THE DEVELOPMENT OF N_2S_2 METAL COMPLEXES AS BIDENTATE LIGANDS FOR ORGANOMETALLIC CHEMISTRY

A Dissertation

by

MARILYN VENA RAMPERSAD

Submitted to the Office of Graduate Studies of
Texas A&M University
in partial fulfillment of the requirements for the degree of

DOCTOR OF PHILOSOPHY

December 2005

Major Subject: Chemistry

THE DEVELOPMENT OF N_2S_2 METAL COMPLEXES AS BIDENTATE LIGANDS FOR ORGANOMETALLIC CHEMISTRY

A Dissertation

by

MARILYN VENA RAMPERSAD

Submitted to the Office of Graduate Studies of
Texas A&M University
in partial fulfillment of the requirements for the degree of

DOCTOR OF PHILOSOPHY

Approved by:

Chair of the committee,	Marcetta Y. Darensbourg
Committee Members,	Stephen A. Miller
	Frank Raushel
	Edward D. Harris
Head of Department,	Emile A. Schweikert

December 2005

Major Subject: Chemistry

ABSTRACT

The Development of N_2S_2 Metal Complexes as Bidentate Ligands for Organometallic Chemistry. (December 2005)

Marilyn Vena Rampersad, B.A., Hunter College of the City University of New York

Chair of Advisory Committee: Dr. Marcetta Y. Darensbourg

Electronic and steric parameters for square planar NiN_2S_2 complexes as bidentate, S-donor ligands have been established. According to the ν(CO) stretching frequencies and associated computed Cotton-Kraihanzel force constants of $(NiN_2S_2)W(CO)_4$ adducts, a ranking of donor abilities and a comparison with classical bidentate ligands are as follows: $Ni(ema)^{=}$ > { $[NiN_2S_2]^0$ } > bipy ≈ phen > $Ph_2PCH_2CH_2PPh_2$ > $Ph_2PCH_2PPh_2$. In addition, we have demonstrated that the NiN_2S_2 ligands are hemilabile as evidenced from CO addition to $(NiN_2S_2)W(CO)_4$, which is in equilibrium with the resulting $(NiN_2S_2)W(CO)_5$ species (K_{eq} = 2.8 M^{-1}, ΔG^o = -1.4 kJ/mole at 50°C). Complete NiN_2S_2 ligand displacement by CO-cleavage of the remaining W-S bond to form $W(CO)_6$ was not observed, indicating that the remaining W-S bond is considerably strengthened upon ring-opening.

Several new cluster compounds based on the NiN_2S_2 ligands bound to Cu^I, Rh^I, Pd^{II} and W^0 are reported. Structural analysis of $(NiN_2S_2)ML_n$ complexes show a unique structural feature defined by the dihedral angle formed by the intersection of NiN_2S_2/WS_2C_2 planes; placing the NiN_2S_2 ligand in closer proximity to one side of the

reactive metal center. This unique orientational feature of the NiN_2S_2 ligands in the series of bimetallic compounds contrasts with classical diphosphine or diimine ligands. The 'hinge angle' ranges in value from 136º as in the (**Ni-1***)$W(CO)_4$ to 101º in the (**Ni-1**)$Pd(CH_3)(Cl)$ complexes. The rigidity of the μ-SR hinge of the nickeldithiolate ligands suggests that they might be suitable for stereochemical and regioselective substrate addition to catalytically active metals such as Rh^I and Pd^{II}.

The structural as well as functional similarities of the acetyl CoA synthase enzyme (ACS) and a palladium-metal based industrial type catalyst led to the preparation of a [(**Ni-1**)$Pd(CH_3)]^+$ bimetallic complex. This complex facilitates CO and ethylene copolymerization to produce polyketone similar to conventional (diphosphine)$Pd(X)_2$ catalysts. However, the diphosphine ligands produce more efficient catalysts as the electron-rich character of the NiN_2S_2 ligand favors the resting state of the catalyst, [(**Ni-1**)$Pd(C(O)CH_3)(CO)]^+$, over the reactive form (**Ni-1**)$Pd(C(O)CH_3)(\eta^2\text{-}C_2H_4)]^+$. An exploratory investigation with the Ni-Pd heterobimetallic showed that this complex also facilitated the C-S coupling reaction to form a thioester similar to the ACS enzyme.

DEDICATION

This dissertation is dedicated to my parents, Ralph and Chanderdai Rampersad, my brother Wayne and sister CindyAnn. To my parents, Ralph and Chanderdai Rampersad, thank you for the sacrifices that you have made over the years so that I could fulfill the dreams you had for me and the ones I had for myself. To my fiancée Ryan Mackiewicz, thank you for being there when I needed you and when I did not. I look forward to the future we will embark on together.

ACKNOWLEDGMENTS

The work enclosed within this dissertation would not have been possible if it were not for my mentor and advisor Dr. Marcetta Y. Darensbourg, who gave me the seed to propagate this scientific project that has blossomed into a tree of many fruitful ideas to come. In many respects she has taught me more about teaching others, perseverance and an appreciation for organometallic chemistry. Thank you for teaching me more than just chemistry and that great things are accomplished only by the perfection of minor details.

I am very appreciative of my committee members, Dr. Raushel, Dr. Miller, and Dr. Harris for their willingness to be on my committee. A special thanks to Dr. Donald J. Darensbourg who has been invaluable towards the development of this project. Our strong collaboration has been extremely rewarding. Thank you for taking the time to listen to me and for your scientific and professional input.

I am grateful to Dr. Joe Reibenspies for getting my feet in X-ray crystallography. Dr. Reibenspies expertise has been extremely valuable. I must also thank Matthew Miller, Jason Yarbrough and Damon Billodeaux for their help and advice on solving crystal structures as well.

I must express my gratitude to the team of students that I became good friends with when I moved to College Station. Each of them mentored me in some way or the other during my development as a graduate student: Dr. Irene Georgakaki, Dr. Rosario Mejia-Rodriguez, Joey (Chao-Yi Chiang). A special thanks to Missy Golden for taking

me under her wings, teaching me scientific independence and for being there to listen. As a pair we taught each other a lot more than we could learn on our own.

A special thanks to past and present members of the DJD group for all the good laughs especially Damon Billodeaux, Cesar Ortiz, and Jody Rogers and the current members, Eric Frantz, Jeremy Andreatta, and Shawn Fitch. Thank you Stephen P. Jeffery for studying long nights with me as I tried to catch up with the rest of my peers and for helping me to develop the NiN_2S_2 ligand. A special thanks to Sue Winters, who has become a good friend the past year when I needed one the most.

To the rest of the MYD group, Scott Brothers, Kayla Green, Ivy Wang, Tianbiao Liu, Michael Singleton, Roxanne Jenkins, and Elky Almaraz, good luck in your endeavors here. I leave to you a few words of advice and inspiration. Keep yourself motivated when things get frustrating. The chemistry and the connections you make are the most exciting part of graduate school.

TABLE OF CONTENTS

CHAPTER Page

LIST OF TABLES

LIST OF FIGURES

FIGURE Page

FIGURE Page

FIGURE Page

FIGURE Page

FIGURE Page

FIGURE Page

CHAPTER I

INTRODUCTION

History has shown that the efficacy of a great catalyst depends on the metal as well as the surrounding ligands providing the steric and electronic environment that influence the performance of the catalyst in terms of rate and selectivity.[1,2] Similarly, ligands coordinated to metals within enzyme active sites may impact the metal in more than one way. For example, they may be involved in the stabilization of the metal during oxidation state changes or promote metal-substrate interactions, both binding and release, during catalysis. The secondary coordination sphere effects by the surrounding protein may also play important roles in fine-tuning the active site during catalysis. Accordingly, in the development of small molecular models of metallo-biological moieties, the type of ligands employed is of utmost importance in order to mimic reactivity in the absence of the surrounding protein.

Indeed, the "art" of homogeneous catalysis typically lies in the minor chemical modifications of steric or electronic properties that tune a metal's ability to control differences in rate and product specificity.[1,2] The discovery of entirely new classes of ligands with unique steric demands or long term stability towards oxidative damage motivates many synthetic efforts. Important technological advances in biomimetic or

---

This thesis follows the style of the *Journal of the American Chemical Society.*

industrial catalyst development and modification rely on the fundamental understanding of ligand properties and their effect on the metal center during catalysis.[1b,3]

Ligand Properties

Ligand properties that influence the performance of the catalyst have been classified as bite angle, steric or electronic features, and ligand flexibility. In order to quantify the effect of these properties on catalysis, several ligand descriptions have been developed. Tolman defined the electronic parameter, χ, as a measure of the electron donating ability of a ligand.[4] The χ value was determined from measuring the CO stretching frequency of $Ni(L)(CO)_3$, utilizing CO reporter ligands as a gauge of electron density transferred to the nickel by various donor ligands (L). Tolman also defined the cone angle (θ) as a means to describe the steric demand of monodentate ligands (Figure I-1, a). This angle simply represents the 'cone" swept out by the ligand attached to a metal center.[4]

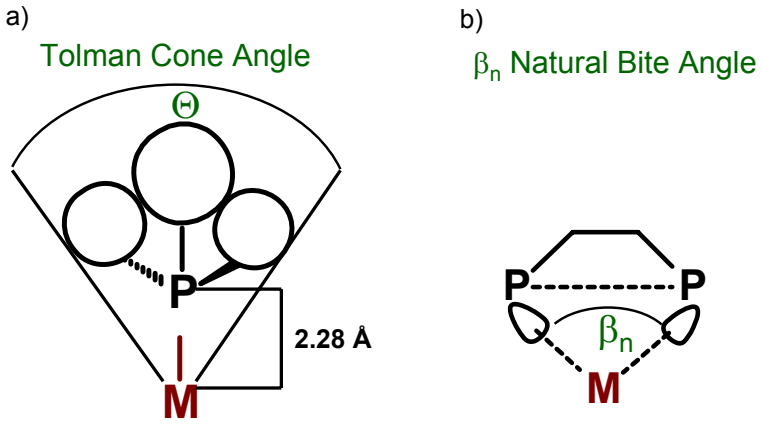

Figure I-1. Ligand parameters defined for steric bulk. a) Tolman cone angle (Θ), and b) natural bite angle (β_n).[4,5]

At the same time, the use of bidentate ligands in catalysis is ubiquitous, and so the need to map the steric and electronic characteristics of bidentate phosphines is also required. Bidentate ligand parameters were initially developed by Tolman and co-workers in the 1970's. Since then other parameters such as the solid angle Ω,[6] the pocket angle[7] and the natural bite angle (β_n)[5] have been put forth. The most widely used is the natural bite angle (β_n), defined as the angle by which two donor atoms bite upon the transition metal center (Figure I-I, b).[1b] Casey and Whiteker calculated this angle by molecular modeling of the ligand backbone as the donor atoms (L) coordinate to a "dummy" metal (M) at fixed L-M bond lengths of 2.315 Å.[5] This method is quite effective in that a crystal structure is not required.[1b,5] A second related parameter, the flexibility range, is defined as the accessible range of bite angles within less than 3 kcal mol^{-1} of strain energy from the calculated bite angle. This parameter estimates the

ligand's ability to stabilize the specific geometry requirements of the metal during catalysis.[5]

The effect of the ligand bite angle during catalysis is best illustrated by van Leeuwen and co-workers in the copolymerization of CO and ethylene with a diphosphine palladium based catalyst, (Figure I-2).[1b] As the number of carbons on the backbone linker increases from one to three, the natural bite angle increases concomitantly with a significant enhancement in productivity or turnover frequency (TOF) (Figure I-2, b). However, the ligand bite angle greater than 91° shows a dramatic decrease in productivity.[1b]

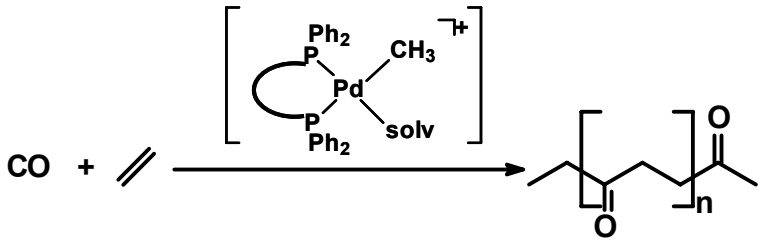

Copolymerization of CO and Ethylene

Ligand	β_n (°)	TOF
$Ph_2P(CH_2)PPh_2$	72	1
$Ph_2P(CH_2)_2PPh_2$	85	1000
$Ph_2P(CH_2)_3PPh_2$	91	6000
$Ph_2P(CH_2)_4PPh_2$	98	2300

TOF = (mole of polymer)/(mol of catalyst)-hour

Figure I-2. Bite angle effects of diphosphines on CO/ethylene copolymerization.[1b]

An emerging attribute of chelating ligands is the ability to possess inert and labile donor groups on the same ligand. Such ligands have been named "hemilabile" ligands; they have the ability to temporarily hold or easily produce open coordination sites on reactive metal centers.[8-10] Evidence for hemilability resulted from ligand substitution reactions wherein the attribute is displayed in the absence or presence of small substrate molecules such as CO, PR_3, ^-CN, NO, etc. (Figure I-3).[8] The stability of the metal complex formed is dependent on the hard-soft acid base character of the metal and donor ligands such that an inert donor side of the ligand will prefer to bind to the soft metal if the ligand is soft and vice versa.[8,10]

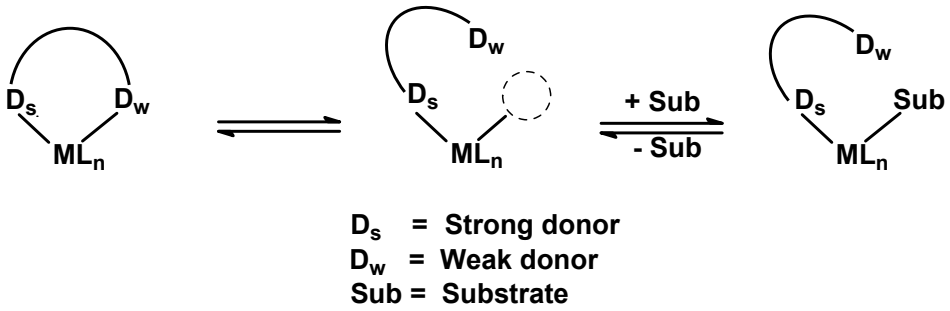

Figure I-3. Hemilabile property of mixed donor bidentate ligands coordinated to transition metals.

Hemilabile ligands have been employed in a broad base of applications in small molecule activation with ligands such as CO and H_2 or in metal complexes that act as small molecule sensors for toxic molecules such as SO_2 and NO.[11-14] The intramolecular dissociation of one arm, also called the "arm off mechanism", has been implicated in many reactions during catalysis.[8] Accordingly, the function of hemilabile ligands during

catalysis has been to stabilize the non-chelate reactive metal complex after the substrate departs or is involved in stabilizing the metal as redox changes occur in which the metal requires specific coordination geometries. A broad range of mixed ligand donor sets accommodate this functionality in which the ligands have a combination of P, N, O, X (halide), S, Se, As, and P=O donor types.[8] Additionally, mixed donor sets have provided a means to chiral ligands of importance to asymmetric catalysis such as hydrosilation and hydroboration.[10,15-16]

Symmetric hemilabile ligands are rare; however, hemilability has been observed with the diimine type ligands and thioether type chelates.[17-19] Van Leeuwen and co-workers have shown that one of the nitrogen donors on tetramethylethylenediamine dissociates, providing an available coordination site on a square planar M^{II} (Pd, Pt) for CO to bind in the C-C coupling of CO and CH_3.[17] A more recent example has been seen with a dithioether ligand coordinated Rh(I) that undergoes oxidative addition of CH_3I. The mechanistic pathway proposed for this reaction includes a dissociation of one thioether donor, providing an electronically and coordinatively unsaturated reactive metal center for oxidative addition to proceed.[18]

Metallodithiolate Complexes as a Novel Class of Ligands

A recent and dramatic discovery of a new ligand class is to be found in the natural assembly of a catalytic reactive center within acetyl CoA synthase (ACS).[20-22] This bimetallic enzyme active site (Figure I-4) has been deconvoluted into a nickel-dithiolate moiety, $N_2S_2Ni_d$, derived from a Cys-Gly-Cys tripeptide bound to a second

catalytically active nickel, Ni_p, through bridging cysteinate sulfur donors.[21,22] The second nickel mediates the assembly of the acetyl CoA thioester from CH_3^+, carbon monoxide, and the elaborate thiolate, coA.[20-22] The role of the first nickel, Ni_d, in N_2S_2 coordination appears to be largely structural, i.e., serving as a template for the tripeptide. The bidentate NiN_2S_2 ligand thus derived has the appropriate electronic (donor) features to support the C-C and C-S coupling chemistry of the second nickel, Ni_p.

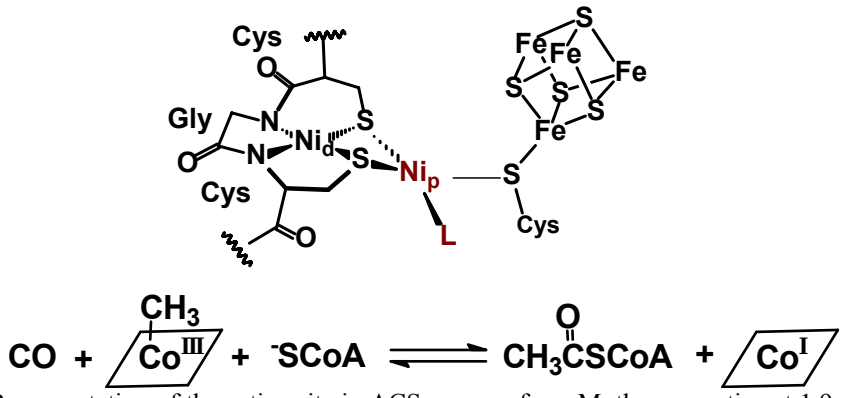

Figure I-4. Representation of the active site in ACS enzyme from M. thermoacetica at 1.9 Å by Darnault and Volbeda et al.[21]

A recent computation designed to understand the role of the metallothiolate moiety in the acetyl CoA synthase enzyme pointed to the fact that the $Ni_dN_2S_2$ ligand in Nature may serve as a hemilabile ligand.[23] That is, one of the Ni_p-S thiolate may dissociate as CO binds, stabilizing the Ni^{2+} metal center. A more detailed account of this computational mechanism is discussed in Chapter V (Figure I-5).

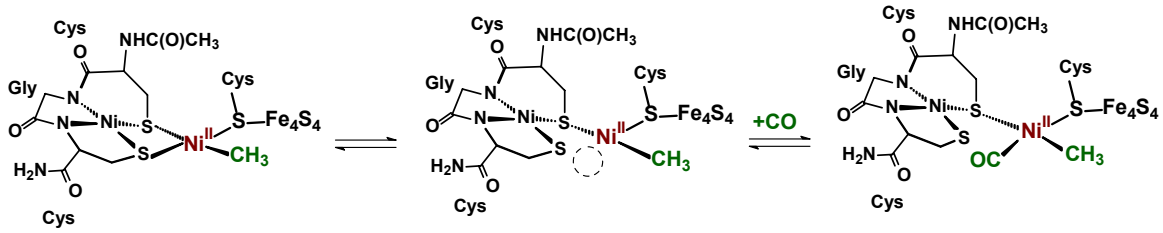

Figure I-5. Representation of hemilabile nature of the $Ni_dN_2S_2$ moiety in the ACS active site as a hemilabile ligand from a computational mechanism by Webster et al.[23].

As the (Cys-Gly-Cys)Ni unit joins a host of synthetic NiN_2S_2 complexes that are well known to form multi-metal clusters through μ-SR interactions, Nature's control of binuclearity in the construction of an organometallic catalyst presents the intriguing possibility that the NiN_2S_2 complexes might be suitable for development as a novel class of ligands for organometallic chemistry and catalysis. From our own work with metallodithiolate ligands, we have seen a wide range of sulfur-based reactivity. We have explored the use of the NiN_2S_2 ligand in sulfur-oxygenation, H-bonding, alkylation, modification leading to coordination sphere expansion, and metallation reactions.[24] Of interest to this present work described herein are the metallation reactions with NiN_2S_2 ligands.[25-40] Similar to classical diphosphine and diimine ligands that bind to metals in a variety of coordination modes, metallodithiolate ligands also bind to a variety of metals in a myriad of oxidation states. Of the structural forms presented in Figure I-6, the NiN_2S_2 ligand, *N,N*'-bis(2-mercaptomethylpropane)-*N,N*'-diazacyclooctane] nickel(II), **Ni-1,** binds to exogenous metals in a bidentate bridging fashion to one or two metals as in the staircase $(\mathbf{Ni\text{-}1})_2Ni^{2+}$ or the $(\mathbf{Ni\text{-}1})_3(CuBr)_2$ structures.[27,29] The **Ni-1** may also utilize only one of the thiolate donors to coordinate to a single metal center as in the (**Ni-**

1)$Fe(CO)_4$.[31] The work illustrated in Figure I-6 evolved over the past 1.5 decades in the Darensbourg labs. In the meanwhile, inspired by the ACS active site the work by Holm, Riordan, Hegg, Mascharak and Schroder has produced many more examples of di and polynuclear structures which are referenced throughout this dissertation.[33-40] Note that the NiN_2S_2 metallation template effect constituted a phenomenon that was observed earlier on by Blinn, Schugar, and others prior to the ACS active site.[35,41]

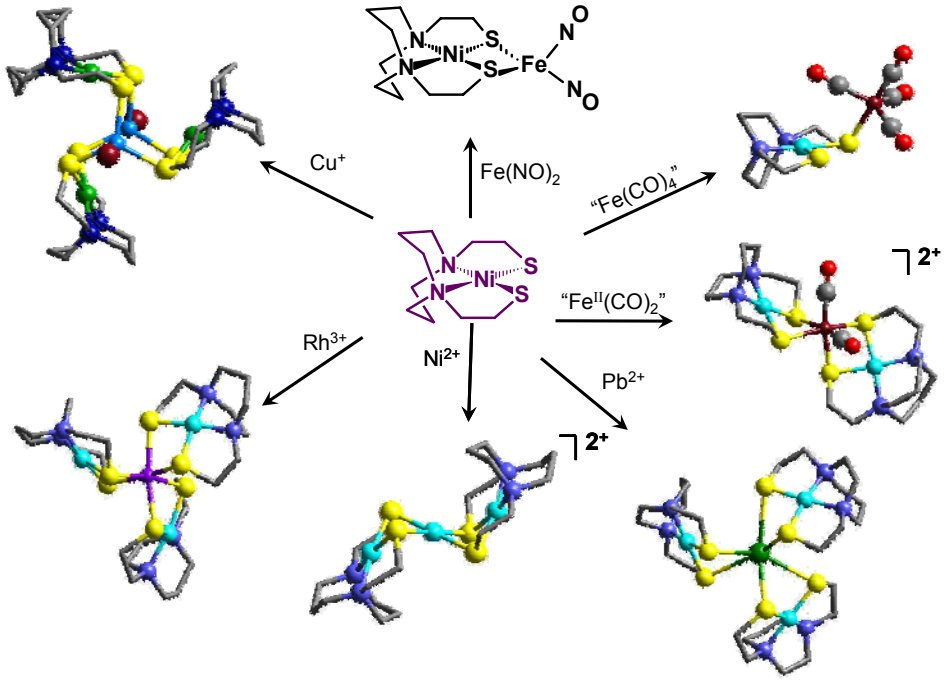

Figure I-6. Cerius model ball-stick-representations of $(NiN_2S_2)_xM_y$ complexes.

Overall, this dissertation details the chemistry of NiN_2S_2 ligands as it relates to enzymes, cluster formation, and possible applications to industrial catalysis. Our efforts primarily focused on four key areas. We have designed bimetallic complexes what have been

using in studying the properties of the ligands and have provided a means to explore the reactivity of the complexes employing the NiN_2S_2 complex as a ligand. The bimetallic complexes with tungsten tetracarbonyl, $(NiN_2S_2)W(CO)_4$, were prepared and used to study the characteristics of NiN_2S_2 complexes as ligands (steric, electronic and hemilabile properties), as well as the stability of the heterometallic complexes formed. Comparison of the structural forms for $(NiN_2S_2)_xCu_y$ aggregates and as well analysis of bimetallic complexes $(NiN_2S_2)ML_n$ are made. Finally, we have examined the reactivity of metal complexes employing NiN_2S_2 ligands in organometallic test reactions for comparison to classical ligands that are industrially and biologically significant.

CHAPTER II

EXPERIMENTAL SECTION FOR CHAPTERS III-VI

GENERAL PROCEDURES AND PHYSICAL METHODS

All manipulations were performed on a double-manifold Schlenk vacuum line under an atmosphere of nitrogen or in an argon-filled glove box. Solvents were reagent grade, pre-dried and deoxygenated according to published procedures under a N_2 atmosphere.[42]

UV-Vis spectra were recorded in CH_3CN or CH_2Cl_2 on a Hewlett Packard HP8552A diode array spectrometer. using quartz cells (1.00 cm path length). Canadian Microanalytical Services, Ltd., Delta, British Columbia, Canada, performed elemental analyses. Infrared spectra were recorded on a Mattson Galaxy Series 6021 FTIR spectrometer or a Bruker Optics 6021 FTIR spectrometer with a DTGS detector. in CaF_2 solution cells of 0.1 mm pathlength.

Mass spectral analyses were done at the Laboratory for Biological Mass Spectroscopy at Texas A&M University. Electrospray ionization mass spectra were recorded using a MDS-Series QStar Pulsar with a spray voltage of 5eV.

---

*Reproduced in part with permission from **"**N_2S_2Ni Metallothiolates as a Class of Ligands that Support Organometallic and Bioorganometallic Reactivity", by Marilyn V. Rampersad, **2005**, *Angew. Chem., Int. Ed..***,** 44, 1217-20. **2005 ,** Angewandte Chemie International Edition.

MALDI-TOFF measurements were performed on the ABI Voyager-DE STR spectrometer, operating in positive reflection mode. Dithranol (1,8,-trihydroxyanthracene) was used as matrix and the polymer was dissolved in hexafluroisopropanol (HFIP).

Conductance measurements were performed using an Orion Model 160 Conductance meter equipped with an Orion two-electrode conductivity cell. The cell constant was determined to be 0.97 at 25^{o}C.

Photolysis experiments were performed using a mercury arc vapor, 450W UV immersion lamp purchased from Ace Glass Co.

^{13}C NMR studies were performed on a INOVA 500 MHz Varian spectrometer. Vis/UV spectra were recorded in CH_2Cl_2 on a Hewlett Packard HP8552A diode array spectrometer. ^{13}C NMR analysis of the polyketone was carried out with a INOVA 400 MHz Varian spectrometer in a 1:1 mixture of hexafluroisopropanol and $CDCl_3$.

Cyclic voltammograms were recorded on a BAS-100A electrochemical analyzer using platinum wire as counter electrode and Ag/Ag^{+}, prepared by anodizing a silver wire in an CH_3CN solution of 0.01 M $AgNO_3$/0.1 M *n*-Bu_4NBF_4, was the reference electrode. The glassy carbon disk (0.071 cm^2) working electrode was polished with 15, 3, and 1 μm diamond pastes, successively, and then sonicated in ultrapure (Millipore) water for 10 min. The solutions were purged with argon for 5-10 min and a blanket of argon was maintained over the solution during the electrochemical measurements. All experiments were performed in CH_3CN solutions containing 0.1 M *n*-Bu_4NBF_4 analyte at room temperature. Since the oxidation peaks for samples were overlapped with the

Cp_2Fe/Cp_2Fe^+ redox wave, Cp^*_2Fe served as internal reference. The measured potential difference between Cp_2Fe/Cp_2Fe^+ and $Cp^*_2Fe/Cp^*_2Fe^+$ was 505 mV. Thus, all potentials are reported relative to the normal hydrogen electrode (NHE) using Cp_2Fe/Cp_2Fe^+ as standard ($E_{1/2}$ = 0.40 V vs NHE in CH_3CN).[43]

EXPERIMENTAL DETAILS FOR CHAPTER III

Materials

The CH_3CN, CH_2Cl_2, diethyl ether, benzene, hexane and tetrahydrofuran (THF) solvents were purified according to published procedures under a N_2 atmosphere.[32] Anhydrous Dimethylformamide (DMF) was purchased from Acros Chemical Company. The **Ni-1***,[44] **Ni(ema)**,[45] **Ni(bme-Me$_2$PDA)**,[46] **Ni-1**,[47] **Ni-1′**,[48] **Ni-1(bmmp-ded)**[49] and the *cis*-$W(CO)_4(pip)_2$,[50] complexes were synthesized according to previously published procedures. Complex **3** was prepared by a graduate student colleague, Stephen P. Jefferey in a similar manner to the other $NiN_2S_2W(CO)_4$ complexes shown below. Definitions: **Ni-1*** = (N,N'-bis-2-mercapto-2-methylpropane-N,N'-diazacyclooctane) nickel(II), **Ni(ema)** = (N,N'-ethylenebis-2-mercaptoacetamide) nickel(II), **Ni(bme-Me2PDA)** = (N,N'-dimethyl-N,N'- bis-2-mercaptoethyl-1,3-propanediamine) nickel(II), **Ni-1** = (N,N'-bis-2-mercaptoethyl-N,N'-diazacyclooctane) nickel(II), **Ni-1'** (N,N'-bis-2-mercaptoethyl)-N,N'-diazacycloheptane) nickel(II), **Ni(bmmp-dmed)** = (N,N'-bis-2-methyl-mercaptopropyl-N,N'-dimethylethylenediamine) nickel(II).

[N,N'-bis-2-mercapto-2-methylpropyl-N,N'-diazacyclooctane] nickel(II) tungsten tetracarbonyl, (Ni-1*)$W(CO)_4$, (1).

The yellow $W(CO)_4(pip)_2$ (0.12 g, 0.26 mmol) was dissolved in 20 mL of CH_2Cl_2 and heated to 40°C for 10 min under a N_2 atmosphere. To this was added dropwise a lilac-purple solution of **Ni-1*** (0.09 g, 0.26 mmol) dissolved in 10 mL of CH_2Cl_2. The resulting red-brown solution was heated for an additional 10 min at 40°C, and stirred at 22°C ultimately producing a brown precipitate. The solvent and piperidine were removed and the brown solid washed with benzene (25 mL x 2) and ether (25 mL x 2). The solid was extracted with CH_2Cl_2 and orange-red crystals were obtained from vapor diffusion of hexane into this solution of (**Ni-1***)$W(CO)_4$, yield 0.11 g (65%) Anal. Cal'd (found) for $C_{18}H_{28}N_2Ni_1O_4S_2W_1$: C, 33.6 (32.1); H, 4.39 (4.49); N, 4.36 (4.49). Vis/UV in DMF solution: λ_{max} (ε)=306 (5002), 372 (1382), 420 (1480), 504 nm (495).

Tetraethylammonium [N,N'-ethylenebis(2-mercaptoacetamide)] nickel(II) tungsten tetracarbonyl, $[Et_4N]_2$[(Ni(ema))$W(CO)_4$], (2).

The yellow $W(CO)_4(pip)_2$ (0.27 g, 0.57 mmol) was dissolved in 20 mL of CH_3CN and heated to 60-70°C for 10 min under an N_2 atmosphere. To this was added dropwise a red solution of $(Et_4N)_2$[**Ni(ema)**] (0.3 g, 0.57 mmol) dissolved in 10 mL of CH_3CN. The resulting olive green-brown solution was heated for an additional 15 min at 60-70°C. The solution was stirred at 22°C for a few hours. The solvent was removed under vacuum and the olive green solid was washed twice with 30 mL benzene to remove excess piperidine and twice with 30 mL ether. The solid was extracted with CH_2Cl_2

olive-green crystals were obtained from vapor diffusion of hexane into this solution of $(Et_4N)_2$[**Ni(ema)**]$W(CO)_4$], yield 0.32 g (67%). The air-sensitive complex was stored in the glove box. Anal. Cal'd (found) for $C_{26}H_{48}N_4Ni_1O_6S_2W_1$: C, 38.1 (37.6); H, 5.90 (5.81); N, 6.85 (6.67). Vis/UV in DMF solution: λ_{max} (ε)=332 (6904), 404 (1967), 478 nm (1120).

[N,N'-bis-2-mercaptoethyl-N,N'-diazacyclooctane] nickel(II) tungsten tetracarbonyl, (Ni-1)W(CO)$_4$, (4).

In an identical manner as (**1)** stated above, a purple solution of **Ni-1** (0.1 g, 0.34 mmol) dissolved in 10 mL of CH_2Cl_2 was added to $W(CO)_4(pip)_2$ (0.16 g, 0.34 mmol) was dissolved in 20 mL of CH_2Cl_2. Isolation yielded 0.14 g (69%). X-ray quality crystals were grown via layering of a DMF solution of the complex with ether to produce crystals. Anal. Cal'd (found) for $C_{14}H_{20}N_2Ni_1O_4S_2W_1$: C, 28.7 (28.2); H, 3.43(3.35); N, 4.77(4.58). Vis/UV in DMF solution: λ_{max} (ε)=308 (6057), 378 (1135), 412 (1136), 488 nm (585).

[N,N'-bis-2-mercaptoethyl-N,N'-diazacycloheptane] nickel(II) tungsten tetracarbonyl, (Ni-1')W(CO)$_4$, (5).

In an identical manner for (**1)** as stated above, the yellow brown slurry of **Ni-1'** (0.10 g, 0.36 mmol) dissolved in 10 mL of CH_2Cl_2 was added to $W(CO)_4(pip)_2$ (0.17 g, 0.36 mmol). Isolation yielded 0.13 g, 61% of (**Ni-1'**)$W(CO)_4$. X-ray quality crystals were grown by diffusion of ether into a DMF solution of the product. Anal. Calcd

(Found) for $C_{13}H_{18}N_2Ni_1O_4S_2W_1$: C, 27.3 (26.9); H, 3.17 (3.67); N, 4.89 (5.27). Vis/UV in DMF solution λ_{max} (ε): 308 (6728), 408 (1169), 450 (985), 512 (494) nm.

[N,N'-bis-2-methyl-mercaptopropyl-N,N'-dimethylethylenediamine] nickel(II) tungsten tetracarbonyl, [Ni(bmmp-dmed)]W(CO)$_4$, (6).

In an identical manner for (**1)** as stated above, a purple solution of Ni(bmmp-dmed) was added to $W(CO)_4(pip)_2$ (0.15 g, 0.31 mmol). Isolation yielded 0.10g, 53% of (Ni(bmmp-dmed))$W(CO)_4$. X-ray quality crystals were grown by vapor diffusion of hexane into a CH_2Cl_2 solution of the product. Anal. Calcd (Found) for $C_{16}H_{26}N_2Ni_1O_4S_2W_1$: C, 31.1 (32.0) ; H, 4.25 (4.75); N, 4.54 (5.01). Vis/UV in DMF solution: λ_{max} (ε) 312 (5725), 388 (609), 440 (565) nm.

[(N,N'-bis-2-mercaptoethyl-N,N'-diazacyclooctane] nickel(II) tungsten pentacarbonyl, (Ni-1)W(CO)$_5$, (7).

A sample of $W(CO)_6$ (0.1 g, 0.28 mmol) in 40 mL of THF under N_2 was photolyzed for 2 hours to yield a yellow solution of the $W(CO)_5$(THF) adduct (ν(CO) = 1975, 1931, 1892 cm^{-1}). Addition of a purple slurry of **Ni-1** (0.08 g, 0.28 mmol) in 20 mL of THF resulted in a red-brown solution that was stirred overnight at 22^{o}C. The volume was reduced in vacuo to about 10 mL; addition of ca. 40 mL of hexane produced a brown solid which was washed with hexane (2 x 40 mL) to remove excess $W(CO)_6$. The solid was further purified by silica gel column chromatography with CH_2Cl_2 as the eluent to remove excess **Ni-1**. The solid was dried under vacuum to yield 0.12 g, 72% of

(**Ni-1**)$W(CO)_5$. Anal. Calcd (Found) for $C_{14}H_{26}N_2Ni_1O_5S_2W_1$: C, 29.3 (28.9); H, 3.28 (2.92); N, 4.56 (4.25). IR (THF, cm^{-1}) υ(CO) 2062 (w), 1974 (m), 1922 (s), 1885 (m). IR (DMF, cm^{-1}) υ(CO) 2062 (w), 1972 (w), 1922 (vs), 1874 (m).

^{13}CO Enrichment.

Carbon-13 enriched $W(CO)_6$ was prepared by addition of ^{13}CO gas to a CH_2Cl_2 solution of [PPN][$W(CO)_5Cl$].[51-52] From tungsten hexacarbonyl the isotopically labeled *cis*-$W(CO)_{4-n}(^{13}CO)_n(pip)_2$ was prepared by the reported method.[41] Replacement of the piperidine with the NiN_2S_2 ligand yielded the $(NiN_2S_2)W(CO)_{4-n}$ $(^{13}CO)_n$ complexes. Samples containing approximately 0.05 – 0.07 mmol of the [$(NiN_2S_2)W(CO)_{4-n}(^{13}CO)_n$] complexes in 0.7 mL of DMF were prepared under Ar and used in the VT NMR studies.

X-ray Crystal Structure Determinations.

Crystal data and details for data collection and refinement are given in Table III-2. The crystals were mounted on a glass fiber at room temperature for the experiment. X-ray data were obtained on a Bruker P4 diffractometer. The space groups were determined on the basis of systematic absences and intensity statistics.[45] Structures were solved by direct methods. Anisotropic displacement parameters were determined for all non-hydrogen atoms. Programs used for data collection and cell refinement, Brucker XSCANS; data reduction, SHELXTL;[53] structure solution, SHELXS-97[54] (Sheldrick); structure refinement, SHELXL-97[55] (Sheldrick), and molecular graphics and preparation of material for publication, SHELXTL-Plus, version 5.1 or later (Bruker).[56]

EXPERIMENTAL DETAILS FOR CHAPTER IV

Materials

The CH_3CN, CH_2Cl_2, diethyl ether, and hexane solvents were purified according to published procedures under a N_2 atmosphere.[42] All other chemicals were purchased from the Aldrich Chemical company. The (TMEDA)Pd$(CH_3)_2$,[57] $H(OEt_2)_2BAr'_4$,[58] (cod)Pd(CH_3)(Cl),[59] and **Ni-1**[47] complexes were synthesized according to published procedures. All compounds were stored under an argon atmosphere at -45°C. The CO gas used was filtered through a Drierite column before introduction to the reactions.

Definitions: cod = cyclooctadiene, $HBAr'_4$ = $[H(OEt_2)_2][(3,5\text{-}[(CF_3)_2C_6H_3)_4B]$, TMEDA = tetramethylethylenediamine, **Ni-1** = [(1,5-bis(2-mercaptoethyl)-1,5-diazacyclooctanato]nickel.

Synthesis of [N,N'-bis-2-mercaptoethyl-N,N'-diazacyclooctane] nickel(II) palladium dimethyl (Ni-1)Pd$(CH_3)_2$.

To a 50 mL Schlenk flask was added (TMEDA)Pd$(CH_3)_2$ (0.30 g, 1.18 mmol) followed by the addition of 15 mL of CH_3CN. To the colorless solution a purple solution of **Ni-1** (0.36 g, 1.25 mmol) dissolved in 20 mL of CH_3CN was added *via* cannula to yield a dark red solution. After stirring overnight at room temperature, the solution was concentrated to about 5 mL. Approximately 40 mL of pentane was added precipitate a red-pink solid. The slurry was washed twice with pentane (2 x 40 mL) and the solid collected by filtration and stored under argon in the refrigerator at -45°C, yielding 0.40

g, 78%. Vis/UV in CH_2Cl_2 solution: λ_{max} (ε) 272 (3272), 280 (3281), 304 (2488), 326 (1930) and 510 (138) nm. Mass spectrum (CH_3CN solution) *m/z* (% abundance relative to base peak = 100 %): 413(82) $[(Ni\text{-}1)Pd(CH_3)]^+$, 454 (100) $[(Ni\text{-}1)Pd(CH_3)(CH_3CN)]^+$, 344 (83) $[(Ni\text{-}1)_2Pd]^{2+}$.

Synthesis of [N,N'-bis-2-mercaptoethyl-N,N'-diazacyclooctane] nickel(II) palladium acetyl carbonyl, [(Ni-1)Pd(C(O)CH$_3$)(CO)][BAr$'_4$].

To a degassed flame-dried Schlenk tube was added HBAr$'_4$ (0.071 g, 0.070 mmol) and (**Ni-1**)$Pd(CH_3)_2$ (0.030 g, 0.070 mmol) under an argon atmosphere which was cooled to -30°C in a dry ice / CH_3CN ice bath. Approximately 5 mL of CH_2Cl_2 was added to the flask taking care to dissolve all of the reactants (CO exposure to (**Ni-1**)$Pd(CH_3)_2$ results in decomposition to Pd black). After stirring for 15 min the red solution was cooled to -78°C in a dry ice / acetone bath and CO gas was sparged vigorously for 5 min. The resulting solution was allowed to stir for an additional 30 min at -78°C. IR (CH_2Cl_2) υ(C≡O, C=O): 2110 (s) cm^{-1} and 1722 (m) cm^{-1}. Vis/UV in CH_2Cl_2 solution: λ_{max} (ε) 236 (185684), 272 (129597), 280 (136897), 328 (58390), 522 (7621) nm.

Synthesis of [(Ni-1)Pd(^{13}C(O)CH$_3$)(^{13}CO)][BAr$'_4$].

The [(**Ni-1**)Pd(C(O)CH$_3$)(CO)][BAr$'_4$] was prepared in a similar manner to that stated above. In a 10 mL degassed flame-dried Schlenk flask was added HBAr$'_4$ (0.071 g, 0.071 mmol) and (**Ni-1**)Pd(CH$_3$)$_2$ (0.030 g, 0.070 mmol). Approximately 5 mL of CH_2Cl_2 was added and the solution was stirred for 15 min before being cooled to -78°C. The argon atmosphere was removed under vacuum and replaced with an atmosphere of isotopically labeled ^{13}CO gas. The red solution was allowed to stir for an additional 30 min at -78°C. IR (CH_2Cl_2) υ(C≡O, C=O): 2062 cm^{-1} (s) and 1862 cm^{-1} (m); ^{13}C NMR (300 mHz, CD_2Cl_2, 25°C): δ= 225.0 ppm (s, C(O)CH$_3$), 175.1 ppm (s, Pd-CO).

Synthesis of [N,N'-bis-2-mercaptoethyl-N,N'-diazacyclooctane] nickel(II) palladium methyl diethyl ether, [(Ni-1)Pd(CH$_3$)(OEt$_2$)][BAr$'_4$].

Under an argon atmosphere the red (**Ni-1**)Pd(CH$_3$)$_2$ (0.030g, 0.070 mmol) and white HBAr$'_4$ (0.071 g, 0.070 mmol) solids were added to a degassed and flame-dried Schlenk tube which was immediately placed in a -30^{0}C dry ice / CH$_3$CN ice bath. A 3:1 v/v mixture of CH_2Cl_2 and diethyl ether was added to the solids taking care to dissolve all of the reactants (CO exposure to unreacted (**Ni-1**)Pd(CH$_3$)$_2$ results in decomposition to Pd black). The orange-red solution was stirred for two hours at -30°C followed by the evaporation of the solvent under vacuum to yield an orange-red solid, 0.068g, 72%. UV-Vis in CH_2Cl_2 solution: λ_{max} (ε, M^{-1} cm^{-1}) 236 (247101), 272 (157731), 280

(154348), 302 (97298), 330 (58341), 396 (14396), 518 (5635) nm. Mass spectrum (CH_3CN solution) *m/z (%* abundance relative to base peak = 100%): 413 [(**Ni-1**)Pd(CH_3)]$^+$ (97%), 454 [(**Ni-1**)Pd(CH_3)(CH_3CN)]$^+$ (100%).

Synthesis of [N,N'-bis-2-mercaptoethyl-N,N'-diazacyclooctane] nickel(II) palladium methyl chloride, (Ni-1)Pd(CH_3)(Cl).

To a degassed sample of (cod)Pd(CH_3)(Cl) (0.20 g, 0.75 mmol) was added 20 mL of CH_2Cl_2 under an N_2 atmosphere. To the colorless solution a purple solution of **Ni-1** (0.22 g, 0.75 mmol) dissolved in 30 mL of CH_2Cl_2 was added. The resulting red-pink solution was stirred for 5 hours at room temperature before the solution was concentrated to about 5 mL resulting in a red precipitate. The slurry was washed with pentane (2 x 20 mL) and then dried under vacuum to yield a red-pink solid of 0.32 g (95%) of (**Ni-1**)Pd(CH_3)(Cl). Anal. Calcd (Found) for $C_{12}H_{25}N_2S_2NiPdCl_3$ ([(**Ni-1**)Pd(CH_3)(Cl)]·CH_2Cl_2): C, 26.2 (27.0); H, 4.94 (4.73); N, 5.86 (5.26). Included in the experimental elemental analysis is a CH_2Cl_2 solvent molecule that was observed in the x-ray diffraction study of the crystals. UV-Vis in CH_2Cl_2 solution: λ_{max} (ε, M^{-1} cm^{-1}) 232 (18014), 262 (13807), 302 (8555), 526 (459) nm. Mass spectrum (CH_3CN solution) *m/z* (% abundance relative to base peak = 100%): 413 [(Ni-**1**)Pd(CH_3)]$^+$ (100%), 454 [(**Ni-1**)Pd(CH_3)(CH_3CN)]$^+$ (22%)

Preparation of [N,N'-bis-2-mercaptoethyl-N,N'-diazacyclooctane] nickel(II) palladium acetyl chloride, (Ni-1)Pd(C(O)CH_3)(Cl).

A sample of the [(**Ni-1**)Pd(CH_3)(Cl) (0.030g, 0.066 mmol) solid was placed in a degassed and flame-dried Schlenk tube under an argon atmosphere which was cooled to -78^{o}C in a dry ice / acetone ice bath. Approximately 5 mL of CH_2Cl_2 was added to the flask followed by sparging of CO gas through the solution vigorously for 5 min. The solution was stirred for an additional 30 min at -78^{o}C. IR (CH_2Cl_2), υ(C=O)): 1692 (s) cm^{-1}.

Stability Studies of [(Ni-1)Pd(CH_3)(OEt_2)][BAr′$_4$] and [(Ni-)Pd(C(O)CH_3)(CO)][BAr′$_4$].

A 0.29 mM sample of [(**Ni-1**)Pd(CH_3)(OEt_2)][BAr′$_4$] in CH_2Cl_2 was added to a flame-dried degassed air tight cuvette fitted with a rubber septum under an N_2 atmosphere. The UV-Vis spectra of the sample were recorded at regular intervals at room temperature for several hours. For the solution stability study of [(**Ni-1**)Pd(C(O)CH_3)(CO)][BAr′$_4$] a fresh sample of the solution was prepared by addition of (**Ni-1**)Pd(CH_3)$_2$ (0.010g, 0.023 mmol) and HBAr′$_4$ (0.024 g, 0.023 mmol) to a flame-dried degassed 10 mL volumetric flask which was immediately cooled to -78^{0}C. To this was added 5 mL of CH_2Cl_2 and after 15 minutes CO gas was sparged through the solution for 5 min to yield the [(**Ni-1**)Pd(C(O)CH_3)(CO)][BAr′$_4$]. The volume of the sample was adjusted to 10 mL with CH_2Cl_2**.** A 0.30 mL aliquot of a 0.30 mM sample

was added to an air-tight cuvette under CO atmosphere containing 2 mL of CH_2Cl_2. The UV-Vis spectra were recorded at regular intervals for 24 hours at room temperature.

Copolymerization of CO and Ethylene.

Samples of (**Ni-1**)Pd$(CH_3)_2$ and HBAr$'_4$ were added to a flame-dried degassed vial and dissolved in 15 mL of CH_2Cl_2. The solution was cooled to -78^oC and left to stir for 10 minutes before being transferred *via* an injection port to a stainless steel 300 mL Parr autoclave at room temperature. The autoclave was pre-dried at 80^oC under vacuum for 8 hours and cooled to room temperature prior to use. The vial was washed with an additional 10 mL of CH_2Cl_2 and the washings were added to the autoclave. The autoclave was then charged with CO gas and then ethylene was added and the contents were heated at the desired temperature and for the designated time. Copolymerization was initiated at the time of monomer addition and was stopped by cooling the autoclave to room temperature and venting the remaining gases in the fume hood. The autoclave was cooled by removing the reactor from the heating mantle, achieving room temperature within a short period. The polymer was extracted from the catalyst by precipitation with an acidic methanol solution (95% CH_3OH and 5% HCl). The grayish to white polymer was collected via filtration in open air, dried and the weight was measured. IR (Hexafluroisopropanol), υ(C=O)): 1704 (s) cm^{-1}. ^{13}C NMR (400 mHz, Hexafluroisopropanol, 25^oC): δ= 220.0 ppm (s, C(O)), 43 ppm (s, α-CH_2).

High Pressure *In Situ* Variable Temperature ^{13}C NMR Study of CO Addition and CO/Ethylene Uptake in $(NiN_2S_2)Pd(L)_2$ Complexes

N.B.: High-pressure sapphire NMR tube: Care must be taken to ensure there are no scratches or microfractures on the tube, which may provide a nucleation point for explosion during pressurization. The tube was cleaned by consecutive rinsings with CH_2Cl_2 and by a gentle scrub using a modified pipe cleaner. These experiments were were carried out in a collaboration with Dr. Piet W.N.M. van Leeuwen, Erik Erik Zuidema, Jan Meine Ernsting.

^{13}C NMR Study of CO Addition to [(Ni-1)Pd(CH_3)(OEt_2)][BAr$'_4$].

To a degassed flame-dried Schlenk tube was added [(**Ni-1**)Pd(CH_3)(OEt_2)][BAr$'_4$] **(**0.053 g, 0.039 mmol) to which 2 mL of anhydrous CD_2Cl_2 was added under an argon atmosphere. The 20 mM solution was transferred *via* a plastic cannula to a high pressure sapphire NMR tube that had been flushed with argon for 15 minutes. The red solution was slightly purged with argon before the stainless steel cap was placed on the top of the tube simultaneously as the plastic cannula was removed. The sample was cooled to -80^{o}C in a dry ice acetone bath and pressurized with 7 bar of isotopically labeled ^{13}CO gas a few minutes prior to transporting the sample to the NMR spectrometer (probe pre-cooled to -80^{o}C). (N.B.: the total pressure in the tube was 8 bar (7 bar CO + 1 bar Ar)). Approximately 5 minutes after CO addition, the NMR tube was wiped dry on the outside, shaken once and inserted into the pre-cooled NMR instrument. Consecutive ^{13}C NMR spectra were recorded over a range from -80^{o}C to 60^{o}C.

^{13}C NMR Study of CO Addition to (Ni-1)Pd(CH_3)(Cl).

In an almost identical procedure for the preparation of the [(**Ni-1**)Pd(CH_3)(OEt_2)][BAr′$_4$] complex for CO addition, the red-pink (**Ni-1**)Pd(CH_3)(Cl) (0.018 g, 0.040 mmol) solid dissolved in 2 mL of anhydrous CD_2Cl_2 in a flame-dried degassed flask under an argon atmosphere. The 20 mM solution was transferred to the sapphire NMR tube (degassed thoroughly in a large schlenk tube under an argon atmosphere) which was cooled to -80^{o}C and charged with 8 bar of isotopically labeled ^{13}CO gas a few minutes prior to transporting the sample to the NMR instrument (probe pre-cooled to -80^{o}C). (N.B.: the total pressure in the tube is 10 bar (8 bar CO + 1 bar Ar)). Approximately 5 minutes after CO addition, the ^{13}C NMR spectra were recorded over a range from -80^{o}C to 30^{o}C.

^{13}C NMR Study of CO and Ethylene Uptake in [(Ni-1)Pd(CH_3)(OEt_2)][BAr′$_4$].

A sample of [(**Ni-1**)Pd(CH_3)(OEt_2)][BAr′$_4$] (0.057 g, 0.042 mmol) dissolved in 2 mL of CD_2Cl_2 was prepared in an identical manner as stated above. The 21 mM sample was pressurized with 7 bar ^{13}CO gas approximately 5 minutes prior to recording the ^{13}C NMR spectrum at -80^{o}C (NMR instrument pre-cooled to -80^{o}C). For the addition of ethylene, the NMR tube was depressurized to 1 bar in a fume hood and charged with 4 bar of ethylene while maintaining a constant temperature of -80^{o}C in a dry ice acetone bath (total pressure = 5 bar). Consecutive ^{13}C NMR spectra were recorded over a range from -80^{o}C to 20^{o}C.

EXPERIMENTAL DETAILS FOR CHAPTER V

Materials

The $CH_3SC(O)Me$, $HS(C_6H_4)Me$ and $NaSCH_3$ were purchased from Aldrich Chemical Co. and used as received without further purification. The synthesis of (**Ni-1**)$Pd(CH_3)_2$ and [(**Ni-1**)$Pd(CH_3)(OEt_2)$][BAr'_4] complexes are described in detail in Chapter IV.

Reactivity of [(Ni-1)Pd(C(O)CH$_3$)(CO)]$^+$ with NaSR (R = Me, (C$_6$H$_4$)Me) and CO

[(**Ni-1**)$Pd(C(O)CH_3)(CO)]^+$ was prepared *in situ* by reacting the (**Ni-1**)$Pd(CH_3)_2$ (0.030 g, 0.070 mmol) and $HBAr'_4$ (0.070 g, 0.070 mmol) solids as described (Chapter IV) in 5 mL of CH_2Cl_2. The solution was transferred to another Schlenk flask containing NaSMe (0.005 g, 0.030 mmol) or $NaS(C_6H_4)Me$ (0.020 g, 0.29 mmol) at -78°C. Consecutive infrared spectra were recorded over 1 hr while stirring.

Reactivity of (Ni-1)Pd(CH$_3$)$_2$ with HS(C$_6$H$_4$)Me and CO.

To a flame-dried degassed Schlenk tube was added (**Ni-1**)$Pd(CH_3)_2$ (0.030 g, 0.070 mmol) under an N_2 atmosphere which was dissolved in 5 mL of CH_2Cl_2. To this solution was added $HS(C_6H_4)Me$ (0.01 g, 0.071 mmol) dissolved in 5 mL of CH_2Cl_2. The resulting solution was cooled to -78^{o}C and stirred for 1 hour. Carbon monoxide gas was sparged through the orange-red solution vigorously for 8 minutes and then consecutive infrared spectra were recorded over 2 h.

Reactivity of [(Ni-1)Pd(C(O)CH_3)(CO)]$^+$ with Acetyl Chloride.

[(**Ni-1**)Pd(C(O)CH_3)(CO)]$^+$ was synthesized as previously described in Chapter IV. The formation of the product was confirmed by infrared spectroscopy. To this solution was added approximately 0.085 mL of acetyl chloride *via* syringe at room temperature, and infrared spectra were recorded over time.

Addition of Acetyl Chloride to Ni-1.

The **Ni-1** (0.022 g, 0.076 mmol) was degassed under a N_2 atmosphere in a 25 mL Schlenk flask. The purple solid was then dissolved in 4 mL of CH_2Cl_2, and acetyl chloride (5.37 μL, 0.076 mmol) was added *via* syringe to yield a brown slurry immediately. The solution was stirred for 15 minutes and an infrared spectrum recorded. IR (CH_2Cl_2, υ(C=O, cm^{-1}) = 1689 cm^{-1}. Mass spectrum (CH_3CN solution) *m/z* (% abundance relative to base peak = 100%): 319 [H(bme-daco)-$(C(O)Me)_2$]$^+$, 100%.

EXPERIMENTAL DETAILS FOR CHAPTER VI

Materials

The CH_3CN, CH_2Cl_2, diethyl ether and hexane were purified according to published procedures under a N_2 atmosphere.[42] The CuBr source and Rh(CO)(PPh_3)(Cl) were purchased from Aldrich Chemical CO. and used as received. The **Ni-1*** and **Ni-1** ligands were synthesized according to published procedures.[44,47]

X-ray Structure Analysis.

X-ray data for all crystal structures were solved at the Crystal and Molecular Structure Laboratory Center for Chemical Characterization and Analysis at Texas A&M University. X-ray diffraction data and analyses were carried out by Dr. Matthew L. Miller or Dr. Joseph H. Reibenspies. Crystals were mounted on a glass fiber at room temperature for the experiment. X-ray data were obtained on a Bruker P4 diffractometer. The structures were solved by direct methods. Anisotropic displacement parameters were determined for all non-hydrogen atoms. Atoms which proved to be nonpositive definite in the $[Ni^{*}\text{-}1]_2(CuBr)_4$ were corrected by including the command ISOR with the "s" parameter set at 0.005 in the instruction file. Programs used for data collection and cell refinement were Brucker XSCANS; data reduction, SHELXTL;[53] structure solution, SHELXS-97 (Sheldrick);[54] structure refinement, SHELXL-97 (Sheldrick),[55] and molecular graphics and preparation of material for publication were SHELXTL-Plus, version 5.1 or later (Bruker).[56] A full list of bond lengths, bond angles can be found in the Supporting Information.

Synthesis of $(Ni\text{-}1^{*})_2(CuBr)_2$.

A sample of CuBr (0.080 g, 0.52 mmol) dissolved in 10 mL CH_3CN was added to a purple solution of **Ni-1*** (0.18 g, 0.52 mmol) dissolved in 20 mL CH_3CN under an N_2 atmosphere. The resulting brown solution was stirred for several hours and precipitated with 30 mL of ether to yield a brown solid. The solid was washed twice with 20 mL of ether and was dried under vacuum, 0.18 g (70%). X-ray quality crystals were obtained

by slow evaporation of ether into a CH_2Cl_2 solution of the product. Anal. Calcd (Found) for $C_{42}H_{85}N_6S_6Ni_3Cu_2Br_2$: C, 26.5 (26.3); H, 4.45 (4.45); N, 4.42 (4.05). UV-Vis in CH_3CN: λ_{max} (ε, M^{-1} cm^{-1}): 220 (43994), 252 (26727), 308 (7999.2), 592 (262.07) nm. Mass spectrum (CH_3CN/CH_2Cl_2 solution) *m/z* (% abundance relative to base peak = 100%): 901 $[(Ni\text{-}1^*)_2Cu_2Br]^+$ (100%), 411 $[(Ni\text{-}1^*)_2Cu_2]^{2+}$ (38%), 757 $[(Ni\text{-}1^*)_2Cu]^+$ (30%), 1045 $[(Ni\text{-}1^*)_2Cu_3Br_2]^+$ (10%).

Synthesis of $[(Ni\text{-}1^*)_3Cu_2][Br_2]$.

In an almost identical procedure as described above, a sample of CuBr (0.040 g, 0.26 mmol) dissolved in 10 mL CH_3CN was added to a purple solution of **Ni-1*** (0.14 g, 0.39 mmol) dissolved in 25 mL CH_3CN under an N_2 atmosphere. The resulting dark orange solution was stirred overnight at room temperature. Addition of 35 mL of ether yielded a brown solid which was dried under vacuum, 0.16 g (93%). X-ray quality crystals were obtained by slow evaporation of ether in a CH_2Cl_2 solution of the product. Anal. Calcd (Found) for ($[C_{42}H_{85}N_6S_6Ni_3Cu_2Br_2]\cdot 2CH_2Cl_2$): C, 34.6 (35.3); H, 6.25 (5.92); N, 5.62 (5.61). Included in the calculated elemental analysis are CH_2Cl_2 solvent molecules that were observed in the crystal packing. UV-Vis in CH_3CN: λ_{max} (ε, M^{-1} cm^{-1}): 220 (66657), 250 (44872), 306 (15612), 388 (3897), 572 (606.63) nm. Mass spectrum (CH_3CN/CH_2Cl_2 solution) *m/z* (% abundance relative to base peak = 100%): 901 $[(Ni\text{-}1^*)_2Cu_2Br]^+$ (100%), 757 $[(Ni\text{-}1^*)_2Cu]^+$ (99%), 411 $[(Ni\text{-}1^*)_2Cu_2]^{2+}$ (77%), 1045 $[(Ni\text{-}1^*)_2Cu_3Br_2]^+$ (11%).

Synthesis of $(Ni\text{-}1^*)_2(CuBr)_4$.

The **Ni-1*** (0.10 g, 0.29 mmol) complex was dissolved in 10 mL of CH_3CN, and to this a solution of CuBr (0.060 g, 0.43 mmol) dissolved in 5mL of CH_3CN was added. The resulting solution was stirred overnight, and a brown solid was precipitated upon the addition 20 mL of ether, 0.13 g (97%). X-ray quality crystals were obtained by slow diffusion of ether into a 50:50 MeCN/MeOH solution of the complex. Anal. Calcd (Found) for $C_{28}H_{56}N_4S_4Ni_2Cu_4Br_4$: C, 34.27 (34.86); H, 5.75 (5.95); N, 5.71 (5.31). UV-Vis in CH_3CN: λ_{max} (ε, M^{-1} cm^{-1}): 216 (46042), 252 (28529), 320 (9708.9), 334 (9603.3), 370 (7207.7) nm. Mass spectrum (CH_3CN/CH_2Cl_2 solution) *m/z* (% abundance relative to base peak = 100%): 1045 $[(Ni\text{-}1^*)_2Cu_3Br_2]^+$ (100%), 901 $[(Ni\text{-}1^*)_2Cu_2Br]^+$ (61%), 1186 $[(Ni\text{-}1^*)_2Cu_4Br]^+$ (38%).

Synthesis of $[(Ni\text{-}1)Rh(CO)(PPh_3)][Cl]$.

A degassed sample of $Rh(CO)(Cl)(PPh_3)_2$ (0.24 g, 0.34 mmol) in 40 mL of CH_2Cl_2 and to this yellow slurry a purple solution of **Ni-1** (0.10 g, 0.34 mmol) dissolved in 10 mL of CH_2Cl_2 was added dropwise. The resulting orange-red slurry was stirred overnight. The solvent was concentrated to about 10 mL, precipitated with 40 mL of pentane, and filtered through a sintered frit. The orange solid was washed twice with 25 mL of ether to remove PPh_3 and dried under vacuum, 0.14 g. (55%) of [(**Ni-1**)$Rh(CO)(PPh_3)$][Cl]. X-ray quality crystals were obtained by layering a CH_2Cl_2 solution of the product with hexane. Anal. Calcd (Found) for $C_{29}H_{35}N_2S_2OPClNiRh$: C, 48.4 (48.2); H, 4.90 (4.54); N, 3.89 (2.98). IR (CH_2Cl_2, υ(CO) cm^{-1}) = 1988 cm^{-1}. UV-

Vis in CH_2Cl_2 solution: λ_{max} (ε, M^{-1} cm^{-1}) 232 (26002), 254 (17552), 282 (15466), 358 (3030), 486 (515) nm. Mass spectrum (CH_3CN/CH_2Cl_2 solution) *m/z* (% abundance relative to base peak = 100%): 683 [(**Ni-1**)Rh(CO)(PPh_3)]$^+$, 100 %.

CHAPTER III

ESTABLISHING THE STERIC AND ELECTRONIC PARAMETER OF NiN_2S_2 COMPLEXES AS SULFUR DONORS OF METALLODITHIOLATE LIGANDS

INTRODUCTION

The chemistry performed by the ACS active site is related to well known organometallic chemistry which takes place at 16-electron square planar complexes, including a current industrial process which has a remarkably similar catalytic motif involving nickel or palladium ligated with diphosphines, diimines, and mixed donor bidentate ligands.[1-3] The CO/R migratory insertion that follows olefin binding to an acetyl-Ni^{II} or -Pd^{II} moiety is a key step in the homogeneous catalysis of CO/olefin copolymerization for production of polyketones.[1-3] As shown in Figure III-1, a metal-mediated C-C coupling via migratory insertion is the function of both the biological and the industrial catalysts.

---

*Reproduced in part with permission from "Characterization of Steric and Electronic Properties of NiN_2S_2 Complexes as S-donor Metallodithiolate Ligands" by Rampersad, M. V., 2005, *Journal of the American Chemical Society,* In Press, copyright 2005 American Chemical Society.

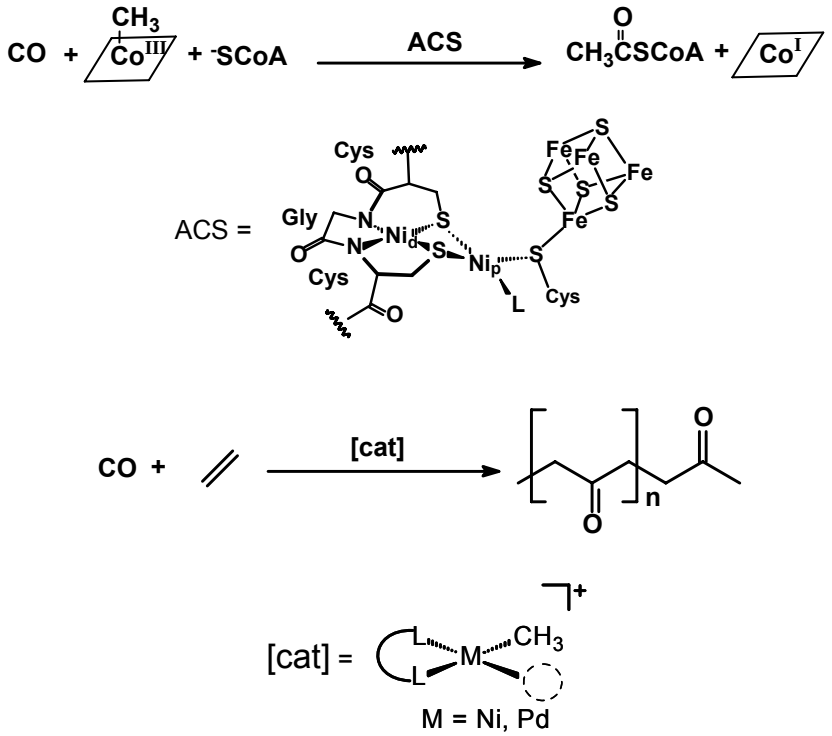

Figure III-1. Demonstration of C-C coupling in both biological and industrial systems.

The NiN_2S_2 complexes may be used as building blocks in the design of polymetallic complexes has been demonstrated for scores of compounds in numerous structural types.[24-31,33-40] The important reaction chemistry observed in the ACS active site pointed to the potential of the NiN_2S_2 complex as a ligand in classic organometallic chemistry (Chapter I).[23,33a,60] Hence, characterization of the intrinsic properties of this class of ligands is of interest.

Historically, the use of metal carbonyls as spectroscopic indicators of the electron-donating abilities of ancillary ligands has been highly successful in the development of homogeneous catalysts. Indeed, the vocabulary of organometallic chemistry that describes electronic and steric characteristics of ligands has its basis in the well known

Tolman parameters.[4] While other approaches and definitions have been put forth over the years,[5-7] those of Tolman, originally developed for monodentate phosphorus-donor ligands in combination with the 16-electron $Ni^0(CO)_3$ as acceptor, remain as the simplest and most widely used (Chapter I). The donor properties of bidentate ligands have been studied by infrared spectroscopy as well as ultraviolet photoelectron spectroscopy (UPS).[61,62] In fact, the validity of the use of CO stretching frequencies as measures of ligand basicity or donor ability has been challenged by results from photoelectron spectra of a series of (P-P)$W(CO)_4$ complexes in which Me and Ph substituents on the P-donors of diphosphines were systematically varied.[61] Nevertheless the ν(CO) frequency values continue to be a reference point for comparisons for classical ligands such as diphosphines, diamines, or diimines.

Several examples of $(NiN_2S_2)M(CO)_x$ complexes have been reported (Figure III-2).[31,41,36,37,63,64,65] From the CO stretching frequencies of a 2,3-pentanedione-bis(β-mercaptoethylimino)nickel-$Mo(CO)_4$ complex, Kang and coworkers concluded that the NiN_2S_2 metallodithiolate ligand was a better donor than phosphines and thioethers and similar to bipyridine.[41] Our own work with various complexes of the NiN_2S_2 metallothiolate ligand, (bme-daco)Ni, **Ni-1**, including [**Ni-1**]$Fe^0(CO)_4$, [**Ni-1**]$_2Fe^{II}(CO)_2^{2+}$, and [**Ni-1**]$Mo^0(CO)_4$ complexes, [31,64] concurred with the kang *et al*., study, and established the nickel thiolate was only slightly poorer than the free, anionic thiolate as an electron donor. In more recent efforts to synthesize model complexes for the [NiFe] hydrogenase enzyme active site, Reynolds *et al.* concluded that the NiN_2S_2 metallothiolate ligands in $[Cp^*Ru(NiN_2S_2)(CO)]^+$ are better electron donors to Ru^{II} than

two monodentate PMe_3 ligands in $[Cp^*Ru(PMe_3)_2(CO)]^+$ or the bidentate diphosphine, $Ph_2PCH_2CH_2PPh_2$, in $[Cp^*Ru(dppe)(CO)]^+$.[37] Other studies by Rauchfuss and co-workers and by Riordan and coworkers established that dianionic N_2S_2Ni complexes containing carboxamido nitrogens within the N_2S_2 donor environment formed dinickel complexes in which the adjacent nickel was Ni^0 in mimicry of a possible redox level in the ACS active site.[36,38] While such isolated reports provide a guide for expectations and design of complexes based on the metallo-ligands, the serial approach found herein broadly establishes ligating properties, including both electronic and steric properties, so that they may be generally applicable. Our study also points to the hemilability of such NiN_2S_2 ligands, a characteristic computed to be of note in the mechanism of the ACS enzyme.[23]

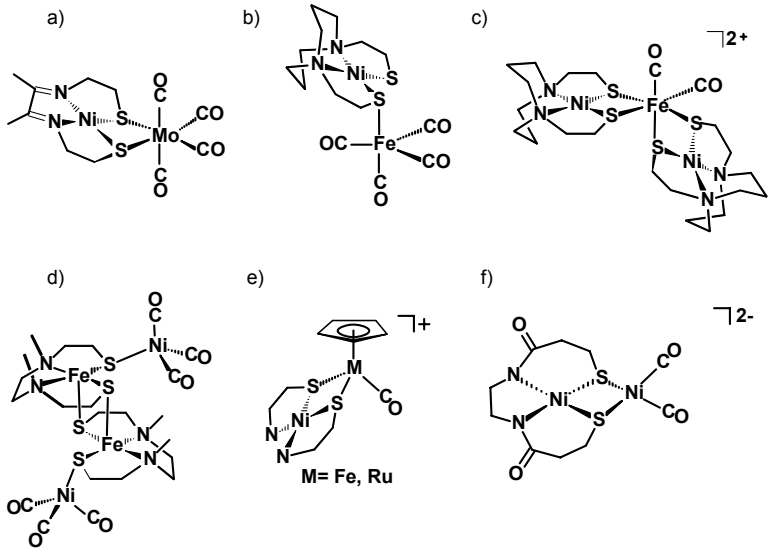

Figure III-2. Representation of $NiN_2S_2M(CO)_x$ complexes, **a)[41], b)[31], c)[64], d)[65], e)[36], f).[37]**

Reported in this chapter is the synthesis of several $W(CO)_4$ derivatives of bidentate NiN_2S_2 complexes; and their IR spectra were recorded in the ν(CO) region. X-ray crystallographic analyses detail the unique spatial characteristics of a series of NiN_2S_2 complexes as ligands to $W(CO)_4$. Carbon-13 NMR spectroscopic studies and electrochemical characterizations are also reported for the series.

RESULTS AND DISCUSSION

Study of Electron Donating Ability by Infrared Spectroscopy

The NiN_2S_2 metallothiolate ligands selected for this study are comprised of a square planar nickel within a N_2S_2 donor set; variations in structures arise from several features (Figure III-3). The diazacyclooctane derivatives **Ni-1** and **Ni-1*** have S-Ni-S ligand angles that are ca. 90°. The **Ni-1´**, based on diazacycloheptane framework, and the open-chain ligand derivative **Ni(bmmp-dmed)** have greater S-Ni-S ligand angles of 95°, resulting from a pinched N-Ni-N angle in both. The **Ni-1*** and **Ni(bmmp-dmed)** compounds possess gem dimethyl groups on the carbon α to the sulfur donor that should provide differences in steric and electron-donating properties of the thiolate sulfur. The **Ni(bme-Me_2PDA)** is a neutral ligand that has a S-Ni-S angle less than 90°. Finally, the dianionic **$[Ni(ema)]^{2-}$** has the largest S-Ni-S ligand angle of 97° and, obviously, the chief capability for donation due to its charge. This last metallodithiolate ligand also bears the closest resemblance to the NiN_2S_2 moiety in the ACS active site.

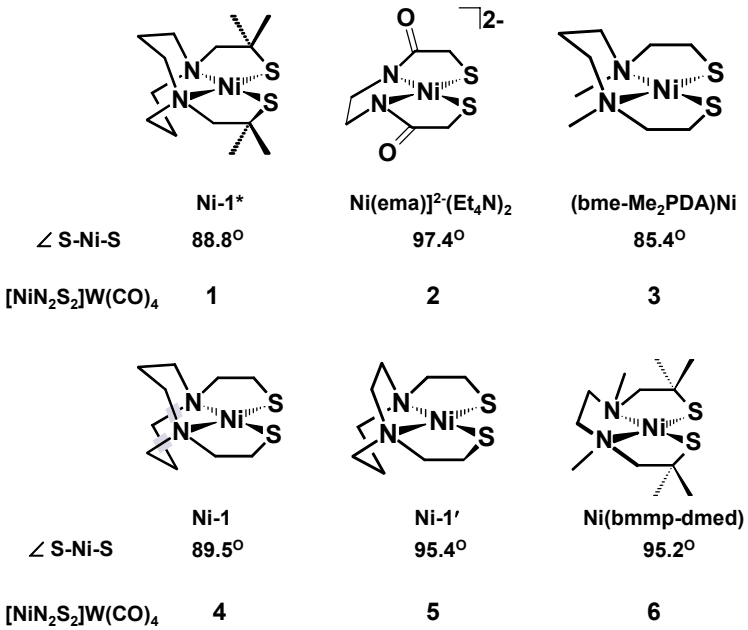

Figure III-3. NiN_2S_2 ligand series, abbreviations, $\angle_{S\text{-}Ni\text{-}S}$ angles, and designations for $W(CO)_4$ derivatives.

The $NiN_2S_2W(CO)_4$ derivatives were synthesized according to the labile-ligand or ligand displacement approach, Figure III-4; simple addition of the NiN_2S_2 complex to the $W(CO)_4(pip)_2$ produced the $NiN_2S_2W(CO)_4$ products which were isolated as crystalline materials, typically in ≥ 60% yields. Complex **4** in this study was prepared and structurally characterized by a fellow a graduate student Stephen P. Jeffery.

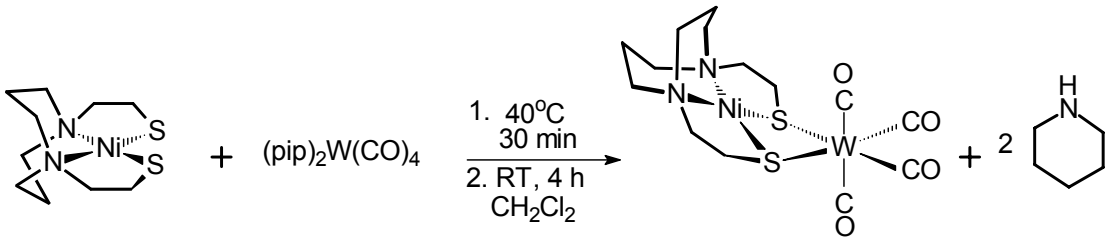

Figure III-4. A method for synthesis for $NiN_2S_2W(CO)_4$.

Due to poor solubility in preferred non-polar solvents, the ν(CO) stretching frequencies for the *cis*-$L_2M(CO)_4$ complexes were measured in DMF. Although this solvent broadens the absorptions, peak maxima selected at ± 3 or 4 wavenumbers produced little differences in the computed Cotton-Kraihanzel (C-K) force constants which were done in collaboration with a fellow graduate student, Dr. Melissa L. Golden.[66] The ν(CO) values and the respective C-K force constants are reported in Table III-1; for comparison, other *cis*-$L_2M(CO)_4$ (L = diphosphine, bipyridine; M = Mo) were prepared and their ν(CO) stretching frequencies also recorded in DMF.

Representative infrared spectra in the ν(CO) region (Figure III-5) display the four absorption bands that are expected for *cis*-$L_2M(CO)_4$ complexes of idealized C_{2v} symmetry, assigned to the two A_1, B_1 and B_2 vibrational modes. It should be noted that the C_{2v} symmetry designation only holds for the immediate $S_2(CO)_4$ donor environment about W; the significant asymmetry deriving from the hinge of the NiN_2S_2 ligand reduces the symmetry to C_S. Assuming C_{2v} symmetry, the CO stretching vibrational mode assignments are according to that of Cotton and Kraihanzel. A_1^1 corresponds to the band with the highest stretching frequency; B_1 has the greatest intensity with a

shoulder or tail corresponding to A_1^2; and the band of lowest frequency corresponds to B_2.[66] In the alternate approach, based on C_S symmetry, the $W(CO)_4$ unit would similarly exhibit four vibrational frequencies of symmetry 3A' + A". In the absence of stereoselectively ^{13}CO labeled species, it is not possible to unequivocally calculate individual force constants for the two different axial CO ligands. Hence, in treating the $W(CO)_4$ moiety as C_{2v} symmetry, an average axial CO force constant, k_2, was calculated. The differentiation of axial CO groups will be addressed in a discussion of the temperature dependent ^{13}C NMR data observed for these complexes, *vide infra*.

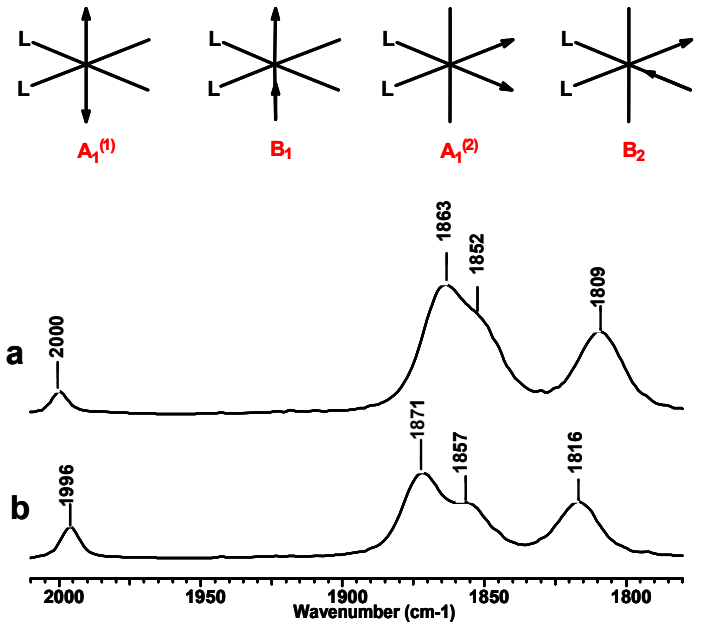

Figure III-5. Comparison of ν(CO) infrared spectra of a) $W(CO)_4(pip)_2$ and b) **(Ni-1*)**$W(CO)_4$.

These are the lowest values of any compounds listed in Table III-1. The neutral NiN_2S_2 sulfur donors result in CO stretching frequencies and force constants of $W(CO)_4$

units that are most like the di-piperidine substituted analogues; they are much better donors than diphosphines.

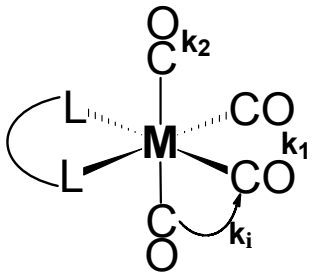

Table III-1. CO Stretching Frequencies (cm^{-1})[a] and Calculated Force Constants (mdyn/Å)[b]

Compound		$\nu(A_1^1)$	$\nu(B_1)$	$\nu(A_1^2)$	$\nu(B_2)$	k_1	k_2	k_i
Ni(bmmp-dmed)W(CO)$_4$	**6**	1998	1878	1854	1821	13.77	15.00	0.38
(Ni-1*)W(CO)$_4$	**1**	1996	1871	1857	1816	13.74	14.99	0.43
(Ni-1´)W(CO)$_4$	**5**	1996	1873	1852	1817	13.74	14.98	0.41
(Ni-1)W(CO)$_4$	**4**	1995	1871	1853	1819	13.77	14.95	0.41
Ni(bme-Me_2PDA)W(CO)$_4$	**3**	1993	1876	1853	1826	13.81	14.91	0.35
[(Ni(ema))W(CO)$_4$]$^{2-}$ ($Et_4N)_2$	**2**	1986	1853	1837	1791	13.41	14.77	0.46
(Ni-1*)Mo(CO)$_4$	**8**	2002	1885	1863	1821	13.80	15.17	0.41
(Ni-1´)Mo(CO)$_4$	**9**	2002	1886	1851	1824	13.81	15.10	0.37
(Ni-1)Mo(CO)$_4$	**10**	2002	1885	1861	1824	13.85	15.13	0.40
(dppm)W(CO)$_4$[c]	**11**	2016	1906	1906	1870	14.50	15.43	0.38
(dppe)W(CO)$_4$[d]	**12**	2015	1900	1900	1870	14.50	15.34	0.38
(dmpm)W(CO)$_4$[e]	**13**	2007	1885	1885	1863	14.39	15.10	0.38
(pip)$_2$W(CO)$_4$[f]	**14**	2000	1863	1852	1809	13.68	14.94	0.46
(bipy)W(CO)$_4$[g]	**15**	2006	1886	1870	1830	13.94	15.19	0.41

[a] IR spectra were recorded in DMF. [b]The convention of modes and the calculated force constants follow that of ref 66. Abbreviations: [c](dppm = bis(diphenylphosphino)methane, [d](dppe = bis(diphenylphosphino)ethane, [e](dmpm = bis(dimethylphosphino)methane, [f](pip = piperidine), and [g](bipy = bipyridine).

Based on electrochemical results ($Ni^{II/I}$ reduction couples) the complex **Ni-1*** with gem dimethyl groups on the carbon α to the sulfur is more electron rich than is **Ni-1**.[67] Nevertheless, using the ν(CO) IR data in Table III-1 as a criterion for donor ability the two metallodithiolate ligands are indistinguishable. A reasonable conclusion is that the

steric hindrance at sulfur prevents optimal close contact of the S-donor site of **Ni-1*** to the tungsten. Such arguments have been made for sterically bulky phosphine ligands in which the spatial requirements of the phosphines impinge on the innate electron-donating ability of the P-donor site, hence obviating a separation of steric and electronic parameters.[61]

Structural Characterization of $NiN_2S_2W(CO)_4$ Complexes

As determined by x-ray diffraction analysis, the molecular structures of complexes, **4-6**, are shown in Figure III-6, adding to the analogous $(NiN_2S_2)W(CO)_4$ complexes **1-3** which were previously reported.[68] Crystallographic data for complexes **4-7** are given in Table III-2. Selected metric data for complexes **1-6** are listed in Table III-3 along with that of the free metallothiolate ligands for comparison. The molecular structure of the monodentate $(NiN_2S_2)W(CO)_5$ complex **7** is given in the figure on page 50 and a selection of distances and angles are given in the figure caption. A full list of bond lengths, bond angles and anisotropic displacement coefficients for complexes **4 - 7** are in the supporting information. X-ray diffraction studies of complexes **3-5** were carried out by a graduate student colleague Stephen P. Jeffery. Ball-and-stick representations for complexes **1-6** are shown in Figure III-8 on page 47 for comparison.

Table III-2. Crystallographic Data for Complexes **4-7**.

	4	**5**	**6**	**7**
Formula	$C_{14}H_{20}N_2NiO_4S_2W$	$C_{13}H_{18}N_2NiO_4S_2W$	$C_{17}H_{28}Cl_2N_2NiO_4S_2W$	$C_{15}H_{20}N_2NiO_5S_2W$
Formula Weight	587.00	572.97	701.99	615.05
Temperature (K)	110(2)	110(2)	110(2)	110(2)
Wavelength (Å)	0.71073	0.71073	0.71073	0.71073
Z	4	4	8	4
D_{calcd} (Mg/cm^3)	2.135	2.247	1.940	2.067
μ (mm^{-1})	7.573	8.162	5.987	7.007
Crystal System	Orthorhombic	Orthorhombic	Orthorhombic	Monoclinic
Space Group	Pnma	Pnma	Pbca	$P2_1/n$
Unit Cell				
a(Å)	13.397(4)	12.721(5)	18.325(11)	7.2847(12)
b(Å)	12.386(4)	12.151(5)	12.748(7)	13.392(2)
c(Å)	11.005(3)	10.959(4)	20.575(12)	20.266(3)
β(°)	90	90	90	92
Volume ($Å^3$)	1826.2(10)	1693.8(11)	4806.5(5)	1976.3(6)
Goodness-of-fit	1.144	1.164	0.992	0.929
R_1[a], wR_2[b](%) [I>2σ(I)]	0.0279, 0.0603	0.0719, 0.1781	0.0490, 0.1078	0.0626, 0.1403
R_1[a], wR_2[b](%) all data	0.0271, 0.0598	0.0800, 0.1842	0.0701, 0.1151	0.1004, 0.1558

[a] $R_1 = \Sigma \big| |F_o| - |F_c| \big| / \Sigma F_o$. [c] $wR_2 = [\Sigma[w(F_o^2 - F^{c2})^2] / \Sigma w(F_o^2)^2]^{½}$.

Table III-3: Selected Bond Distances and Bond Angles of Complexes **1-6.**

	1	**Ni-1*** ref. 44	**2**	**[Ni(ema)]$^{2-}$** ref. 45	**3**	**Ni(bme-Me$_2$PDA)** ref. 46	**4**	**Ni-1** ref. 47	**5**	**Ni-1'** ref. 48	**6**	**Ni(bmmp-dmed)** ref. 49
Ni-W	3.389		2.928		3.033		3.35		3.249		3.021	
Ni-C(1)	3.726		2.954		2.856		3.561		3.388		3.24	
W-C(1)	2.001(14)		1.978(13)		2.023(13)		2.023(15)		2.03(4)		2.052(9)	
W-C(2)	2.037(12)		2.042(12)		2.057(12)		2.047(11)		2.03(8)		2.040(9)	
W-C(3)	1.951(10)		1.939(12)		1.952(8)		1.957(6)		1.96(15)		1.970(9)	
W-C(4)	1.951(10)		1.937(12)		1.952(8)		1.957(6)		1.96(15)		1.944(9)	
W-S$^a_{avg}$	2.589(3)		2.616(3)		2.591(2)		2.5792(14)		2.6(2)		2.621(2)	
Ni-S$^a_{avg}$	2.170(3)	2.152(1)	2.172(3)	2.179(1)	2.190(2)	2.175(1)	2.1893(15)	2.159(3)	2.17(16)	2.164(1)	2.155(2)	2.153(10)
Ni-N$^a_{avg}$	1.986(8)	1.995(3)	1.855(8)	1.857(3)	1.995(6)	2.005(3)	1.974(5)	1.979(7)	1.93(14)	1.940(4)	1.994(7)	1.940(3)
C(1)-W-C(2)	165.5(5)		176.5(5)		170.0(4)		172.4(3)		172.6(10)		165.5(3)	
C(3)-W-C(4)	91.3(6)		90.8(5)		89.9(4)		90.7(3)		91(9)		91.3(4)	
W-C(1)-O(1)	171.5(13)		173.4(11)		172.9(9)		171.7(7)		174.7(11)		173.8(8)	
W-C(2)-O(2)	173.3(12)		179.3(11)		170.8(8)		175.5(8)		174.9(10)		178.8(8)	
S(1)-W-S(2)	70.92(12)		75.06(9)		68.75(9)		72.08(6)		75(8)		71.16(6)	
S(1)-Ni-S(2)	87.62(15)	88.8(1)	94.42(11)	97.44(8)	83.83(11)	85.37(4)	87.76(8)	89.4(1)	92(9)	95.4(1)	91.49(9)	95.16(4)
N(1)-Ni-N(2)	92.2(5)	90.4(1)	86.04(4)	85.6(2)	98.3(4)	97.3(1)	91.5(3)	89.3(4)	83(7)	82.5(2)	89.8(3)	88.11(12)
Dihedral[b]	135.9		107		106.8		132.5		127.5		114.4	

[a] Averaged bond distances and estimated standard deviations given in parentheses. [b]Angle between best planes of NiN_2S_2 and $S_2W(CO)_2$.

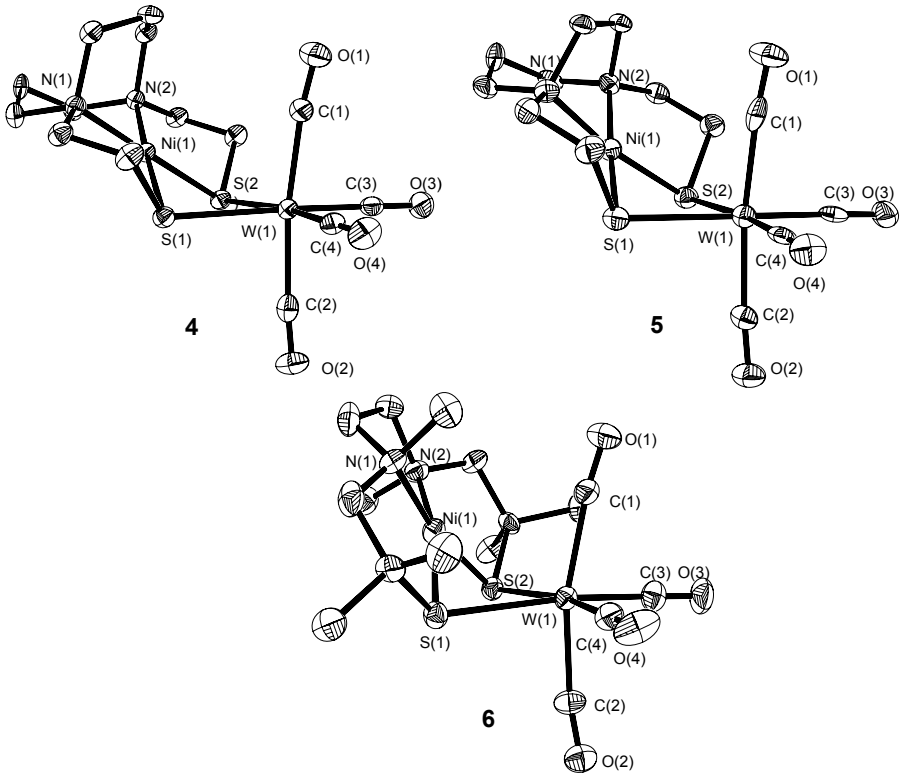

Figure III-6. Thermal ellipsoid plots (50% probability) of the molecular structures for complexes **4 - 6** with select atoms labeled and hydrogen atoms omitted.

A common characteristic of the $(NiN_2S_2)W(CO)_4$ structures is that the ca. square planar NiN_2S_2 complexes bind as bidentate, S-donor ligands to W^0, largely maintaining the structural features of the parent NiN_2S_2 complex with only minor deviations in metric parameters. In the case of $Ni(ema)^=$ however, the substantially planar structure changes into one with a Td twist of 8.6° on binding to $W(CO)_4$, while the Ni-1' distorts even more from planar (Td twist of only 2.1°) to a Td twist of 11.1° in the $(Ni\text{-}1')W(CO)_4$ complex. Interestingly, the NiN_2S_2 parent (free) ligand of complex **6** has a Td twist of 14.4° and has only a minor distortion to 16.5° on binding to $W(CO)_4$.

A second notable feature of the $(NiN_2S_2)W(CO)_4$ structures is that the NiN_2S_2 plane in each case connects into the $S_2W(CO)_2$ plane of the pseudo-octahedral tungsten complex with a hinge at the sulfurs. This hinge, a consequence of the directionality of the sulfur lone pairs, is the hallmark of a majority of thiolate bridged dinuclear compounds typically referred to as butterfly complexes; it is presumably a consequence of the directionality of the sulfur lone pairs. Rotation of the structural representation used that focuses on the octahedral geometry of the $S_2W(CO)_4$ coordination sphere into a form that better displays the butterfly character of the complexes, Figure III-7, illustrates the difference in chemical environment of the two CO groups that are mutually cis to the S-donors and trans to each other. In fact, the CO that is under the Ni----W vector is ideally situated to be in a semi-bridging position. That it is strictly terminal is evident by the Ni-C(1) distances in the series of six complexes, which range from 2.85 – 3.72 Å, and are beyond bonding. The shorter of these actually are within the sum of Ni + C van der Waals radii (1.63 + 1.77 = 3.33 Å), suggesting the possibility of at least some orbital overlap. While there is no indication from ν(CO) infrared data of a low frequency CO that might indicate bridging character, NMR spectroscopic studies described below find two distinct resonances for the mutually trans CO carbons.

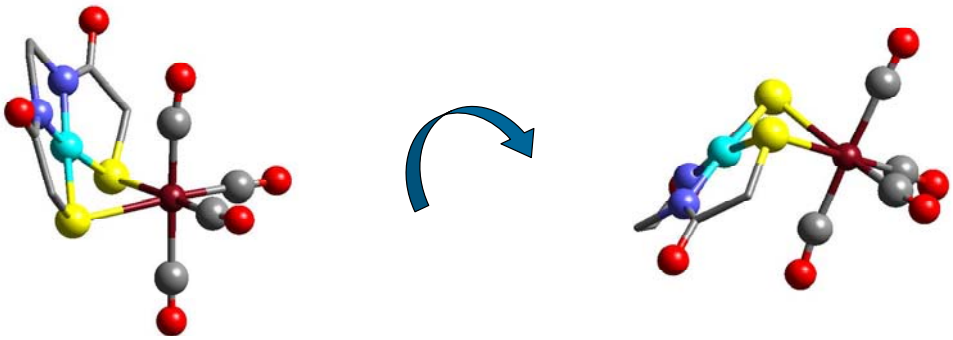

Figure III-7. The butterfly core defined by the $(\mu\text{-SR})_2$ bridge in complex **2**.[68]

The Ni---W distance range, 2.92 – 3.39 Å, is also beyond bonding; individual values largely correlate with the dihedral angle (d.a.) made by the intersecting NiN_2S_2 and WC_2S_2 planes which cover a range of 107 to 136°. Inspection of the crystal packing diagrams and metric analysis find that, in general, the closest intermolecular non-bonding contacts, in the range of 3.08 to 3.2 Å, are related to carbonyl oxygen orientations towards each other between layers of the neutral complexes. In the $[NEt_4]_2$[**Ni(ema)**$W(CO)_4$] salt, tetraethyl ammonium cations intersperse between rows comprised of pairings of interdigitated anions. We conclude that the values of the dihedral angles in the series of complexes are only influenced by intramolecular electronic and steric interactions.

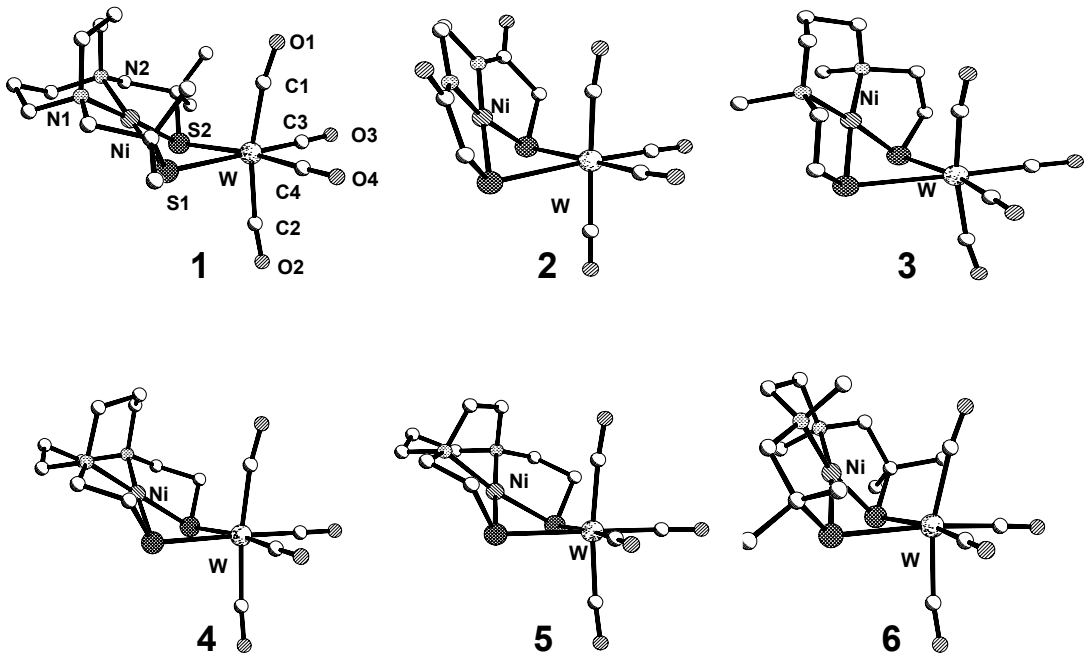

Figure III-8. Ball-and-stick representations of compounds **1-6** on which x-ray crystallographic studies were performed.

Analysis of the differences in dihedral plane values benefits from comparisons of pairs of complexes in the series of six compounds. While the complexes with gem dimethyl groups on the carbon α to sulfur are expected to have the greatest spatial requirement within the $W(CO)_4S_2$ coordination sphere, in fact complex **1** with d.a. = 135.6° realizes this prediction and complex **6** does not (d.a. = 114°). Inspection of the structures of complexes **1** and **6** finds a distinct difference in the orientation of the gem-dimethyl groups in the two complexes, Figure III-9. Whereas in complex **1** two of the C_α-CH_3 vectors from each of the α-carbons are parallel and pointed in the vicinity of the W-C(1) bond vector, the open chain framework of complex 6 allows the analogous methyl groups to be splayed and oriented outwardly from the Ni(μ-SR)$_2$W unit, offering

little steric hindrance towards the $W(CO)_4$ unit. Thus in the solid state at least, the steric encumbrance of the diazacycle-containing complex **1** is much greater than that of the open-chain complex **6**.

Complexes **4** and **5** also have large dihedral angles compared to other members of the series. In both cases the C-C unit that links S to N are eclipsed across the NiN_2S_2 plane. The pucker in the 5-membered $NiSC_2N$ rings displaces the C that is α to S in each case towards the W-C(1) bond vector, imposing steric hindrance from the H atoms of the α-CH_2 groups in **4** and **5** that is nearly as great as the methyl substituent of complex **1**.

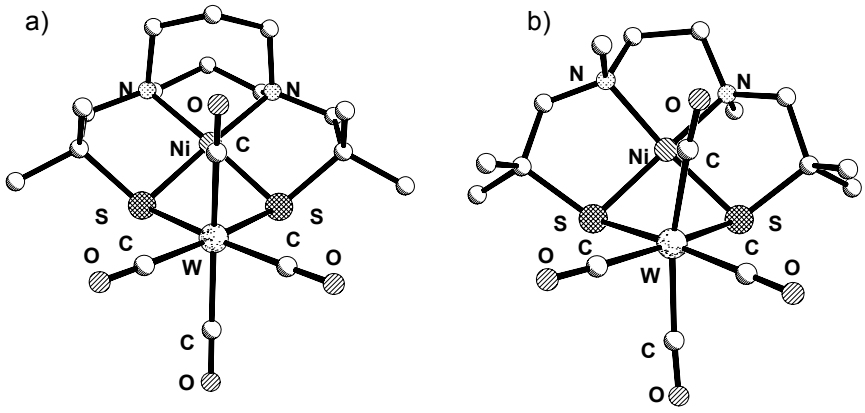

Figure III-9. Ball-and stick representations of alternate views for a) [(**Ni-1***)$W(CO)_4$] and b) [(**Ni(bmmp-dmed**)$W(CO)_4$], complexes **1** and **6**, with focus on the orientation of the gem-dimethyl groups of the carbons α to the S-donor atoms—the origin of the steric difference in the two molecules as displayed in the NiN_2S_2/WS_2C_2 dihedral or hinge angles: 136° for the former and 114° for the latter.

Complexes **2** and **3** have the smallest dihedral angles, 107°. The nearly flat character of the carboxamido N to S linkers accounts for the small steric requirement of complex **2**. The open-chain SNNS ligand of **3** finds the CH_2-CH_2 units connecting N to S eclipsed across the N_2S_2Ni plane, however unlike complexes **4** and **5**, both carbons α to S in the $NiSC_2N$ 5-membered rings are oriented down and away from the W-C(1) region. Hence there is no obvious steric hindrance from the hydrogen atoms on that carbon.

There is no apparent correlation of dihedral or hinge angle with other metric data of the complexes such as the S-W-S bite angle or W-S distances. The former ranges from 69 to 75° deriving from S-Ni-S angles of 83 to 98°. In all members of this series, the S-Ni-S angle decreases (by 1 to 4°) upon binding of the NiN_2S_2 ligand to tungsten, forming the $W(CO)_4$ derivatives, Table III-3.

Minor differences in metric data exist in the Ni-S distances in members of the series of Ni-W bimetallics as compared to the free NiN_2S_2 ligands, see Table III-3. Taken individually, these differences would not be statistically significant. From the series however, the consistent observation of a slight increase in Ni-S bond length upon complexation to W, along with a concomitant decrease in Ni-N bond length from that of the precursor NiN_2S_2, is convincing evidence of change, presumably a decrease, in Ni-S bond character in the heterobimetallics. A different result is observed for the **Ni(ema)**$^{2-}$ metallodithiolate ligand. The Ni-S as well as the Ni-N distances slightly decrease (or remain the same) on binding to W. The greater Ni(d_π)-S(p_π) antibonding interaction in the dianionic complex and its partial relief on binding to tungsten could account for

enhanced bonding in the Ni-W complex. The W-S bond distance in the **Ni(ema)**$W(CO)_4^{2-}$ complex **2**, of 2.616 Å is, however, within the range of that of the neutral compounds, 2.58 to 2.62 Å.

Crystals of complex **7** were obtained inadvertently during crystallization attempts for complex **4**. Complex **7** was subsequently prepared by the labile ligand approach from the $W(CO)_5(THF)$ adduct. Views of its molecular structure are given in Figure III-10. The square planar NiN_2S_2 complex is again largely unchanged from that of the parent free ligand (least-squares plane deviation of Ni, N, and S = 0.0698 Å) and the thiolate pendant arms are in the eclipsed position. The mono-dentate binding of the **Ni-1** unit to W produces a long Ni-W metal distance of 3.89 Å, resulting from a W-S-Ni angle of 109.8°. At 2.176 Å the Ni-S(1) distance for the tungsten-bound thiolate of **7** is .01 Å larger than that of the unbound Ni-S(2), 2.164 Å.

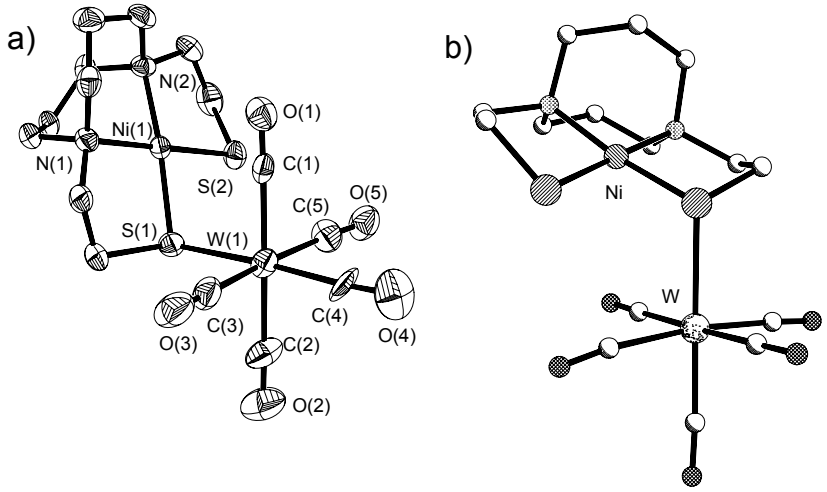

Figure III-10. Two views of the molecular structures of complex **7**, [(**Ni-1**)W(CO)$_5$]: **a**) thermal ellipsoid plot (50% probability) with atom labels and hydrogen atoms omitted, and **b**) ball-and-stick drawing. Selected averaged distances (Å) and angles (deg): Ni-S(1), 2.176(3); Ni-S(2), 2.164(3); W-S(1), 2.577(3); Ni-N$_{avg}$, 1.985(8); Ni···W, 3.894; S-Ni-S, 88.5(11); N-Ni-N, 89.5(3); W-C(1)-O(1), 178.3(9), W-C(2)-O(2), 177.5(12); W-C(4)-O(4), 176.5(11); W-C(5)-O(5), 172.6(11); Ni-S(1)-W, 109.8(11).

Within the **Ni-1** unit of complex **7** both Ni-S bond distances are increased as compared to those for the free **Ni-1** ligand (2.159 Å). Both are shorter than the Ni-S$_{avg}$ = 2.189 Å observed in the (**Ni-1**)W(CO)$_4$ complex. The W-S$_{avg}$ distance of (**Ni-1**)W(CO)$_4$, 2.579 Å, is the same as in (**Ni-1**)W(CO)$_5$, 2.577 Å. Only one W-C-O linkage deviates significantly from linearity (172.6°) and it is that closest to the unbound thiolate. Nevertheless the S(2) – C(5) and S(2) – O(5) distances of 3.485 and 3.331, respectively are beyond bonding interactions.

^{13}CO NMR Spectroscopy.

The ^{13}C NMR spectra of complexes **1** through **5**, recorded at room temperature, 22°C, in DMF solvent on both natural abundance and randomly enriched C-13 samples, display three signals in the M-CO region of the spectrum in approximately 2:1:1 intensity ratio; as example, the spectrum of complex **4** is shown in Figure III-11.

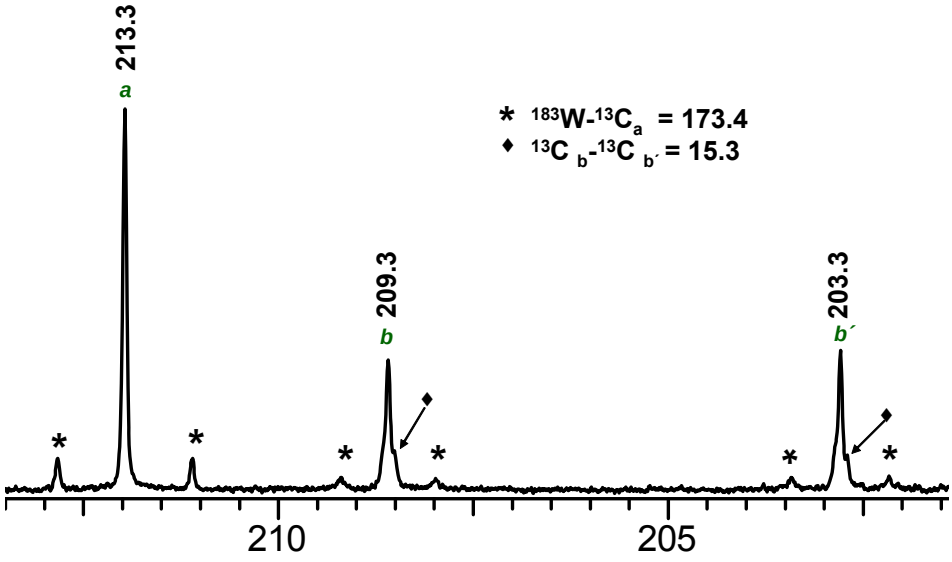

Figure III-11. ^{13}C NMR spectrum of [(**Ni-1**)W(CO)$_4$] in DMF at 22°C in the low-field CO region. *Asterisks indicate ^{183}W satellites and ♦ indicate ^{13}C-^{13}C coupling. Assignments refer to structure shown in Table III-4.

Chemical shifts for all complexes are listed in Table III-4. The most intense resonance is assigned to the equivalent CO groups mutually trans to the S-donors of the NiN_2S_2 ligands and mutually cis to each other, labeled **a** and **a'** in Table III-4. Note that only for the highly unsymmetrical complex **6** are both **a** and **a'** distinct; in all others **a** = **a'**,

consistent with the mirror plane in the solid state structures of all except complex **6**. The non-equivalence of the carbonyls labeled **b** and **b'** is imposed by the orientation of the NiN_2S_2 ligand. The assignment of **b** and **b'** to specific resonances is not straightforward. From the dependence of C-13 chemical shifts of metal-bound carbonyls on electron density displaced onto the carbons, that carbon responsible for the resonance nearest to the position of the **a/a'** carbonyl carbon is the more electron-rich. Whether this CO is closest in proximity to the NiN_2S_2 plane, or opposite, in closer proximity to the remaining lone pairs on S, is, at this time, not known.

The CO-carbon resonances in the carbon-13 enriched samples have satellites that derive from ^{183}W-^{13}C and ^{13}C -^{13}C coupling, see Figure III-11 and Table III-4. The coupling constants for the CO ligands trans to the thiolate donors, $J(^{183}W\text{-}^{13}C)_{trans\text{-}COa}$, are on the order of 170 Hz; they are larger than the coupling constants for the non-equivalent CO ligands cis to the thiolate donors: $J(^{183}W\text{-}^{13}C)_{cis\text{-}COb}$ = 130 Hz and $J(^{183}W\text{-}^{13}C)_{cis\text{-}COb'}$ = 128 Hz, respectively.[69]

Table III-4. ^{13}C NMR Data, 22ºC in DMF Solution Except Where Noted, for the Carbonyl Carbons in $[(NiN_2S_2)W(CO)_4]$ Complexes with the CO Designations.

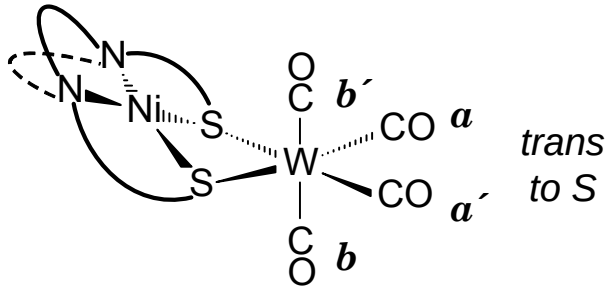

		^{13}C Resonance, ppm			
Ligand	**Complex**	**CO (trans to S)**		**CO (cis to S)**	
		a	***a´***	***b***	***b´***
Ni-1*	**1**[a]	212.2 ^{183}W-$^{13}C_a$ (172.0)		212.0 ^{183}W-$^{13}C_b$(129.7) $^{13}C_b$-$^{13}C_{b'}$(15.1)	202.8 ^{183}W-$^{13}C_{b'}$(127.7) $^{13}C_b$-$^{13}C_{b'}$(15.1)
Ni(ema)$^{2-}$	**2**[b]	216.7		209.1	207.1
Ni(bme-Me$_2$PDA	**3**	213.4		210.1	204.2
Ni-1	**4**	213.3 ^{183}W-$^{13}C_a$ (173.4)		209.3 ^{183}W-$^{13}C_b$(123.2) $^{13}C_b$-$^{13}C_{b'}$(15.3)	203.3 ^{183}W-$^{13}C_{b'}$(127.5) $^{13}C_b$-$^{13}C_{b'}$(15.3)
Ni-1´	**5**[a]	211.7		208.4	203.8
Ni(bmmp-dmed)	**6**	213.5	211.7	210.1	202.8

[a] ^{183}W-^{13}C and ^{13}C-^{13}C coupling measured on ^{13}C enriched compounds. [b] CD_3CN.

Variable-Temperature (VT) ^{13}C NMR Studies of [$(NiN_2S_2)W(CO)_{4-n}(^{13}CO)_n$].

In order to determine the extent of CO site exchange in the $W(CO)_4$ unit, particularly whether the CO's labeled **b** and **b'** might undergo rapid interconversion of sites, the temperature dependence of C-13 NMR spectra of selected complexes in the $(NiN_2S_2)W(CO)_4$ series were recorded on samples dissolved in DMF randomly enriched in ^{13}CO. Displayed in Figure III-12 are the spectra of [(**Ni-1***)$W(CO)_{4-n}(^{13}CO)_n$] measured over the range of 22 to 90 °C. The three characteristic resonances described above for complex **1** are seen in the 22 °C spectrum. The more intense resonance which is assigned to the equivalent CO ligands trans to the thiolate donors, **a**, retains a narrow peak width over the temperature range. The resonances assigned to the non-equivalent CO ligands, **b** and **b'**, are sharp at 22 °C, they broaden as the temperature is raised, and they coalesce into the baseline at 90 ^{o}C. At the high temperature limit of our experiment, 120 °C, there is evidence within the significant noise of the background at higher temperatures of the appearance of the site-averaged **b** + **b'** signal at 208.4 ppm. On cooling the sample, the resonances of **b** and **b'** reappear. Hence we conclude that the observed CO site equilibration is a reversible phenomenon and is limited in this temperature range to the CO groups that are trans to one another.

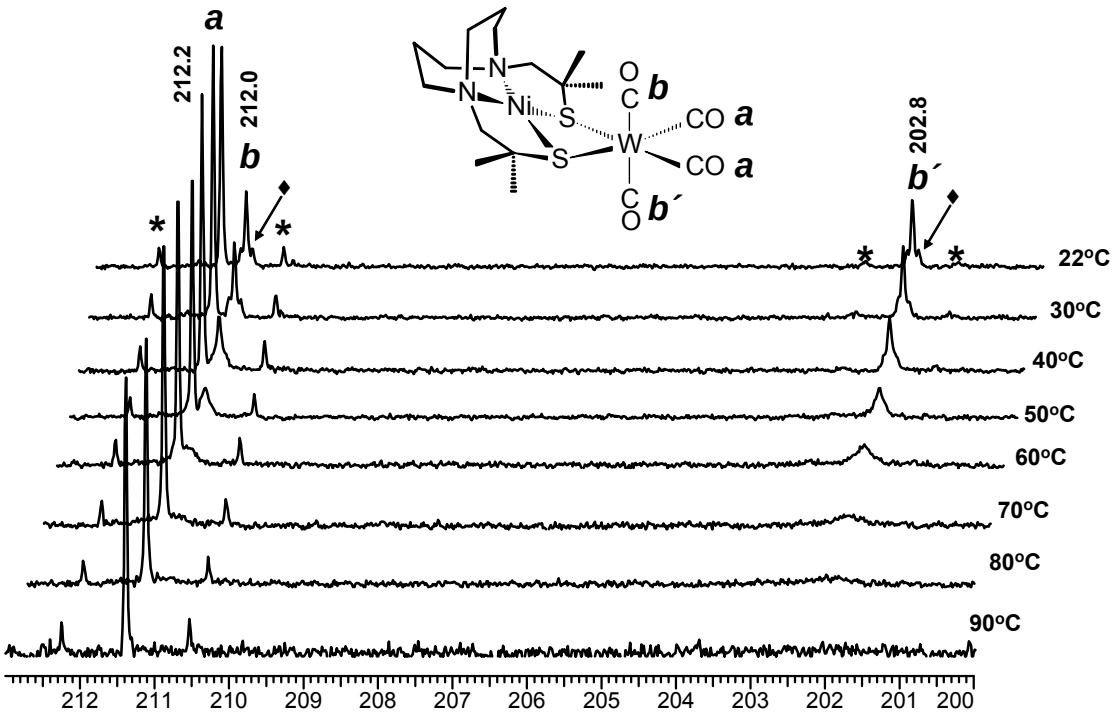

Figure III-12. Variable-temperature ^{13}C NMR spectra of [(**Ni-1***)$W(CO)_4$] in DMF in the low-field CO region. *Asterisks indicate ^{183}W satellites and ♦ indicate ^{13}C-^{13}C coupling shown in the 22°C spectrum. Assignment of b and b' are unconfirmed.

A coalescence of resonances for carbonyls **b** and **b'** as seen for complex **1** did not occur at 90 °C or even above 100 °C, for the neutral $(NiN_2S_2)W(CO)_4$ complexes **4** and **5**. Likewise, the four resonances of complex **6** retained their integrity up to 110°C; higher temperatures were not experimentally accessible. Analogous VT-NMR studies of the dianionic complex **2** were compromised by the ring-opening of the $Ni(ema)^{=}$ followed by a cannabolism process that produced a pentacarbonyl species analogous to complex **7**.

Activation barriers for the $(CO)_b/(CO)_b'$ site permutations in complex **1** were estimated from the following equations: $k = 1/\tau$; $\tau_{coalesence} = ((\sqrt{2})\pi\Delta\nu)^{-1}$; and $\Delta G^{\ddagger} = RT$

[ln(R/Nh) - ln (k/T)]). For complex **1** the exchange rate constant was calculated at the coalescence temperature of 90 °C (363 K) and the error indicated for the activation barrier is from computations made for coalescence temperatures of ± 10° on either side of 363 K.

$$\tau = 2.45 \times 10^{-4} \text{ s (at 363 K)}$$

$$k = 4.08 \times 10^{3} \text{ s}^{-1} \text{ (at 363 K)}$$

$$\Delta G^{\ddagger} = 64.4 (\pm 2.0) \text{ kJ/mol (at 363 K)}$$

The process which equilibrates the $(CO)_b$ and $(CO)_b'$ sites in complex **1** is expected to be a mutual buckling of the NiN_2S_2 and $W(CO)_4$ units at the sulfur hinges; alternatively this may be described as a double inversion at the sulfurs (Figure III-13). Notably the molecular mobility is greatest for the complex of greatest steric encumbrance and largest hinge angle.

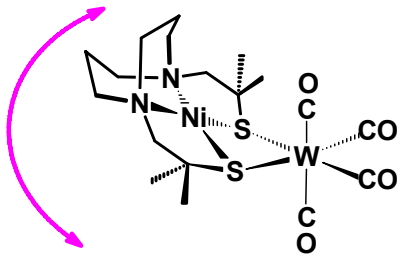

Figure III-13. Mutual buckling of the NiN_2S_2 and $W(CO)_4$ units.

Electrochemical Studies. Cyclic voltammograms (CV's) of the $(NiN_2S_2)W(CO)_4$ complexes were recorded at room temperature in CH_3CN solutions containing 0.1 M *n*-

Bu_4NBF_4 as supporting electrolyte. These studies were done in collaboration with Dr. Jonghyuk Lee. For direct comparison, CV's of the NiN_2S_2 metallothiolate ligands were examined under identical conditions; these are overlaid with their respective $W(CO)_4$ derivatives in Figure III-14. The electrochemical data are summarized in Table III-5.

In general, all of the neutral $(NiN_2S_2)W(CO)_4$ complexes undergo one reversible reduction and one quasi-reversible oxidation within the acetonitrile solvent window. As the $(pip)_2W(CO)_4$ complex shows no reductions, the reversible reductions, found in the range of -1.36 to -1.64 V for complexes **1**, **3** and **6** are assigned as the $Ni^{II/I}$ redox couple. The shift to more positive potentials by ca. 0.50 V as compared to the ca. -2 V, $Ni^{II/I}$ redox event in the free NiN_2S_2 ligand, is compatible with formation of a Lewis base-Lewis acid adduct with the $W(CO)_4$ acceptor which withdraws electron density from the metallo ligand via the bridging thiolate sulfurs. In contrast, the oxidation event seen in the neutral NiN_2S_2 ligands in the 0.20 – 0.40 V range is barely changed in the $(NiN_2S_2)W(CO)_4$ complexes; these were proposed to be sulfur-based in the NiN_2S_2 free ligands.[67] A second oxidative process, proposed to be nickel-based, is observed for the **Ni-1*** and **Ni(bmmp-bmed)** free ligands, but is shifted out of the CH_3CN solvent window in the $(NiN_2S_2)W(CO)_4$ complexes **1** and **6**. Thus if indeed the more accessible oxidation process is sulfur-based, it would appear to be less dependent on the formation of the $W(CO)_4$ complex than are the Ni-based redox events. It should be mentioned that there is an irreversible oxidation in the CV of the $(pip)_2W(CO)_4$ complex at ca. + 0.5 V. Hence the assignment of the oxidation events displayed in Figure III-14 to the $Ni^{II/III}$ couple are not definite.

As shown in Figure III-14(d), the only redox event in the CV of CH_3CN solutions of $(Et_4N)_2$[**Ni(ema)**] is a reversible oxidation at –0.30 which earlier was assigned by Holm and coworkers to $Ni^{II/III}$; the assignment was supported by EPR spectroscopy.[45] In contrast, the CV of the tungsten derivative of **Ni(ema)**$^{2-}$, [**Ni(ema)** $W(CO)_4]^{2-}$, also as its Et_4N^+ salt, reveals both an irreversible oxidation at –0.21 V and an irreversible reduction at -2.34 V under the same experimental conditions as used for study of **Ni(ema)**$^{2-}$. Making the assumption that the complexation of the $NiN_2S_2^{2-}$ by $W(CO)_4$ shifts the $Ni^{II/I}$ reduction potential at minimum by the same amount as in the neutral compounds, the $Ni^{II/I}$ reduction in the free **Ni(ema)**$^{2-}$ can be estimated to be - 2.8 V or even more negative.

As the shifts in $Ni^{II/I}$ reduction potentials reflect the drain of electron density from the NiN_2S_2 coordination environment upon formation of the $W(CO)_4$ adduct, one might expect a correlation of the differences in reduction potential with the ν(CO) IR data. That is, the greater shift in the value $E_{1/2}$ for the $Ni^{II/I}$ couple in the **Ni(bme-Me$_2$PDA)** vs. complex **3** as contrasted to analogous features in complex **1**, would appear to indicate better donor properties for the **Ni(bme-Me$_2$PDA)** ligand over the **Ni-1*** ligand. Unfortunately the infrared and force constant data are fairly indistinguishable within the series of neutral Ni-W compounds. It is not known whether the lack of correlation of ν(CO) and the $Ni^{II/I}$ couple $E_{1/2}$ values is due to an inherent insensitivity of the former to small differences in donor property, or whether there should be such a correlation at all.

Table III-5. Half-Wave and Anodic Potentials for Reductions and Oxidations of NiN_2S_2 and $[NiN_2S_2]W(CO)_4$ Complexes.[a]

	$E_{1/2}$ (V)	E_{pa} (V)	
Compound	reduction	1st oxidn.	2nd oxidn.
Ni-1	-2.02	0.17	
Ni-1′	-2.03	0.21	
Ni-1*	-2.11	0.30	1.15
Ni(bmmp-dmed)	-1.97	0.38	1.04
Ni(bme-Me$_2$PDA)	-2.00	0.34	
[**Ni(ema)**]$(Et_4N)_2$		-0.30[b]	
(**Ni-1**)$W(CO)_4$	-1.56	0.25	
(**Ni-1′**)$W(CO)_4$	-1.51	0.30	
(**Ni-1***)$W(CO)_4$	-1.64	0.36	
[**Ni(bmmp-dmed)**]$W(CO)_4$	-1.42	0.35[c]	
[**Ni(bme-Me$_2$PDA)**]$W(CO)_4$	-1.36	0.36	
[**Ni(ema)**$W(CO)_4$]$(Et_4N)_2$	-2.34[d]	-0.12	

a All potentials scaled to NHE referenced to a Cp_2Fe/Cp_2Fe^+ standard ($E_{1/2}^{NHE}$ = 0.40 V; see Experimental Section). In CH_3CN solutions, 0.1 M *n*-Bu_4NBF_4 electrolyte, glassy carbon working electrode, measured vs $Ag/AgNO_3$ reference electrode. *b* This oxidation peak is coupled to a return peak E_{pc} at –0.38 V. *c* This reduction peak is coupled to a return peak E_{pc} at 0.28 V. *d*This value is for an irreversible reduction peak.

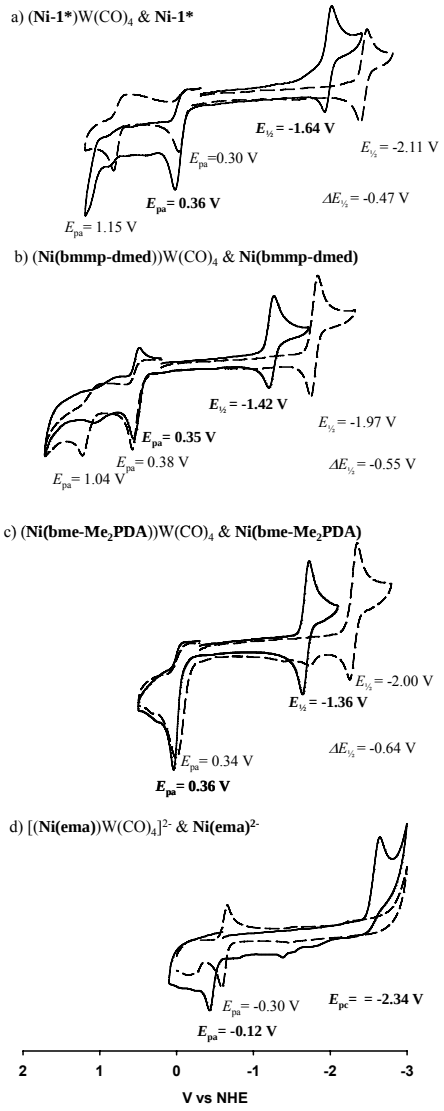

Figure III-14. Cyclic voltammograms of NiN_2S_2 (dashed line) and $[NiN_2S_2]W(CO)_4$ (solid line) complexes in CH_3CN solutions, 0.1 M *n*-Bu_4NBF_4 at a scan rate of 200 mV/S.

Stability of the $(NiN_2S_2)W(CO)_4$ complexes.

The neutral complexes of this type have considerable thermal stability, even in solution, as evidenced by the VT NMR studies which demonstrated complex integrity at temperatures ≥ 100 °C. With the exception of the $(Et_4N)_2$[**Ni(ema)**$W(CO)_4$] all of the $NiN_2S_2W(CO)_4$ are, for practical purposes, air stable. As described above in the isolation of complex **7**, thermal decomposition of complex **4** over a one week period in a sealed vial where any liberated CO could be taken up by another molecule of **4** resulted in the pentacarbonyl species and conversion of the bidentate into a monodentate ligand. Subsequent studies of this hemilabile property with the deliberate addition of exogeneous CO has shown that the pentacarbonyl complexes do not easily undergo complete CO displacement of the NiN_2S_2 ligand. Furthermore, preliminary studies find in all cases the ring closing, reformation of the tetracarbonyl, is in equilibrium with the opening/CO capture process, Figure III-15. The ring-opening characteristic of the Ni(μ-$SR)_2W$ core that produces an open site on the $W(CO)_4$ moiety, yet persists as a nickel-thiolato ligand, is an attractive feature for catalyst design. A related scenario is prominent in the computed mechanism for the ACS enzyme activity.[23]

Exploring the Hemilabile Property of NiN_2S_2 Ligands.

An interesting observation was made upon the addition of isotopically labeled ^{13}CO gas (1 atm) to (**Ni-1***)$W(CO)_4$ in a DMF solution. After 30 minutes, the ^{13}C NMR spectrum of the reaction showed a growth of resonances assigned to the CO ligands mutually cis to each other (**a** and **a´**) and trans with respect to the sulfur donors, and the

appearance of a resonance assigned to the (**Ni-1***)$W(CO)_5$ species, (Figure III-15, b). Additional isotopic enrichment is observed after 120 min under a ^{13}CO atmosphere (Figure III-15, b). This suggested that the mutually cis CO ligands (**a** and **a´**) were isotopically enriched at a much faster rate than the mutually trans CO ligands (b and b´).

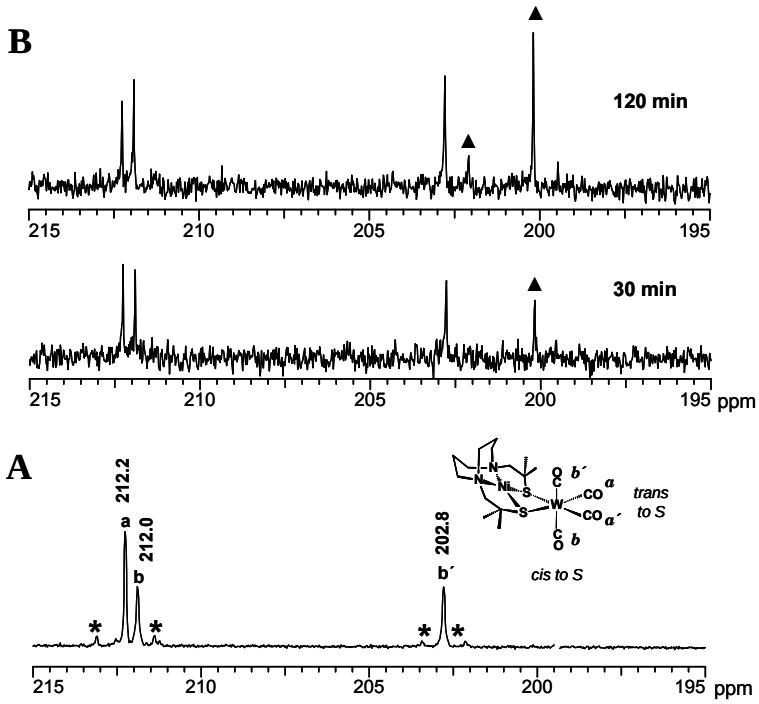

Figure III-15. A. Natural abundance ^{13}C NMR spectrum of CO resonances in complex **1**. **NOTE:** Ratio of combined equatorial CO signals (**b** and **b'**) to the axial CO signal (**a**) is 1.0. Peaks marked by asterisks correspond to ^{183}W–^{13}C coupling. **B.** ^{13}C NMR spectra of carbonyl resonances resulting from **1** + ^{13}CO ⇆ **2**. After 30 and 120 min reaction periods at 50ºC in DMF the ratios of (**b** and **b'**)/**a** are 1.80 and 2.70, respectively. Peaks marked with ▲ at 202.1 and 200.1 ppm are due to ^{13}CO enriched complex **2**.

This observation suggested that ^{13}CO addition to complex **1**, (**Ni-1***)$W(CO)_4$, to form the pentacarbonyl, (**Ni-1***)$W(CO)_5$, is stereo-selective, and the reformation of the (**Ni-1***)$W(CO)_4$ by means of CO loss was also stereo-selective and is best illustrated by

Figure III-16. CO ligand loss from the 5 coordinate intermediate **2-^{13}CO**, (**Ni-1***)W(CO)$_4$(^{13}CO), can occur by three possible routes, **Int-1**, **Int-2** and **Int-3**. Ring-closure in **Int-2** and **Int-3** lead to twice as much isotopic ^{13}CO enrichment in the **b**, and **b´** as in the **a** position. These results are in agreement with *cis*-labilization arguments by Brown and co-workers.[70]

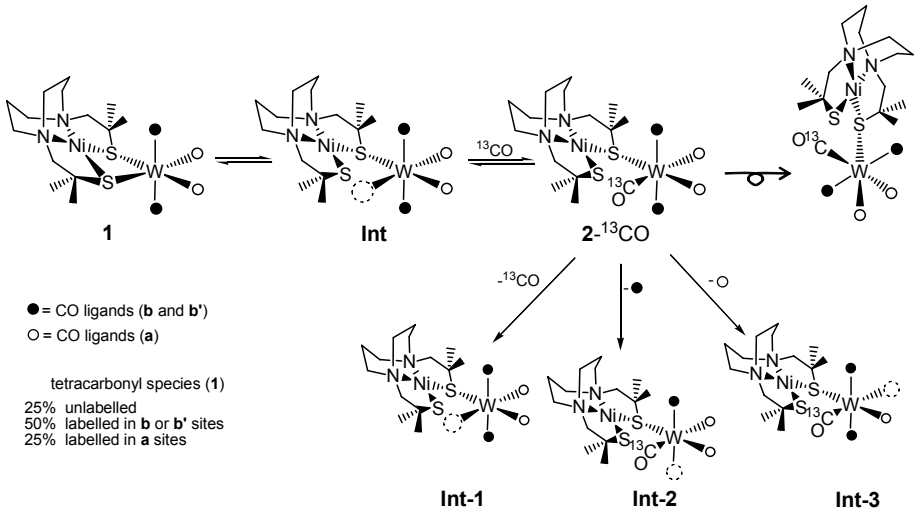

Figure III-16. A. Proposed mechanism of ^{13}CO enrichment.

A kinetic study of the ring-opening process in $(NiN_2S_2)W(CO)_4$ complexes as they take up CO and convert to$(NiN_2S_2)W(CO)_5$ as depicted in Figure III-17 was the subject of an investigation done and reported separately by Dr. Donald J. Darensbourg and Dr. Andrea Phelps.[71]

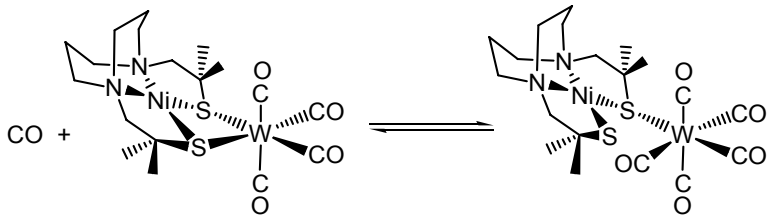

Figure III-17. Conversion of a tetracarbonyl species into a pentacarbonyl species in the presence of CO.

In their study, the (**Ni-1***)$W(CO)_4$ complex was pressurized with moderate CO pressures between 400-1400 psi in a stainless steel Parr reactor modified to accommodate an ASI ReactIR SiComp probe in DMF. Spectral changes in the infrared spectra of (**Ni-1***)$W(CO)_4$, (ν(CO) = bands at 1996, 1871, 1857, and 1816 cm^{-1}), were monitored over time as (**Ni-1***)$W(CO)_4$ was converted to the (**Ni-1***)$W(CO)_5$ species (ν(CO) = 2061, 1920, and 1874 cm^{-1}). The CO substitution reaction was monitored by the appearance of a strong isolated band at 1920 cm^{-1} in the (**Ni-1***)$W(CO)_5$ species. From this study it was determined that the reaction does not go to completion so there is equilibrium distribution of (**Ni-1***)$W(CO)_4$ + CO and (**Ni-1***)$W(CO)_5$. More importantly, the **Ni-1***$W(CO)_5$ derivative does not react further with CO to afford the $W(CO)_6$ species.

The equilibrium constant determined at 50°C for the conversion of the tetracarbonyl complex in the presence of CO to the pentacarbonyl species was determined to be 2.8 M^{-1} or $\Delta G° = -1.4$ kJ/mole. The activation parameters determined for the ring-opening process was calculated to be $\Delta H^{\neq} = 89.1$ kJ-mol^{-1} and $\Delta S^{\neq} = -37.2$ J-$mol^{-1}K^{-1}$, which suggested a solvent-assisted, concerted ring-opening mechanism. Similar values were reported by Dobson and coworkers in four-membered chelated dithioether derivatives of Mo and W in the presence of alkyl- and arylphosphites.[71-74]

This indicated that the second W-S bond is considerably strengthened upon dissociation of the first W-S bond and further supports the theoretical mechanism for NiN_2S_2M ring-opening proposed by Webster and co-workers for the ACS enzyme.[23]

COMMENTS AND CONCLUSIONS

This detailed inspection of a series of NiN_2S_2 derivatives of $W(CO)_4$ has identified a unique steric property of the metallodithiolate ligands to lie in the hinge angle imposed by the bridging thiolate sulfurs and their remaining quiescent lone pairs. There is no obvious correlation of the hinge angle with other metric data of the complexes such as the S-W-S bite angle or W-S distances. A detailed molecular mechanics analysis is necessary in order to assess all of the torsion angles within the polydentate ligand framework that influence the S-donor site and the dihedral or hinge angle. Nevertheless from the crystallography data produced for this set of six complexes, we can conclude that substituents and orientations at the C_α to S produce the principal steric deviation from the inherent dihedral angle of the NiN_2S_2 / $S_2W(CO)_2$ planes as set by the S-lone pair/W acceptor orbital interactions. The overlay of structures in Figure III-19 show an impressive range of the steric effect for the $W(CO)_4$ series of complexes. The smallest of these is only 6 degrees larger than the 101.3° dihedral angle observed for the (**Ni-1**)PdMeCl complex shown below (Figure III-18).[75]

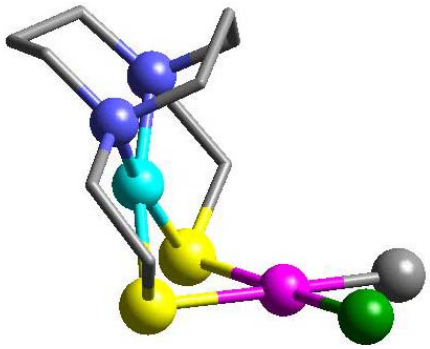

Figure III-18. Ball-and-stick representation of (**Ni-1**)PdMeCl[74].

With no steric interactions possible in the two hinged square planes, the (**Ni-1**)PdMeCl complex could represent the natural dihedral angle limit for NiN_2S_2 derivatives. We have noted that such a steric effect as defined for the NiN_2S_2 ligands may become a benefit for substrate orientation in palladium-promoted coupling reactions. Importantly, the VT NMR studies establish that this orientation is fixed, appearing to be mobile at relatively high temperatures.

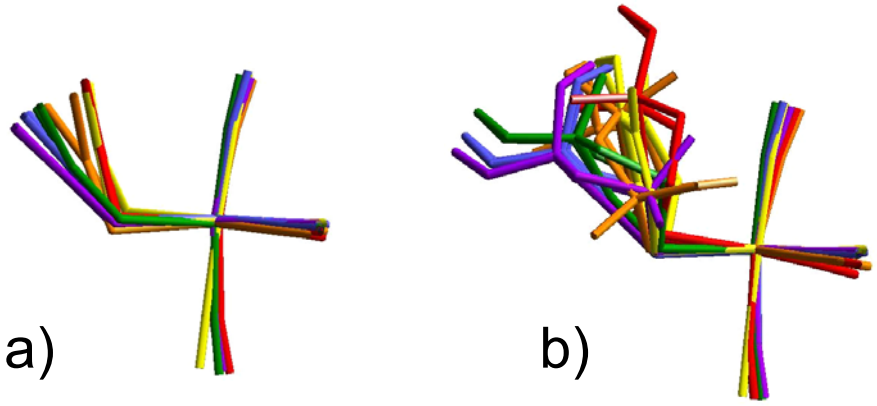

Figure III-19. Structural overlay of $(NiN_2S_2)W(CO)_4$ complexes in order of decreasing dihedral angle with hydrogen atoms omitted. **purple** (Ni-1*)$W(CO)_4$, **blue** (Ni-1*)$W(CO)_4$, **green** (Ni-1')$W(CO)_4$, **orange** (Ni(bmmp-dmed))$W(CO)_4$, **yellow** $[NEt_4]_2$[(Ni(ema))$W(CO)_4$], **red** (Ni(bme-Me_2pda))$W(CO)_4$. **a)** bond representations as cylinders using $NiN_2S_2W(CO)_4$ only; **b)** hydrocarbons added.

The electron-donating ability of the NiN_2S_2 ligands, related to each other and to other neutral donors to a first approximation through the ν(CO) stretching frequencies of $W(CO)_4$ adducts, find close analogies to N-donor ligands such as piperidine or bipyridine; the ranking is as follows (Figure III-20):

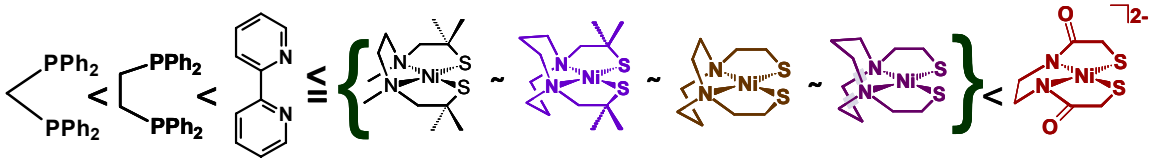

Figure III-20. Order of electron donating ability for common bidentate ligands and NiN_2S_2 complexes determined in this study.

While the vibrational spectroscopy data does not distinguish between the neutral NiN_2S_2 ligands, the dianionic [Ni**(ema)**]$^{2-}$ ligand significantly enriches the $W(CO)_4$ moiety with electron density as contrasted to the neutral analogues. . Interestingly, the average ν(CO) for [**Ni(ema)**$W(CO)_4$] $^{2-}$, 1867 cm^{-1}, is only 18 cm^{-1} lower than the average ν(CO) values of the neutral complexes, 1885 cm^{-1}. In contrast, the average ν(CO) value of a dianionic dithiolate, (S,S-C_6H_4)$W(CO)_4^{2-}$ is 1850 cm^{-1} and that for a dithioether, ($Bu^tS(CH_2)_2SBu^t$)$W(CO)_4$, is 1920 cm^{-1}, a 70 cm^{-1} difference.[76,77] In summary, the electron density transferred to the $W(CO)_4$ unit from the various bidentate S-donors is ranked:

$$RS\text{-}R'\text{-}SR << Ni(SR)_2 < Ni(SR)_2^{2-} < {}^{-}SR'S^{-}$$

Electrochemical studies find significant differences in accessibility of the $Ni^{II/I}$ redox couple in the NiN_2S_2 metallothiolate ligands upon coordination of the thiolate

sulfurs lone pairs to an exogeneous metal. The differences in reduction potential appear to be more ligand dependent than are the ν(CO) and force constant values. Hence while the IR spectroscopic analysis finds no differences in donor ability of the neutral NiN_2S_2 metallothiolate ligands, the $Ni^{II/I}$ redox couples, specifically the difference between the $E_{1/2}$ of the $Ni^{II/I}$ couple in the free NiN_2S_2 ligand vs. that bound to $W(CO)_4$, suggest the order of electron withdrawal from the NiN_2S_2 ligands by $W(CO)_4$ to be:

$$\text{Ni(bme-Me}_2\text{PDA)} > \text{Ni(bmmp-dmed)} > \textbf{Ni-1'} > \textbf{Ni-1} \approx \textbf{Ni-1*}$$

Interestingly there is a reasonable, and as of now ill-defined, correlation of the hinge angles with the differences in $\Delta E_{1/2}$ of the $Ni^{II/I}$ redox couples ($\Delta E_{1/2} = E_{1/2}(Ni^{II/I}$ of $NiN_2S_2W(CO)_4) - E_{1/2}$ ($Ni^{II/I}$ of NiN_2S_2)), the understanding of which will require computational chemistry.

Notably, the dianionic [**Ni(ema)**]$^{2-}$ complex, that which most faithfully models the Ni(Cys-Gly-Cys) moiety in the ACS enzyme, was found within our series, to most prominently display the property of hemilability, releasing one S-W bond and opening up a site on the $W(CO)_4$ moiety for the uptake of CO, producing a $W(CO)_5$ complex in which the $NiN_2S_2^{2-}$ ligand is monodentate. This observation is consistent with the *in silico* mechanism for the ACS enzyme active site in which the Ni(Cys-Gly-Cys)$^{2-}$ ligand switches into a monodentate form to accommodate addition of CO and switches back to reform the resting state of the enzyme.[23,59] Another interesting feature of the dianionic [**Ni(ema)**]$^{2-}$ complex ligand is how easily it fits into the overall spectroscopic and reactivity pattern of the neutral NiN_2S_2 ligands. This result is compatible with the work of Hegg, et al. which demonstrated an array of electrophile reactivity with [**Ni(ema)**]$^{2-}$

that mirrored the S-based reactivity of neutral NiN_2S_2 complexes.[34] Consistent with these similarities is the small change in ν(CO) stretching frequencies of the $W(CO)_4$ derivatives of the dianionic as compared to the neutral nickel dithiolato complexes described above. Thus in addition to moderation of charge by the nickel ion, it appears to buffer the donor ability.

For the purposes of synthetic design and for analysis of donor properties, we have treated the NiN_2S_2 complexes as "innocent" ligands.[78] This very useful assumption, is arguably correct for the firm binding site for nickel in the tetradentate, square planar N_2S_2 coordination environment in combination with soft and low-valent metals such as W^0, Pd^{2+} and $Ni^{(I/0)}$. It provides a rationale for the assembly of the ACS active site, a rationale that can possibly be extended to other binuclear active sites in biology and presumably in organometallic applications. However whether this innocence will be maintained in combination with all metals is not known. The full potential of these ligands should be addressed through systems designed to take advantage of their unique properties some of which we have identified, and some of which await further studies.

CHAPTER IV

CO AND ETHYLENE MIGRATORY INSERTION REACTIONS AND COPOLYMERIZATON INVOLVING PALLADIUM COMPLEXES WITH A NiN_2S_2 METALLODITHIOLATE LIGAND

INTRODUCTION

Inspired by a heterobimetallic biological catalyst, acetyl CoA synthase (ACS), we endeavored to develop a host of NiN_2S_2 metal complexes as a new class of ligands for organometallic chemistry. The active site of the enzyme contains a Ni(CysGlyCys) moiety coordinated to a second catalytically active nickel in which the Ni(CysGlyCys) moiety serves as a ligand stabilizing the metal in sequential C-C and C-S coupling reactions. These were presented in the Chapter I.[20-22] This natural NiN_2S_2 ligand is similar to a library of synthetic analogues in which we investigated several distinctive steric, electronic and structural properties well established through derivatives of tungsten tetracarbonyl which were described in Chapter III. The series of metallodithiolate ligands explored were found to be more electron rich donors than the conventional ligands (diphosphines and diimines) in such $L_2W^0(CO)_4$ complexes.

---

*Reproduced in part with permission from **"**N_2S_2Ni Metallothiolates as a Class of Ligands that Support Organometallic and Bioorganometallic Reactivity", by Marilyn V. Rampersad, **2005**, *Angew. Chem., Int. Ed.*.**,** 44, 1217-20. **2005 ,** Angewandte Chemie International.Edition.

The heterobimetallic complex, (Ni-1)Pd(CH_3)(Cl), Figure IV-1 was designed to mimic structural as well as functional features of the ACS enzyme active site as well as a palladium catalyst employed in C-C coupling reactions.[75] Its structural analysis along with several NiN_2S_2M complexes presented a unique structural feature of the ligand when bound to a second metal. The μ-SR bridge formed between the Ni^{2+} in the N_2S_2 chelate and a Pd^{2+} metal center shows a classic butterfly core often observed in heterobimetallic active sites as in acetyl CoA synthase (Figure IV-1).[20-22] This unique feature in which the ligand is almost perpendicular to the metal center where catalysis occurs might allow for stereo- and regioselective substrate addition.

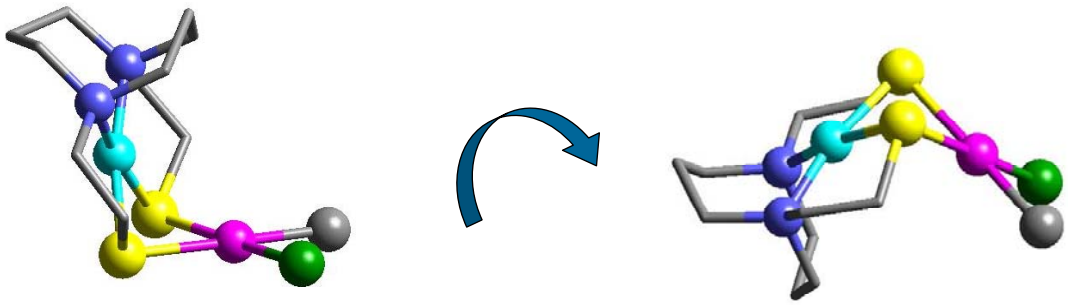

Figure IV-1. The butterfly core defined by the $(\mu\text{-SR})_2$ bridge (**Ni-1**)Pd(CH_3)(Cl).

An added functionality of metallodithiolate ligands is their ability to serve as hemilabile ligands. Sulfur-catalytic metal bond dissociation provides an open site on an otherwise coordinatively saturated metal center, or it may stabilize the catalytic metal as it undergoes coordination geometry changes.

The use of a metal complex as a ligand in which the metal center is incorporated within the ligand framework is not a new idea; as metal complexes with phosphine donors have been utilized in a variety of industrially significant reactions. For example, 1,1 bis(diorganylphosphino)metallocene ligands (M=Fe, Ru, Co) coordinated to palladium has shown reactivity towards cross coupling,[79] the Heck reaction,[80] hydroamination of alkenes[81] and CO/ethylene copolymerizaton.[82] Catalysts employing novel ligands capable of producing functional polymers from inexpensive monomers such as CO and olefin are of continuous interest. Copolymerization of CO and olefin to form alternating polyketone opens a door to a host of new functional materials with valuable engineering properties for high performance thermoplastics.[1,2] Important properties include, chemical resistance, strength, heat resistance, and UV stabilities; that are applicable to automotive components, gears, fittings, fibers and packaging.[1] Usually the alternating polyketones have molecular weights of 10^4-10^6, high melting points (T_m) up to 260^{o}C, glass transition temperatures (T_g) near 15^{o}C and density of 1.24 g/cm^3.[2] Copolymerization of CO/ethene/propene to form terpolymers (PK-EP) produces very different properties for practical purposes. For example, PK-EP when cross linked with diamines have been known to produce thermoset systems referred to as CARILITE^{TM} that are found in coatings and adhesives.[83] The production of polyketone is also very environmentally friendly such that the monomers used are from available or renewable feedstocks like ethanol, rather than petrochemical resources and the production of other less valuable monomers as waste are minimial.[2] In addition, these copolymers are useful in the reduction of hydrocarbon emissions from vehicles by hydrocarbon incorporated

polyketone fuel based systems.[2] The array of commercial applications support the need for catalyst systems capable of producing functional polymers. The possibility that NiN_2S_2 complexes could serve as ligands capable of stabilizing low oxidation stable metals in simple organometallic reactions like that observed in CO/C_2H_2 copolymerization would be intriguing and novel.

The initial steps to CO/C_2H_4 copolymer formation involve two consecutive insertions reactions: migratory CO insertion into a Pd-alkyl bond (Figure 4-2) followed by migratory ethylene insertion into a Pd-acetyl bond (Figure IV-2).[2,84,85] Sen et al. has shown that double CO insertion is thermodynamically unfavorable and that double insertion of ethylene is retarded by the high affinity of Pd^{II} metal centers for CO.[86-88]

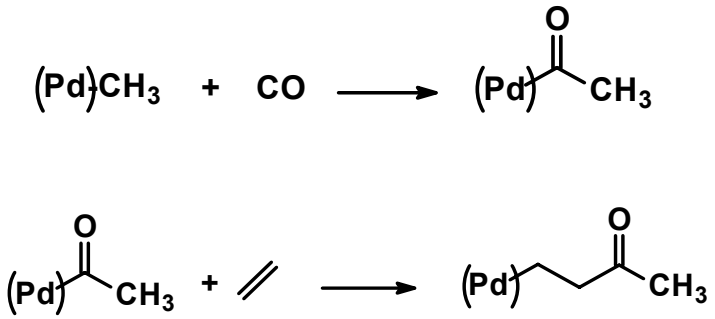

Figure IV-2. Reaction steps observed during CO ethylene copolymerization.

Elegant mechanistic studies by Brookhart[85], Drent[89], and van Leeuwen[17] over the last decade have provided substantial mechanistic information that highlight the key steps of CO/ethylene chemistry and delineate the formation of palladium-catalyzed, perfectly alternating polyketone. These mechanistic studies have also provided model

compounds upon which to study the elementary steps in C-C coupling reactions as well as spectroscopic sigNatures of key intermediates during copolymer formation.

The lower reactivity of the Palladium-based cationic systems with bidentate nitrogen ligands were amenable systems for observing intermediates on CO/C_2H_4 copolymer formation. Shown in Figure IV-3 is Brookhart's mechanistic cycle for polyketone formation; NMR and IR spectroscopy were the main tools used to observe the alleged intermediates.[85] With the α-diimine ligand (o-phenanthroline) the resting state of the catalyst was found to be the open-chain acetyl carbonyl, $[(o\text{-}phen)Pd(C(O)Me)(CO)]^+$, since CO has a greater binding affinity than ethylene for the metal center, resulting in CO insertion rate approximately 2000 times that of ethylene insertion. That is $k_{-1}>>k_1$, therefore ethylene displacement of CO to form the ethylene acetyl intermediate, $[(o\text{-}phen)Pd(C(O)Me)(\eta^2\text{-}CH_2CH_2)]^+$ is a rare occurrence.[85] The rapid rate of β-acetyl migration to ethylene in such derivatives is then followed by rapid CO trapping of the open site, followed by CO insertion to form the alkyl CO species, $[Pd\text{-}(C(O)Me)(CO)]^+$, once more ensuring no significant formation of the 5-and 6-membered keto-chelate complexes that would otherwise stabilize the open site on the metal and inhibit catalysis (Figure IV-3).

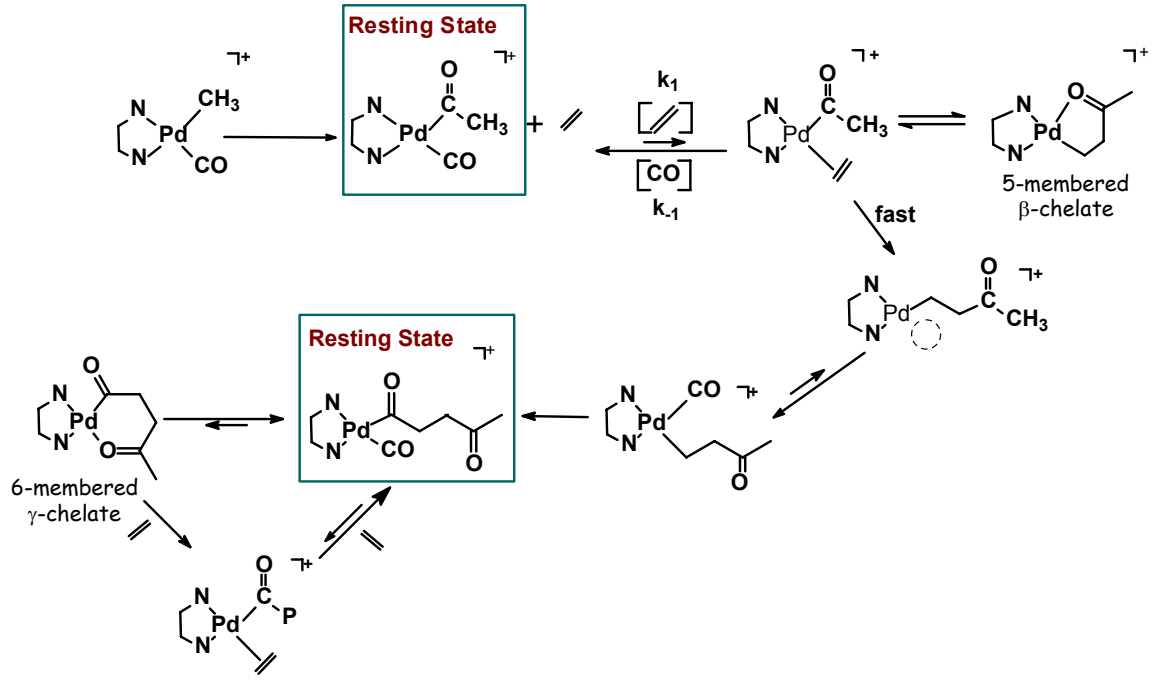

Figure IV-3. Proposed mechanism for the copolymerization of CO/C_2H_4 employing palladium diimine catalysts.[85]

Drent and co-workers utilized polarization modulation reflection absorption infrared spectroscopy (PM-ARIRS) as a spectroscopic tool to look at the important steps in C-C coupling reactions during the addition of CO/C_2H_4 gas to the catalyst $(dppp)Pd(CH_3)^+(OTf)$ (dppp = bisdiphenylphosphinopropane), in microcrystalline state.[89] Based on the absence of a ν(CO) stretch in the infrared spectrum that would signify a terminal bound CO in the open-chain form of the carbonyl acetyl complex, $[(o\text{-}phen)Pd(C(O)Polymer)(CO)]^+$ the resting states of the catalysts were found to be the α,β-keto-chelate complexes with the diphosphine ligand. Drent and co-workers also found that CO replacement of the palladium-bound ketone in the γ-chelate reduces steric crowding, facilitates the side on approach of ethylene, and results in more facile

CO/C_2H_4 exhange and C_2H_4 nsertion.[89] In contrast, Brookhart and co-workers suggested that relatively flat Nature of phenanthroline ligand provided less steric crowding facilitating the direct ketone displacement by ethylene.[90]

In addition to the differences between the resting states of the catalyst during copolymer formation there exists differences between the mechanistic route to CO addition in neutral $(L_2)Pd(CH_3)(X)$ cationic and $[(L_2)Pd(CH_3)]^+(X)^-$ metal complexes.[17,89] These differences may depend on the ligand's steric and electronic components as well as the charge and coordination geometry of the overall complex.[17] In this study we employed the use of a electron rich metallodithiolate ligand on a palladium metal center to study CO addition and to determine the ligand effect in the copolymerization of ethylene and CO.

RESULTS AND DISCUSSION

Syntheses of $(NiN_2S_2)Pd(L)_2$ Complexes

Initial attempts to prepare complex **4-1**, (**Ni-1**)$Pd(CH_3)_2$, by Cesar Ortiz *via* a well known TMEDA ligand displacement route developed by Boersma *et al*.[51] found that the complex was reactive towards chlorinated solvents forming the chloro-methyl derivative (Figure IV-4).[75] A modified procedure using CH_3CN produced the (**Ni-1**)$Pd(CH_3)_2$ as red-pink solid as evidenced by mass spectral analysis and was found to be stable at low temperature for an extended period of time (Figure IV-4).

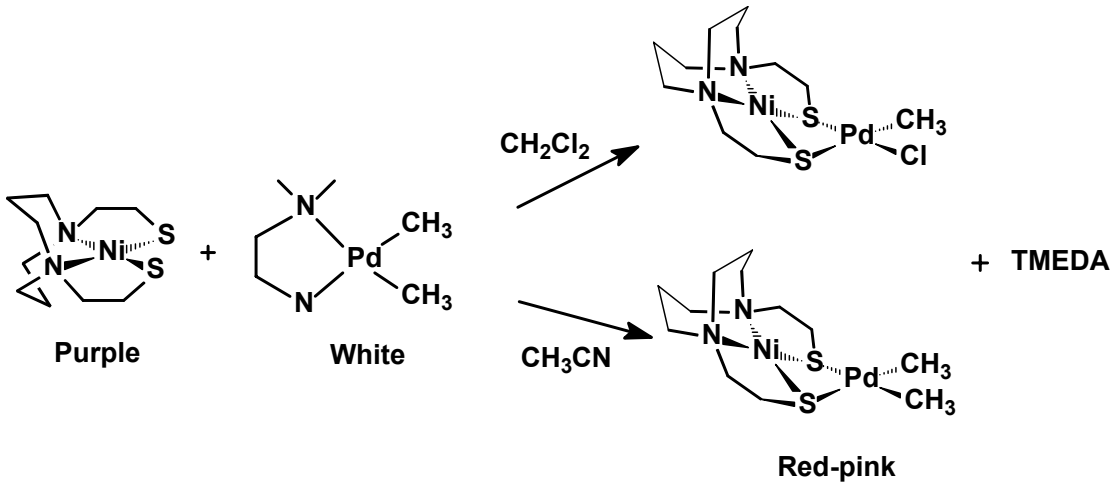

Figure IV-4. Reaction pathway for the synthesis of (**Ni-1**)Pd(CH_3)$_2$.

According to the experimental protocol laid out by Brookhart *et al.*[85] the mono-methyl derivative, [(**Ni-1**)Pd(CH_3)(OEt_2)][BAr ′$_4$] was prepared from the (**Ni-1**)Pd(CH_3)$_2$ precursor and release of CH_4 (Figure IV-5). This complex was an extremely useful precursor that is stable as a solid at low-temperature. The weakly coordinating ether ligand can be easily displaced. Mass spectral analysis of a sample of the compound dissolved in acetonitrile confirmed that 100% of the compound is the acetonitrile adduct [(**Ni-1**)Pd(CH_3)(CH_3CN)]$^+$ with a mass to charge ratio of 454 demonstrating the ease with which ether can be displaced by more donating solvents.

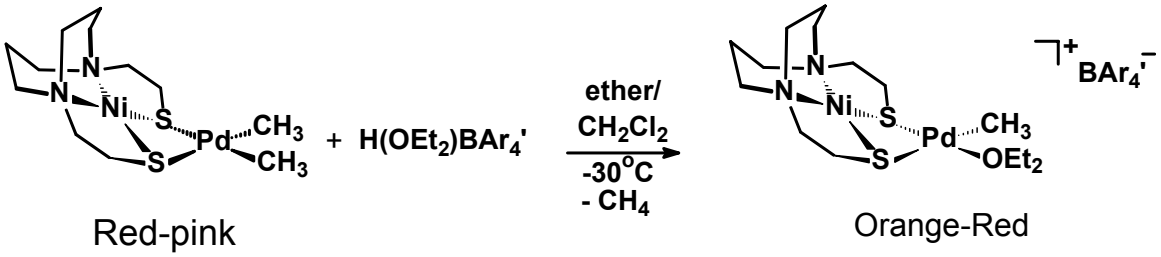

Figure IV-5. Reaction pathway for the synthesis of the cationic palladium complex utilized as a catalyst throughout this chapter.

For the preparation of (**Ni-1**)Pd(CH_3)(Cl), a ligand displacement route developed by van Leeuwen and co-workers was adopted.[59] This route provided a direct and facile synthesis of the compound by metallodithiolate ligand substitution of the cyclooctadiene in (cod)Pd(CH_3)(Cl) in 95% yield (Figure IV-6). Mass spectral analysis of the product in acetonitrile also confirmed that 100% of the compound was [(**Ni-1**)Pd(CH_3)]$^+$ with a mass to charge ratio of 413 while 22% was the acetonitrile adduct [(**Ni-1**)Pd(CH_3)(CH_3CN)]$^+$.

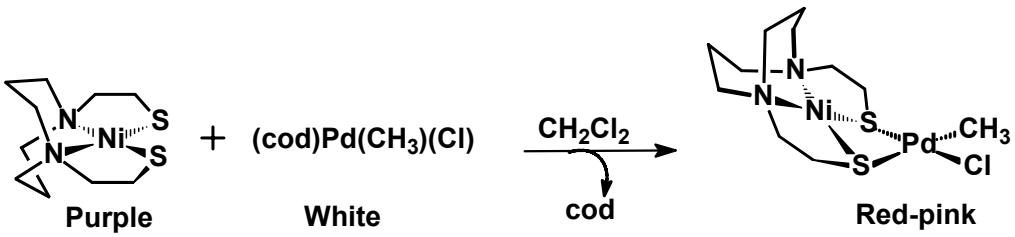

Figure IV-6. Reaction pathway for the formation of (**Ni-1**)Pd(CH_3)Cl complex.

Infrared Study of CO Addition to the Cationic [(Ni-1)Pd(CH_3)(OEt_2)][BAr'_4].

The [(**Ni-1**)Pd(CH_3)(OEt_2)]$^+$ complex was prepared in a CH_2Cl_2 solution from the (**Ni-1**)Pd(CH_3)$_2$ and $HBAr'_4$ precursors at -30°C. On cooling the orange-red solution to -78°C and purging with CO, a maroon red solution was produced with ν(CO) infrared bands at 2110 and 1722 cm^{-1}. These bands were assigned to a terminal bound and acetyl CO group consistent with the structure proposed in Figure IV-7, a). The assumed terminal bound derivative, [(L_2)Pd(CH_3)(CO)]$^+$, that is observed with traditional bidentate ligands was not observed. Addition of isotopically labeled ^{13}CO to [(**Ni-1**)Pd(CH_3)(OEt_2)]$^+$ (95% enriched), shifts both bands which match the calculated predictions of ν(^{13}CO) bands at 2061 and 1685 cm^{-1}, respectively, thus supporting the assignments (Figure IV-7, b)). Interestingly, the analogous [(o-phen)Pd(C(O)CH_3)(CO)]$^+$ complex, have ν(CO) infrared bands at 2127 and 1745 cm^{-1} reflecting the poor electron-donating ability the diimine ligand in comparison to the Ni-1 towards the Pd^{2+} metal center.[85]

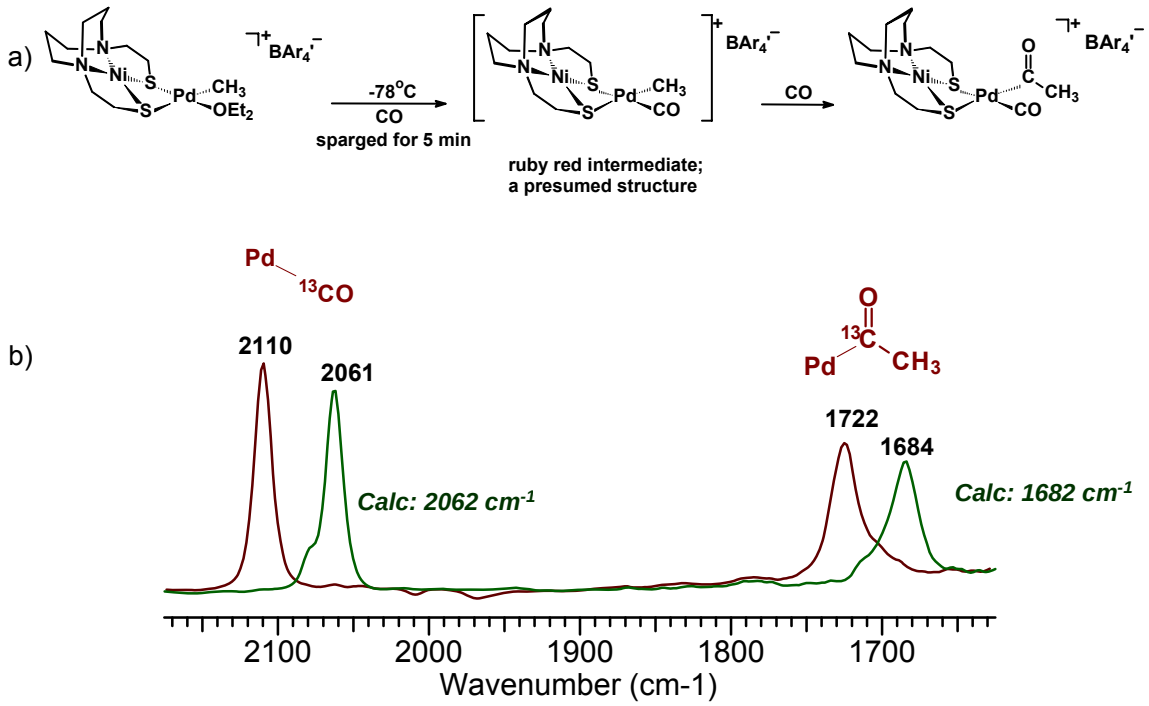

Figure IV-7. a) Reaction of [(**Ni-1**)Pd(CH_3)(OEt_2)]$^+$ with CO. b) IR spectra of the reaction product and of the ^{13}C-labelled product with the calculated isotopic-shift bands.

Infrared Study of ^{13}CO Exchange with [(Ni-1)Pd(C(O)CH_3)(CO)][BAr$'_4$]

To explore the exchange reaction of Pd-bound CO with free ^{13}CO in [(**Ni-1**)Pd(CO)(C(O)Me)]$^+$ the following isotopic labeling experiment was conducted. A CH_2Cl_2 solution of [(**Ni-1**)Pd(CO)(C(=O)Me)]$^+$ was placed under a ^{13}CO atmosphere over the course of 30 minutes at -78°C (Figure IV-8, a)). The IR spectrum of the solution showed ca. 75% enrichment of the terminal CO position while the acetyl ^{12}CO band remained the major species. Nevertheless, there was some build-up of a shoulder on the lower energy side of the 1722 cm^{-1} band that indicated minor incorporation of ^{13}CO into the acetyl position (Figure IV-8, b)). The facile Nature of the terminal CO exchange with free ^{13}CO at -78°C will be commented on later.

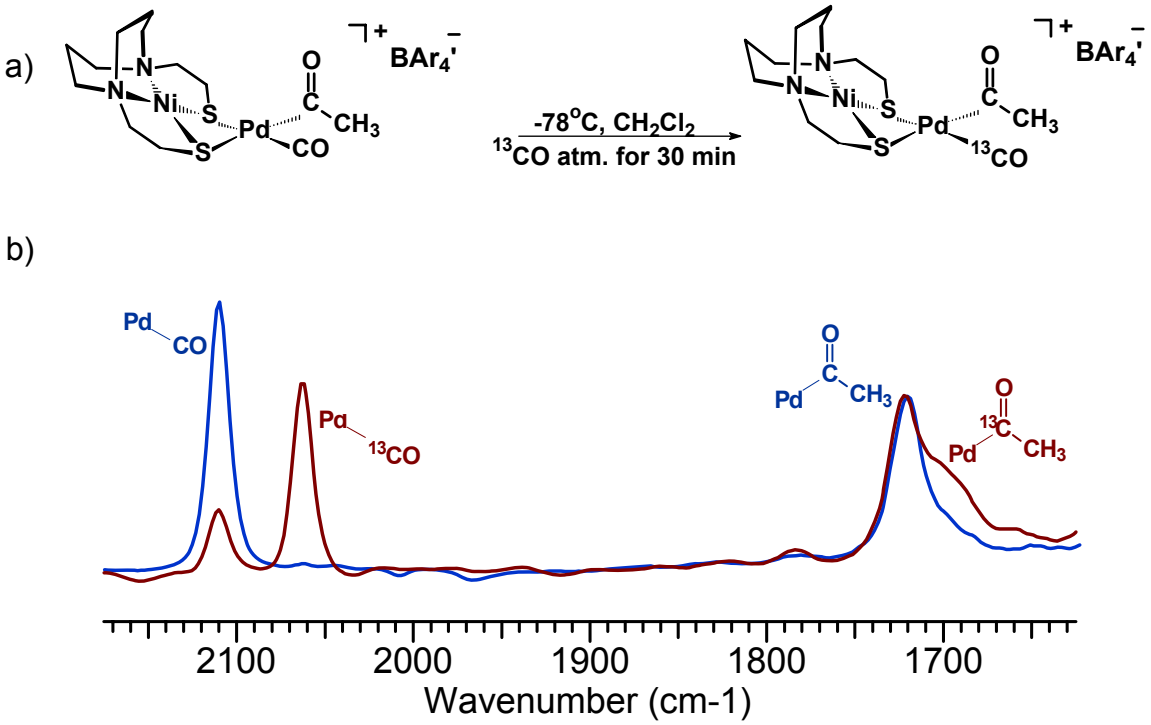

Figure IV-8. a) Reaction of [**Ni-1**]Pd(C(O)CH_3)(OEt_2)]$^+$ with ^{13}CO. b) IR spectra of the reaction product and of the ^{13}C-labelled product.

Solution Stability of [(Ni-1)Pd(CH_3)(OEt_2)][BAr′$_4$] and [(Ni-1)Pd(C(O)CH_3)(CO)][BAr′$_4$]

A sample of [(**Ni-1**)Pd(CH_3)(OEt_2)][BAr′$_4$] in CH_2Cl_2 was monitored via UV-Vis spectroscopy at room temperature to determine the stability of the complex. The red solution of the complex displayed several characteristic charge transfer and d-d transitions, however for the purpose of this study only d-d transitions at 394 nm and 522 nm were monitored over several hours. Shown in Figure IV-9, are the UV-Vis spectral changes that were observed after 2 hours. More prominent spectral changes in UV-Vis occurred overnight showing a dramatic increase in absorbance with a concurrent shift in the absorptions of the starting complex to 402 nm and 520 nm respectively. These

spectroscopic features are consistent with the formation of trimetallic complexes such as the dark purple $[(\textbf{Ni-1})_2Pd]^{2+}(Cl)_2$ (λ_{max} at 408 (5245), 522 (3730) in CH_3OH) that has been structurally characterized.[27] The trimetallic complex, $[\textbf{Ni-1}]_2Pd[BAr_4']_2$, and Pd^0 black are products of a well known thermal decomposition reaction of $L_2Pd(CH_3)_2$ complexes.[51] As a solid, the complex is stable at low temperature but, as observed in the room temperature UV-Vis spectra, the complex is at best stable for 2 hours in non-coordinating solvents before thermal decomposition occur.

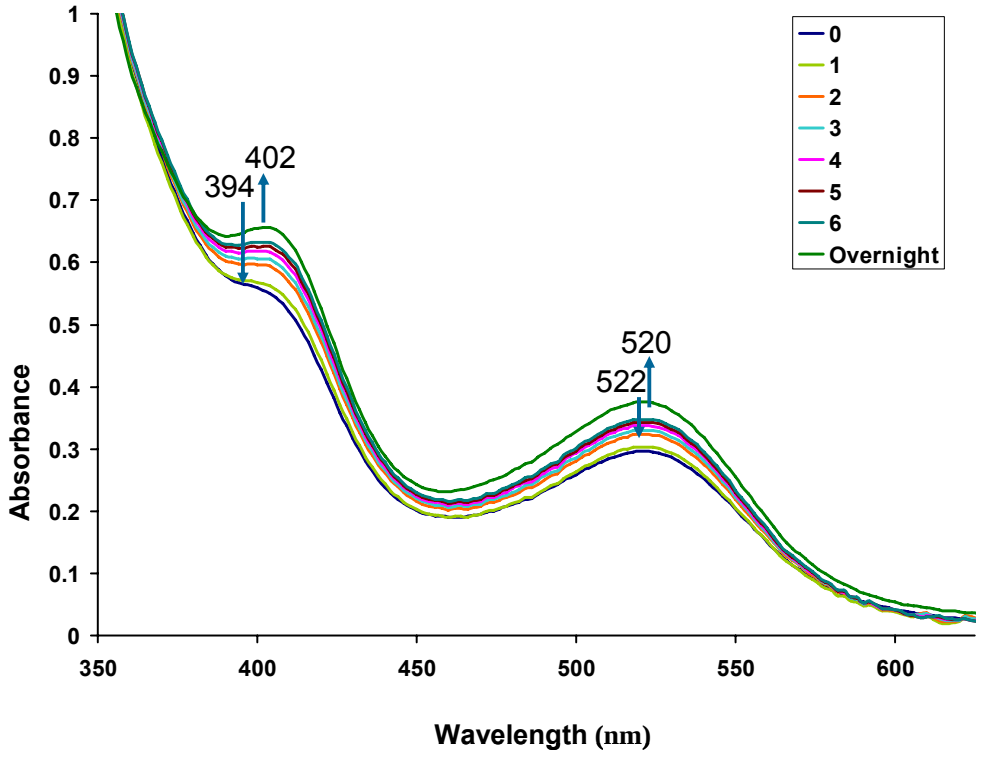

Figure IV-9. UV-Vis spectra of $[(\textbf{Ni-1})Pd(CH_3)(OEt_2)][BAr_4']$ was monitored in CH_2Cl_2 at 22°C.

Shown in Figure IV-10 are the UV-Vis spectra of a CH_2Cl_2 solution of [(**Ni-1**)Pd($C(O)CH_3$)(CO)][BAr'_4] under a CO atmosphere monitored over time to determine the relative stability of the complex. The maroon red complex exhibits similar d-d transitions to the [(**Ni-1**)Pd(CH_3)(OEt_2)]$^+$ derivative at 396 nm and 522 nm except for differences in molar absorptivities. Subtle spectral changes were observed after 6 hours indicating the formation of the trimetallic species in solution. The stability of the species was also monitored by infrared spectroscopy at 22°C, which confirms that under an atmosphere of CO the carbonylated derivative, [(**Ni-1**)Pd($C(O)CH_3$)(CO)]$^+$ is stable at for several hours. The lifetime of the product was enhanced when the solution was kept cold. Attempts to isolate the acetyl complex under a N_2 atmosphere thus far have been unsuccessful due to gradual decarbonylation. Regardless, under catalytic conditions addition of CO to the compound at 22°C under high pressure should not lead to rapid decomposition of the catalyst to form the trimetallic species.

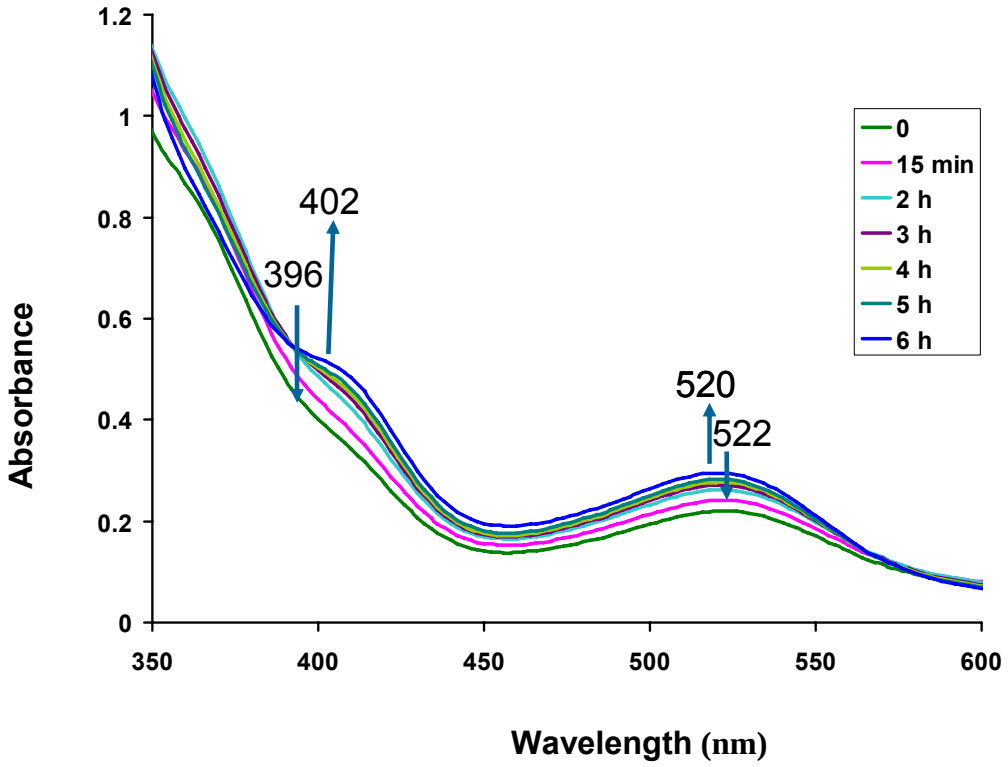

Figure IV-10. UV-Vis spectra of [(**Ni-1**)Pd(C(O)CH_3)(CO)][BAr′$_4$] was monitored in CH_2Cl_2 at 22°C.

^{13}C NMR Study of CO Addition to [Ni-1)Pd(CH_3)(OEt_2)][BAr′$_4$]

In order to study the migratory insertion chemistry of [(**Ni-1**)Pd(CH_3)(OEt_2)]$^+$ a 20 mM sample of the complex as its [BAr′$_4$]$^-$ salt was prepared at room temperature and cooled to -80°C prior to the addition of 7 bar ^{13}CO gas in a high pressure sapphire NMR tube (Figure IV-11). The ^{13}C NMR spectrum was recorded within 5 minutes of CO addition and transportation of the cold NMR tube to the NMR instrument that was pre-cooled to -80°C.

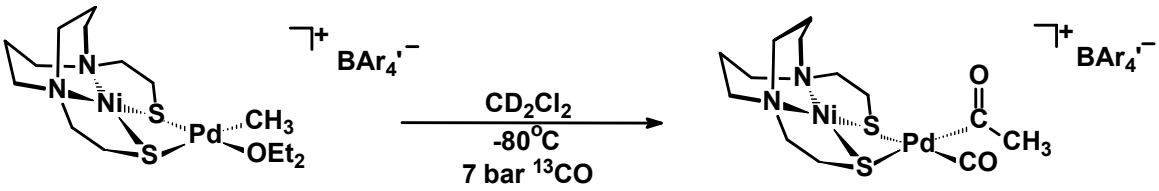

Figure IV-11. Reaction pathway used to observe the formation of the [(**Ni-1**)Pd(C(O)CH_3)(CO)][BAr $'_4$].

The ^{13}C NMR spectra were recorded at -80°C and at 10°C increments thereafter as the temperature was increased to 60°C (Figure IV-12). At -80°C the ^{13}C NMR spectrum displays three sharp signals in the CO region (Figure IV-12, a)). The large resonance at 185 ppm is assigned to free ^{13}CO dissolved in CD_2Cl_2. The signal at 225 ppm, shifted downfield from free ^{13}CO, is assigned to the carbonyl carbon of the acetyl group, (CO_a), coordinated to the palladium metal center while the resonance at 176 ppm, upfield from free ^{13}CO, is assigned to carbon of a terminal bound CO ligand, (CO_t). Resonances with asterisks represent minor impurities. The assignments were consistent with that of the [(o-phen)Pd(C(O)CH_3)(CO)]$^+$ complex reported by Brookhart and co-workers.[85] On warming the sample the resonance of the acetylated carbonyl derivative observed at -80°C does not grow in intensity. This suggested that CO/CH_3 migratory insertion was complete at -80°C. Consequently, the rate of insertion could not be determined. The fast rate of CO reaction and insertion with [(**Ni-1**)Pd(C(O)CH_3)(CO)]$^+$ thus limited the possibility of observing mechanistic intermediates prior to insertion such as the methyl carbonyl intermediate, [(L_2)Pd(CH_3)(CO)]$^+$ that was observed with the traditional ligands. Quantitative studies with classical ligands have determined the rate constant for migratory insertion in a diphosphine derivative, [(dppp)Pd(CH_3)(CO)]$^+$, is k_{obs} = 4.5x10$^-$

[5] sec^{-1} ($\Delta G^{\ddagger}$ = 14.8(1) kcal/mole, -81.7°C) and with a diimine derivative, [(o-phen)Pd(CH_3)(CO)]$^+$, is k_{obs} = 2.5x10^{-4} sec^{-1}, ($\Delta G^{\ddagger}$ = 15.4 kcal/mole, -66°C), respectively.[85,90] In these cases the methyl-CO intermediate could be observed. Thus it is evident that the rate of methyl migration on the palladium metal center is extremely rapid in the presence of the metallodithiolate ligand when compared to the classical ligands in similar cationic complexes.

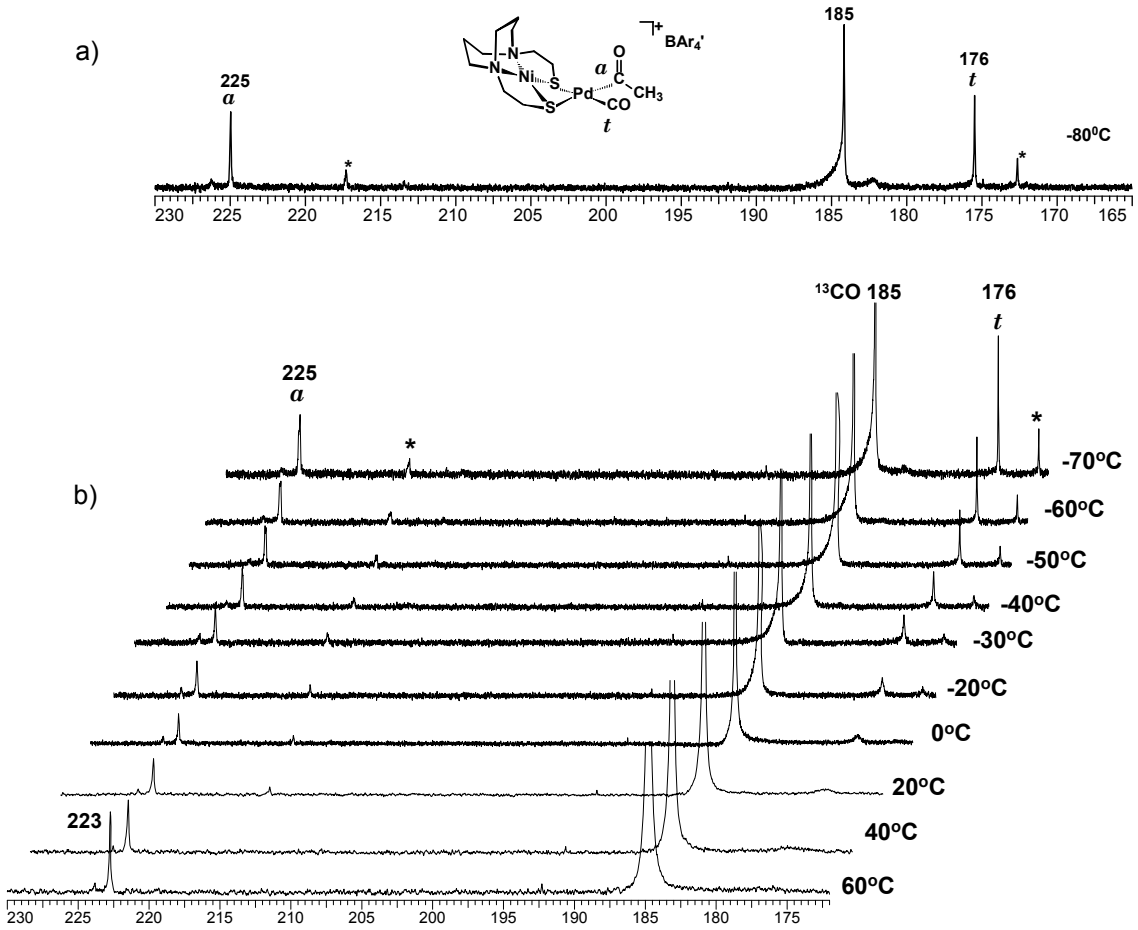

Figure IV-12. ^{13}C NMR study of CO uptake by the [(**Ni-1**)Pd(CH_3)(OEt_2)]$^+$ complex, a) -80°C and b) monitor of effect of temperature rise from -70°C to 60°C in a high pressure sapphire NMR tube at 7 bar of ^{13}CO. *Asterisks indicate minor impurities.

^{13}CO Exchange in [(Ni-1)Pd(C(O)CH$_3$)(CO$_t$)]$^+$

The ^{13}C NMR spectra of [(**Ni-1**)Pd(C(O)CH$_3$)(CO$_t$)]$^+$ between -80°C and 60°C illustrate that as the sample is warmed the terminal-bound CO$_t$ resonance at 176 ppm disappears with concomitant broadening of the free ^{13}CO signal at 185 ppm. This effect is the result of rapid ligand exchange between the terminal bound CO$_t$ and free ^{13}CO dissolved in solution. The acetyl signal at 225 ppm remains relatively sharp upon warming the sample indicating that this species is stable. A slight shift in resonance upfield to 223 ppm will be addressed later.

The rate of exchange and the activation barrier for the (Pd-^{13}CO$_t$)/free (^{13}CO) exchange in [(**Ni-1**)Pd(C(O)CH$_3$)(CO$_t$)]$^+$ was calculated from the following equations: $k_r = 1/\tau$; $\tau_{coalesence} = (\sqrt{2}\pi\Delta\nu)^{-1}$; and $\Delta G^{\ddagger} = -RT\,[\ln(k/T) + \ln(h/k_b)]$). The exchange rate constant was calculated at the coalescence temperature of 40°C (313 K) and the error indicated for the activation barrier is from calculations made for coalescence temperatures of ± 10°K on either side of 313 K.

$$\tau = 2.06 \times 10^{-4}\ k^{-1} \quad \text{(at 313 K)}$$

$$k_r = 4.80 \times 10^{3}\ s^{-1} \quad \text{(at 313 K)}$$

$$\Delta G^{\ddagger} = 54.8\ (\pm 1.8)\ \text{kJ/mol (at 313 K)}$$

Rapid terminal CO_t exchange may occur via a dissociative or associative pathway, Figure IV-13. Ligand dissociation *via* Ni-S or Pd-CO bond breaking (path B or C would result in the formation of a 14-electron intermediate with an open site for CO to bind resulting in a stable square planar 16-electron complex. However, such a process is unlikely at low temperature. An associative pathway is a more reasonable and thermodynamically favored route to ligand exchange (path A) concomitantly forming a 5-coordinate square pyramidal, 18-electron species, Figure IV-13. A 5-coordinate associative pathway would also account for the deinsertion process that is required for the apparent incorporation of some of the 13-C label into the acetyl site observed in the infrared ^{13}CO exchange study in $[(\mathbf{Ni\text{-}1})Pd(C(O)CH_3)(CO)]^+$. This is similar to a ligand exchange process confirmed to be associative by Brookhart and co-workers in which the alkyl carbonyl complex, (o-phen)$Pd(CH_3)(^{12}CO)$, underwent rapid exchange in the presence of ^{13}CO.[85] On the other hand, the Pd-S bond strength in the NiS_2Pd chelate system is unknown and the breaking of one NiS_2—Ni bond in the theoretical model of acetyl CoA synthase was computed as a probable route for creating the open site required for CO uptake and catalysis.[23]

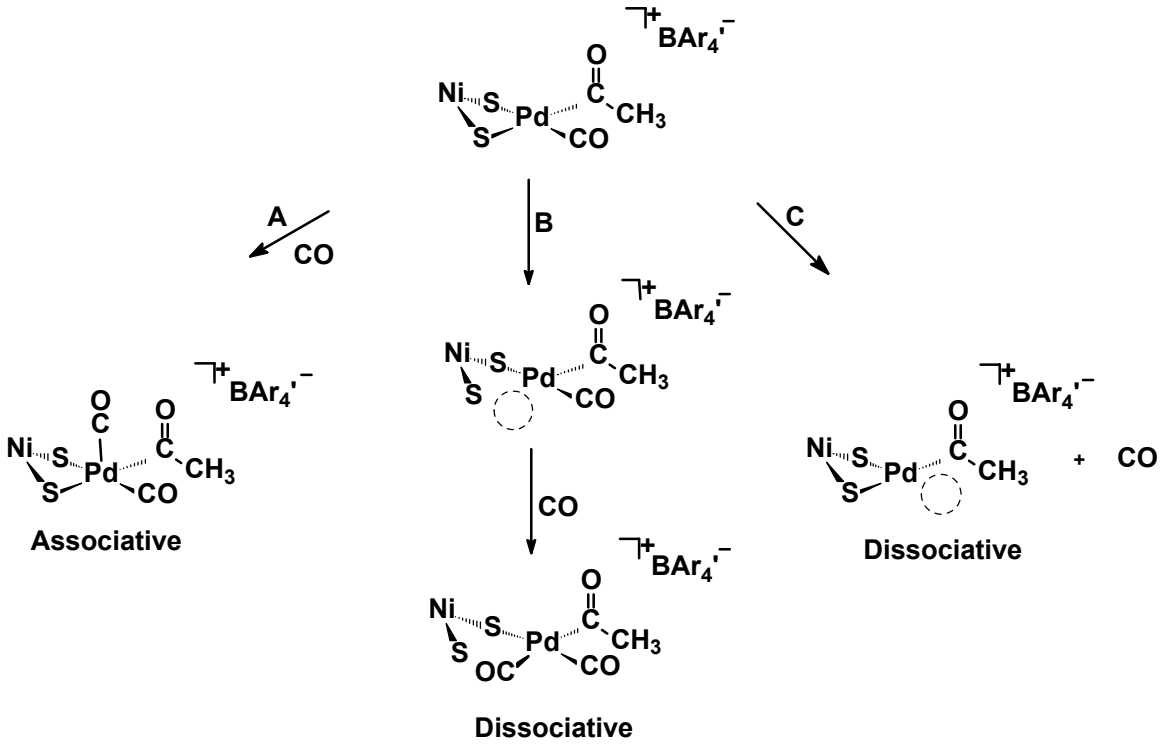

Figure IV-13. Possible reaction mechanism for CO exchange in [(**Ni-1**)Pd(C(O)CH$_3$)(CO)]$^+$.

^{13}C NMR Study of CO Addition to (Ni-1)Pd(CH$_3$)(Cl)

The same procedure as described above was applied for CO addition to the neutral (**Ni-1**)Pd(CH$_3$)(Cl) complex as shown in Figure IV-14. A 20 mM sample was pressurized with 8 bar of isotopically labeled ^{13}CO gas at -80^{o}C and the ^{13}C NMR spectrum was recorded in the pre-cooled NMR probe 5 minutes after CO addition.

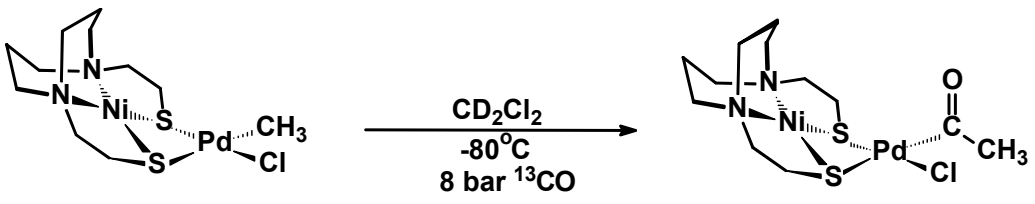

Figure IV-14. Reaction pathway used to observe the formation of (**Ni-1**)Pd(C(O)CH$_3$)(Cl).

The ^{13}C NMR spectrum of this solution recorded at -80^{o}C in CD_2Cl_2 displays three sharp resonances in the CO region, Figure IV-15. The resonance for free ^{13}CO dissolved in solution is observed at 185 ppm while the signal shifted downfield relative to free ^{13}CO at 226 ppm is assigned to the carbon of the acetyl, (CO_a), on the palladium metal center. This is in agreement with CO addition to similar neutral complexes of the type $L_2Pd(CH_3)(Cl)$ complex (L = diimine) to form the acetylated derivatives, $L_2Pd(C(O)CH_3)(Cl)$.[91] The infrared spectrum of the acetylated (**Ni-1**)Pd(C(O)CH_3)(Cl) also show an ν(C=O) stretch at 1692 cm^{-1}, in agreement with the ν(C=O) stretching frequency (1690 cm^{-1}) of the (bipy)Pd(C(O)CH_3)(Cl) complex.[17] It is important to note that a terminal bound CO ligand was not observed in the CO region of the NMR spectrum. Upon warming the solution from -70°C to 20°C, the resonance assigned to the carbon of the acetyl ligand did not intensify. This signifies that CO addition to the neutral complex, (**Ni-1**)Pd(CH_3)(Cl), was complete at -80°C and hence it was surprising to note that the rate of insertion was as rapid as the cationic [(Ni-1)Pd(CH_3)(OEt_2)]$^{+}$derivative. The rate of CO/CH_3^{+} migratory insertion with (bipy)Pd(CH_3)(Cl) was determined to be $k_r = 4.05x10^{-4}$ s^{-1} at 20°C.[17]

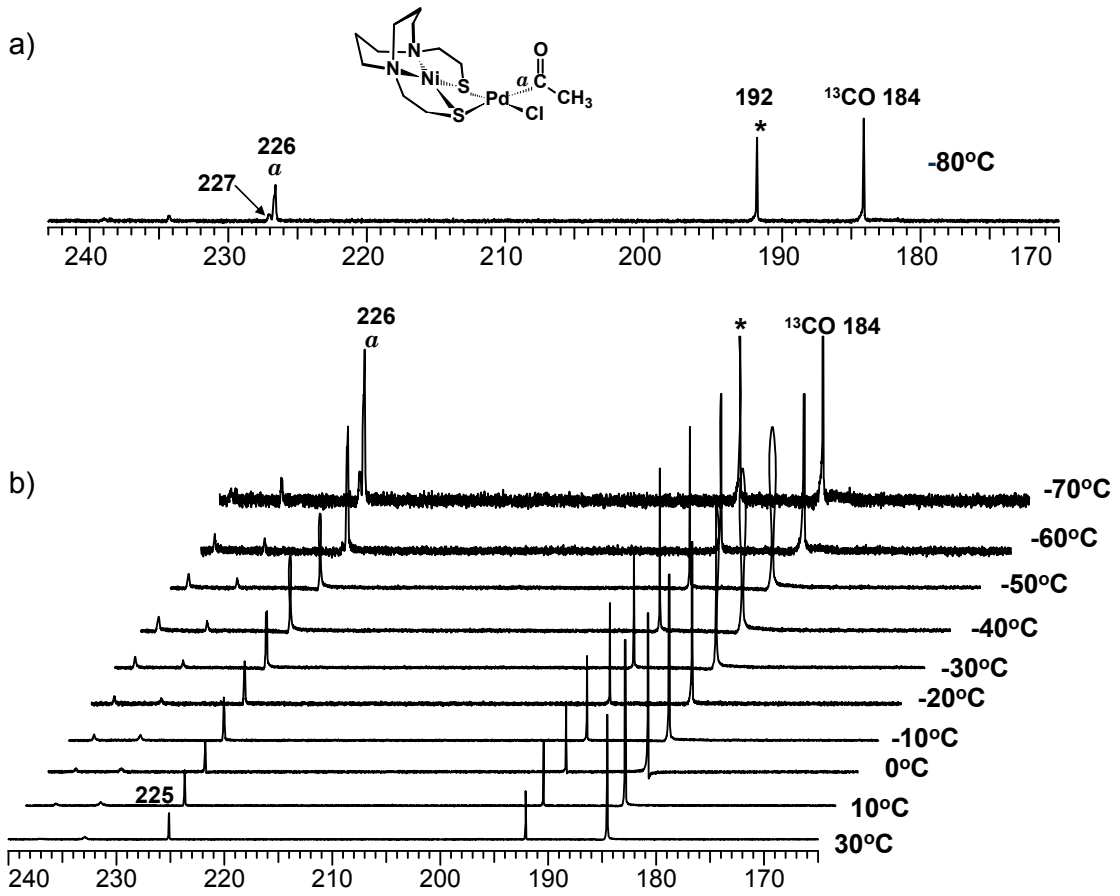

Figure IV-15. ^{13}C NMR spectra of CO uptake by (**Ni-1**)Pd(CH_3)(Cl). a) -80°C b) monitor of effect of temperature rise from -70°C to 30°C. in a high pressure sapphire NMR tube at 8 bar of ^{13}CO. *Asterisks indicate $Ni(CO)_4$ an unfortunate impurity from the regulator.

The large resonance observed at 192 ppm is assigned to the carbonyl ligands of $Ni(CO)_4$, an unfortunate impurity from a reaction between ^{13}CO gas trapped in a gas regulator composed of a nickel alloy. The chemical shift of the carbonyl ligands in $Ni(CO)_4$ in CD_2Cl_2 was consistent with that reported by Levason et al. at 192 ppm.[92]. That the $Ni(CO)_4$ formation was not the result of a decomposition reaction formed by oxidation of the thiolate donors to form disulfide reducing Ni^{2+} to Ni^0 in the presence of CO was explored by the following experiment. Addition of ^{13}CO to the free

metallodithiolate ligand over an extended period did not result in $Ni(CO)_4$ formation. In addition, two unidentifiable smaller resonances were observed downfield from the carbon acetyl signal at 234 and 239 ppm respectively. The ^{13}C NMR spectrum of the sample after being depressurized of CO followed by a slight argon purge at 20°C showed a significant decrease in the resonance signals for free ^{13}CO and $Ni(CO)_4$ dissolved in solution. The carbonyl acetyl signal however remained sharp and unchanged, re-affirming that the (Ni-1)Pd(C(O)CH_3)(Cl) species was stable. Other interesting features observed in the ^{13}C NMR spectra is a small resonance at 227 ppm and the slight line broadening of the acetyl signal that occurs as the temperature. This will be addressed later.

Possible Mechanism of CO Addition/Migratory Insertion to (Ni-1)Pd(CH_3)(Cl)

The observance of an acetyl group on a neutral 16-electron square planar metal center raised several important mechanistic questions concerning how CO addition occurred and the enhanced rate of migratory insertion observed on a neutral (L_2)Pd(CH_3)(X) complex. In addition to the preliminary results reported herein, the following proposed mechanism is based on a large part from conclusions drawn by van Leeuwen *et al.* about CO addition/migratory insertion reactions in neutral methyl(chloro) palladium(II) complexes with α-diimine type ligands.[17] Whereas chloride dissociation would provide an open site for CO addition followed by migratory insertion (Figure IV-16, path A), this is an unlikely route since a ligand dissociation pathway at low temperature is thermodynamically unfavorable. Additionally, the absence of a terminal-

bound CO in the terminal bound CO region of the NMR spectrum at -80°C disfavors a Cl^- dissociation pathway.

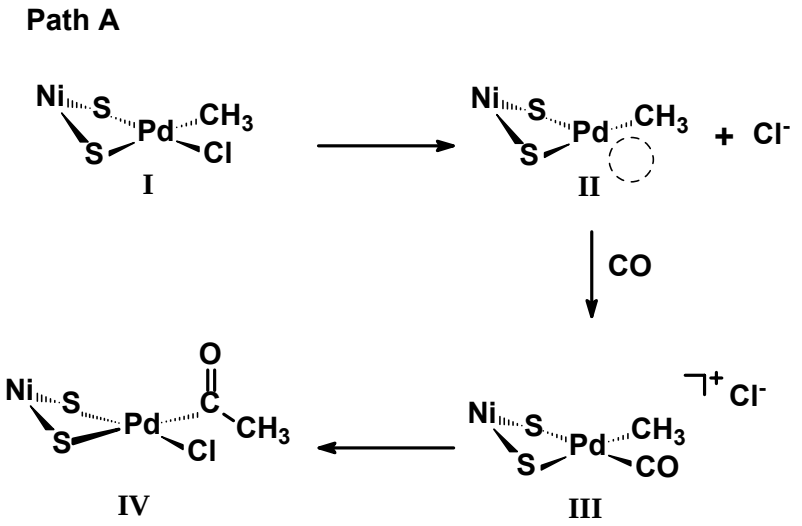

Figure IV-16. Possible reaction pathway for CO addition/insertion in (**Ni-1**)Pd(CH_3)(Cl).

Alternatively, in the tentatively proposed mechanism by van Leeuwen and co-workers, the α-diimine has the ability to coordinate in a bidentate fashion or monodentate fashion largely governed by bulky subsituents that are close in proximity to one of the nitrogen donors on a bidentate ligand.[17] Metallodithiolate ligands can also adopt mono- and bidentate coordination modes.[25,31] In Chapter III the hemilabile property of NiN_2S_2 ligands was explored in which M-S bond breaking was found to occur at room temperature to open up coordination sites on coordinatively saturated metal centers. However, it is less likely that ligand dissociation by Pd-S bond breaking opening a coordination site (**V**) for CO addition (**VI)** followed by isomerization (**VII**)

such that the CO and CH_3 are mutually cis to each (Figure IV-17, path A) at low temperature. Even if ligand dissociation occurred, migratory insertion will not occur when the CH_3 is trans to the Cl^-. This intermediate would have to submit to partial Cl^- dissociation followed by reassociation to form a 5-coordinate intermediate (**VIII**) that would be more favored. It is noteworthy to mention that in a dissociative pathway CO addition would be in competition with ring closing (**XII**) so there would not be an appreciative amount of the terminal-bound CO accumulation that would be observable by NMR spectroscopy. An associative pathway is a more conceivable direct route for CO addition to the square planar complex (**I**) to form the (**Ni-1**)Pd(C(O)CH_3)(Cl)(CO) intermediate (**VIII**) followed by migratory insertion (**X**) (Figure IV-17, path C). Van Leeuwen has suggested that regardless of the mechanistic path, an intermediate such as (**VIII**) would be distorted from planarity, positioning the CO and CH_3 groups closer together for migratory insertion, whereas a trigonal bipyrimidal intermediate (**IX**) would hinder migration and would not be a likely intermediate.[17] In addition, Natile and co-workers have shown that ligands that are a good π acceptors such as CO in a 5 coordinate complex would relieve some of the electron density from the metal center facilitating insertion.[93] Hence, 5 coordinate intermediate with a metallodithiolate ligand with a small S-Pd-S bite angle (77°) would be a reasonable intermediate for CO insertion and would account for the rapid rate of migratory insertion in a neutral square planar 16 electron complex with no open coordination sites for CO to bind.

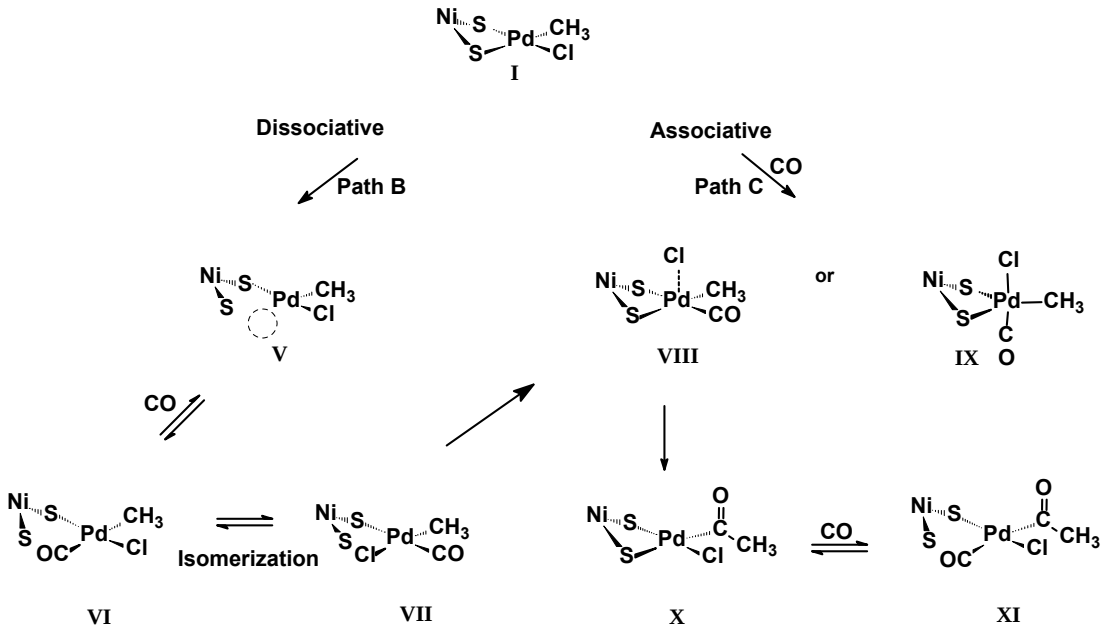

Figure IV-17. Alternative reaction pathways B and C for CO addition/insertion in (**Ni-1**)Pd(CH_3)(Cl).

CO addition to (Ni-1)Pd(CH_3)(Cl) Monitored by Infrared Spectroscopy

Infrared spectroscopy can provide additional information about short-lived intermediates that are not observed by NMR spectroscopy. Hence the infrared spectrum of (**Ni-1**)Pd(CH_3)(Cl) following CO addition in CH_2Cl_2 was also recorded. The infrared spectrum at approximately -78°C shows two bands in the ν(C=O) region; a strong infrared active band at 1692 cm^{-1} and a shoulder at 1663 cm^{-1}, indicative of metal-bound acetyl ligands (Figure IV-18). At room temperature, the infrared spectrum of the carbonylated derivative shows an additional ν(CO) stretch at 2041 cm^{-1} in the terminal bound CO region, which increases in intensity upon standing. This band was shifted by 45 cm^{-1} to 1996 cm^{-1} in the presence of ^{13}CO gas (10 min reaction time) and disappears upon removal of the solvent under vacuum leaving the ν(CO) stretch of the Pd-acetyl

intact. A ^{13}C NMR spectrum of an isotopically enriched sample prepared at 25°C and left over several hours displays the characteristic resonances at 20°C in addition to a signal at 166 ppm. While this resonance might suggest a terminal bound CO ligand, the chemical shift is further upfield in the NMR spectrum to where a signal for a terminal bound CO would be expected.

Based on these results it is tempting to assign ν(CO) stretches at 2041 and 1663 cm^{-1} to an acetylated carbonyl complex, (**Ni-1**)Pd(C(O)CH_3)(Cl)(CO), however, at this point there is no direct evidence to support these assignments. The fact that the intensity of the acetyl band at 1663 cm^{-1} does not increase or shift in the infrared spectrum with concurrent growth of the ν(CO) stretch at 2041 cm^{-1} is evidence that the ligands are not within the same chemical environment. Hence, any assignments that would be made for the proposed solution structures of the terminal CO-bound pentacoordinate (**Ni-1**)Pd(C(O)CH_3)(CO)(Cl) or tetracoordinate (**Ni-1**)Pd(C(O)CH_3)(Cl)(CO), (**XI**), intermediates would be unfounded. It is interesting to note that similar intermediates have been spectroscopically observed by infrared and NMR spectroscopy with bidentate mixed phosphine-nitrogen donor ligands on methyl-chloro Pt metal complexes.[94] Alternatively, while the formation of $Pd^0(CO)_4$ is a possibility, the ^{13}C NMR of the isotopically labeled product did not provide any evidence in the 190 ppm region that would suggest the formation of this species at room temperature. At this point, no tentative conclusion about the identity of this product observed at 2041 cm^{-1} can be made.

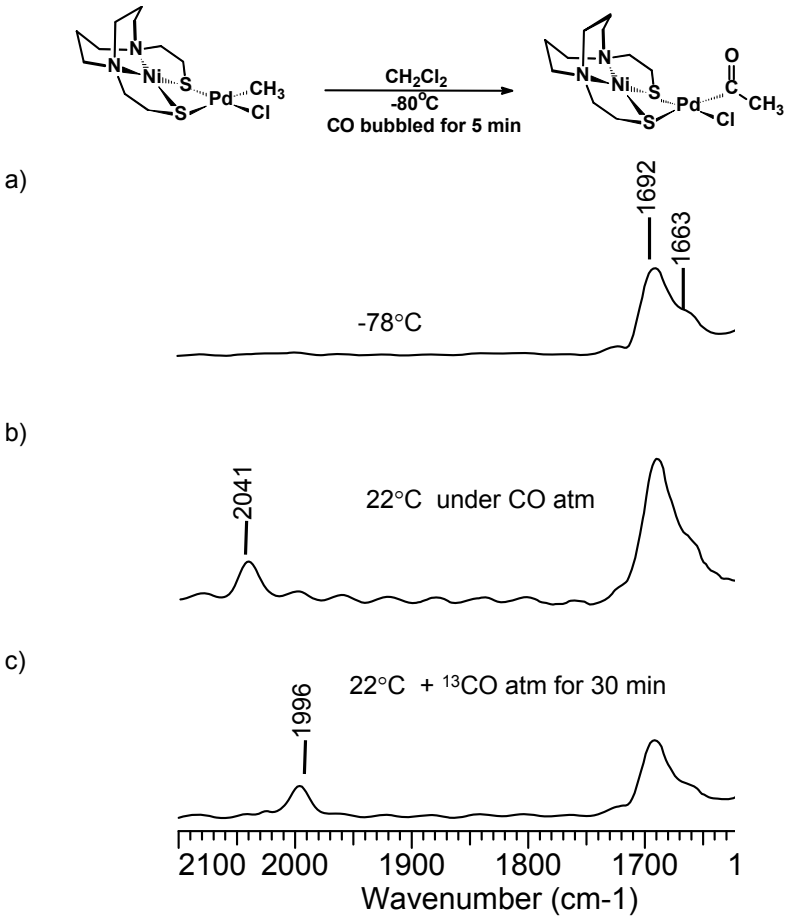

Figure IV-18 Infrared spectra of CO addition to (**Ni-1**)Pd(CH_3)(Cl) at a) -78°C, b) 22°C under a CO atmosphere and c) after 30 min under a ^{13}CO atmosphere at 22°C.

^{13}C NMR Spectroscopic Monitor of (Ni-1)Pd(C(O)CH_3)(Cl) on Warming

The ^{13}C NMR spectrum at -80°C of the (**Ni-1**)Pd(C(O)CH_3)(Cl) complex showed a small secondary feature at 227 ppm slightly downfield from the carbon of the acetyl resonance at 226 ppm. This resonance feature suggested the presence of a second chemically distinct acetyl group. Upon warming the sample to -50°C the signals at 226 ppm and 227 ppm diminish and only one resonance is apparent at 225 ppm at 30°C. Resolution enhancement of this resonance was achieved by applying a sine bell function

during data processing. This technique indicated two chemically distinct signals between -50°C and -10°C (Figure IV-19). Upon warming the sample both signals shift concurrently as the signal at 227 ppm grew in intensity and that at 226 ppm diminished. Therefore, only one signal was observed at 225 ppm at 0°C.

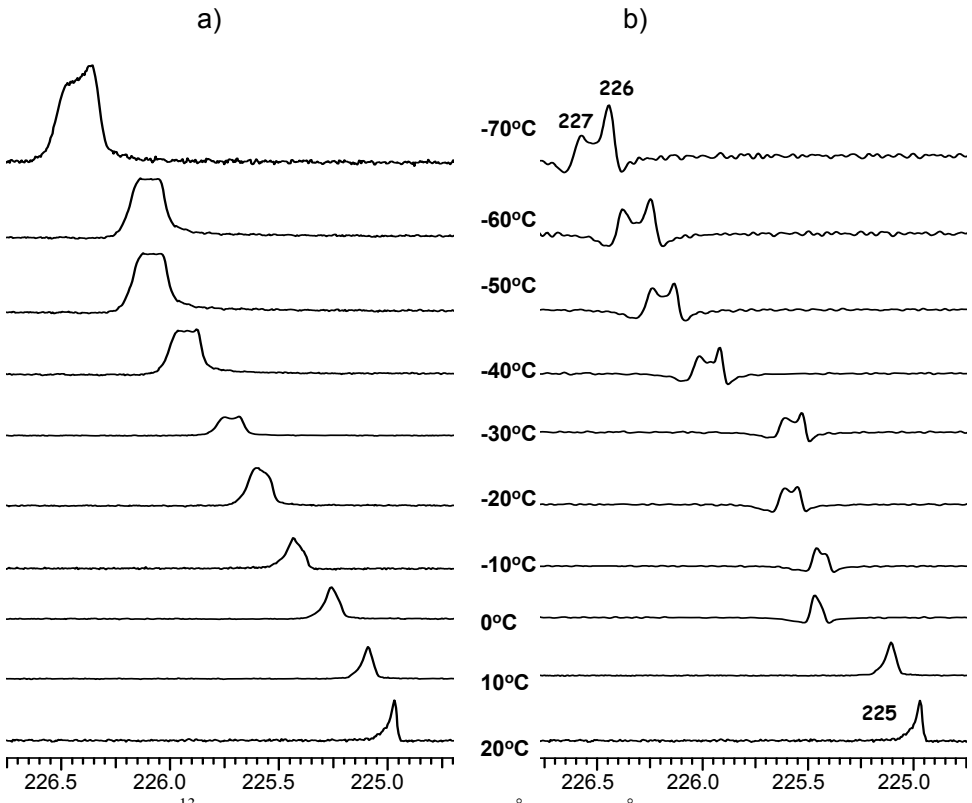

Figure IV-19 a) Low field ^{13}C NMR spectra between -70°C and 20°C of CO acetyl resonance of (**Ni-1**)Pd(C(O)CH_3)(Cl). a) normal resolution and b) resolution enhancement by a sine bell function (sb = 0.130 sec).

This behavior on the NMR time scale might best be explained by analysis the solid state structure of (**Ni-1**)Pd(CH_3)(Cl) and a suggested solution structure of (**Ni-**

1)Pd(C(O)CH)$_3$(Cl) at low temperature. The solid state structure of the (**Ni-1**)Pd(CH)$_3$(Cl) has a dihedral angle (defined by the intersection of the NiN_2S_2 plane and $PdS_2Cl(CH_3)$ plane of 101.3° (Figure IV-20, a).[75] The molecular structures of several acetyl palladium compounds illustrate that the acetyl ligand is oriented perpendicular to the square plane of the metal center (defined by PdL_2C_2 plane) as seen with the (L_2) Pd(C(O)CH$_3$)(X).[85,17] A qualitative view of the suggested solution structures of (**Ni-1**)Pd(C(O)CH)$_3$(Cl) position the acetyl group perpendicular to the PdS2CCl plane (Figure IV-20, b) in close contact with the CH_2 groups of the diazacycle backbone with the CH_3 group oriented below the square plane. An alternative solution structure (Figure IV-19, c)) features the carbonyl of the acetyl ligand rotated away from the metallodithiolate ligand so that there is less steric influence by the CH_2 groups from the diazacycle backbone of the NiN_2S_2 ligand, which positions the CH_3 group in closer contact with the NiN_2S_2 ligand.

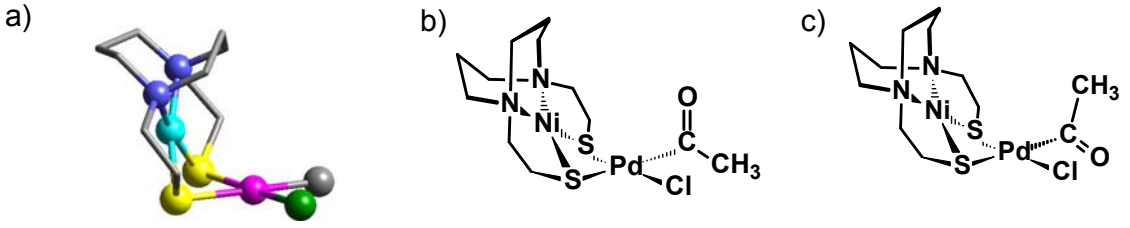

Figure IV-20 a) Ball-and-stick representation of (**Ni-1**)Pd(CH$_3$)(Cl) illustrating the small dihedral angle of 101.3°. The suggested stick drawings of the solution structure of acetyl derivative, (**Ni-1**)Pd(C(O)CH)$_3$(Cl) a) carbonyl perpendicular to the PdS_2CCl plane c) carbonyl rotation of 180° away from the NiN_2S_2 plane.

The degree of steric influence imposed on a acetyl group by the **Ni-1** ligand in a suggested solution structure of (**Ni-1**)Pd(C(O)CH_3)(Cl) is best illustrated by a Cerius model overlay of the molecular structure of (**Ni-1**)Pd(CH_3)(Cl) and [(o-phen)Pd(C(O)CH_3)(CO)]$^+$ complex (Figure IV-21).

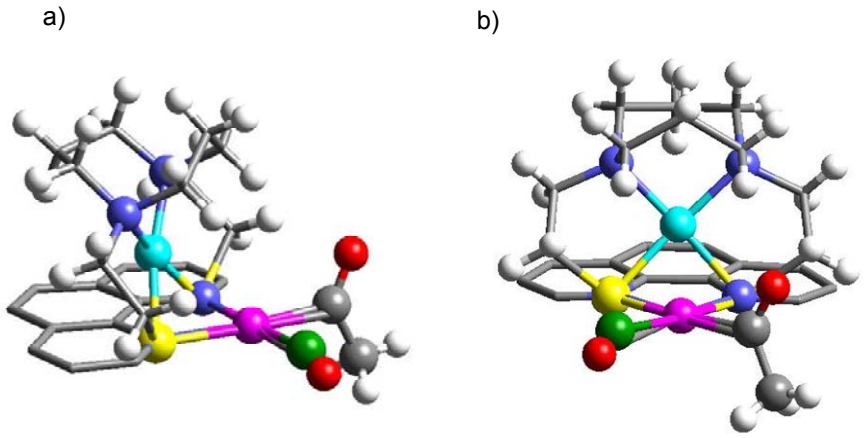

Figure IV-21 Two molecular views of the overlay of (**Ni-1**)Pd(CH_3)(Cl) and [(o-phen)Pd(C(O)CH_3)(CO)]$^+$ illustrating the orientation acetyl group perpendicular to the PdS_2CCl and the steric influence by **Ni-1**. Hydrogen atoms added on the Ni-1 ligand and the CH_3 group of the acetyl.

At -80°C the low thermal motion of the molecule renders the ligands in a relatively rigid position so that the chemically distinct resonance at 226 ppm is favored over the smaller signal at 227 ppm. As the temperature is raised, the metallodithiolate might rotate *via* inversion at the sulfur hinge or the carbonyl group of the acetyl rotate by 180° away from the NiN_2S ligand so there is minimal contact between the ligands

(Figure IV-22). At 30°C the rotational process is rapid so only one signal is observed at 225 ppm.

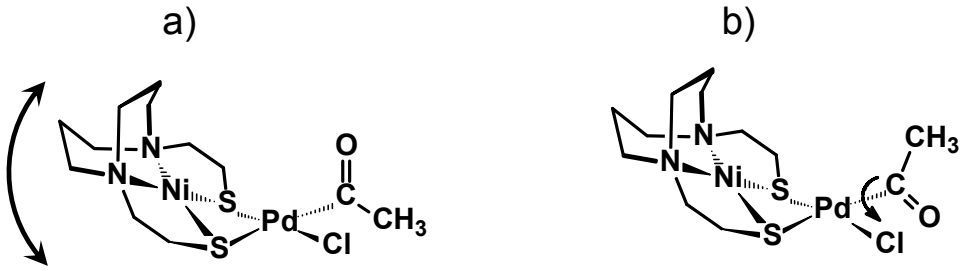

Figure IV-22. Stick drawings illustrating a) mutual buckling of the NiN_2S_2 ligand and $Pd(C(O)CH_3(Cl)$ unit at the sulfur hinges and b) carbonyl acetyl bond rotation.

Evidence for the mutual buckling of the NiN_2S_2 ligand and the $Pd(C(O)CH_3(Cl)$ unit at the sulfur hinges comes from a variable temperature study of a $NiN_2S_2W(CO)_4$ complex, (**Ni-1***)$W(CO)_4$, in which the mutually trans CO ligands equilibrated at 90°C as discussed in Chapter III. When the sample is cooled back to -30°C both carbonyl signals reappear indicating the process is reversible. It is also worth mentioning that this same behavior was also observed for the $[(\textbf{Ni-1})Pd(C(O)CH_3)(CO)]^+$ complex. This rotational behavior in the $[(\textbf{Ni-1})Pd(C(O)CH_3)(CO)]^+$ and (**Ni-1**)$Pd(C(O)CH_3)(Cl)$ complexes delineates the line broadening observed between -70°C and 40°C and between -70°C and 0°C respectively.

^{13}C NMR Study of CO and Ethylene Uptake by [Ni-1)Pd(CH_3)(OEt_2)][BAr'_4]

To observe possible intermediates during copolymer formation the reaction progress of ^{13}CO and ethylene gas uptake was monitored by ^{13}C NMR spectroscopy. A 21 mM sample of [(**Ni-1**)Pd(CH_3)(OEt_2)]$^+$ in CD_2Cl_2. was pressurized with 8 bar of ^{13}C-labeled CO gas at -80°C and the ^{13}C NMR spectrum was recorded within a 5 minute time period with results as described above (Figure IV-12), i.e., two resonances appear at 225 ppm and 176 ppm characteristic of the acetyl carbonyl complex, [(**Ni-1**)Pd(C(O)CH_3)CO)]$^+$. In addition the two resonances observed for free ^{13}CO and $Ni(CO)_4$ were evident.

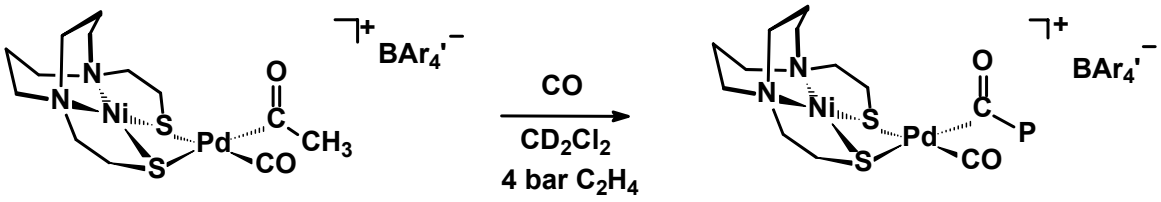

Figure IV-23. Reaction pathway for ethylene addition to [(**Ni-1**)Pd(C(O)CH_3)CO)]$^+$.

While maintaining a constant temperature at -80°C, the sample was depressurized to 1 bar followed by addition of ethylene to a total pressure of 5 bar (Figure IV-23). The ^{13}C NMR was spectra recorded at -80°C within a 5-minute period and at temperature increases in every 10°C increments thereafter. There was no spectral change within 5 minutes of ethylene addition. Upon warming the sample the only spectral change observed is that previously described for [(**Ni-1**)Pd(C(O)CH_3)CO)]$^+$ complex. In the

temperature range of -20°C to 20°C, the growth and disappearance of several new resonances between 230 ppm and 205 ppm were observed, (Figure IV-21). The carbon of the acetyl shifts slightly to 224 ppm at 0°C while another signal at 225 ppm, CO_c, suggests an additional acetyl ligand (Figure IV-23, b). This resonance might be a [(**Ni-1**)Pd(C_c(O)CH_3)(η^2-CH_2=CH_2)]$^+$ intermediate. Brookhart and co-workers have shown that the carbonyl resonances of [(o-phen)Pd(C(O)CH_3)(η^2-CH_2=CH_2)]$^+$ shifted by ca. 6 ppm upfield relative to the carbon acetyl resonance of [(o-phen)Pd(C(O)CH_3)(CO)]$^+$ (Table 4-1).[85] However, the difference in chemical shift is much greater with the diimine ligand than the metallodithiolate, **Ni-1**, ligand.

Table IV-1. Comparison of ^{13}C NMR Shifts of [(L_2)Pd(C(O)CH_3)(η^2-CH_2=CH_2)]$^+$ and [(L_2)Pd(C(O)CH_3)(CO)]$^+$ Complexes with the NiN_2S_2 and o-phen Ligands.

Ligand	[(L_2)Pd(C(O)CH_3)(CO)]$^+$	[(L_2)Pd(C(O)CH_3)(η^2-CH_2=CH_2)]$^+$
	^{13}C NMR (ppm)	
o-phen	217	223
Ni-1	224	225

The resonances at 20°C observed downfield relative to the acetyl signal at 208, 207 and 206 ppm were assigned to the carbon signals from ketone-like end groups after three consecutive CO/ethylene insertions in [(**Ni-1**)Pd(C(O)CH_3)CO)]$^+$ forming a growing polymer chain (Figure IV-24, c). This is consistent with a decrease in the concentration of free ^{13}CO in solution. No change was observed in the intensity of the

resonance at 192 ppm assigned to $Ni(CO)_4$. Note that solubility of a growing polymer chain is limited in CD_2Cl_2 so that polymer begins to precipitate out of solution.

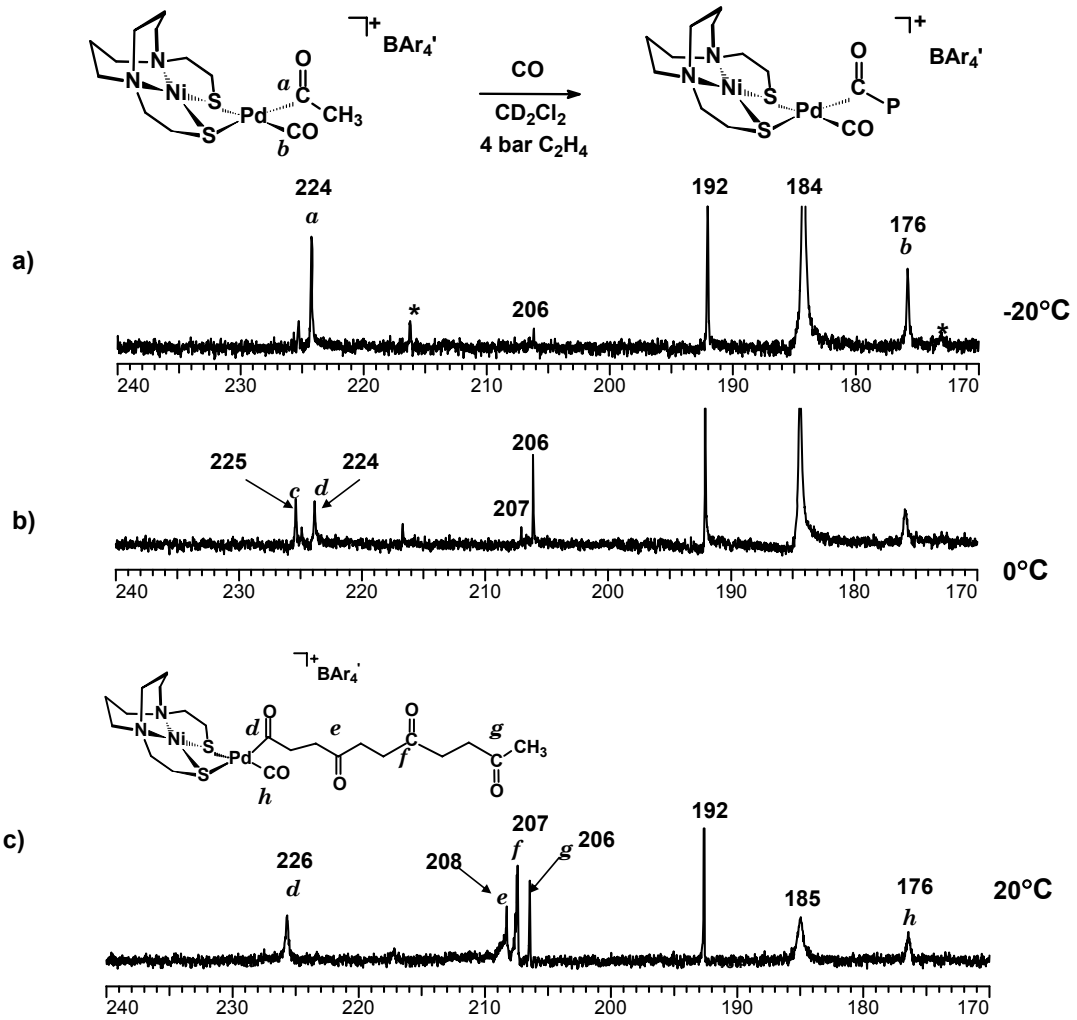

Figure IV-24. ^{13}C NMR spectra monitor of the reaction of ethylene with $[(\textbf{Ni-1})Pd(C(O)CH_3)CO)]^+$ over a temperature range of -20°C to 20°C.

Since no spectral changes were observed at temperatures lower than -20°C it can be concluded that ethylene does not replace CO easily. The appearance of new signals at T > -20°C suggests that that a CO/CH_2=CH_2 reaction has occurred along with some ethylene insertion. As shown in Figure IV-25, ethylene displacement of CO in the resting state of the catalyst, [(o-phen)Pd(C(O)CH_3)(CO)]$^+$, to form the ethylene acetyl complex, [(o-phen)Pd(C(O)Me)(η^2-CH_2CH_2)]$^+$, is thermodynamically uphill.[85] Therefore, it is reasonable that a metal center with a very electron rich ligand will prefer to have a good π acceptor ligand like CO rather than ethylene as evidenced by the presence of a Pd bound terminal CO trapped species during the reaction. Hence, the resting state of the catalyst with a metallodithiolate ligand is the [(Ni-1)Pd(C(O)CH_3)(CO)]$^+$ (a) species and ethylene insertion is slow due high binding affinity of CO for the Pd^{2+} metal center (Figure IV-25).

The absence of resonances in the 240 ppm region, indicate that the CO trapping of the ethylene inserted species is highly favorable such that 5-membered β-chelate (c) and 6-membered γ-chelate (d) intermediates (Figure IV-25) were not observed during the CO/C_2H_4 reaction as was seen with the diimine Pd-metal based systems.[85] The catalytic resting state in the presence of a metallodithiolate ligand therefore is a contrast to the resting states observed for the diphosphine ligands in which the chelate forms are predominant.[89]

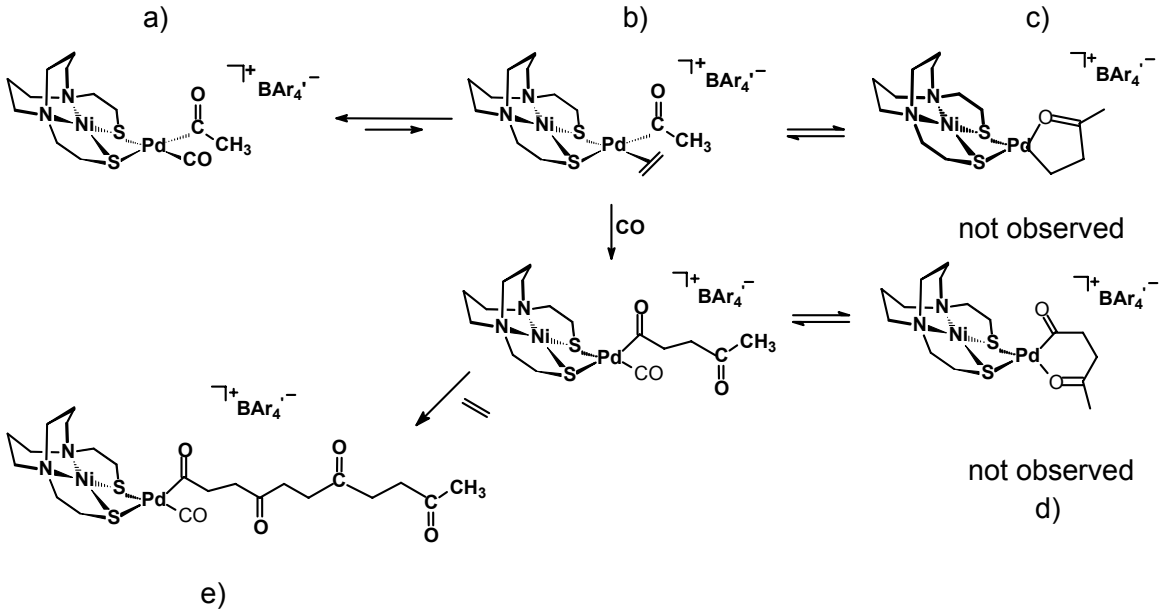

Figure IV-25. Proposed mechanistic cycle for CO/C_2H_4 migratory insertion.

CO/Ethylene Copolymerization with [(Ni-1)Pd(CH_3)(OEt_2)][BAr′$_4$]

Having shown that CO and ethylene insertion can occur with the [(**Ni-1**)Pd(CH_3)(OEt_2)]$^+$, bulk copolymerization studies were conducted. The catalytic species was formed *in situ* by reacting the (**Ni-1**)Pd(CH_3)$_2$ and HBAr′$_4$ precursors in pre-dried glassware. The catalyst was pressurized in a stainless steel high pressure Parr autoclave at room temperature with CO followed by ethylene. Over the course of 24 hr at room temperature, a light gray to white product precipitated from the reaction mixture that is characteristic of polyketone. Polyketones are known to be soluble in polar and acidic solvents such as hexafluroisopropanol, which allowed for easy analysis by NMR, IR and Mass Spectroscopy. Shown in Figure IV-26 is a typical infrared spectrum of the polymer with a distinctive ν(C=O) stretch at 1704 cm^{-1} in the C=O region (ν(C=O), KBr

= 1692 cm^{-1}) from subsequent CO groups incorporated in the polymer backbone. This is consistent previous with results by Sen and co-workers; ν(C=O) stretch of 1695 cm^{-1} (KBr) for alternating polyketone.[86]

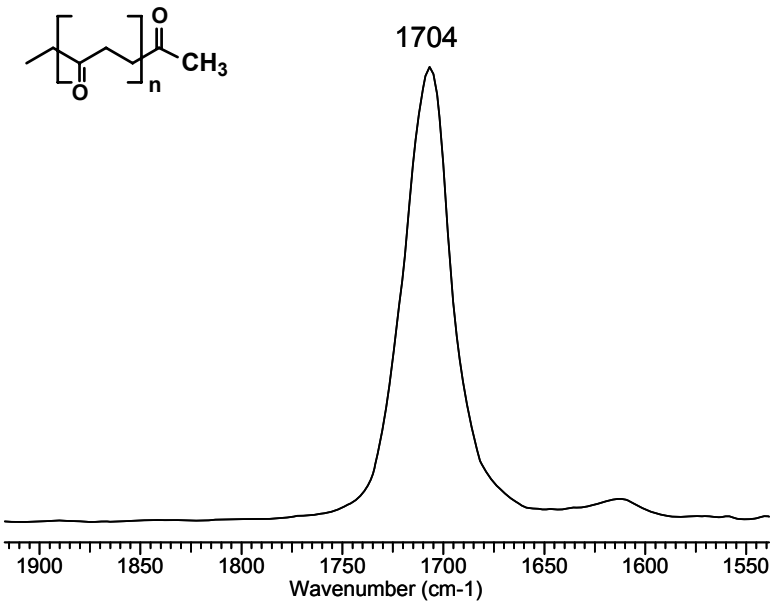

Figure IV-26: Infrared spectrum of alternating CO/C_2H_4 copolymer dissolved in hexafluroisopropanol at 22°C with the [(**Ni-1**)Pd(CH_3)(OEt_2)]$^+$ catalyst.

The room temperature ^{13}C NMR spectrum of the copolymer displays two resonances at 220 ppm and 43 ppm, corresponding to the C=O moiety and α-CH_2 groups from ethylene insertion respectively (Figure IV-27). Again, this is similar to literature reports.[95]

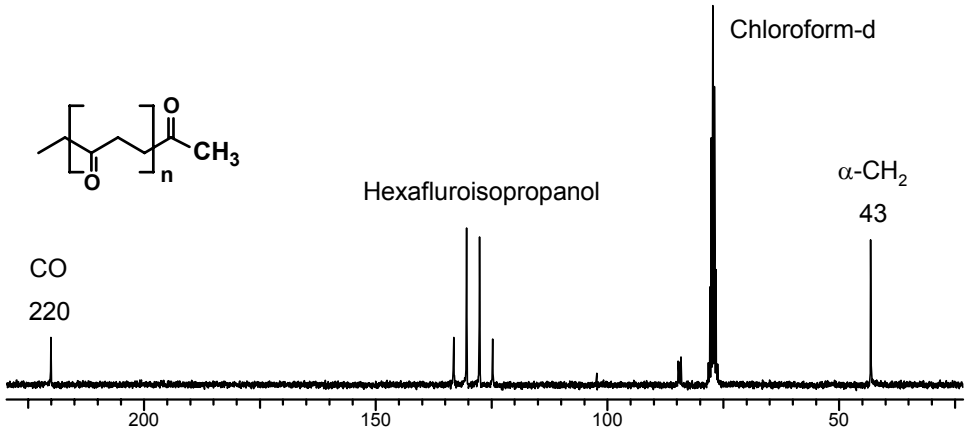

Figure IV-27. Typical ^{13}C-NMR spectrum of alternating CO/C_2H_4 copolymer dissolved in a mixture of hexafluroisopropanol (60%) and $CDCl_3$ (60%) at 22°C in which the catalyst was [(**Ni-1**)Pd(CH_3)(OEt_2)]$^+$.

Mass spectral analysis of the red product collected after several polymer runs in CH_2Cl_2 and CH_3CN confirm the presence of the trimetallic species, $[(Ni\text{-}1)_2Pd]^{2+}$ species. This is reasonable product since monomer release from high pressure and chain termination by an acidic methanol solution would give an aldehyde end group on one end of the chain with a ketone end group on the other. End group analysis by ^{1}H NMR analysis shows a small resonance of the methylene protons of ketonic end group at 2.17 ppm slightly upfield from the resonance of the α-CH_2 groups at 2.73 ppm concurrent with that reported within the literature.[96] MALDI-TOF analysis of the copolymer confirmed that the end group is a ketone (Figure IV-28). The polymer was characterized by the presence of the cationic (adducts of potassium) oligomers that differ from each other by the mass of one repeat unit (56 m/z).

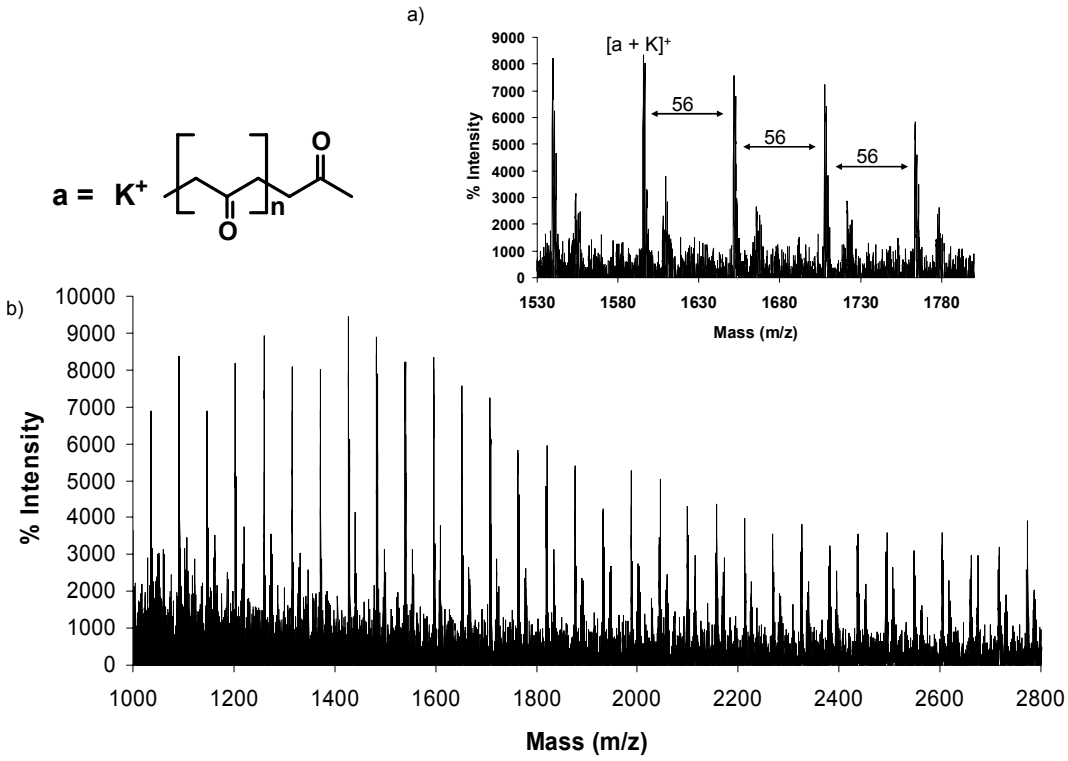

Figure IV-28: MALDI-TOF mass spectrum in hexafluroisopropanol of a CO/C_2H_2 copolymer prepared in CH_2Cl_2 at 30°C the [(**Ni-1**)Pd(CH_3)(OEt_2)]$^+$. a) An enlarged region and b) a full spectrum.

The Effect of Monomer Concentration [BAr′$_4$][(Ni-1)Pd(CH_3)(OEt_2)]

To examine the effect of monomer concentration the CO pressure was kept constant while the ethylene concentration was varied with 75 mg of the [(**Ni-1**)Pd(CH_3)(OEt_2)]$^+$ catalyst in 25 mL of CH_2Cl_2 at 30°C over 24 hr reaction periods (Table IV-2). Figure IV-29 clearly illustrates that an increase in ethylene monomer concentration has a significant influence on the turnover number (TON) or turnover frequency (TOF). These results are consistent with findings by Brookhart and co-workers where ethylene displacement of CO was found to be thermodynamically and kinetically disfavored.[85] Hence, a greater concentration of ethylene should push the

reaction equilibrium towards the ethylene bound side. A current diphosphine based industrial catalyst, (diMe-Si-AXPHS)Pd^{2+} (diMe-Si-AXPHS = di-*o*-anisylphosphinodimethylsilane) , produce a TOF of 40,000 g of polyketone with 50 bar of CO/ethylene at 90°C in methanol.[97] Our catalyst, [(**Ni-1**)$Pd(CH_3)(OEt_2)]^+$, with a nickeldithiolate ligand only produced a TOF of 2.5 g at 30°C under 6.89 bar of CO. The low productivity is likely due to the very stable resting state, [(**Ni-1**)$Pd(C(O)CH_3)(CO)][BAr'_4]$. The possibility that dormant states of the catalyst formed *in situ* during copolymerization render the catalyst inactive cannot be ruled out. A dormant state observed in the diphosphine and diimine Pd-based system is a $[L_2Pd]_2^{2+}$ dimer that can be re-activated with the addition of oxidants such as 1,4 benzoquinone (BQ).[98] In our system, a dormant state could possibly be the $[(\textbf{Ni-1})_2]Pd^{2+}$ trimetallic formed from the well-known aggregative tendency of metallodithiolate ligands. Addition of BQ might reactivate the catalyst to the (**Ni-1**)Pd^{2+} form, however, further speculation is unwarranted at this time.

Table IV-2. The Effect of [CO] and [Ethylene] on Productivity.

Run	CO (psi)	$CH_2=CH_2$ (psi)	Yield (g)	[a]TON	[b]TOF
1	100	100	0.1	9.4	0.4
2	100	200	0.3	45.8	1.9
3	100	300	0.4	60.0	2.5

[a]TON = g of Polyketone / g Pd. [b]TOF = g of Polyketone / g Pd•hour. Volume of Solvent = 25 mL CH_2Cl_2. [catalyst] = 0.056 mmol. Temperature = 30°C. Run time = 24 hr.

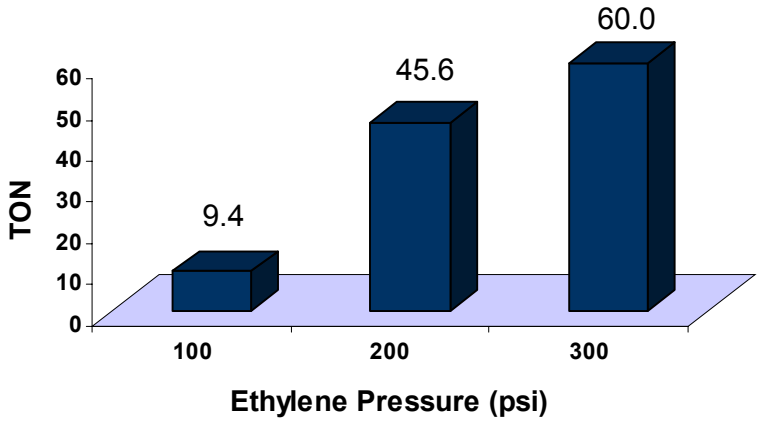

Figure IV-29. CO/C_2H_4 copolymerization: effect of monomer concentration on polyketone production. Catalyst: [(**Ni-1**)Pd(CH_3)(OEt_2)][BAr′$_4$]. Reactions conditions: n_{Pd} = 0.056 mmol; solvent = 25 mL CH_2Cl_2 , P_{CO} = 100 psi, T = 30°C, *t* = 24 h.

Effect of Solvent on Copolymer Formation with [(Ni-1)Pd(CH_3)(OEt_2)][BAr′$_4$]

To explore the effect of solvent on productivity and quality of polyketone formed the catalytic runs were carried out in several solvents with [(**Ni-1**)Pd(CH_3)(OEt_2)]$^+$ as the catalyst under the conditions specified in Table IV-3. Copolymerization reactions conducted in more donating solvents such as CH_3CN and THF had lower productivities

than CH_2Cl_2 (Figure IV-30). Brookhart and co-workers have shown that coordinating solvents such as CH_3CN bind equally to the Pd^{2+} open site necessary for the binding/insertion of ethylene.[85] THF is a reasonable coordinating solvent that would have much a higher binding affinity to the open site than ethylene. For this reason, competition for the open site by ethylene with a good donor solvent explains the lower productivity. Non-coordinating solvents, while ideal for the above reasons are not practical for copolymerization with our catalyst system because of solubility problems. Importantly, regardless of the solvent the ^{13}C NMR analysis showed that the copolymer remained alternating.

Table IV-3. The Effect of Solvent on Productivity

Solvent	Time	Yield (g)	[a]TON	[b]TOF
CH_2Cl_2	24	0.056	14.1	0.6
CH_3CN	24	0.035	8.9	0.4
THF	24	0.031	7.8	0.3

[a]TON = g of Polyketone / g Pd. [b]TOF = g of Polyketone / g Pd•hour. Volume of Solvent = 25 mL. [catalyst] = 0.037 mmol. Temperature = 30°C. Run time = 24 hr. $CO/CH_2{=}CH_2$ (100:200 psi)

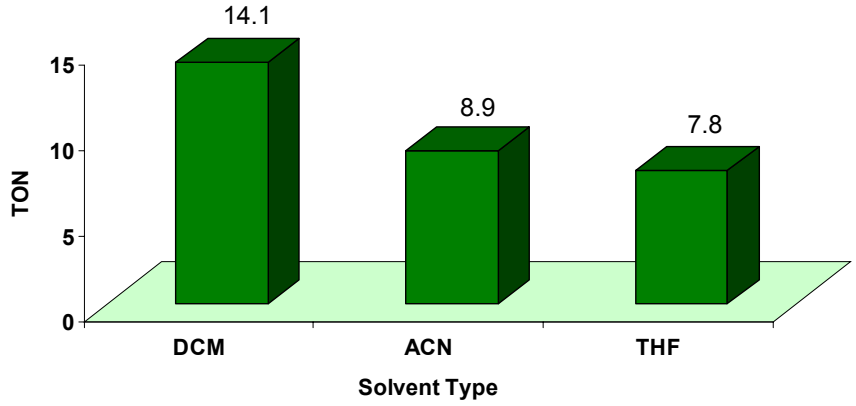

Figure IV-30. CO/C_2H_4 copolymerization: effect of solvent on polyketone production. Catalyst: [(**Ni-1**)Pd(CH_3)(OEt_2)]$^+$. Reactions conditions: n_{Pd} = 0.037 mmol, solvent = 25 mL, P_{CO} = 100 bar, $P_{Ethylene}$ = 200 bar, T = 30°C, *t* = 24 h. Dichloromethane (DCM), acetonitrile (ACN), and tetrahydrofuran (THF).

COMMENTS AND CONCLUSIONS

The heterobimetallic complexes presented within this chapter, in which the NiN_2S_2 complex is a bidentate ligand coordinated to a low valent exogenous metal, Pd^{2+}, opens the door to a new class of ligands for organometallic chemistry. Reactivity studies with CO show that the nickeldithiolate ligand is capable of stabilizing low oxidation state metals in simple organometallic reactions at a single metal site that are of biological and industrial significance.

Owing to the immeasurably fast (in our hands) CO/CH_3^+ migratory insertion observed at low temperature in the neutral (**Ni-1**)Pd(CH_3)(Cl) and cationic [(**Ni-1**)Pd(CH_3)(OEt_2)]$^+$ complexes; a full kinetic and thermodynamic study necessary to assemble an accurate model of the migratory insertion processes involved in CO/C_2H_2

copolymerization is lacking. Nonetheless, several assumptions were still made regarding the enhanced rate of migratory insertion and the resting state of the catalyst.

While the rate of CO/R migratory insertion was expected to be slower for the neutral square planar 16-electron complex, (**Ni-1**)Pd(CH_3)(Cl), both systems appeared to have migratory insertion rates that were faster than the classical Pd-metal based systems employing diphosphine and diimine ligands. Literature precedents find that the driving force for CO insertion in the classical system may be different depending on the ligand properties; such properties include the steric and electronic components as well as bite angle.[1b,3] For the metallodithiolate ligand, **Ni-1**, an electronic argument has been made concerning the fast rate of insertion such that the electron rich Nature of the ligand governs the rate of the reaction. In a system with a very electron rich ligand it is reasonable that CO will have a strong affinity towards the metal center, since the metal will prefer to have a good π acceptor, ligand, CO, therefore migratory insertion is more facile. Being that the S-Pd-S ligand bite in [(**Ni-1**)Pd(CH_3)(Cl) is 77°, constrained by the Ni metal ion linker in the ligand backbone, the bite angle may be less influential than in cases where larger ligand bite angles (~ 91°) have been known to enhance the rate of migratory insertion.[1b] For the neutral complex an associative pathway involving a 5-coordinate intermediate similar to that suggested for neutral diimine Pd-metal based complexes might also be a contributing factor for fast CO insertion. The steric effect of the ligand on the rate of the migratory insertion reactions has not yet been.

From this study, it is apparent that the Nature of the ligand has a direct effect on the initial steps in migratory insertion which affect copolymerization of CO/C_2H_4.

While the electron rich Nature of the ligand stabilizes the metal center for rapid CO insertion into the Pd-alkyl bond it also attracts CO as a poison; such that CO binds to the metal very strongly so that ethylene displacement of CO is difficult in the second migratory insertion step of Pd-acetyl required for copolymerization. Other more electron rich ligands such as the dianionic $Ni(ema)^{2-}$ discussed in Chapter III would not be suitable for this type of reaction. It is evident that the carbonyl acetyl intermediate is the most prevalent species in the copolymerization cycle, as ethylene displacement of CO does not occur very readily. Five and six membered chelates are also not observed, but due to the extremely fast reaction rate, these complexes cannot be eliminated as possible intermediates. A greater concentration of ethylene is necessary to push the equilibrium towards ethylene addition/insertion. As a result, copolymerization is greatly affected by the slow binding of ethylene producing lower TOF and by strongly coordinating solvents that compete with ethylene for the open site. In addition, because of the large CO binding affinity it is also unlikely that consecutive insertions occurred during copolymerization.

While it seems that the electron rich metallodithiolate hinders some aspects of C-C coupling chemistry, these NiN_2S_2 ligands may be useful to facilitate other organometallic reaction chemistry in which the metal undergoes oxidation state changes. The unique structural feature of the ligand when bound to an exogenous metal also presents an opportunity to do stereo- and regioselective chemistry with other olefin substrates such as styrene.

CHAPTER V

EXPLORATORY C-C AND C-S COUPLING REACTIONS RELEVANT TO ACETYL COENZYME-A SYNTHASE ENZYME

INTRODUCTION

The recent discovery of the active site of the Acetyl CoA synthase enzyme from *Moorella thermoacetica* led synthetic chemists in a race to design model complexes that would exhibit similar structural as well as functional features (Figure V-1).[20-22] Required structural features include a Ni^{2+} coordinated to two carboxamido-nitrogen and two thiolate sulfur donors in a rigid square planar coordination environment. The $Ni_dN_2S_2$ moiety must be able to coordinate to a second metal, M_p, (M = Ni, Cu, Zn) in a bidentate fashion through both thiolate sulfur donors. As nickel, Ni_p, the second metal is the catalytically active metal and is bridged to a Fe_4S_4 cubane, it must be able to adopt a square planar or tetrahedral geometry when necessary. A labile ligand coordinated to Ni_p should be easily displaced. Another necessary feature is the ability to mimic a Ni(I) state that would afford a NiFeC signal with g = 2.08 in the EPR.[99]

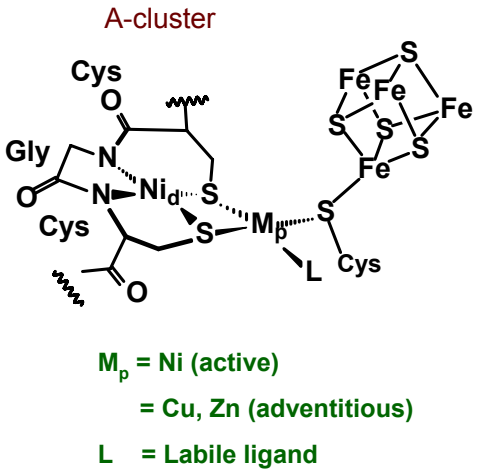

Figure V-1. Required structural features of the ACS active site needed for a biomimetic model.[20-22]

In terms of functional features, the model must be able to bind CO and CH_3^+ substrates on Ni_p with a ν(CO) stretch at 1996 cm^{-1}.[100] In addition, the CO/CH_3^+ complex must be able to react with a thiol to form a thioester in a sequential pair of C-C and C-S coupling reactions (ACS reactivity).

A well established library of NiN_2S_2 complexes provided a variety of models for the Ni_d centers but also presented many synthetic challenges due to their well-known aggregative tendency with exogenous metals.[24-31,33-41] Control of aggregate formation has been explored with the use of sterically hindering metallodithiolate ligands or the use of exogenous metal precursors containing steric blocks such as phosphines or inert ligands such as CO that are often difficult to displace.[36-41,101,102] Many synthetic models thus far have ignored Fe_4S_4 clusters and have focused on the $(NiN_2S_2)M_d$ site, using an approach in which the NiN_2S_2 complex is reacted with ML_n. The L ligands need to be

displaceable by one NiN_2S_2 and incoming substrates. The challenge is to limit the NiN_2S_2 moieties to one unit, as in Figure V-2, rather than multiple units.

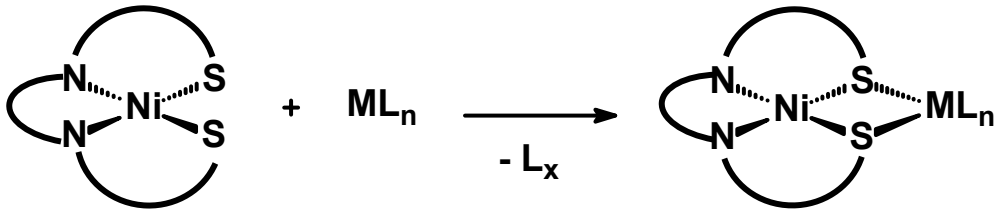

Figure V-2. Synthetic methodology for the synthesis of heterobimetallic complexes.

$(Ni_dN_2S_2)Ni_p$ Structural Models of Acetyl CoA Synthase Active site

The first bimetallic nickel model complex of the ACS active site was reported by Rauchfuss in which the soft thiolate donors of an anionic NiN_2S_2 ligand stabilized a tetrahedral Ni^0 metal center with two CO ligands (ν(CO) at 1948 and 1866 cm^{-1}).[36] The CO ligands stabilize the Ni^0 metal center under an inert atmosphere but upon exposure to air degrades to the trimetallic, $[(NiN_2S_2)_2Ni]^{2-}$ species (Figure V-3, b).[36] More recently, Riordan and co-workers have employed a Cys-Gly-Cys tripeptide to chelate a Ni^{II} in K_2[Ni(CysGlyCys], complementary to the active site.[38] This natural metallodithiolate ligand was used as a template to build trimetallic and bimetallic models of the active site with Ni (Figure V-3, c) and d)).[38] The bimetallic models that featured a NiN_2S_2 moiety bridged to a NiP_2S_2 unit, Figure V-3 d) and e); provided a $Ni^{II}Ni^{I}$ redox active state when electrochemically reduced which could bind CO.[38-40]

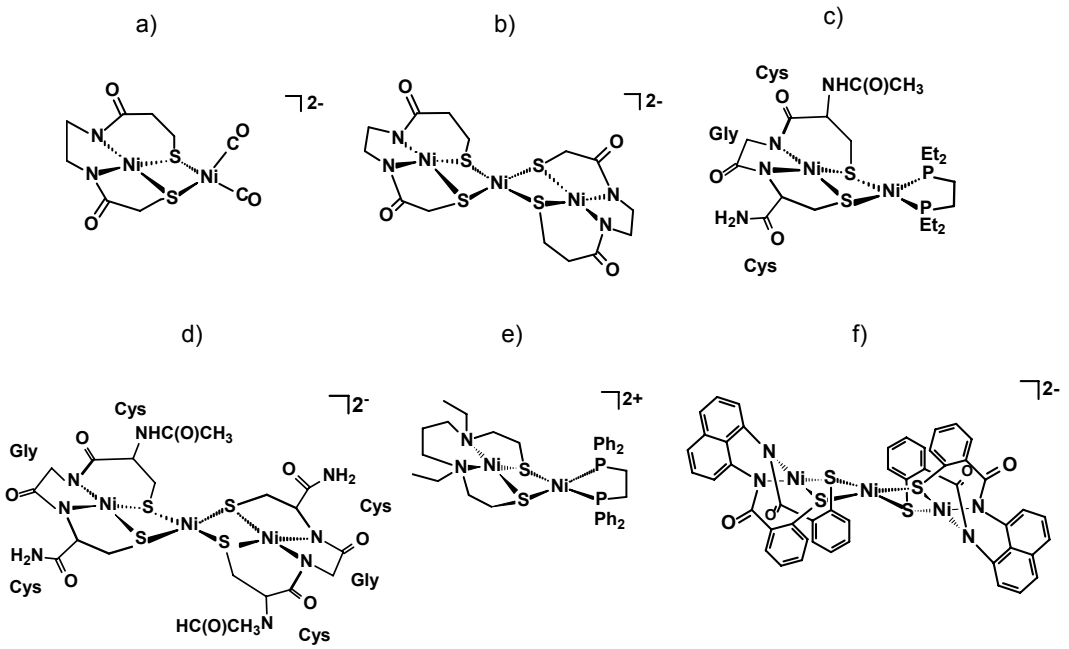

Figure V-3 ($Ni_dN_2S_2$)Ni_p structural models of the ACS enzyme active site. **a)-b)**[36], **c)-d)**[38], **e)**[39] and **f)**[40]

Functional Models of the ACS Enzyme

Before the structure of the ACS active site was elucidated by crystallography, most models were designed as mononuclear Ni^{II} complexes. Holm and co-workers designed the first functional model that exhibited thioester formation. This model featured a tripodal NS_3 ligand with thioether donors bound to Ni^{II} (Figure V-4).[103] Oxidative addition of CH_3^+ in the presence of CO produced an acetyl complex (ν(CO) = 1670 cm^{-1}), which was reactive toward $^-$SR. Nucleophilic attack by a thiol, $^-$SR, reductively eliminated a thioester transferring two electrons to Ni^{2+} to form a Ni^0 and a proton to the NS_3 thioether ligand, forming a tertiary amine.[103] This was the first time intermediates similar to the reactivity of the ACS enzyme had been spectroscopically observed.

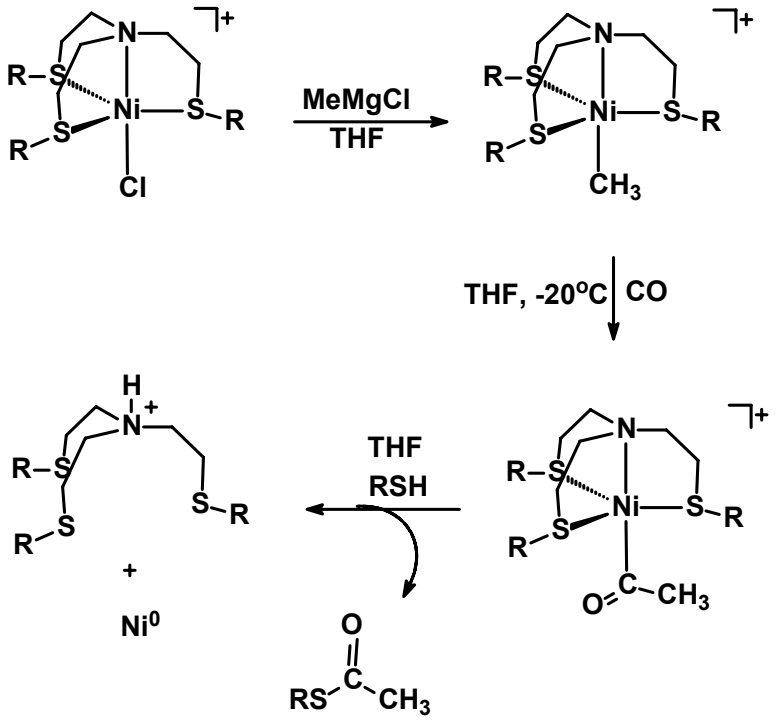

Figure V-4. Reaction sequence for the formation of a thioester by a mononuclear nickel complex designed by Holm and co-workers.[103]

Holm and co-workers also demonstrated ACS reactivity with a less traditional supporting ligand in the (bipy)Ni(CH_3)$_2$ complex (Figure V-5).[104] Addition of RSH protonated one of the CH_3 groups to eliminate one molecule of CH_4 to form a metal-bound thiolate ligand. Unlike the previous reaction sequence in which CO was added before the thiol, this protocol demonstrated acetyl formation on a square planar Ni^{2+} with a metal-bound $^{-}$SR ligand. Thioester formation occurred by direct internal nucleophilic attack on the acetyl ligand by $^{-}$SR.[104] Under a large excess of CO, the Ni^0 species formed from reductive elimination was stabilized by two CO ligands and bipyridine, (bipy)Ni(CO)$_2$ (ν(CO) = 1872, 1973 cm^{-1}). Even though both mononuclear metal model

complexes did not structurally mimic the active site, they were functional and pointed to the fact that thioester formation can occur *via* two separate mechanistic pathways.

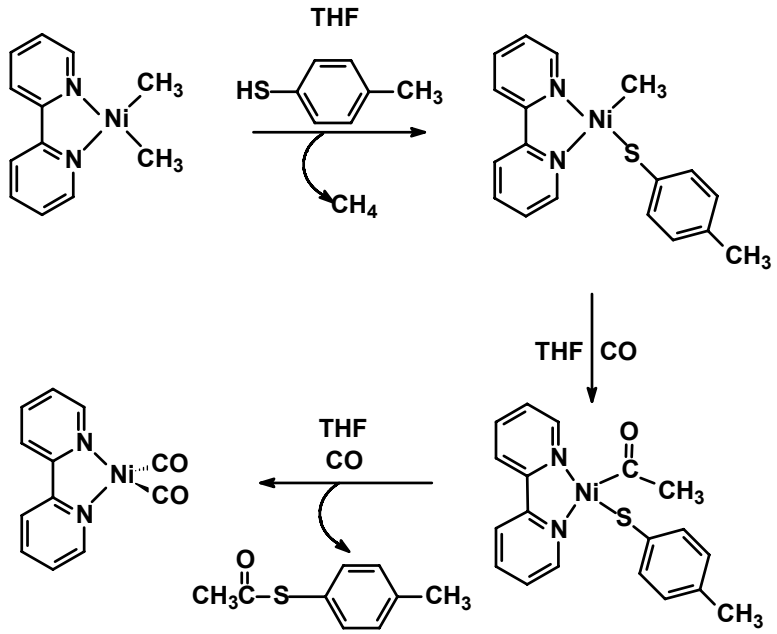

Figure V-5. Reaction sequence for the formation of thioesters by a neutral **(**bipy)Ni(CH_3)$_2$ utilizing a classical ligand in organometallic chemistry.[104]

Theoretically Proposed Mechanisms for Acetyl CoA Synthase Reactivity

Two theoretical mechanisms have recently been proposed for acetyl CoA synthesis utilizing a (NiN_2S_2)Ni bimetallic catalyst.[23,60] These mechanisms point to several possible intermediates that are integral components during the catalytic cycle that may be experimentally observed. Such intermediates have been observed in similar systems consistent with classical organometallic chemistry.

Computational Mechanism A

The computational mechanism proposed by Webster, Hall, Lindahl and Darensbourg suggested that the $Ni_dN_2S_2$ moiety serve as a bidentate ligand that stabilizes a tetrahedral Ni^0 metal prior to oxidative addition by $^+CH_3$ forming a square planar Ni(II) (Figure V-6).[23] CO addition destabilizes one of the Ni_p-S bonds, forcing it to break while the other Ni_p-S is strengthened. Methyl migration/CO insertion produces a Ni(II) with an open site for ^-SR ligand to coordinate. Internal nucleophilic attack followed by reductive elimination of a thioester completes the catalytic cycle. Note that the overall charge on the Fe_4S_4 cluster remains neutral throughout the process.[23] In this mechanism the C-C coupling reaction occurs strictly on the Ni_p metal center while the $Ni_dN_2S_2$ moiety is inferred to act as a hemilabile ligand that stabilizes the Ni^0 metal center during catalysis.[23]

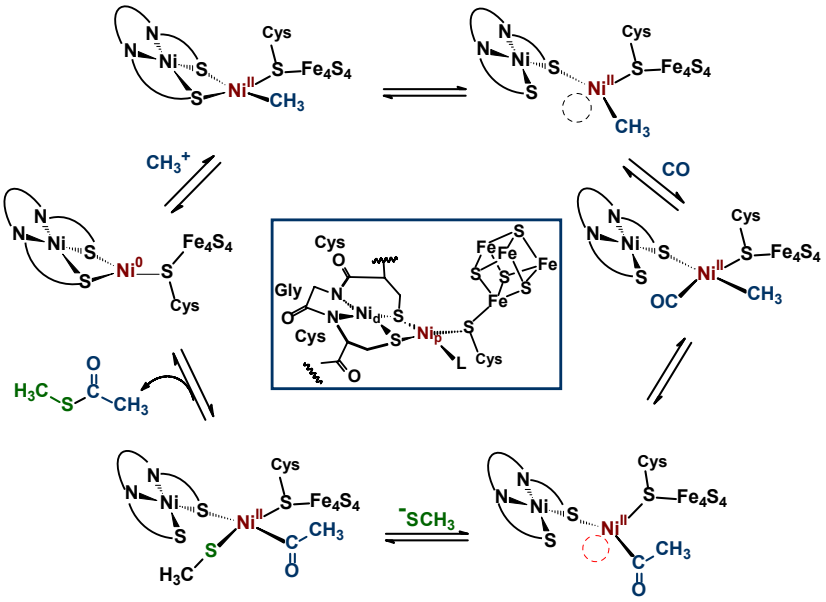

Figure V-6. Computational mechanism A proposed by Webster, Hall, Lindhal and Darensbourg.[23]

Computational Mechanism B

The second theoretically proposed mechanism suggests that the active site is in the $Ni^{II}Ni^{I}$ oxidation state that would be consistent with the experimentally observed NiFeC signal in the EPR (Figure V-7).[60,99] Carbon monoxide addition forms a $Ni^{II}Ni^{I}$ heterobimetallic bridged to a $[Fe_4S_4]^{+}$ cluster still in the oxidized form (S = ½). Oxidative addition of CH_3^{+} forms a square planar $Ni^{II}Ni^{II}$ species next to a $[Fe_4S_4]^{2+}$ cluster. Isomerization positions the CH_3^{+} and CO cis to each other for methyl migration to occur and produces a metal-bound acetyl species which undergoes external nucleophilic attack by ^{-}SR to complete the catalytic cycle.[60] It is unclear at this point what the sequence of the reactions are as proposed by results from the experimentally developed model or the theoretically proposed mechanism.

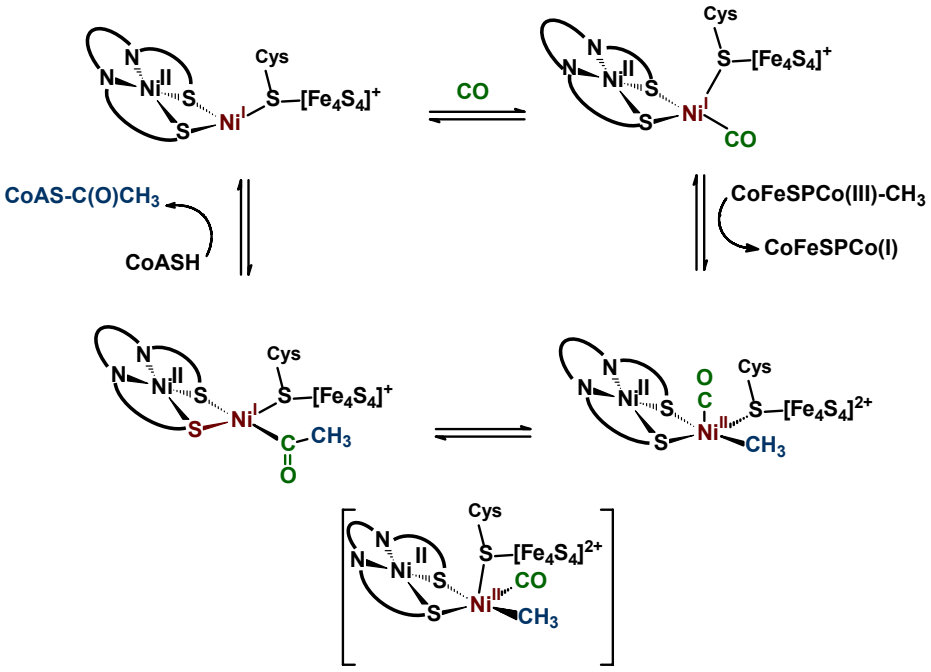

Figure V-7. Computational mechanism B by Fontecilla-Camps and Volbeda.[60]

The [(**Ni-1**)PdCH$_3$(OEt$_2$)]$^+$ heterobimetallic complex exhibits similar structural characteristics similar to the ACS active site.[21-22] It has a bidentate ligand that stabilizes the Pd^{2+} with an alkyl group and a labile Et_2O ligand that is easily replaced by CO and good donor solvents. As palladium has similar chemical properties to nickel, this heterobimetallic provided an opportunity to test for ACS reactivity.

RESULTS AND DISCUSSION

Studies of [(Ni-1)Pd(CH$_3$)(OEt$_2$)]$^+$ and (Ni-1)Pd(CH$_3$)$_2$ Complexes as Biomimetic Models for the ACS active site.

The preparation of the model complexes for each of the following studies was described in Chapter IV. Two types of reactions were carried out: 1) carbon monoxide was added to metal complex prior to the addition of a thiolate source, and 2) the thiolate was added the metal precursor prior to addition of CO. The progress of the reactions was monitored over time by infrared spectroscopy.

Reactivity of [(Ni-1)Pd(CH$_3$)(OEt$_2$)]$^+$ with CO and a thiolate source, $^-$SR.

A solution of [(**Ni-1**)Pd(C(O)CH$_3$)(CO)]$^+$ was added to the NaSR thiolate source (R = Me, (C$_6$H$_4$)Me) (Figure V-8, a)) at -78°C. Infrared spectra of the reaction mixture recorded over time at room temperature, (Figure V-8, b)), showed the disappearance of the ν(CO) stretching frequencies assigned to the Pd-bound terminal CO and Pd-acetyl at 2110 cm^{-1} and 1722 cm^{-1} with concomitant appearance of a band at 1686 cm^{-1}. This

ν(CO) stretch was assigned to the carbonyl group in the thioester and is in agreement with a bona fide sample of the thioester, $CH_3SC(O)CH_3$ (ν(CO) at 1689 cm^{-1}).

A UV-Vis spectrum of a sample of the dark red-black solution reaction mixture after $NaSCH_3$ addition showed two absorptions at λ_{max} of 404 nm and 520 nm, which were assigned to the [**Ni-1**]$_2Pd^{2+}$ trimetallic species in CH_3CN. This is consistent with a known sample of [**Ni-1**]$_2Pd^{2+}$ in methanol (λ_{max} of 408 nm and 522 nm)[27] and is supported by ESI (Electron Spray Ionization) mass spectral analysis, which showed that 100% of the species had a mass to charge ratio of 344, as does [**Ni-1**]$_2Pd^{2+}$. The observation of trace amounts of Pd^0 black in solution is evidence that some reductive elimination of the thioester had occurred. The observation of [**Ni-1**]$_2Pd^{2+}$ is best explained by a competing reaction between the free **Ni-1** and the added $^-$SR source in towards the reactive [(**Ni-1**)Pd(C(O)CH_3)(CO)]$^+$ complex, and is consistent with the well-known aggregative tendency of NiN_2S_2 ligands. The addition of another thiolate source, $NaS(C_6H_4)Me$), produced similar results. A ν(CO) stretch at 1702 cm^{-1} in the product mixture was assigned to the carbonyl ligand of the thioester, $CH_3(C_6H_4)SC(O)CH_3$.

The infrared spectrum of the reaction mixture upon NaSMe addition to [(**Ni-1**)Pd(C(O)CH_3)(CO)]$^+$ after 1 hour at room temperature shows the appearance of a band in the terminal CO region of the infrared at 2041 cm^{-1} and one in the C=O region at 1766 cm^{-1}. The 2041 cm^{-1} also grows in intensity over time and is similar to an unidentified species in the reaction between CO and the (Ni-1)Pd(CH_3)(Cl) complex (Chapter IV).

At this point, the identity of these species at 2041 and 1766 cm^{-1} are unknown, as attempts to isolate these species have not been made yet.

From this exploratory investigation, it appears that the [(**Ni-1**)Pd($C(O)CH_3$)(CO)]$^+$ is capable of a C-S coupling reaction similar to the enzyme to produce a thioester. Whether thioester formation is the result of external nucleophilic attack or internal nucleophilic attack by $^-$SR from displacement of CO is unknown at this point. Kinetic and thermodynamic studies are required to provide information about the rates of the reaction in addition to activation parameters ($\Delta G^{\ddagger}$, $\Delta H^{\ddagger}$,$\Delta S^{\ddagger}$) which will elucidate whether C-S coupling occurs *via* internal or external nucleophilic attack.

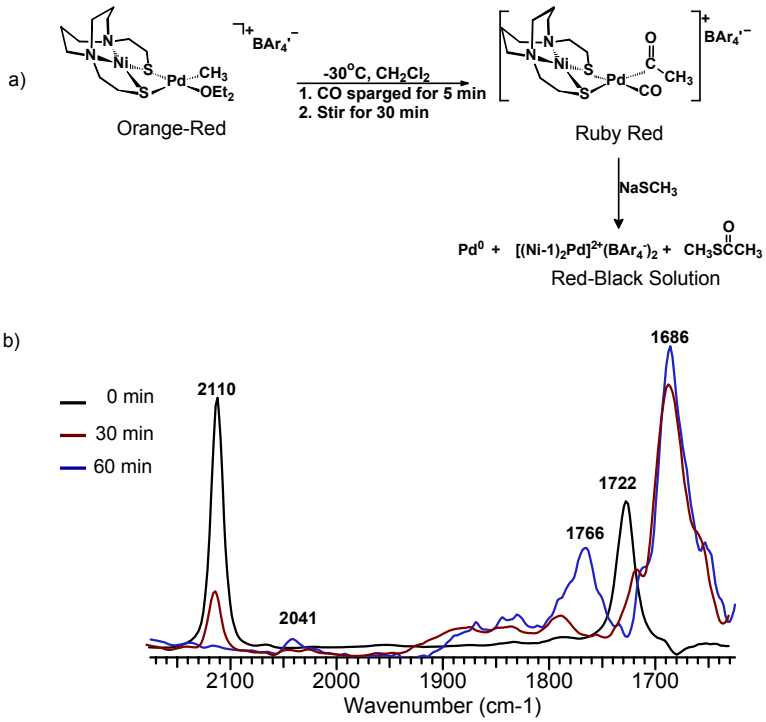

Figure V-8. A test for ACS reactivity. A) reaction protocol of [(**Ni-1**)Pd(CH_3)(OEt_2)]$^+$ with CO and a NaSR source. b) Infrared monitor of CO and NaSR addition to [(**Ni-1**)Pd(CH_3)(OEt_2)]$^+$ at room temperature in CH_2Cl_2 from 0 -60 min.

Reactivity of [(Ni-1)Pd(CH_3)$_2$ with HS(C_6H_4)Me and CO

In a similar protocol utilized by Holm and co-workers,[104] the HS(C_6H_4)CH_3 thiol was added to the (**Ni-1**)Pd(CH_3)$_2$ precursor in CH_2Cl_2, eliminating one equivalent of CH_4 (Figure V-9). Carbon monoxide gas was sparged through the cold solution of the reaction, and the progress of this reaction was followed by infrared spectroscopy (Figure V-10).

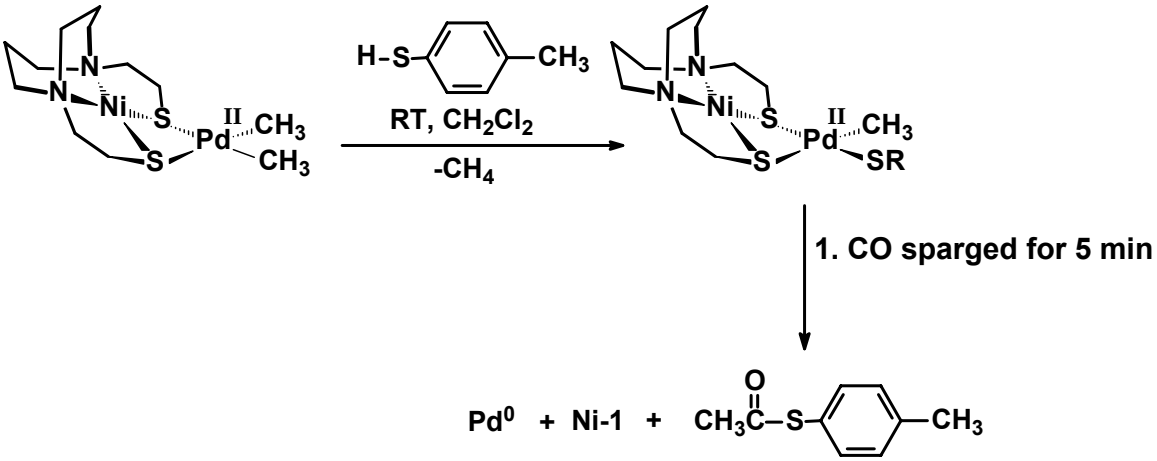

Figure V-9. A test for ACS reactivity with [(**Ni-1)**Pd(CH_3)$_2$ after HS(C_6H_4)CH_3 and CO addition.

The infrared spectrum of a cold solution of the reaction subsequent to addition of CO after 1 hour of stirring at -78°C provided a ν(CO) stretching frequency at 1685 cm^{-1}, assigned to the carbonyl of a palladium-bound acetyl ligand (Figure V-10). The ν(CO) stretch at 1604 cm^{-1} is assigned to the aromatic ring of the thiolate. This is in agreement with the low stretching frequency observed for the (bipy)Ni(C(O)Me)(SR) intermediate observed by Holm *et al.* with a ν(CO) stretch at 1632 cm^{-1} ($^{-}$SR = S-2,6-$C_6H_3Cl_2$).[104] A

similar ν(CO) was observed in the infrared spectrum from the reaction monitor of [(**Ni-1**)Pd(C(O)CH_3)(CO)]$^+$ with NaS(C_6H_4)CH_3. Upon warming the solution to room temperature, the infrared spectrum of the black-purple mixture shows the disappearance of the ν(CO) stretch at 1685 while a new ν(CO) at 1702 cm^{-1} appears. The latter was assigned to the carbonyl of the thioester, $CH_3(C_6H_4)SC(O)CH_3$. Concurrently, ν(CO) stretching frequencies at 2043 cm^{-1} and 1766 cm^{-1} also appeared. We speculate that these infrared bands should be assigned to a 5-coordinate intermediate with a terminal bound CO in [(**Ni-1**)Pd(C(O)CH_3)(SR)(CO)].

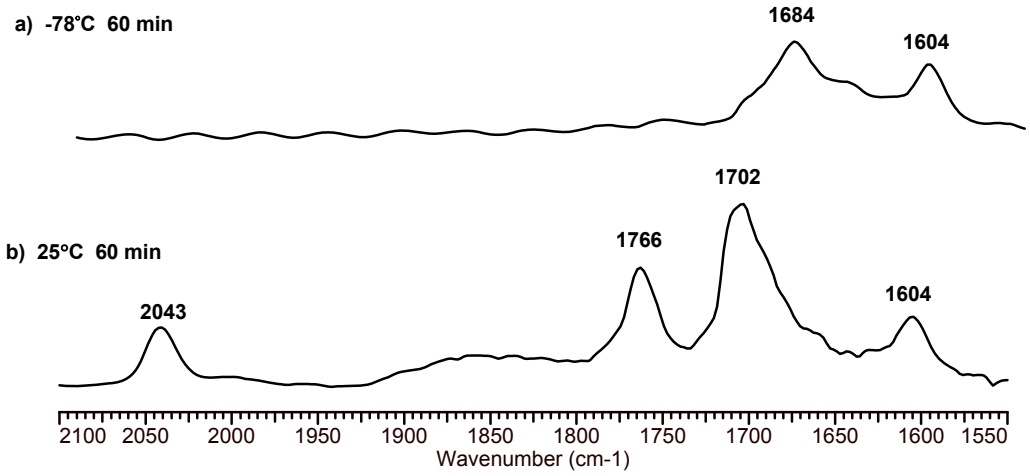

Figure V-10. Infrared monitor of the reaction of [(**Ni-1)**Pd$(CH_3)_2$ with HS(C_6H_4)CH_3 and CO in CH_2Cl_2. a) 60 min at -78°C and b) 60 min at 25°C.

In Holm's reaction under an large excess of CO, the (bipy)Ni^0 species formed from reductive elimination of the thioester reacted with CO to produce a dicarbonyl

adduct, (bipy)$Ni^0(CO)_2$ (ν(CO) stretching frequencies at1973 cm^{-1} and 1864 cm^{-1})[104]. In our system, a dicarbonyl adduct was not observed. While traces of Pd^0 were observed after the reaction, perhaps a (Ni-1)$Pd^0(CO)_2$ species did not form because enough CO gas was not present in solution. Thioester formation is evidence that acetyl formation is not required prior to $^-$SR addition. It may very well be on the metal center before CO/CH_3^+ addition. More importantly, these results suggest that thioester formation could proceed via internal nucleophilic attack. A full kinetic and thermodynamic study is necessary to substantiate this hypothesis.

Acetyl Migration Within the [(Ni-1)Pd(C(O)CH_3)(CO)]$^+$ Complex

To investigate whether acetyl migration from the Pd^{2+} could indeed produce a metallodithiolate thioester (Figure V-11), the following control experiments were conducted.

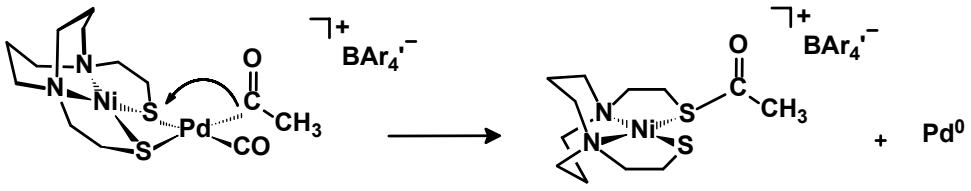

Figure V-11. Possible expected reaction for acetyl migration as $[C(O)Me]^+$ to the bridging S in the metallodithiolate ligand.

The first experiment required the addition of acetyl chloride to a purple solution of **Ni-1** in CH_2Cl_2, which turns to a brown slurry immediately. An infrared spectrum of the supernatant showed a ν(CO) stretch at 1689 cm^{-1} (Figure V-12). The structure of the chloride derivative of [(**Ni-1**)C(O)Me]$^+$ is most likely analogous to the Ni(bme-dach),

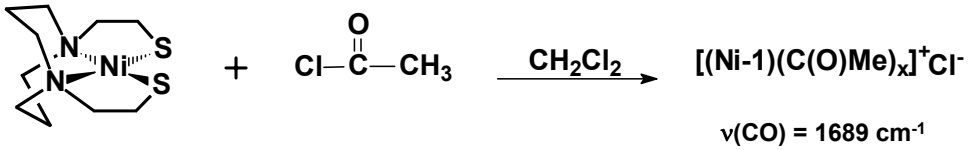

Figure V-12. Acetyl chloride addition to **Ni-1** to form a metallothiolate-thioester, [(**Ni-1**)C(O)Me]$^+$.

Ni-1′, derivative (**Ni-1′)**$(C(O)Me)_2(Cl)_2$ shown in (Figure V-13, a) in which one thiolate arm dangling while the other is coordinated.[105] The ν(CO) frequencies for the (**Ni-1′)**$(C(O)Me)_2(Cl)_2$ was 1737(m), 1710(sh) and 1695(s) cm^{-1}. Golden reports that upon demetallation with KCN only one ν(CO) stretch was observed at 1741 cm^{-1}, ascribed to the nickel-free acetylated N_2S_2 ligand.[105] Acetyl addition to the NiN_2S_2 thiolate donors are in agreement with the well-known sulfur nucleophilicity. The structure of the **Zn-1′**derivative, (**Zn-1′)**$(C(O)Me)_2(Cl)_2$, shows the acetyl ligands coordinated to the dangling thiolate sulfur donors that are not coordinated to the metal center with a ν(CO) stretch at 1692 cm^{-1} (Figure V-13, b), and would explain by only one ν(CO) stretch was observed. However, ESI mass spectral analysis show that 100% of a positively charged species with a mass to charge ratio of 319 is [H(bme-daco)-$(C(O)Me)_2$]$^+$ in which the Ni^{2+} has been removed from the N_2S_2 chelate after acetylating the **Ni-1** ligand . In light

of ESI results, an alternative structure is $[H(bme\text{-}daco)\text{-}(C(O)Me)_2]^+$ without the Ni^{2+} metal center.

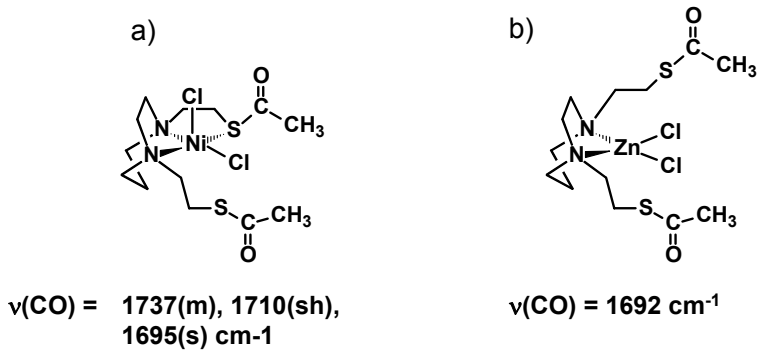

Figure V-13. Structural representations of the acetylated MN_2S_2 ligands. a) (**Ni-1′**)$(C(O)Me)_2(Cl)_2$ and b) (**Zn 1′**)$(C(O)Me)_2(Cl)_2$ from acetyl chloride addition.[105]

The second experiment examined the activity of the remaining lone pair on the thiolate sulfur toward a nucleophile when bound to a Pd^{2+} metal center. Acetyl chloride was added to a CH_2Cl_2 solution of $[(\mathbf{Ni\text{-}1})Pd(C(O)CH_3)(CO)]^+$ at room temperature, and the infrared spectra of this solution was recorded over an extended period. The characteristic bands at 2110 cm^{-1} and 1722 cm^{-1} remained unchanged after consecutive measurements, suggesting that the $[(\mathbf{Ni\text{-}1})Pd(C(O)CH_3)(CO)]^+$ was stable and that the remaining lone pair on the thiolate was inactive towards the electrophilic acetyl as evidence by the absence of an infrared band at ca. 1689 cm^{-1}. The ν(CO) stretch for acetyl chloride at 1804 cm^{-1} also remained unchanged. Metallation deactivates the second lone pair, rendering it non-reactive towards electrophiles such as acetyl; therefore, acetyl migration from the Pd^{2+} metal center is not possible upon metallation.

COMMENTS AND CONCLUSIONS

This work provides some evidence for thioester formation as mediated by NiN_2S_2Pd heterobimetallic. The present investigations also demonstrated and concurred with Holm *et al*. that thioester formation can occur via two separate pathways in the mechanistic cycle. The first pathway for acetyl formation precedes nucleophilic attack by a thiolate while the second pathway suggests the thiolate substrate binds first before acetyl formation to produce the thioester. The second pathway lends more support to internal nucleophilic attack on the Pd-bound acetyl ligand to reductively eliminate a thioester.

Control experiments suggest that while the free ligand, **Ni-1**, is reactive with electrophiles such as acetyl chloride, but when to a second metal the remaining lone pairs are deactivated. Hence, the acetyl formed at Pd from the CO/CH_3 migratory insertion process does not result in internal reductive elimination at the Ni-bound thiolate sulfur atom. Rather an exogenous thiolate is required for thioester formation. From this exploratory work employing a NiN_2S_2Pd heterobimetallic, $[(\mathbf{Ni\text{-}1})Pd(CH_3)(OEt_2)]^+$ suggests that this complex is a viable source for further studies of ACS reactivity.

CHAPTER VI

METALLATION REACTIONS OF COPPER AND RHODIUM WITH METALLOTHIOLATE LIGANDS

INTRODUCTION

The development of NiN_2S_2 complexes as ligands in molecules designed to mimic biological active sites require synthetic strategies to limit the aggregative tendencies of metallodithiolate ligands.[24-31,33-40] Fortunately, combinations of the low valent $W(CO)_4$ moiety and several NiN_2S_2 ligands (Chapter III) have yielded Ni-W heterobimetallic compounds in which the strong W-CO bonds block polymetallic cluster formation. Other heterobimetallic $(NiN_2S_2)Pd$ complexes (Chapter IV) utilized $Pd(CH_3)_2$ and $Pd(CH_3)(Cl)$ reaction precursors containing the labile TMEDA (tetramethylethylenediamine) and cod (cyclooctadiene) ligands that are easily displaced. In this case, the M-CH_3 bond is evidently stronger than the M-(μ-SR), hence aggregation stops at the heterobimetallic NiPd complex.

Several binuclear complexes resembling the active site of the ACS enzyme (Chapter V) utilized chelating diphosphine ligands (Figure VI-1, a) and c)) as a form of steric block.[38-40,] The $Ni^{II}Ni^0$ heterobimetallic in Figure VI-1 (b) is the most representative structural model of the ACS enzyme synthesized thus far, in which carbonyl ligands temporarily stabilize the Ni^0 oxidation state.[36] With large R groups on the thiolate pendant arms the NiN_2S_2 ligand itself may aid in limiting cluster size.

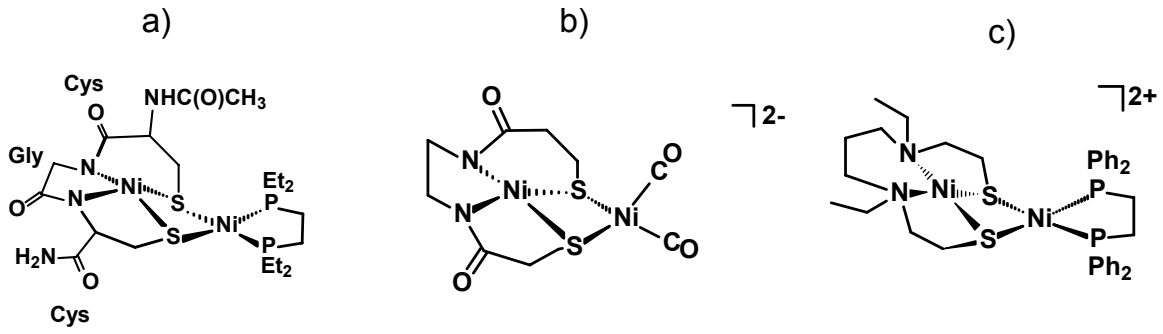

Figure VI-1. Representations of $(NiN_2S_2)Ni$ heterobimetallics as models of the ACS enzyme active site: a)[38], b)[36] and c)[39]

While there are several models of the $(NiN_2S_2)Cu$ form of the ACS active site in which large phosphines stabilize the Cu^I trigonal planar geometry, due to the extreme sulfophilicity of Cu^I, a large number of higher order aggregates are predominant (Figure VI-2).[36,101,102] Metallodithiolate reactions with copper have provided an interesting library of structural forms (Figure VI-2), which vary depending on the stoichiometric ratio of NiN_2S_2 ligand to Cu^I source. Structural analysis finds that the ligands bind to copper in a bidentate fashion as in the staircase or paddlewheel structures or in a bidentate bridging fashion to either one or two metal centers. The geometry of the copper in these structural forms extends from linear to trigonal planar and tetrahedral.

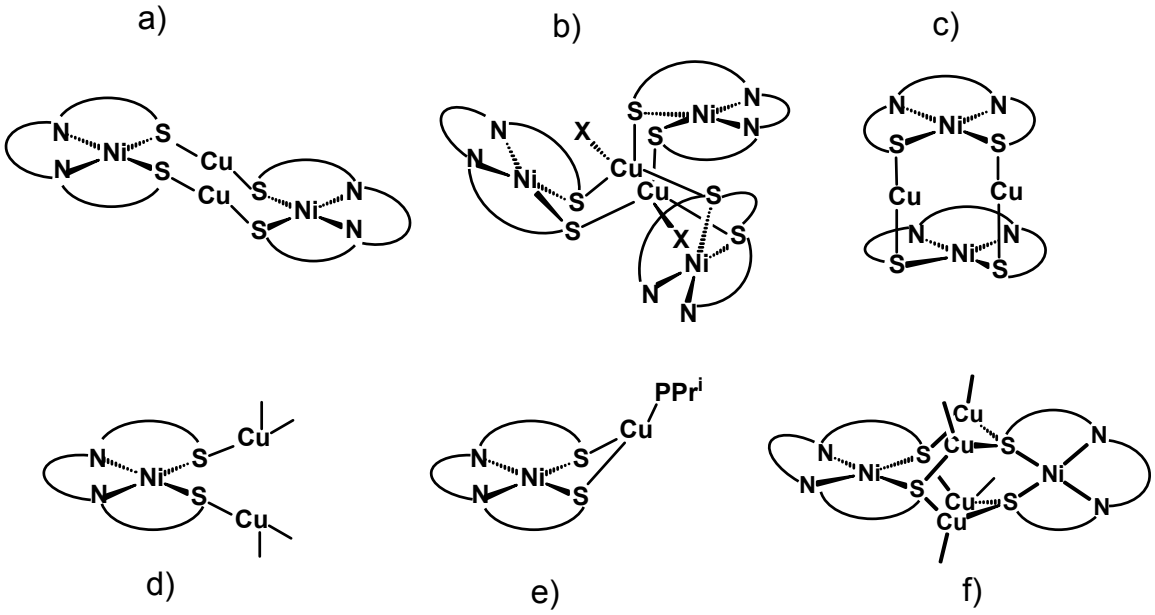

FigureVI-2. Representations of various structural forms of polymetallic (NiN_2S_2)Cu clusters: **a)**[36], **b)**[29], **c)-e)**[33a,101,102] and **f)**[26,35].

From our work with the **Ni-1**, **Ni-1´** and **Ni-1*** metallodithiolate ligands, the "pinwheel" (Figure VI-2, b) and "adamantane-like" (Figure VI-2, f) nickel-copper aggregates were produced.[24,26,29] Of particular interest are the structural differences in aggregates with the **Ni-1** and **Ni-1*** ligands, where the stoichiometric ratio of metallodithiolate ligand to Cu ion is varied. For example, the **Ni-1*** ligand which possesses gem dimethyl groups on the carbon α to the sulfurs produced a novel hexametallic cluster.[26] It became of interest therefore to evaluate what combination of steric hindrance on the ligand and stoichiometric control of ligand to metal ratio will produce lower order aggregates. Reactions of NiN_2S_2 complexes with copper and rhodium were investigated in order to extend our knowledge of cluster formation,

thereby adding to the library of structural forms, so that we may effectively understand and ultimately control the product structure.

RESULTS AND DISCUSSION

Syntheses of $(NiN_2S_2)Cu^I$ and $[(NiN_2S_2)Rh$ Complexes

Figure VI-3 displays the synthesis of different polymetallic $(NiN_2S_2)_XCu_Y$ aggregates in various Cu^I to **Ni-1*** stiochiometric ratios. Dark brown solutions of the polynuclear aggregates were obtained upon addition of CuBr to a purple solutions of **Ni-1*** in collaboration with Dr. Mathew L. Miller. These complexes were isolated as solids in >70% yields and found to be very soluble in CH_2Cl_2 and CH_3CN but insoluble in ether. As seen in Figure VI-3, Ni^{II}-S-Cu^I bridging interactions of various types are constructed such that two types of bridging modes were observed. The structural forms presented are a direct result of varying the stoichiometric ratio of ligand to metal. The recrystallized products were characterized by ESI mass spectroscopy and x-ray diffraction studies. It is also worth mentioning that the predominant species observed in the ESI mass spectra of the **(Ni-1*)**$_2(CuBr)_2$ and $[$**(Ni-1*)**$_3Cu_2][Br_2]$ complexes was the positively charged $[$**(Ni-1*)**$_2Cu_2Br]^+$ species, while only minor amounts of $[$**(Ni-1*)**$_2Cu_3Br_2]^+$ were observed. The ESI mass spectra for **(Ni-1*)**$_2(CuBr)_4$ showed that 100% of the species with a mass to charge ratio of 1045 was $[$**(Ni-1*)**$_2Cu_3Br_2]^+$. Hence, upon ionization, the most stable species that forms is $[$**(Ni-1*)**$_2Cu_2Br_2]^+$. However, this is only true when there is less copper. In the presence of excess copper, the remaining

lone pairs are metallated, and the $[(\mathbf{Ni\text{-}1^*})_2Cu_3Br]^+$ is the most prevalent species after electrospray ionization.

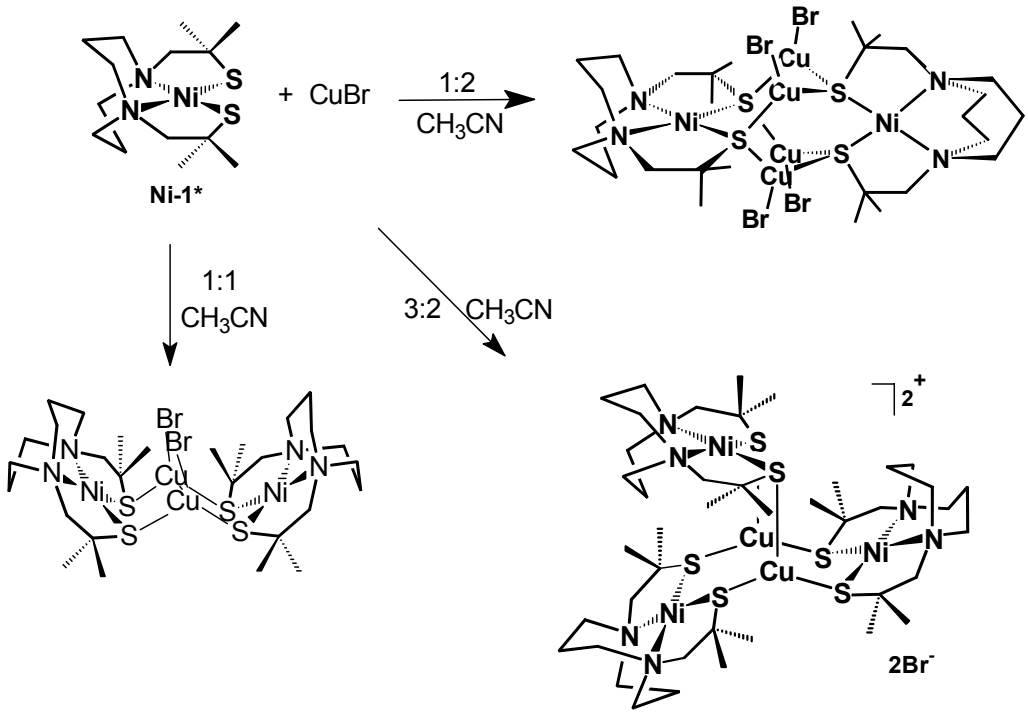

Figure VI-3. Preparation of polymetallic (NiN_2S_2)Cu clusters in various **Ni-1*** to Cu^I ratio.

The synthesis of the $[(\mathbf{Ni\text{-}1})Rh(CO)(PPh_3)][Cl]$ complex proceeds *via* ligand displacement of a PPh_3 and a chloride ion from $Rh(CO)(PPh_3)_2(Cl)$ (Figure VI-4). The orange solid in solution has a ν(CO) stetch in the terminal CO bound region of the infrared spectrum at 1988 cm^{-1}, a 10 cm^{-1} difference from the starting complex (ν(CO) 1978 cm^{-1}). ESI mass spectroscopy confirmed that 100% of the product was $[(\mathbf{Ni\text{-}1})Rh(CO)(PPh_3)]^+$, with a mass to charge ratio of 683. No other clusters of higher

nuclearity were observed in the mass spectra, indicating that this species forms relatively easily upon electrospray ionizataion.

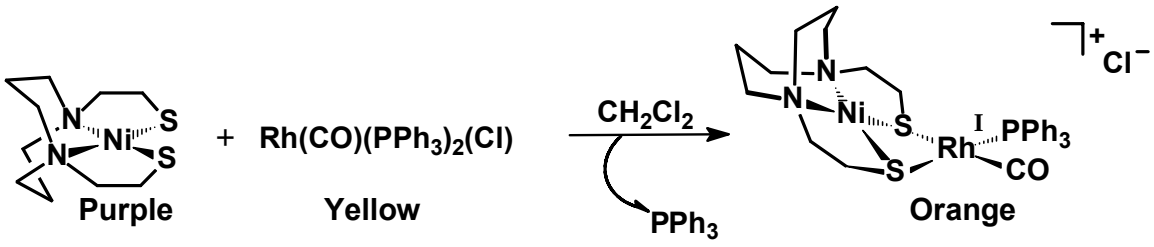

Figure VI-4. Synthesis of [(**Ni-1**)Rh(CO)(PPh_3)][Cl] *via* ligand displacement.

Solid State Characterization of (NiN_2S_2)Cu^IComplexes

The molecular structures of (**Ni-1***)$_2$($CuBr)_2$, [(**Ni-1***)$_3Cu_2$][Br_2] and (**Ni-1***)$_2$($CuBr)_4$ were obtained from X-ray diffraction studies and are shown as ball-and-stick representations throughout the text. The experimental crystallographic data are listed in Table VI-1, and the selected metric data are listed in Table VI-2. Selected metric data corresponding to the free metallodithiolate are also included for comparison. In all three complexes, the diazacycle ligand framework remains in the usual boat/chair configuration with respect to the Ni and the thiolate pendant arms are eclipsed with respect to each other across the N_2S_2 plane. Upon metallation, the Ni-N bond distances are shortened with a concurrent increase in Ni-S bond distances.

Table VI-1. Crystallographic Experimental Data for (**Ni-1***)$_2$(CuBr)$_2$, [(**Ni-1***)$_3$Cu$_2$][Br$_2$], (**Ni-1***)$_2$(CuBr)$_4$ and [(**Ni-1**)Rh(CO)(PPh$_3$)][Cl].

	(Ni-1*)$_2$(CuBr)$_2$	[(Ni-1*)$_3$Cu$_2$][Br$_2$]	(Ni-1*)$_2$(CuBr)$_4$	[(Ni-1)Rh(CO)(PPh3)][Cl]
Formula	$C_{28}H_{56}Br_2Cu_2N_4Ni_2S_4$ (CH$_3$CN)	$C_{42}H_{85}Br_2Cu_2N_6Ni_3S_6$ 3(CH$_2$Cl$_2$)	$C_{56}H_{112}Br_8Cu_8N_4Ni_3S_4$ 8(CH$_3$CN)	$C_{29}H_{37}ClN_2NiO_2PRhS_2$ H$_2$O
Temperature (^{0}K)	110(2)	110(2)	110(2)	110(2)
Wavelength (Å)	0.71073	0.71073	0.71073 Å	0.71073
Z	8	8	4	2
D_{calcd} (g/cm^3)	1.706	1.557	1.867	1.67
μ μχ($^{1-}$)	42.32	30.48	57.8	15.32
Crystal System	Orthorhombic	Monoclinic	Monoclinic	Triclinic
Space Group	Pbca	C2/c	P2(1)/n	P-1
Unit Cell				
a(Å)	14.1557(15)	42.629(4)	13.5542(12)	9.119(5)
b(Å)	20.801(2)	13.7696(13)	32.169(3)	11.111(5)
c(Å)	27.034(3)	24.700(2)	23.427(2)	14.916(5)
β(°)	90	109.534(2)	100.459(2)	79.333(5)°.
Volume (Å^3)	7960.0(15)	13664(2)	10044.9(15)	1467.5(12)
Goodness-of-fit	0.879	1.001	0.918	1.078
R_1[b], wR_2[c](%) [I>2σ(I)]	0.0616, 0.1385	0.0709, 0.1770	0.0859, 0.1925	0.0562, 0.1327
R_1[b], wR_2[c](%) all data	0.1148, 0.1606	0.1216, 0.2210	0.2504, 0.2613-3	0.0715, 0.1429

[a] Obtained using graphite-monochromatized Mo-Kα at 110K.
[b] $R_1 = \Sigma \big| |F_o| - |F_c| \big| / \Sigma F_o$. [c] $wR_2 = [\Sigma[w(F_o^2 - F_c^2)^2] / \Sigma w(F_o^2)^2]^{½}$.

Table VI-2: Selected Averaged Distances (Å) and Angles (°) for (**Ni-1***)$_2$(CuBr)$_2$, [(**Ni-1***)$_3$Cu$_2$][Br$_2$]and (**Ni-1***)$_2$(CuBr)$_4$.

	(**Ni-1***)$_2$Cu$_2$Br$_2$	[(**Ni-1***)$_3$Cu$_2$][Br$_2$]	(**Ni-1***)$_2$(CuBr)$_4$	**Ni-1***
Cu----Cu(Å)	3.481	3.054	3.167-4.866	
Ni----Cu (Å)	3.375	3.383	3.128-4.164	
Cu-S $^a_{avg}$ (Å)	2.258(2)	2.281(3)	2.241(6)	
Ni-S $^a_{avg}$ (Å)	2.167(2)	2.172(3)	2.185(6)	2.152(1)
Ni-N $^a_{avg}$ (Å)	1.987(7)	1.980(8)	1.982(16)	1.995(3)
N-Ni–S $^a_{avg}$ (^{o})	90.6(2)	91.2(3)	89.2(5)	
N-Ni-N $^a_{avg}$ (^{o})	90.7(3)	89.7(3)	90.7(7)	90.4(1)
S-Ni-S $^a_{avg}$ (^{o})	88.2(9)	87.8(11)	91.1(2)	88.8(1)
S-Cu-S	117.8(9)	119.9(11)	114.4(12)	
S-Cu-Br	120.3(7)	-	123.6(18)	

[a] Averaged bond distances and estimated standard deviations given in parentheses.

A tetranuclear complex of the formulation (**Ni-1***)$_2$(CuBr)$_2$, synthesized from equal molar amounts of both **Ni-1*** and CuBr, shows that the **Ni-1*** ligand coordinates two Cu^I metal ions in a bidentate bridging fashion (Figure VI-5). When viewed from the side, this complex resembles that of the letter "W" in which the **Ni-1*** unit comprises the "outer leg" and the Cu_2S_2 plane comprises the "inner leg" of the letter. The Ni^{2+} metal ions retain their square planar geometry, while the Cu atoms are trigonal planar with a Cu----Cu interaction of 3.48 Å. The folding angle calculated between the best plane of the Cu_2S_2 unit and of each the NiN_2S_2 units is 99.9° for Ni(1) and 104.3° for Ni(2), respectively. The larger folding angle with the Ni(2) unit is also reflected by the 0.06 Å increase in Ni----Cu metal interaction. Certainly, this unique polymetallic has not been observed before and does not resemble the stair case structural form presented in Figure

VI-2. The Cu----Cu interaction is 0.7 Å longer than the staircase structure in $[(NiN_2S_2)_2Cu_2]^{2+}$ (NiN_2S_2 = hexamethylated diamino dithiolate, Cu----Cu = 2.82 Å) and 0.8 Å longer than the rhombic $[(Ni(L_H\text{-}N_2S_2)_2Cu_2]^{2+}$ ($Ni(L_H\text{-}N_2S_2)^{2-}$ = N,N'-ethylenebis(2-mercaptoisobutyramide)), Cu----Cu = 2.64 Å) structure in which the Cu^I atoms have a linear geometry.[33a,36]

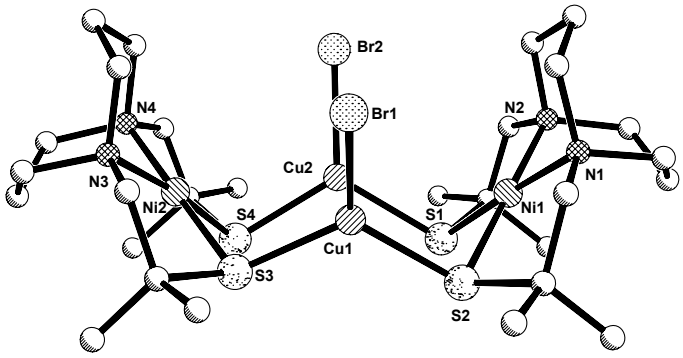

Figure VI-5. Ball-and-stick representation of structure of $[(\mathbf{Ni\text{-}1^*})_2Cu_2][Br_2]$ with hydrogen atoms omitted.

The pentanuclear complex, $[(\mathbf{Ni\text{-}1^*})_3Cu_2][Br_2]$, was derived from mixing **Ni-1*** and CuBr in a 3:2 molar ratio. The molecular structure of $[(\mathbf{Ni\text{-}1^*})_3Cu_2][Br_2]$ (Figure VI-6) is reminiscent of the C_3 zinc and copper pinwheel complexes utilizing the **Ni-1** ligand.[106,29] There are three square planar **Ni-1*** units as paddles and an "axle" along the bridging Cu atom without bromide ion coordination. In fact, the bromide ligands are not located within the coordination sphere of the Cu(I) ions, leaving copper in a trigonal planar geometry within the S_3 plane (Cu(I)----Br(I) interactions ranging from 8.3-9.5 Å). As a result, the Cu----Cu interaction increases as Cu^I goes from a trigonal planar to

tetradrahedral geometry in which the bromide ions pulls the Cu^{I} out of the S_3 plane in the zinc and copper pinwheels. The Cu----Cu interaction with the trigonal planar copper paddlewheel, [(**Ni-1***)$_3$Cu$_2$][Br$_2$], is 3.054 Å, while the tetrahedral copper and zinc complexes have a Cu----Cu and Zn----Zn interaction of 4.053Å and 4.35Å, respectively.[29,106] It is possible that a small amount of steric hindrance from the gem dimethyl groups on the thiolate pendent arms may have an influence on the coordination of the bromide counterion. This is the only structural variation between the **Ni-1** and **Ni-1*** ligands, which have similar $\angle_{S\text{-}Ni\text{-}S}$ angles (ca. 90°) . The folding angle between the NiN_2S_2 plane and the Cu_2S_2 plane is ca. 103°, again showing that as the folding angle increases, the Ni----Cu interaction also increases so there is less metal-metal interaction.

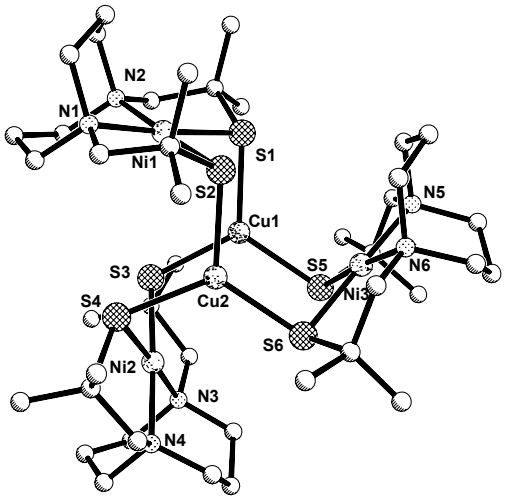

Figure VI-6. Ball-and-stick representation of [(**Ni-1***)$_3$Cu$_2$]Br$_2$ with hydrogen atoms omitted.

The (**Ni-1***)$_2$(CuBr)$_4$ admantane-like complex derived from a 1:2 ligand to metal ratio is structurally very similar to the (**Ni-1***)$_2$(CuCl)$_4$ analogue.[26] The only structural difference lies in the asymmetric unit, which consists of two admantane-like structures and the metal halide source employed. One structure shows a Cu metal atom in a tetrahedral geometry, coordinated by two sulfur donors, a bromide and a CH_3CN solvent molecule (Figure VI-7). The rest of the Cu atoms in both structures assumes a trigonal planar geometry. Note that there are no other solvent metal interactions similar to that observed in the crystal packing of the (**Ni-1***)$_2$(CuCl)$_4$ analogue.[26] Each nickeldithiolate sulfur donor is ligated to two Cu atoms, and the NiN_2S_2 planes are oriented perpendicular to each other.

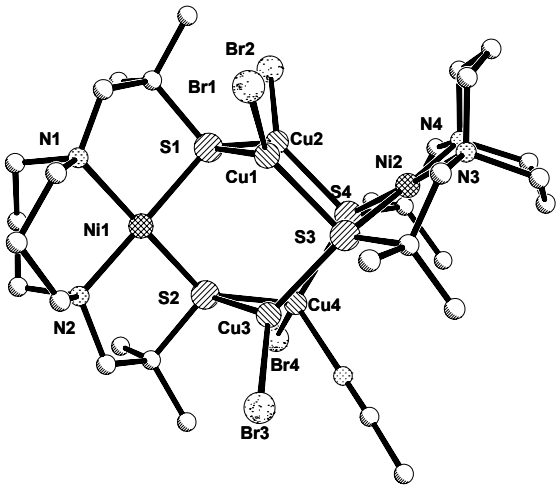

Figure VI-7. Ball-and-stick representation of [(**Ni-1***)$_2$(CuBr)$_4$(CH_3CN)] with hydrogen atoms omitted.

In general, the $\angle_{S\text{-}Ni\text{-}S}$ angles vary in all three structures and are largely defined by the number of Cu^{I} ions bridging the NiN_2S_2 units as well as the coordination geometry of the Cu metal center. The $\angle_{S\text{-}Ni\text{-}S}$ angle of the "W-shape" complex, [(**Ni-1***)$_2$Cu$_2$][Br$_2$], is greater than the "Cu-paddlewheel" complex, [(**Ni-1***)$_3$Cu$_2$]Br$_2$, where a third NiN_2S_2 positions itself in place of the bromide counterions, satisfying the coordination sphere of Cu^{I}. Consequently, the Cu----Cu metal interaction decreases by ca. 0.43Å as the bidentate ligand bites down on the two Cu metal atoms. Both the "W-shape" and "paddlewheel" complexes have $\angle_{S\text{-}Ni\text{-}S}$ angles ca. 4° smaller than that of "adamantane-like" complex in which four Cu^{I} ions are coordinated to two NiN_2S_2 units (Cu----Cu interactions range between 3.128–4.164 Å). This formulation is not surprising, since the remaining lone pair on the each thiolate donor remains accessible for metal coordination, and thiolates are known to have strong binding affinites for sulfur.[30] The average $\angle_{N\text{-}Ni\text{-}N}$ and $\angle_{S\text{-}Ni\text{-}S}$ angles remain relatively unchanged upon metallation except for the $\angle_{S\text{-}Ni\text{-}S}$ angle of the admantane-like structure, which opens up ca. 2° from the parent complex. This is reasonable since there are more CuBr units located within the S_4 cavity.

Of the structural forms presented, indeed the size of the cluster is dependent on the NiN_2S_2 ligand to Cu^{I} ion metal ratio and is less dependent on the relatively small steric hindrance the gem dimethyl groups provide. The smallest polymetallic cluster obtainable had a ligand to metal ratio of 1:1; however, in the presence of excess Cu^{I} or **Ni-1*,** the [(**Ni-1***)$_3$Cu$_2$][Br$_2$], and (**Ni-1***)$_2$(CuBr)$_4$ complexes are easily formed.

Solid State Characterization of [(Ni-1)Rh(CO)(PPh_3)][Cl]

While several polynuclear aggregates were synthesized by the use of metal halide sources, the [(**Ni-1**)Rh(CO)(PPh_3)][Cl] complex is an excellent example of aggregative control by using metal sources other than metal halides that promote aggregation. The molecular struture of [(**Ni-1**)Rh(CO)(PPh_3)][Cl] is shown in a ball-and-stick representation with selected metric data in the figure caption (Figure VI-8). The rigid square planar **Ni-1** unit coordinates to the Rh^I metal center in a bidentate mononucleating fashion. The Rh^I also adopts a square planar geometry with the CO and PPh_3 ligand completing the coordination sphere. A non-coordinated chloride ion stabilizes charge on the Rh^I heterobimetallic and a H_2O water molecule is also located in the unit cell (Rh----Cl interaction of 7.671 Å). A decrease in the Ni-N distance and increase in Ni-S are also observed upon metallation. The $\angle_{S\text{-}Ni\text{-}S}$ angle is pinched ca. 4° from the parent **Ni-1*** complexes as the thiolates form a μ-SR bridge to the Rh metal center, which opens up the $\angle_{N\text{-}Ni\text{-}N}$ by 2°. The μ-SR bridge formed between Rh^I and Ni^{II} metal centers positions the NiN_2S_2 ligand almost perpendicular to the Rh metal center with a dihedral angle of 115° (dihedral angle defined by the intersection of the NiN_2S_2 and RhS_2CP planes) with a Ni----Rh interaction of 2.996 Å. It is interesting to note that the dihedral angle is ca. 11° larger than that observed for the (**Ni-1**)Pd(CH_3)(Cl) heterobimetallic. This is perhaps due to the bulky PPh_3 group that is positioned opposite to the NiN_2S_2 ligand.[74] One of the aromatic rings on the PPh_3 group is above the RhS_2PC plane in front of the CH_2 groups of the diazacyle backbone, while the other two aromatic rings are below the plane. Most of the steric bulk by the ligands is above the

RhS_2PC plane, which adds an attractive stereo-chemical feature similar to (**Ni-1**)$Pd(CH_3)(Cl)$.

Derivatization of the Ni-Rh heterobimetallic complex could lead to viable precursors for catalysis such as oxidative addition by CH_3^+, a preliminary step in the Monsanto acetic acid process. Hydride addition to [(**Ni-1**)$Rh(CO)(PPh_3)$][Cl] to form a $(L_2)RhH(CO)$ complex would also be a suitable precursor for hydroformylation. The electron rich Nature of the metallodithiolate ligand makes these heterobimetallic systems suitable for stabilizing the metal center during catalysis, where oxidation state changes are required.

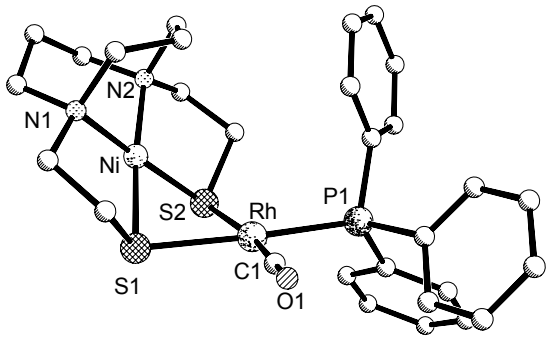

Figure VI-8. Ball-and-stick representation of [(**Ni-1**)$Rh(CO)(PPh_3)$][Cl] with hydrogen atoms omitted. Selected averaged distances (Å) and angles (deg): Ni-S_{avg}, 2.165(14); Rh-$S1_{avg}$, 2.386(13); Ni-N_{avg}, 1.963(4); Rh-P_{avg}, 2.271(13); Ni···Rh, 2.996; S-Ni-S, 85.4(5); N-Ni-N, 91.4(16); N-Ni-S_{avg}, 91.4(12); P1-Rh-C1, 91.7(15), C1-Rh-S2, 167.9(15); C1-Rh-S2, 92.3(15); P1-Rh-S1, 175.7(4); P1-Rh-S2, 99.9(5).

Electronic Spectra and Molar Conductance of (NiN_2S_2)Cu Polymetallics

Ni-1* is a distinctive purple solution that changes color immediately upon addition of the pale yellow CuBr solution, forming polynuclear aggregates that have subtle color differences both in the solid and solution states. Shown in Table VI-3 are the electronic absorptions and molar absorptivites for the mixed valent species. **Ni-1*** exhibits ligand field (LF) d-d electronic absorptions at 350 (ε = 143 $M^{-1}cm^{-1}$) and 438 nm (ε = 90 $M^{-1}cm^{-1}$). Comprehensive assignments of mixed metal-copper systems were made by Shugar *et al.* in similar (NiN_2S_2)Cu clusters.[35a]

Table VI-3. UV-Vis Spectroscopy and Conductivity Measurements of (NiN_2S_2)Cu Aggregates.

Compound	**Ni-1***	[(**Ni-1***)$_2$($CuBr)_2$]	[(**Ni-1***)$_3Cu_2$][Br_2]	[(**Ni-1***)$_2$($CuBr)_4$]
Color	Blue-purple	Brown	Dark Brown	Orange-Brown
UV[a] (nm(ε))[b]	350nm (143) 438 (90)	220 (43994) 252 (26727) 308 (7999.2) 592 (262.07)	220 (66657) 250 (44872) 306 (15612) 388 (3897) 572 (606.63)	216 (46042) 252 (28529) 320 (9708.9) 334 (9603.3) 370 (7207.7)
Molar Conductance[c]		72	196	20

[a]Data obtained in CH_3CN. [b] Molar absorptivity = ε in $M^{-1}cm^{-1}$. [c] Molar conductance = $\Lambda(cm^2mol^{-1}ohm^{-1})$

All of the complexes exhibit three or four bands in their UV-Vis spectra that are characteristic of ligand-field (LF) charge transfer electronic transitions as evidenced by the large molar absorptivity as seen in Table VI-3. The number of LF charge transfer transitions increase with an increase in the **Ni-1*** to Cu^I ratio and would account for the

slight variations in color. A plot of absorbance versus wavelength (Figure VI-8) elucidates the difference in the electronic absorptions of the d-d transitions of the $(NiN_2S_2)Cu$ polymetallics. (**Ni-1***)$_2$(CuBr) and [(**Ni-1***)$_3$Cu$_2$][Br$_2$] exhibit relatively strong d-d electronic absorptions whereas [(**Ni-1***)$_2$(CuBr)$_4$] shows extremely weak d-d electronic absorptions.

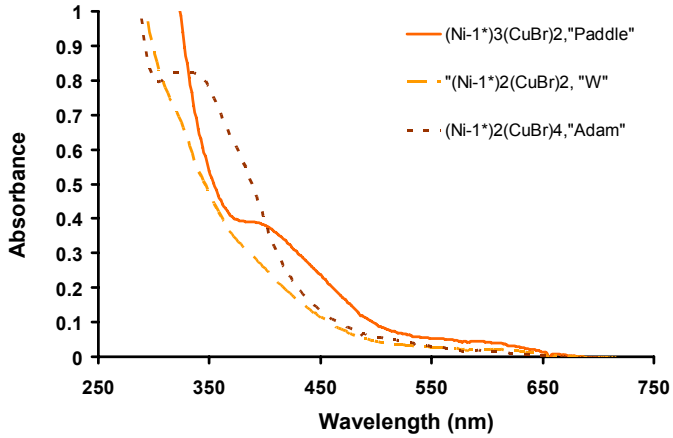

Figure VI-9. UV-Vis spectral overlay of d-d transitions of **(Ni-1***)$_2$(CuBr)$_2$, [(**Ni-1***)$_3$Cu$_2$][Br$_2$]and (**Ni-1***)$_2$(CuBr)$_4$ polymetallic clusters in CH_3CN between 300 nm and 600 nm.

Conductivity measurements were performed to determine if the aggregates maintain their structural integrity in solution. The molar conductivity of $1.0x10^{-3}$M samples of (**Ni-1***)$_2$Cu$_2$Br$_2$ and [(**Ni-1***)$_2$(CuBr)$_4$] in CH_3CN gave a $\Lambda(cm^2mol^{-1}ohm^{-1})$ of 72 and 20 suggesting that few ions were present in the solution**.** Measurements for [(**Ni-1***)$_3$Cu$_2$][Br$_2$] gave a $\Lambda(cm^2mol^{-1}ohm^{-1})$ of 196 suggesting two or three ions were present in solution. The number of ions present in solution for all three mixed valent systems were consistent with that obtained in the solid state structure. The lack of

dissociation in solution also suggests that the complexes are very stable aggregates in solution.

Electrochemistry

The cyclic voltammograms (CV) of the $(NiN_2S_2)Cu$ aggregates were recorded in CH_3CN and were scanned beginning in the negative potential direction (Figure VI-10, page 153) . Two redox events were observed in the cathodic region for (Ni-**1***)$_2(CuBr)_2$ and [(**Ni-1***)$_3Cu_2$][Br_2] as shown in Table VI-4. The first redox event is *quasi-reversible,* while the second event is *irreversible*. These consecutive redox events in the cathodic region are assigned to a $Ni^{II/I}$ redox couple and not a $Cu^{I/0}$ redox event, in which the Ni^{2+} from each NiN_2S_2 unit is electrochemically reduced to Ni^{+1}.

Table VI-4. Comparison of $Ni^{II/I}$ Reduction Potentials for $(NiN_2S_2)Cu$ Clusters.

Complex	E ½ $Ni^{II/I}$[V]	$^{2nd}E_{pc}$ [V]	ΔE^b [V]
Ni-1*	-2.12		
[(Ni-1*)$_2(CuBr)_2$	-1.28	-2.14	0.86
[(Ni-1*)$_3Cu_2$][Br_2]	-1.31	-2.11	0.80
(Ni-1*)$_2(CuBr)_4$	-1.42	-	-

[a] All potentials scaled to NHE referenced to a Cp_2Fe^+/Cp_2Fe standard ($E_{1/2}$=0.4V) at 25°C. In CH_3CN solutions, 0.1M n-Bu_4NBF_4 electrolyte, measured vs. Ag/$AgNO_3$ reference electrode. [b] Difference between the first and second reduction.

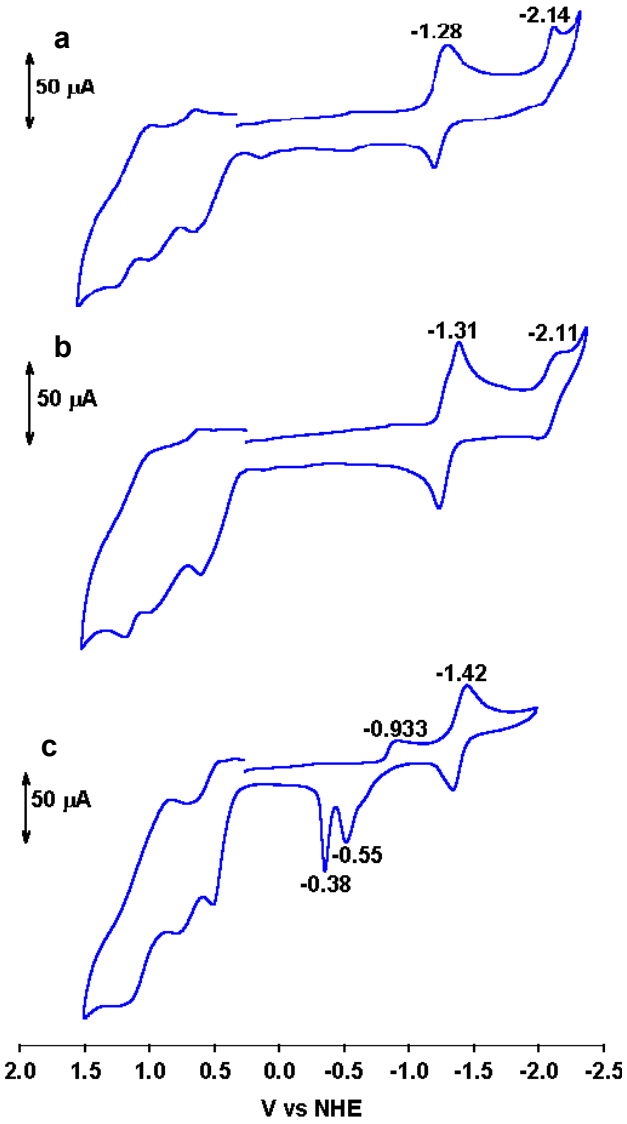

Figure VI-10: Cyclic voltammograms of 1.0 mM solutions of (a) (**Ni-1***)$_2$(CuBr$_2$), b) [(**Ni-1***)$_3$Cu$_2$][Br$_2$], (c) (**Ni-1***)$_2$(CuBr)$_4$ in a 0.1M n-Bu$_4$NBF$_4$ with a glassy carbon electrode at a scan rate of 200 mV/s. All potentials are scaled to NHE.

These assignments are consistent with polymetallic compounds in which the metal in the N_2S_2 chelate is reduced first and not the metal in the S_4 core.[27] A third $Ni^{II/I}$ redox event was not observed for $[(\mathbf{Ni\text{-}1^*})_3Cu_2][Br_2]$, since it probably extends beyond the CH_3CN solvent window concurrent in aggreement with that observed for the $(Ni\text{-}\mathbf{1^*})_3(ZnBr)_2$.[27] Multiple oxidations in the anodic region are assumed to be either metal-based or sulfur based.[27] The interpretation of the two redox events as explained above show that regardless if the metal (M) is two or four Cu^I metal ions in the non-chelating sulfur donor environment is best illustrated in Figure VI-11.

$$\mathbf{[(Ni^{II}\text{-}1)(M^I)_x(Ni^{II}\text{-}1)]^{2+} \overset{e^-}{\rightleftharpoons} [(Ni^{I}\text{-}1)(M^I)_x(Ni^{II}\text{-}1)]^{+} \overset{e^-}{\rightleftharpoons} [(Ni^{I}\text{-}1)(M^I)_x(Ni^{I}\text{-}1)]^{2+}} \quad \mathbf{(1)}$$

$\mathbf{x = 2, 4}$

Figure VI-11. Mechanism of redox reactions observed during cyclic voltammetry.

The CV of $Ni_2Cu_4S_4$adam is reminiscent of that observed for the $(\mathbf{Ni\text{-}1^*})_2(CuCl)_4$ derivative with a reversible redox event at -1.42V, attributed to a $Ni^{II/I}$ event (Figure VI-9, c) . A second redox couple within the permitted solvent window was not observed. As established for the $(\mathbf{Ni\text{-}1^*})_2(CuCl)_4$ analogue, the two irreversible oxidative events at -0.55V and -0.38V are reminiscent of (diphos)CuCl, which suggests that the metallothiolates have phosphine-like abilities.[26]

For all complexes, the $Ni^{II/I}$ redox couple is shifted to positive potentials from the parent complex ($Ni^{II/I}$ = -2.12 V), indicating that the $Ni^{II/I}$ couple is more accessible upon metallation.[27] It is interesting to note that the $Ni^{II/I}$ redox couple in the adamantane-like complex, (**Ni-1***)$_2$(CuBr)$_4$, has the most negative redox potential, which suggests that the Ni^{2+} ions are more difficult to reduce in this cluster. One might expect the opposite, since metallation by the remaining lone pairs on the sulfur atoms should draw more electron density away from the Ni center, which becomes more positively charged and easily reduced. However, in this case, this effect seems to be overridden by the electron density added by the copper ions. Finally, the difference between the 1st and 2nd reduction potentials is taken as a measure of electron delocalization in the mixed valent species formed on the initial reduction. [(**Ni-1***)$_3$Cu$_2$]Br$_2$ has an ΔE of 0.80V which signifies that the electron density is more delocalized than in [(**Ni-1***)$_2$(CuBr)$_2$.

COMMENTS AND CONCLUSIONS

The aggregative tendency of metallodithiolates with exogenous metals to produce polymeric species has been an overwhelming factor and a challenge for synthetic chemists interested in designing biomimetic models of enzyme active sites with thiolate ligands. Polymetallic complexes are often unreactive towards any type of substrate addition or modification. In our efforts to produce heterobimetallic complexes employing NiN_2S_2 ligands with Cu^I salts, we have found that the size of the cluster can be controlled to some degree by varying the ligand to metal ratio. However, due to the thiophilicity of copper, a 1:1 equimolar ratio of Ni-1* to Cu^I did not produce the desired heterobimetallic. The steric influence of the gem dimethyl groups on the dithiolate

pendent arms do not sufficiently control aggregation, as evidenced by other similar heterobimetallic nickel-copper clusters.[24,26,29,33a,35,36,40,101,102] In this chapter, the synthesis and structural characterization of three additional Ni-Cu polymetallic complexes containing four to six metal ions with the methylated N_2S_2 derivative were presented. The tetranuclear (**Ni-1***)$_2Cu_2Br_2$, pentanuclear [(**Ni-1***)$_3Cu_2$][Br_2], and hexanuclear (**Ni-1***)$_2(CuBr)_4$ complexes add to the library of other well known structural forms of (NiN_2S_2)Cu polymetallic clusters. These complexes remain intact as aggregates, indicating that these complexes have a strong binding affinity for the metal center, in agreement with Golden *et al.* where the Cu^I binding affinity is found to be 10 times greater in solution.[30]

The use of extremely large R groups on the pendent thiolate arms provides its own synthetic challenges and thus far has not been investigated. For now the construction of heterobimetallic complexes with functional metal centers relies on using metal sources with a combination of sterically bulky ligands and labile ligands. The synthesis of heterobimetallic complexes like the [(**Ni-1**)Rh(CO)(PPh_3)][Cl] is additional evidence for utilizing this type of synthetic strategy.

CHAPTER VII

CONCLUDING REMARKS

The discovery of the ACS active site renewed interest in the use of NiN_2S_2 complexes as building blocks for the construction of small molecule mimics of bimetallic enzyme active sites. The striking resemblance of the $Ni_dN_2S_2$ moiety within the active site to biomimetic NiN_2S_2 complexes found within the literature was unexpected, yet not entirely surprising. Several synthetic groups have established that NiN_2S_2 thiolate donors have a high binding affinity for exogenous metals and form a broad range of aggregates. A synthetic challenge for many chemists interested in designing heterobimetallic complexes with the NiN_2S_2 ligands as a building blocks has been how to control the degree of polynucleation.

From synthetic efforts described in this dissertation, we have successfully designed several new bimetallic complexes by coordinating the bidentate NiN_2S_2 ligands to an appropriate choice of metal precursor. The selected metal precursor required some form of inert ligand component (in most cases a carbon moiety such as CH_3 or CO) in addition to labile ligands that were easily displaced by one NiN_2S_2 ligand to form the heterobimetallic complex. Several $(NiN_2S_2)M(L)_x$ complexes of W^0, Pd^{2+} and Rh^I were prepared and characterized. Derivatives of metal halide source, such as CuBr, yielded small clusters with the NiN_2S_2 ligands; the clusters ranged from a small tetranuclear to a large hexanuclear species in which the nickeldithiolates utilized all available lone pairs on the sulfur to coordinate to copper. We conclude that the best route to bimetallic

complexes employing NiN_2S_2 complexes is through labile ligand displacement reactions on organometallic compounds (Figure VII-1).

The synthesis of the bimetallic complexes presented within this dissertation has allowed us to explore NiN_2S_2 complexes as ligands. A comparison of the ν(CO) stretching frequency of $NiN_2S_2W(CO)_4$ complexes with the classical diimine and diphosphine ligands to tungsten tetracarbonyl metal centers showed that NiN_2S_2 ligands are more electron rich. How much the Ni^{2+} metal tunes the donor property of the dithiolate is still relatively unknown. A different metal in the N_2S_2 core is expected to play a role in tuning the ligand and studies of the CoNO analogue, (bme-daco)CoNO, are currently being investigated. My work has established the first electron donor scale for a series of nickeldithiolate ligands that are neutral and anionic. As more MN_2S_2 ligands are synthesized or modified, this scale provides a reference point for other metallodithiolate ligands.

Structural analysis of all the compounds has shown a unique structural feature of the μ-SR bridge between the Ni^{2+} in the N_2S_2 core and the metal (M) to which the ligand is bound (M= W^0, Pd^{2+} and Rh^I), that produces a hinge at the μ-SR unit. This feature, as is an attractive one for stereo- and regioselective substrate addition as it places the NiN_2S_2 unit on one side of a reactive metal center. The degree of asymmetry by the NiN_2S_2 unit varies in all the bimetallic models explored this far and is a defining characteristic of these ligands. Whether this is due to steric influence of other ligands on the adjacent metal center or the directionality of the lone pairs on the dithiolate ligand has not been determined at this point. Molecular modeling studies are required to

explore this possibility. In addition to the steric and electronic properties established for this novel class of ligands, the NiN_2S_2 ligands were demonstrated to behave as hemilabile ligands. The arm-off possibility for the bidentate NiN_2S_2 was illustrated by CO addition studies to $NiN_2S_2W(CO)_4$ complexes; such hemilability supports computational mechanism proposed by Webster *et al*. for the ACS active site. [23]

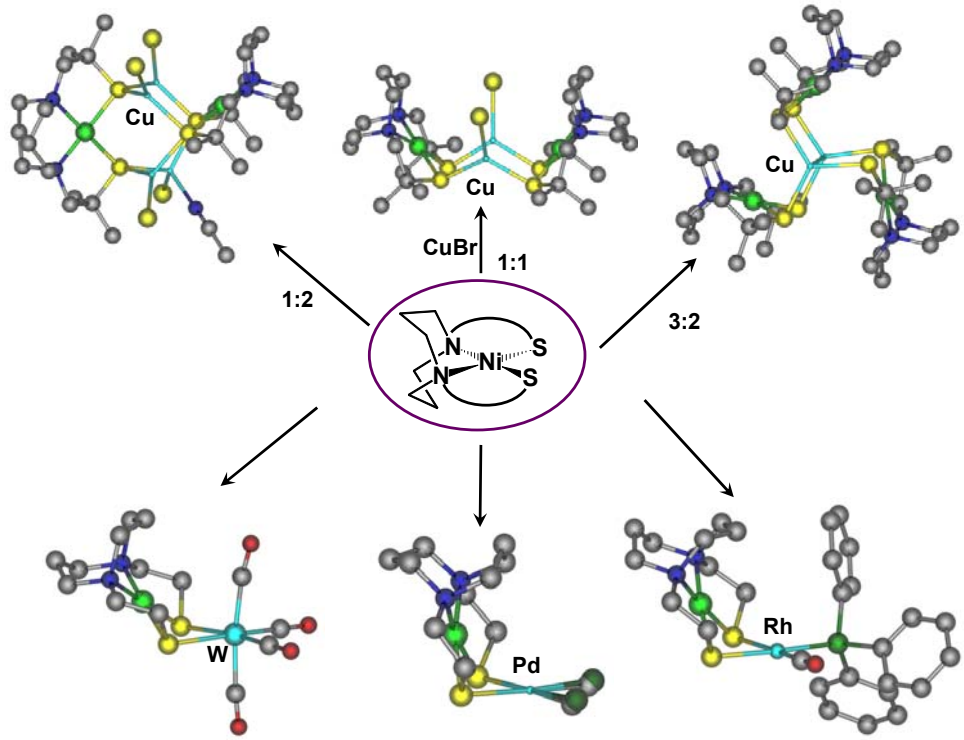

Figure VII-1. POV-Ray models of new heterobimetallic complexes, $(NiN_2S_2)_xM_y$ complexes.

The bimetallic models of an industrial catalyst and the ACS enzyme active site provided the method to test the capability of metallodithiolate ligands to support

catalysis at a palladium metal center. Our studies have shown that the NiN_2S_2 ligand, **Ni-1**, is capable of stabilizing the Pd^{2+} metal center in C-C coupling reactions. The [(**Ni-1**)$Pd(CH_3)]^+$ is a catalyst for an industrially significant process, but the electron rich Nature of the ligand hinders its development for CO/ethylene copolymerization. The use of the less electron rich MN_2S_2 ligands for this process has not been explored and might be fruitful. However, the NiN_2S_2ligands may be better suited for other types of reactions in which the metal undergoes oxidation state changes. The asymmetric feature of these metal complexes as described above also point to their potential stereo-selective substrate reactions such as in styrene/CO copolymerization.

We are already well on our way to employing the [(**Ni-1**)$Rh(CO)(PPh_3)$][Cl] bimetallic complex in oxidative addition reactions, which are required in the initial steps in the Monsanto acetic acid process. A preliminary investigation using [(**Ni-1**)$Rh(CO)(PPh_3)$][Cl] has suggest that this complex should be pursued as a precursor towards hydroformylation of 1-octene to produce linear and branched aldehydes. Alternatively, the [(**Ni-1**)Rh(CO)(*p*-$P(tolyl)_3$)][Cl] derivative has been prepared by a fellow graduate student, Shawn Fitch, who will be exploring copolymerization of CO_2 and aziridines to produce poly-β-peptoids.

With regards to the enzyme, acetyl CoA synthase that inspired the development of metallodithiolate ligands for organometallic chemistry, our exploratory studies show that the [(**Ni-1**)$Pd(CH_3)]^+$ complex is capable of both C-C and C-S coupling reactions with CH_3^+, CO and $^-$SR substrates similar to the enzyme. While this reactivity is exciting, the door is left ajar for further studies with the [(**Ni-1**)$Pd(CH_3)]^+$ complex. A

full kinetic and thermodynamic study to elucidate thioester formation and quantitative analysis of the yield and catalytic capability towards thioester formation are also necessary in order to produce a fully functional biological mimic of the enzyme that will aid in elucidating the mechanism of thioester formation. In addition, the use of NiN_2S_2 ligands that are more similar in charge and structure, such as the **Ni(ema)$^{2-}$** and Ni(CysGlyCys) ligands, is also required to develop a good synthetic analogue that would be able to stabilize a Ni^I or Ni^0 oxidation state bridged to a Fe_4S_4 cluster. Whether such a structural and functional analogue once achieved would be able to produce the same catalytic capability in the absence of the secondary coordination sphere effects of the surrounding protein is another question. Perhaps the incorporation larger superstructures are required and others are invited to build a new classes of inorganic supramolecular transition metal catalysis; which are already underway by several other groups.[107-110.]

To this end, our work has only touched the surface of the development of metallodithiolate complexes as a new class of ligands whose full potential remains to be explored. "The journey of a thousand miles beings with a single step." We have taken that step.

REFERENCES

1. a) Van Leeuwen, P. W. N. M. *Homogeneous Catalysis, Understanding the Art;* Kluwer Academic Publishers: Netherlands, 2004. b) Van Leeuwen, P. W. N. M.; Kamer, P. C. J.; Reek, J. N. H; Dierkes, P. *Chem. Rev.* **2000**, *100*, 2741-2769.
2. Sen, A. *Catalytic Synthesis of Alkene-Carbon Monoxide Copolymers and Cooligomers*; Kluwer Academic Publishers: Netherlands, 2003.
3. Ledford, J.; Shultz, S. C.; Gates, D. P.; White, P. S.; DeSimone, J.; Brookhart, M. *Organometallics,* **2001**, *20*, 5266-5276.
4. Tolman, C. A.; *Chem. Rev.* **1977**, *77*, 313-348.
5. Casey, C. P.; Whiteker, G. T. *Isr. J. Chem.* **1990**, *30*, 299-304.
6. a) Koide, Y.; Bott, S. G.; Barron, A. R. *Organometallics* **1996**, *15*, 2213-2226. b) Hirota, M.; Sakakibara, K.; Komatsuzaki, T.; Akai, I. *Comput. Chem*. **1991**, *15*, 241-248.
7. White, D.; Taverner, B. C.; Coville, N. J.; Wade, P. W. *J. Organomet. Chem.* **1995**, *495*, 41-51.
8. Slone, C. S.; Weinberger, D. A.; Mirkin, C. A. *Prog. Inorg. Chem.* **1999**, *48*, 233-350.
9. Jeffery, J. C.; Rauchfuss, T. B. *Inorg. Chem*. **1979**, *18*, 2658-66.
10. Espinet, P.; Soulantica, K. *Coord. Chem. Rev*. **1999**, *193-195*, 499-556.
11. Rauchfuss, T. B.; Patino, F. T.; Roundhill, D. M. *Inorg. Chem*., **1975**, *14*, 652-656.

12. Lindner, E.; Schober, U.; Fawzi, R.; Hiller, W., Englert, U.; Wegner, P. *Chem. Ber*., **1987**, *120*, 1621-1628.

13. Lindner, E; Haustein, M.; Fawzi, R.; Steimann, M.; Wegner, P. *Organometallics* **1994**, *13*, 5021-5029.

14. Del Zotto, A.; Rigo, P. *Inorg. Chim. Acta*, **1988**, *147*, 55-59.

15. Nishibayashi, Y. Segawa, K.; Ohe, K.; Uemura, S. *Organometallic*s **1995**, *14*, 5486-5487

16. Valk, J. M.; Whitloch, G. A.; Layzell, T. P.; Brown, J. M.; *Tetrahedron Assymmetry* **1995**, *6*, 2593-2596.

17. Rülke, R. E.; Delis, J. G. P.; Groot, A. M..; Elsevier, C. J.; Van Leeuwen, P. W. N. M.; Vrieze, K.; Goubitz, K.; Schenk, H. *J. Organometallic Chem.* **1996**, *508*, 109-120.

18. Bassetti, M.; Capone, A.; Salamone, M. *Organometallics*. **2004**, *23*, 247-252.

19. Lindner, E.; Schmid, M.; Wegner, P.; Nachtigal, C.; Steimann, M.; Fawzi, R. *Inorg. Chim. Acta.* **1999**, *296*, 103-113.

20. Dokov, T. I; Iverson, T. M; Seravalli, J.; Ragsdale, S. W.; Drennan, C. L. *Science*. **2002**, *298*, 567-572.

21. Darnault, C.; Volbeda, A.; Kim, E. J.; Legrand, P.; Vernède, X.; Lindahl, P. A.; Fontecilla-Camps, J. C. *Nat. Struc. Biol*. **2003**, *10*, 271-279.

22. Svetlitchnyi, V.; Dobbek, H.; Meyer-Klaucke, W.; Meins, T.; Thiele, B.; Romer, P.; Huber, R.; Meyer, O. *PNAS* **2004**, *101*, 446-451.

23. Webster, C. E.; Darensbourg, M. Y.; Lindahl, P. A.; Hall, M. B. *J. Am. Chem. Soc.* **2004**, *126*, 3410-33411.

24. Farmer, P. J.; Reibenspies, J. H.; Lindahl, P. A.; Darensbourg, M. Y. *J. Am. Chem. Soc.* **1993**, *115*, 4665-4674.

25. Golden, M. L.; Jeffery, S. P.; Miller, M. L.; Reibenspies, J. H.; Darensbourg, M. Y. *Eur. J. Inorg. Chem.* **2004***,* 231-236.

26. Miller, M. L.; Ibrahim, S. A.; Golden, M. L.; Darensbourg, M. Y. *Inorg. Chem.* **2003**, *42*, 2999-3007.

27. Musie, G.; Farmer, P. J.; Tuntulani, T.; Reibenspies, J. H.; Darensbourg, M.Y. *Inorg. Chem.* **1996**, *35*, 2176-2183.

28. Jeffery, S. P.; Lee, J.; Darensbourg, M. Y. *Chem. Comm.* **2005**, *9*, 1122-1124.

29. Golden, M. L; Rampersad, M. V.; Reibenspies, J. H.; Darensbourg, M. Y. *Chem.Comm.* **2003**, *15*, 1824-1825.

30. Golden, M. L.; Whaley, C. M.; Rampersad, M. V.; Reibenspies, J. H.; Hancock, R. D.; Darensbourg, M. Y. *Inorg. Chem*. **2005**, *44*, 875-883.

31. Lai, C.-H.; Reibenspies, J. H.; Darensbourg, M. Y. *Angew. Chem., Int. Engl*. **1996**, *35*, 2390-2393.

32. Jicha, D. C.; Busch, D. H. *Inorg. Chem.* **1962**, *1*, 872-877.

33. a) Rao, P. V.; Bhaduri, S.; Jiang, J.; Holm, R. H. *Inorg. Chem.* **2004**, *43*, 5833-5859. b) Rao, P. V.; Bhaduri, S.; Jiang, J.; Hong, D.; Holm, R. H. *J. Am. Chem. Soc.* **2005**, *127*, 1933-1945.

34. Hatlevik, O.; Blanksma, M. C.; Mathrubootham, V.; Arif, A. M.; Hegg, E. L. *JBIC*. **2004**, *9(2)*, 238-246.

35. a) Stibrany, R.T.; Fikar, R.; Brader, M.; Potenza, M.N.; Potenza, J.A.; Schugar, H.J. *Inorg. Chem*. **2002**, *41*(20), 5203-5215. b) Stibrany, R. T.; Schugar, H. J.; Potenza, J. A. *Acta. Cryst.* **2003**, *59*, 630-632.

36. Linck, R. C.; Spahn, C. W.; Rauchfuss, T. B.; Wilson, S. R. *J. Am. Chem. Soc*. **2003**, *125*, 8700-8701.

37. Reynolds, M. A.; Rauchfuss, T. B.; Wilson, S. R. *Organometallics*. **2003**, *22*, 1619-1625.

38. Krishnan, R.; Riordan, C. G. *J. Am. Chem. Soc.* **2004**, *126*, 4485-4485.

39. Wang, Q.; Blake, A. J.; Davies, E. S.; McInnes, E. J. L.; Wilson, C.; Schröder, M. *Chem. Commun*. **2003**, 3012.

40. a) Harrop, T. C.; Olmstead, M. M.; Mascharak, P. K. *Chem. Comm.* **2004**, *15*, 1744-1745. b) M. M.; Mascharak, P. K. *Chem. Comm.* **2004**, *15*, 1744-1745.

41. Kang, D.-X.; Poor, M.; Blinn, E. L. *Inorg. Chimca. Acta.* **1990**, 209-214.

42. Gordon, A. J; Ford, R. A. *The Chemist's Companion*; Wiley and Sons: New York. 1972; pp 429-436.

43. Gagne, R. R.; Koval, C. A.; Lisensky, G. C. *Inorg. Chem.* **1980**, *19*, 2854-2855.

44. Darensbourg, M. Y.; Font, I.; Pala, M.; Reibenspies, J. H. *J. Coord. Chem.* **1994**, *32*, 39-49.

45. Kruger, H. J.; Peng, G.; Holm, R. H.; *Inorg. Chem.* **1991**, *30*, 734-742.

46. Colpas, G. J.; Kumar, M.; Day, R. O.; Maroney, M. J.; *Inorg. Chem.* **1990**, *29*, 4779-4788.

47. Mills, D. K.; Reibenspies, J. H.; Darensbourg, M. Y. *Inorg. Chem.* **1990**, *29*, 4364-4366.

48. Smee, J. J.; Miller, M. L.; Grapperhaus, C. A.; Reibenspies, J. H.; Darensbourg, M. Y. *Inorg. Chem*. **2001**, *40*, 3601-3605.

49. Grapperhaus, C. A.; Mullins, C. S.; Kozlowski, P. M.; Mashuta, M. S. *Inorg. Chem.* **2004**, *43*, 2859-2866.

50. Darensbourg, D. J; Kump, R. L. *Inorg. Chem*. **1978**, *17*, 2680-2682.

51. Cotton, F. A.; Darensbourg, D. J.; Kolthammer, B. W. S. *J. Am. Chem. Soc.* **1981**, *103*, 398-405.

52. Darensbourg, D. J.; Gray, R. L. *Inorg. Chem*. **1985**, *23*, 2993-2996.

53. Sheldrick, G. (1990) *SHELXTL-PLUS* revision 4.11V, *SHELXTL-PLUS* users manual, Siemens Analytical X-ray Inst. Inc., Madison WI, U.S.A.

54. Sheldrick, G. (1997) *SHELXS-97 Program for Crystal Structure Solution*, Institüt für Anorganische Chemie der Universität, Tammanstrasse 4, D-3400 Gottingen, Germany.

55. Sheldrick, G. (1997) *SHELXL-97 Program for Crystal Structure Refinement*, Institüt für Anorganische Chemie der Universität, Tammanstrasse 4, D-3400 Gottingen, Germany.

56. *SHELXTL*, version 5.1 or later; Bruker Analytical X-ray Systems: Madison, WI. 1998.

57. De Graaf, W.; Boersma, J.; Smeets, J. J.; Spek, A. L.; van Koten, G. *Organometallics*, **1989**, *8*, 2907-2917.

58. Brookhart, M.; Grant, M.; Volpe, A. F. *Organometallics* **1992**, *11*, 3920-3922.

59. Rülke, R. E.; Ernsting, J. M.; Spek, A. L.; Elsevier, C. J.; Van Leeuwen, P. W. N. M.; Vrieze, K. *Inorg. Chem*. **1993**, *32*, 5769-5778.

60. Amara, P.; Volbeda, A.; Fontecilla-Camps, J. C.; Field, M. J. *J. Am. Chem. Soc*. **2005**, *127*, 2776-2785.

61. Bancroft, G. M.; Dignard-Bailey, L.; Puddephatt, R. J.; *Inorg. Chem.* **1986**, *25*, 3675-3680.

62. Lichtenberger, D. L.; Jatcko, M. E. *J. Coord. Chem,* **1994**, *32*, 79-101.

63. Yoo, J.; Ko, J.; Park, S. *Bull. Korean, Chem. Soc.* **1994**, *15(9)*, 803-805

64. Chojnacki, S. S; Hsiao, Y.-M.; Darensbourg, M. Y; Reibenspies, J. H. *Inorg. Chem*, **1993**, *32*, 3573-3576.

65. Bouwman, E.; Henderson, R. K.; Spek, A. L.; Reedijk, H. *Eur. J. Inorg. Chem.* **1999**, 217-219.

66. Cotton, F. A; Kraihanzel, C. S. *J. Am. Chem. Soc*. **1962**, *85*, 4432-4438.

67. Buonomo, R. M.; Font, I.; Maguire, M. J.; Reibenspies, J. H.; Tuntulani, C.; Darensbourg, M. Y. *J. Am. Chem. Soc*. **1995**, *117*, 963-973.

68. Rampersad, M.V.; Jeffery, S.P.; Reibenspies, J.H.; Ortiz, C.G.; Darensbourg, D.J.; Darensbourg, M.Y. *Angew. Chem. Int. Ed*. **2005**, 44, 1217-1220.

69. Buchner, W.; Schenk, W. A. *Inorg. Chem.* **1985**, *23*, 132-137.

70. (a) Atwood, J. D.; Brown, T. L. *J. Am. Chem. Soc.* **1976**, *98*, 3160-3166. (b) Atwood, J. D.; Brown, T. L. *J. Am. Chem. Soc.* **1975**, *97*, 3380-3385. (c) Atwood, J. D.; Brown, T. L. *J. Am. Chem. Soc.* **1976**, *98*, 3155-3159. (d) Cohen, M. A.; Brown, T. L. *Inorg. Chem.* **1976**, *15*, 1417-1423. (e) Lichtenberger, D. L.; Brown, T. L. *J. Am. Chem. Soc.* **1978**, *100*, 366-373.

71. Phelps, A. L.; Rampersad, M. V.; Fitch, S. B.; Darensbourg, D. J.; Darensbourg, M. Y. *Inorg. Chem*, **2005**, *Submitted for publication.*

72. Dobson, G. R.; Faber, G. C. *Inorg. Chem.* **1968**, *7*, 585-588.

73. Awad, H. H.; Dobson, C. B.; Dobson, G. R.; Leipoldt, J. G.; Schneider, K.; van Eldik, R.; Wood, H. E. *Inorg. Chem.* **1989**, *28*, 1654-1657.

74. Dobson, G. R.; Cortés, J. E. *Inorg. Chem.* **1988**, *27*, 3308-3314.

75. Ortiz, C. G.; PhD Dissertation. Texas A&M University College Station, TX, 2004.

76. Dobson, G. R. *Inorg. Chem.* **1969**, *8*, 90-95.

77. Darensbourg, D. J.; Draper, J. D.; Frost, B. J.; Reibenspies, J. H. *Inorg. Chem.* **1999**, *38*, 4705-4714.

78. The term “innocent” in this case refers to the stability of the Ni^{II} and RS^{-} redox levels throughout the reactions explored. However, the combination of a redox active metal and thiolate sulfurs lends caution to this assumption. Ray, K.; Weyhermüller, T.; Neese, F.; Wieghardt, K. *Inorg. Chem.* **2005**, *44*, 5345-5360.

79. a) Ogasawara, M.; Yoshida, K.; Hayashi, T. *Organometallics*, **2000**, *19*, 1567. b) Bosch, B. E.; Brümmer, I.; Kunz, K.; Erker, G.; Frölich, R.; Kotila, S. *Organometallics* **2000**, *19*, 1255-1261.

80. Jutand, A.; Hii, K. K.; Thornton-Pett, M.; Brown, J M. *Organometallics*, **1999**, *18, 5367*.

81. Li, K.; Hii, K. K.; Horton, P. N.; Hursthouse, M. B.; Hii, K. K. J.; *Organometallics*, **2003**, *665, 250*.

82. Bianchini, C.; Meli, A.; Oberhauser, W.; Parisel, S. *Organometallics*, **2005**, 1018-1030.

83. Mul, W. P.; Dirkzwager, H.; Broekhuis, A. A.; Heeres, H. J.; van der Linden, A. J.; Orpen, A. G. *Inorg. Chim. Act.* **2002**, 327, 147-159.

84. Drent. E.; Budzelaar, P. H. M. *Chem. Rev.* **1996**, 663-681.

85. Rix, F. C.; Brookhart, M.; White, P. S. *J. Am. Chem. Soc.* **1996**, *118*, 4746-4764.

86. Lai, T. W.; Sen, A. *Organometallics*, **1994**, *3*, 866-870.

87. Chen, J. T.; Sen, A. *J. Am. Chem. Soc*. **1985**, *106*, 1506.

88. Sen, A.; Chen, J. T.; Vetter, W. M.; Whittle, R. R. J. *J. Am. Chem. Soc*. **1987**, *109*, 148.

89. Mul, W. P.; Oosterbeek, H.; Beitel, G. A.; Kramer, G.; Drent. E. *Angew. Chem., Int. Ed*. **2000**, *39*, 1858-1851.

90. Shultz, C.; Ledford, J.; DeSimone, J.; Brookhart, M. *J. Am. Chem. Soc.* **2000**, *122*, 6351-6356.

91. van Asselt, R.; Gielens, E. C. G.; Rülke, R. E.; Elsevier, C. J. *J. Chem. Soc., Chem. Commun*. **1993**, 1203-1205.

92. Hill, A. M.; Levason, W.; Webster, M.; Albers, I. *Organometallics* **1997**, *16*, 5641-5647

93. a) Fanizzi, F. P.; Maresca, L.; Natile, G.; Lanfranchi, M.; Tiripicchio, A.; Pacchioni, G. *J. Chem. Soc., Chem. Commun*. **1992**, 333-335. b) Fanizzi, F. P.; Lanfranchi, M.; Natile, G.; Tiripicchio, A. *Inorg. Chem.*. **1994**, *33*, 3331-3339.

94. Dekker, G. P. C. M.; Buijs, A.; Elsevier, C. J.; Vrieze, K. *Organometallics*. **1992**, *11*, 1937-1948.

95. Zhao, A. X.; Chien, J. C. W. *J. Polym. Sci. Polym. Chem*. **1992**, *30*, 2735.

96. Wu, T. K.; Ovenall, D. W.; Hoen, H. H. in *Applications of Polymer Spectroscopy,* 1st ed. Brame, E.G. Ed. Academic Press Inc: New York, 1978, p. 19.

97. Sen, A. *Catalytic Synthesis of Alkene-Carbon Monoxide Copolymers and Cooligomers*; Kluwer Academic Publishers: Netherlands, 2003, p. 104.

98. Sen, A. *Catalytic Synthesis of Alkene-Carbon Monoxide Copolymers and Cooligomers*; Kluwer Academic Publishers: Netherlands, 2003, p. 129.

99. Xia, J.; Hu, Z.; Popescu, C.V.; Lindahl, P. A.; Münck, E. *J. Am. Chem. Soc*. **1997**, *119*, 8301-8312.

100. Chen, J.; Huang, S.; Seravalli, J.; Gutzman, Jr. H.; Swartz, D. J.; Ragsdale, S. W.; Bagley, K. A. *Biochemistry* **2003**, 42, 14822.

101. Krishnan, R.; Voo, J. K.; Riordan C. G.; Zahkarov, L.; Rheinold, A. L. *J. Am. Chem. Soc*. **2003**, *125*, 4422-23

102. Ohrenberg, C.; Riordan C. G.; Liable-Sands, L. M.; Rheinold, A. L. *Inorg. Chem*. **2001**, *40*, 4276-4283.

103. Stavropoulos, S.; Muetterties, M. C.; Carrie, M.; Holm, R. H. *J. Am. Chem. Soc.* **1991**, *113*, 8585-8592.

104. G.C. Tucci, R.H Holm. *J. Am. Chem. Soc.* **1995**, *117*, 6489-6496.

105. Golden, M. L.; PhD Dissertation. Texas A&M University College Station, TX, 2004.

106. Tuntulani, T.; Reibenspies, J. H.; Farmer, P. J.; Darensbourg, M. Y. *Inorg. Chem*, **1992**, *31*, 3497-3499.

107. Collot, J.; Gradinaru, N.; Humbert, M.; Shanker, M.; Zoochi, A.; Ward, T. R. *J. Am. Chem. Soc.* **2003**, *125*, 9030-9031.

108. Wilson, M. E.; Whitesides, G. M. *J. Am. Chem. Soc.* **1978**, *100*, 306-307.

109. Kaiser, E. T.; Lawrence D. S. *Science*, **1985**, *226*, 505-511.

110. Wilkinson, M. J.; Van Leeuwen, P. W. N. M, Reek, J. N. H. *Org. Biomol. Chem.* **2005**, *3*, 2371-2383.

APPENDIX A

CRYSTAL STRUCTURE DATA

Table A-1. Crystal data and structure refinement for (**Ni-1**)$W(CO)_4$.

Identification code	niwco4	
Empirical formula	C14 H18 N2 Ni O4 S2 W	
Formula weight	585.98	
Temperature	293(2) K	
Wavelength	0.71073 Å	
Crystal system	Orthorhombic	
Space group	Pnma	
Unit cell dimensions	a = 13.397(4) Å	α= 90°.
	b = 12.386(4) Å	β= 90°.
	c = 11.005(3) Å	γ = 90°.
Volume	1826.2(10) $Å^3$	
Z	4	
Density (calculated)	2.128 Mg/m^3	
Absorption coefficient	7.573 mm^{-1}	
F(000)	1128	
Crystal size	? x ? x ? mm^3	
Theta range for data collection	2.39 to 27.43°.	
Index ranges	-9<=h<=11, -16<=k<=8, -11<=l<=13	
Reflections collected	4764	
Independent reflections	1608 [R(int) = 0.1131]	
Completeness to theta = 27.43°	73.6 %	
Absorption correction	None	
Refinement method	Full-matrix least-squares on F^2	
Data / restraints / parameters	1608 / 0 / 121	
Goodness-of-fit on F^2	1.144	
Final R indices [I>2sigma(I)]	R1 = 0.0330, wR2 = 0.0886	
R indices (all data)	R1 = 0.0341, wR2 = 0.0895	
Largest diff. peak and hole	2.355 and -0.986 $e.Å^{-3}$	

Table A-2. Atomic coordinates (x 10^4) and equivalent isotropic displacement parameters (Å^{2}x 10^3) for (**Ni-1**)W(CO)$_4$. U(eq) is defined as one third of the trace of the orthogonalized U^{ij} tensor.

	x	y	z	U(eq)
W(1)	1520(1)	2500	4426(1)	18(1)
Ni(2)	1723(1)	2500	7460(1)	16(1)
S(5)	2183(1)	1275(1)	6140(1)	18(1)
C(7)	152(6)	1450(4)	8851(5)	22(2)
O(2)	919(4)	736(4)	2526(3)	33(1)
N(2)	1285(5)	1358(4)	8592(4)	20(1)
C(2)	1158(6)	1377(5)	3256(5)	25(2)
C(1)	67(11)	2500	4928(7)	32(3)
C(6)	1487(5)	244(5)	8091(5)	20(2)
O(1)	-811(7)	2500	5070(7)	45(2)
C(4)	2921(8)	2500	3686(7)	22(2)
C(10)	1668(7)	2500	10454(6)	12(2)
C(11)	-281(8)	2500	8394(7)	22(2)
C(12)	1320(6)	255(4)	6721(5)	26(2)
C(13)	1879(6)	1461(5)	9754(5)	22(2)
O(4)	3685(6)	2500	3192(7)	34(2)

Table A-3. Bond lengths [Å] and angles [°] for (**Ni-1**)$W(CO)_4$.

		C(1)-W(1)-S(5)#1	97.57(19)
W(1)-C(2)	1.957(6)	C(4)-W(1)-S(5)#1	88.57(19)
W(1)-C(2)#1	1.957(6)	C(2)-W(1)-S(5)	98.53(18)
W(1)-C(1)	2.023(15)	C(2)#1-W(1)-S(5)	170.1(2)
W(1)-C(4)	2.047(11)	C(1)-W(1)-S(5)	97.57(19)
W(1)-S(5)#1	2.5792(14)	C(4)-W(1)-S(5)	88.57(19)
W(1)-S(5)	2.5792(14)	S(5)#1-W(1)-S(5)	72.08(6)
Ni(2)-N(2)#1	1.974(5)	N(2)#1-Ni(2)-N(2)	91.5(3)
Ni(2)-N(2)	1.974(5)	N(2)#1-Ni(2)-S(5)#1	90.34(14)
Ni(2)-S(5)#1	2.1893(15)	N(2)-Ni(2)-S(5)#1	177.54(15)
Ni(2)-S(5)	2.1893(15)	N(2)#1-Ni(2)-S(5)	177.54(15)
S(5)-C(12)	1.828(6)	N(2)-Ni(2)-S(5)	90.34(14)
C(7)-C(11)	1.510(7)	S(5)#1-Ni(2)-S(5)	87.76(8)
C(7)-N(2)	1.549(10)	C(12)-S(5)-Ni(2)	93.9(2)
O(2)-C(2)	1.173(7)	C(12)-S(5)-W(1)	116.4(2)
N(2)-C(6)	1.511(7)	Ni(2)-S(5)-W(1)	88.88(5)
N(2)-C(13)	1.512(7)	C(11)-C(7)-N(2)	112.2(6)
C(1)-O(1)	1.188(14)	C(6)-N(2)-C(13)	107.0(5)
C(6)-C(12)	1.524(7)	C(6)-N(2)-C(7)	108.1(5)
C(4)-O(4)	1.158(12)	C(13)-N(2)-C(7)	110.7(4)
C(10)-C(13)#1	1.526(7)	C(6)-N(2)-Ni(2)	111.7(3)
C(10)-C(13)	1.526(7)	C(13)-N(2)-Ni(2)	108.5(4)
C(11)-C(7)#1	1.510(7)	C(7)-N(2)-Ni(2)	110.8(3)
		O(2)-C(2)-W(1)	177.1(6)
C(2)-W(1)-C(2)#1	90.7(3)	O(1)-C(1)-W(1)	171.7(7)
C(2)-W(1)-C(1)	86.6(3)	N(2)-C(6)-C(12)	109.1(5)
C(2)#1-W(1)-C(1)	86.6(3)	O(4)-C(4)-W(1)	175.5(8)
C(2)-W(1)-C(4)	88.0(3)	C(13)#1-C(10)-C(13)	115.0(6)
C(2)#1-W(1)-C(4)	88.0(3)	C(7)#1-C(11)-C(7)	118.9(8)
C(1)-W(1)-C(4)	172.4(3)	C(6)-C(12)-S(5)	105.0(4)
C(2)-W(1)-S(5)#1	170.1(2)	N(2)-C(13)-C(10)	113.6(6)
C(2)#1-W(1)-S(5)#1	98.53(18)		

Symmetry transformations used to generate equivalent atoms: #1 x,-y+1/2,z

Table A-4. Crystal data and structure refinement for (**Ni-1´**)$W(CO)_4$.

Identification code	ddni	
Empirical formula	C13 H18 N2 Ni O4 S2 W	
Formula weight	572.97	
Temperature	293(2) K	
Wavelength	0.71073 Å	
Crystal system	Orthorhombic	
Space group	Pnma	
Unit cell dimensions	a = 12.721(5) Å	α= 90°.
	b = 12.151(5) Å	β= 90°.
	c = 11(2) Å	γ = 90°.
Volume	1694(309) $Å^3$	
Z	4	
Density (calculated)	2.247 Mg/m^3	
Absorption coefficient	8.162 mm^{-1}	
F(000)	1104	
Crystal size	? x ? x ? mm^3	
Theta range for data collection	2.45 to 23.46°.	
Index ranges	0<=h<=14, -13<=k<=13, -12<=l<=12	
Reflections collected	7249	
Independent reflections	7249 [R(int) = 0.0000]	
Completeness to theta = 23.46°	97.8 %	
Absorption correction	None	
Refinement method	Full-matrix least-squares on F^2	
Data / restraints / parameters	7249 / 0 / 116	
Goodness-of-fit on F^2	1.164	
Final R indices [I>2sigma(I)]	R1 = 0.0717, wR2 = 0.1761	
R indices (all data)	R1 = 0.0800, wR2 = 0.1815	
Largest diff. peak and hole	3.481 and -1.047 e.$Å^{-3}$	

Table A-. Atomic coordinates (x 10^4) and equivalent isotropic displacement parameters (Å^{2}x 10^3) for (**Ni-1´**)W(CO)$_4$. U(eq) is defined as one third of the trace of the orthogonalized U^{ij} tensor.

	x	y	z	U(eq)
W(1)	3344(1)	2500	-528(1)	24(1)
Ni(1)	3110(1)	2500	2425(1)	22(1)
S(1)	2658(1)	1214(1)	1159(1)	25(1)
O(1)	5738(6)	2500	342(7)	46(2)
O(2)	4023(4)	670(4)	-2376(4)	34(1)
O(3)	1138(5)	2500	-1920(6)	38(2)
N(1)	3732(4)	1442(4)	3526(5)	23(1)
C(1)	4851(9)	2500	86(8)	31(2)
C(2)	3779(5)	1346(6)	-1677(6)	24(2)
C(3)	1919(7)	2500	-1359(9)	26(2)
C(4)	3700(5)	275(6)	1670(6)	28(2)
C(5)	3695(5)	287(6)	3055(6)	25(2)
C(6)	4853(5)	1856(6)	3597(6)	26(2)
C(7)	3240(5)	1456(6)	4753(6)	27(2)
C(8)	3419(7)	2500	5454(8)	26(2)

Table A-6. Bond lengths [Å] and angles [°] for (**Ni-1´**)$W(CO)_4$.

W(1)-C(2)	1.96(15)	C(3)-W(1)-S(1)#1	91(7)
W(1)-C(2)#1	1.96(15)	C(1)-W(1)-S(1)#1	95(6)
W(1)-C(3)	2.03(8)	C(2)-W(1)-S(1)	97(8)
W(1)-C(1)	2.03(4)	C(2)#1-W(1)-S(1)	171.8(3)
W(1)-S(1)#1	2.6(2)	C(3)-W(1)-S(1)	91(7)
W(1)-S(1)	2.6(2)	C(1)-W(1)-S(1)	95(6)
Ni(1)-N(1)#1	1.93(14)	S(1)#1-W(1)-S(1)	75(8)
Ni(1)-N(1)	1.93(14)	N(1)#1-Ni(1)-N(1)	83(7)
Ni(1)-S(1)	2.17(16)	N(1)#1-Ni(1)-S(1)	171.1(7)
Ni(1)-S(1)#1	2.17(16)	N(1)-Ni(1)-S(1)	92(8)
S(1)-C(4)	1.85(3)	N(1)#1-Ni(1)-S(1)#1	92(8)
O(1)-C(1)	1.164(17)	N(1)-Ni(1)-S(1)#1	171.1(7)
O(2)-C(2)	1.17(9)	S(1)-Ni(1)-S(1)#1	92(9)
O(3)-C(3)	1.17(6)	C(4)-S(1)-Ni(1)	93(4)
N(1)-C(6)	1.501(8)	C(4)-S(1)-W(1)	111(3)
N(1)-C(7)	1.5(2)	Ni(1)-S(1)-W(1)	86(10)
N(1)-C(5)	1.50(3)	C(6)-N(1)-C(7)	110(4)
C(4)-C(5)	1.5(3)	C(6)-N(1)-C(5)	111.2(5)
C(6)-C(6)#1	1.564(14)	C(7)-N(1)-C(5)	108(4)
C(7)-C(8)	1.50(7)	C(6)-N(1)-Ni(1)	101.3(4)
C(8)-C(7)#1	1.50(7)	C(7)-N(1)-Ni(1)	113(8)
		C(5)-N(1)-Ni(1)	113(7)
C(2)-W(1)-C(2)#1	91(9)	O(1)-C(1)-W(1)	174.7(11)
C(2)-W(1)-C(3)	88(6)	O(2)-C(2)-W(1)	178.6(6)
C(2)#1-W(1)-C(3)	88(6)	O(3)-C(3)-W(1)	174.9(10)
C(2)-W(1)-C(1)	87(5)	C(5)-C(4)-S(1)	107(3)
C(2)#1-W(1)-C(1)	87(5)	N(1)-C(5)-C(4)	111(3)
C(3)-W(1)-C(1)	172.6(10)	N(1)-C(6)-C(6)#1	109.6(3)
C(2)-W(1)-S(1)#1	171.8(3)	N(1)-C(7)-C(8)	114(6)
C(2)#1-W(1)-S(1)#1	97(8)	C(7)-C(8)-C(7)#1	115(9)

Symmetry transformations used to generate equivalent atoms: #1 x,-y+1/2,z

Table A-7. Crystal data and structure refinement for (**Ni(bmmp-dmed)**)$W(CO)_4$.

Identification code	mdni	
Empirical formula	C17 H28 Cl2 N2 Ni O4 S2 W	
Formula weight	701.99	
Temperature	110(2) K	
Wavelength	0.71073 Å	
Crystal system	Orthorhombic	
Space group	Pbca	
Unit cell dimensions	a = 18.3245(11) Å	α= 90°.
	b = 12.7485(7) Å	β= 90°.
	c = 20.5750(12) Å	γ = 90°.
Volume	4806.5(5) $Å^3$	
Z	8	
Density (calculated)	1.940 Mg/m^3	
Absorption coefficient	5.987 mm^{-1}	
F(000)	2752	
Crystal size	0.31 x 0.21 x 0.12 mm^3	
Theta range for data collection	2.18 to 25.00°.	
Index ranges	-21<=h<=17, -15<=k<=14, -24<=l<=24	
Reflections collected	22168	
Independent reflections	4089 [R(int) = 0.1057]	
Completeness to theta = 25.00°	96.6 %	
Max. and min. transmission	25.00 and 2.18	
Refinement method	Full-matrix least-squares on F^2	
Data / restraints / parameters	4089 / 0 / 268	
Goodness-of-fit on F^2	1.090	
Final R indices [I>2sigma(I)]	R1 = 0.0477, wR2 = 0.0979	
R indices (all data)	R1 = 0.0693, wR2 = 0.1034	
Largest diff. peak and hole	2.783 and -1.099 $e.Å^{-3}$	

Table A-8. Atomic coordinates (x 10^4) and equivalent isotropic displacement parameters (Å^{2}x 10^3)for (**Ni(bmmp-dmed)**)$W(CO)_4$. U(eq) is defined as one third of the trace of the orthogonalized U^{ij} tensor.

	x	y	z	U(eq)
Ni(1)	2257(1)	1700(1)	853(1)	23(1)
W(1)	819(1)	1427(1)	1541(1)	22(1)
Cl(1)	8398(2)	4519(2)	1557(2)	64(1)
Cl(2)	9624(2)	4562(2)	658(1)	52(1)
S(1)	2153(1)	829(2)	1737(1)	24(1)
S(2)	1371(1)	853(2)	407(1)	25(1)
O(1)	1057(4)	3865(5)	1681(3)	44(2)
O(2)	290(4)	1775(5)	2957(3)	46(2)
O(3)	311(3)	-897(5)	1869(3)	38(2)
O(4)	-724(3)	1885(5)	983(3)	40(2)
N(1)	3175(4)	2254(5)	1149(3)	25(2)
N(2)	2261(4)	2727(5)	134(3)	26(2)
C(1)	1005(5)	3009(7)	1599(4)	31(2)
C(2)	482(5)	1665(7)	2438(5)	32(2)
C(3)	525(5)	-88(7)	1709(4)	30(2)
C(4)	-150(5)	1712(7)	1201(5)	32(2)
C(5)	2748(5)	1671(6)	2260(4)	24(2)
C(6)	3317(5)	919(7)	2587(4)	36(2)
C(7)	2298(5)	2204(7)	2792(4)	33(2)
C(8)	3100(5)	2535(7)	1850(4)	28(2)
C(9)	3356(5)	3185(7)	739(4)	33(2)
C(10)	3060(5)	3010(8)	79(4)	36(2)
C(11)	1959(5)	2255(7)	-455(4)	34(2)
C(12)	1247(5)	1606(6)	-359(4)	27(2)
C(13)	550(5)	2214(8)	-361(5)	41(2)
C(14)	1209(6)	808(7)	-906(4)	37(2)
C(15)	3761(5)	1450(7)	1025(4)	31(2)
C(16)	1857(5)	3705(7)	296(4)	36(2)
C(17)	9339(6)	4385(7)	1474(4)	39(2)

Table A-9. Bond lengths [Å] and angles [°] for (**Ni(bmmp-dmed)**)$W(CO)_4$.

Ni(1)-N(1)	1.929(7)
Ni(1)-N(2)	1.959(6)
Ni(1)-S(2)	2.153(2)
Ni(1)-S(1)	2.156(2)
Ni(1)-W(1)	3.0208(11)
W(1)-C(4)	1.942(10)
W(1)-C(2)	1.971(9)
W(1)-C(3)	2.036(9)
W(1)-C(1)	2.048(9)
W(1)-S(1)	2.591(2)
W(1)-S(2)	2.649(2)
Cl(1)-C(17)	1.741(10)
Cl(2)-C(17)	1.773(9)
S(1)-C(5)	1.872(8)
S(2)-C(12)	1.865(8)
O(1)-C(1)	1.108(10)
O(2)-C(2)	1.132(10)
O(3)-C(3)	1.151(10)
O(4)-C(4)	1.165(10)
N(1)-C(8)	1.473(10)
N(1)-C(9)	1.495(11)
N(1)-C(15)	1.507(10)
N(2)-C(11)	1.462(11)
N(2)-C(16)	1.497(11)
N(2)-C(10)	1.512(11)
C(5)-C(7)	1.529(11)
C(5)-C(8)	1.541(11)
C(5)-C(6)	1.568(12)
C(9)-C(10)	1.479(12)
C(11)-C(12)	1.557(12)
C(12)-C(13)	1.495(13)
C(12)-C(14)	1.520(11)

Table A-9. Continued

N(1)-Ni(1)-N(2)	89.8(3)	O(3)-C(3)-W(1)	171.5(8)
N(1)-Ni(1)-S(2)	168.2(2)	O(4)-C(4)-W(1)	178.4(8)
N(2)-Ni(1)-S(2)	91.8(2)	C(7)-C(5)-C(8)	108.0(6)
N(1)-Ni(1)-S(1)	89.3(2)	C(7)-C(5)-C(6)	108.8(7)
N(2)-Ni(1)-S(1)	168.2(2)	C(8)-C(5)-C(6)	113.5(7)
S(2)-Ni(1)-S(1)	91.53(9)	C(7)-C(5)-S(1)	110.6(6)
N(1)-Ni(1)-W(1)	130.3(2)	C(8)-C(5)-S(1)	109.4(5)
N(2)-Ni(1)-W(1)	115.7(2)	C(6)-C(5)-S(1)	106.5(5)
S(2)-Ni(1)-W(1)	58.77(6)	N(1)-C(8)-C(5)	113.9(7)
S(1)-Ni(1)-W(1)	57.18(6)	C(10)-C(9)-N(1)	108.4(7)
C(4)-W(1)-C(2)	91.2(4)	C(9)-C(10)-N(2)	108.8(7)
C(4)-W(1)-C(3)	89.8(4)	N(2)-C(11)-C(12)	115.5(7)
C(2)-W(1)-C(3)	85.4(4)	C(13)-C(12)-C(14)	107.8(7)
C(4)-W(1)-C(1)	89.4(4)	C(13)-C(12)-C(11)	116.1(7)
C(2)-W(1)-C(1)	81.2(3)	C(14)-C(12)-C(11)	107.5(7)
C(3)-W(1)-C(1)	165.5(4)	C(13)-C(12)-S(2)	112.2(6)
C(4)-W(1)-S(1)	166.7(3)	C(14)-C(12)-S(2)	106.4(6)
C(2)-W(1)-S(1)	101.3(3)	C(11)-C(12)-S(2)	106.4(6)
C(3)-W(1)-S(1)	86.8(3)	Cl(1)-C(17)-Cl(2)	111.8(5)
C(1)-W(1)-S(1)	97.1(3)		
C(4)-W(1)-S(2)	94.9(3)		
C(2)-W(1)-S(2)	171.1(3)		
C(3)-W(1)-S(2)	89.1(3)		
C(1)-W(1)-S(2)	105.4(2)		
S(1)-W(1)-S(2)	72.19(7)		
C(4)-W(1)-Ni(1)	127.2(3)		
C(2)-W(1)-Ni(1)	134.5(3)		
C(3)-W(1)-Ni(1)	114.9(3)		
C(1)-W(1)-Ni(1)	76.7(3)		
S(1)-W(1)-Ni(1)	44.38(5)		
S(2)-W(1)-Ni(1)	44.02(5)		
C(5)-S(1)-Ni(1)	98.2(3)		
C(5)-S(1)-W(1)	118.1(3)		
Ni(1)-S(1)-W(1)	78.44(7)		
C(12)-S(2)-Ni(1)	100.3(3)		
C(12)-S(2)-W(1)	123.4(3)		
Ni(1)-S(2)-W(1)	77.21(7)		
C(8)-N(1)-C(9)	111.9(6)		
C(8)-N(1)-C(15)	113.3(7)		
C(9)-N(1)-C(15)	106.6(6)		
C(8)-N(1)-Ni(1)	108.9(5)		
C(9)-N(1)-Ni(1)	107.5(5)		
C(15)-N(1)-Ni(1)	108.5(5)		
C(11)-N(2)-C(16)	109.6(7)		
C(11)-N(2)-C(10)	113.7(7)		
C(16)-N(2)-C(10)	108.0(7)		
C(11)-N(2)-Ni(1)	109.9(5)		
C(16)-N(2)-Ni(1)	112.9(5)		
C(10)-N(2)-Ni(1)	102.6(5)		
O(1)-C(1)-W(1)	172.9(8)		
O(2)-C(2)-W(1)	178.3(8)		

Table A-10. Crystal data and structure refinement for (**Ni-1**)$W(CO)_5$.

Identification code	mdmr16m	
Empirical formula	C15 H20 N2 Ni O5 S2 W	
Formula weight	615.01	
Temperature	293(2) K	
Wavelength	0.71073 Å	
Crystal system	Monoclinic	
Space group	P2(1)/n	
Unit cell dimensions	a = 7.2857(12) Å	α= 90°.
	b = 13.392(2) Å	β= 91.712(3)°.
	c = 20.266(3) Å	γ = 90°.
Volume	1976.3(6) $Å^3$	
Z	4	
Density (calculated)	2.067 Mg/m^3	
Absorption coefficient	7.007 mm^{-1}	
F(000)	1192	
Crystal size	0.3 x 0.1 x 0.1 mm^3	
Theta range for data collection	2.94 to 28.29°.	
Index ranges	-7<=h<=9, -16<=k<=16, -26<=l<=23	
Reflections collected	12098	
Independent reflections	4473 [R(int) = 0.0851]	
Completeness to theta = 28.29°	91.2 %	
Absorption correction	None	
Refinement method	Full-matrix least-squares on F^2	
Data / restraints / parameters	4473 / 0 / 235	
Goodness-of-fit on F^2	0.929	
Final R indices [I>2sigma(I)]	R1 = 0.0626, wR2 = 0.1404	
R indices (all data)	R1 = 0.1004, wR2 = 0.1559	
Largest diff. peak and hole	5.571 and -1.626 e.$Å^{-3}$	

Table A-11. Atomic coordinates (x 10^4) and equivalent isotropic displacement parameters ($Å^2$x 10^3) for (**Ni-1**)$W(CO)_5$. U(eq) is defined as one third of the trace of the orthogonalized U^{ij} tensor.

	x	y	z	U(eq)
C(1)	4169(14)	6305(8)	9593(4)	30(2)
C(2)	6875(19)	8944(8)	9820(5)	51(3)
C(3)	7344(16)	6956(8)	10350(5)	43(3)
C(4)	4064(19)	7946(9)	10491(6)	55(4)
C(5)	3428(17)	8313(8)	9183(6)	47(3)
C(6)	9485(13)	6614(7)	8949(5)	36(2)
C(7)	8922(13)	5553(7)	9024(5)	32(2)
C(8)	6963(14)	4250(7)	8592(5)	34(2)
C(9)	5994(15)	3717(8)	8022(5)	41(3)
C(10)	4571(14)	4327(7)	7685(5)	36(2)
C(11)	9282(13)	4957(7)	7874(5)	35(2)
C(12)	8674(13)	5377(8)	7205(5)	36(2)
C(13)	6804(13)	5056(7)	6916(5)	35(2)
C(14)	3652(14)	5696(8)	6986(5)	36(2)
C(15)	3883(16)	6782(9)	6894(5)	47(3)
N(1)	7905(11)	5185(6)	8504(4)	30(2)
N(2)	5253(11)	5269(6)	7382(4)	29(2)
Ni(1)	6175(2)	6221(1)	8064(1)	27(1)
O(1)	3452(10)	5558(6)	9528(4)	45(2)
O(2)	7694(14)	9688(7)	9895(5)	78(3)
O(3)	8293(12)	6552(6)	10725(4)	62(2)
O(4)	3145(13)	8109(8)	10924(4)	70(3)
O(5)	2181(12)	8704(6)	8949(4)	55(2)
S(1)	7459(4)	7349(2)	8698(1)	32(1)
S(2)	4265(4)	7350(2)	7707(1)	36(1)
W(1)	5515(1)	7621(1)	9724(1)	35(1)

Table A-12. Bond lengths [Å] and angles [°] for (**Ni-1**)$W(CO)_5$.

C(1)-O(1)	1.134(11)	C(11)-C(12)-C(13)	118.0(8)
C(1)-W(1)	2.031(11)	N(2)-C(13)-C(12)	112.3(8)
C(2)-O(2)	1.169(13)	C(15)-C(14)-N(2)	110.6(8)
C(2)-W(1)	2.036(12)	C(14)-C(15)-S(2)	108.1(7)
C(3)-O(3)	1.147(12)	C(8)-N(1)-C(7)	106.2(7)
C(3)-W(1)	2.019(11)	C(8)-N(1)-C(11)	109.4(7)
C(4)-O(4)	1.140(13)	C(7)-N(1)-C(11)	109.4(7)
C(4)-W(1)	1.955(13)	C(8)-N(1)-Ni(1)	112.7(6)
C(5)-O(5)	1.140(13)	C(7)-N(1)-Ni(1)	110.4(6)
C(5)-W(1)	2.067(12)	C(11)-N(1)-Ni(1)	108.6(6)
C(6)-C(7)	1.488(13)	C(10)-N(2)-C(14)	106.1(7)
C(6)-S(1)	1.833(10)	C(10)-N(2)-C(13)	110.9(7)
C(7)-N(1)	1.522(11)	C(14)-N(2)-C(13)	108.5(7)
C(8)-N(1)	1.483(12)	C(10)-N(2)-Ni(1)	111.6(6)
C(8)-C(9)	1.515(13)	C(14)-N(2)-Ni(1)	111.6(6)
C(9)-C(10)	1.473(14)	C(13)-N(2)-Ni(1)	108.1(6)
C(10)-N(2)	1.493(12)	N(2)-Ni(1)-N(1)	89.5(3)
C(11)-N(1)	1.522(11)	N(2)-Ni(1)-S(2)	90.9(2)
C(11)-C(12)	1.523(13)	N(1)-Ni(1)-S(2)	179.0(2)
C(12)-C(13)	1.528(13)	N(2)-Ni(1)-S(1)	171.4(2)
C(13)-N(2)	1.521(11)	N(1)-Ni(1)-S(1)	91.3(2)
C(14)-C(15)	1.476(15)	S(2)-Ni(1)-S(1)	88.45(11)
C(14)-N(2)	1.508(12)	C(6)-S(1)-Ni(1)	96.9(3)
C(15)-S(2)	1.829(11)	C(6)-S(1)-W(1)	108.0(3)
N(1)-Ni(1)	1.985(8)	Ni(1)-S(1)-W(1)	109.76(11)
N(2)-Ni(1)	1.982(8)	C(15)-S(2)-Ni(1)	95.1(4)
Ni(1)-S(2)	2.164(3)	C(4)-W(1)-C(3)	87.8(5)
Ni(1)-S(1)	2.176(3)	C(4)-W(1)-C(1)	91.5(5)
S(1)-W(1)	2.577(3)	C(3)-W(1)-C(1)	90.3(4)
		C(4)-W(1)-C(2)	90.2(5)
O(1)-C(1)-W(1)	178.3(9)	C(3)-W(1)-C(2)	90.8(5)
O(2)-C(2)-W(1)	177.5(12)	C(1)-W(1)-C(2)	178.0(4)
O(3)-C(3)-W(1)	175.7(11)	C(4)-W(1)-C(5)	85.1(5)
O(4)-C(4)-W(1)	176.5(11)	C(3)-W(1)-C(5)	172.8(4)
O(5)-C(5)-W(1)	172.6(10)	C(1)-W(1)-C(5)	88.6(4)
C(7)-C(6)-S(1)	108.6(7)	C(2)-W(1)-C(5)	90.5(5)
C(6)-C(7)-N(1)	110.7(8)	C(4)-W(1)-S(1)	175.3(4)
N(1)-C(8)-C(9)	114.2(8)	C(3)-W(1)-S(1)	94.4(3)
C(10)-C(9)-C(8)	113.5(9)	C(1)-W(1)-S(1)	92.7(3)
C(9)-C(10)-N(2)	114.9(8)	C(2)-W(1)-S(1)	85.6(3)
N(1)-C(11)-C(12)	112.0(8)	C(5)-W(1)-S(1)	92.8(3)

Table A-13. Crystal data and structure refinement for **[(Ni-1*)$_2$Cu$_2$Br$_2$].**

Identification code	mmmb	
Empirical formula	C30 H59 Br2 Cu2 N5 Ni2 S4	
Formula weight	1022.38	
Temperature	110(2) K	
Wavelength	0.71073 Å	
Crystal system	Orthorhombic	
Space group	Pbca	
Unit cell dimensions	a = 14.1557(15) Å	α = 90°.
	b = 20.801(2) Å	β = 90°.
	c = 27.034(3) Å	γ = 90°.
Volume	7960.0(15) Å^3	
Z	8	
Density (calculated)	1.706 Mg/m^3	
Absorption coefficient	4.232 mm^{-1}	
F(000)	4176	
Crystal size	0.2 x 0.15 x 0.1 mm^3	
Theta range for data collection	2.47 to 25.00°.	
Index ranges	-16<=h<=12, -22<=k<=24, -32<=l<=31	
Reflections collected	40702	
Independent reflections	7009 [R(int) = 0.1333]	
Completeness to theta = 25.00°	99.9 %	
Refinement method	Full-matrix least-squares on F^2	
Data / restraints / parameters	7009 / 0 / 415	
Goodness-of-fit on F^2	0.879	
Final R indices [I>2sigma(I)]	R1 = 0.0616, wR2 = 0.1385	
R indices (all data)	R1 = 0.1148, wR2 = 0.1606	
Largest diff. peak and hole	1.946 and -0.708 e.Å^{-3}	

Table A-14. Atomic coordinates (x 10^4) and equivalent isotropic displacement parameters ($Å^2$x 10^3) for **[(Ni-1*)$_2$Cu$_2$Br$_2$]**. U(eq) is defined as one third of the trace of the orthogonalized U^{ij} tensor.

	x	y	z	U(eq)
Br(1)	3277(1)	1599(1)	3720(1)	30(1)
Br(2)	3311(1)	4061(1)	4376(1)	31(1)
Ni(1)	5745(1)	2729(1)	4488(1)	22(1)
Ni(2)	3349(1)	3680(1)	2857(1)	22(1)
Cu(1)	4527(1)	2308(1)	3464(1)	26(1)
Cu(2)	4621(1)	3912(1)	3830(1)	27(1)
S(1)	5994(2)	2246(1)	3789(1)	24(1)
S(2)	6054(2)	3616(1)	4112(1)	26(1)
S(3)	4336(1)	2886(1)	2760(1)	25(1)
S(4)	4529(2)	4294(1)	3053(1)	26(1)
N(1)	5519(5)	1898(3)	4821(2)	25(2)
N(2)	5548(5)	3203(3)	5125(2)	26(2)
N(3)	2320(5)	3136(3)	2603(2)	28(2)
N(4)	2447(4)	4407(3)	2956(2)	24(2)
C(1)	4527(5)	1897(4)	5026(3)	23(2)
C(2)	4391(6)	2366(4)	5448(3)	26(2)
C(3)	4581(6)	3064(4)	5311(3)	32(2)
C(4)	6259(6)	2971(4)	5507(3)	29(2)
C(5)	6802(6)	2380(4)	5353(3)	28(2)
C(6)	6223(6)	1786(4)	5232(3)	29(2)
C(7)	5531(6)	1348(4)	4459(3)	29(2)
C(8)	6222(6)	1439(4)	4040(3)	27(2)
C(9)	7271(6)	1401(4)	4188(3)	33(2)
C(10)	6055(6)	927(4)	3647(3)	33(2)
C(11)	5604(6)	3914(4)	5050(3)	29(2)
C(12)	6294(6)	4123(4)	4658(3)	28(2)
C(13)	7331(6)	4034(5)	4795(4)	38(2)
C(14)	6113(6)	4828(4)	4520(3)	36(2)
C(15)	1681(5)	4212(4)	3300(3)	24(2)
C(16)	1039(6)	3690(4)	3113(3)	32(2)
C(17)	1569(6)	3075(4)	2985(3)	29(2)
C(18)	1914(6)	3443(4)	2140(3)	24(2)
C(19)	2249(6)	4127(4)	2058(3)	30(2)
C(20)	2039(6)	4612(4)	2463(3)	34(2)
C(21)	2938(6)	4966(4)	3203(3)	32(2)
C(22)	3937(6)	5083(4)	3064(3)	25(2)
C(23)	4082(7)	5373(4)	2544(3)	41(3)
C(24)	4408(6)	5515(5)	3442(3)	36(2)
C(25)	2632(5)	2460(4)	2495(3)	24(2)
C(26)	3631(6)	2413(4)	2309(3)	23(2)
C(27)	3794(6)	2676(5)	1794(3)	35(2)
C(28)	3951(6)	1713(4)	2326(3)	38(2)
N(1S)	5361(6)	9401(4)	4141(3)	49(2)
C(1S)	4722(7)	9687(4)	4281(3)	31(2)
C(2S)	3898(6)	10043(4)	4443(3)	36(2)

Table A-15. Bond lengths [Å] and angles [°] for **[(Ni-1*)$_2$Cu$_2$Br$_2$].**

Br(1)-Cu(1)	2.4044(14)	C(1S)-C(2S)	1.449(13)
Br(2)-Cu(2)	2.3918(14)	N(1)-Ni(1)-N(2)	90.9(3)
Ni(1)-N(1)	1.975(7)	N(1)-Ni(1)-S(2)	177.3(2)
Ni(1)-N(2)	2.006(7)	N(2)-Ni(1)-S(2)	90.7(2)
Ni(1)-S(2)	2.149(2)	N(1)-Ni(1)-S(1)	91.0(2)
Ni(1)-S(1)	2.169(2)	N(2)-Ni(1)-S(1)	177.8(2)
Ni(2)-N(3)	1.969(7)	S(2)-Ni(1)-S(1)	87.37(9)
Ni(2)-N(4)	1.997(7)	N(3)-Ni(2)-N(4)	90.5(3)
Ni(2)-S(4)	2.168(2)	N(3)-Ni(2)-S(4)	173.8(2)
Ni(2)-S(3)	2.180(2)	N(4)-Ni(2)-S(4)	90.8(2)
Cu(1)-S(1)	2.258(2)	N(3)-Ni(2)-S(3)	89.7(2)
Cu(1)-S(3)	2.269(2)	N(4)-Ni(2)-S(3)	179.2(2)
Cu(2)-S(4)	2.250(2)	S(4)-Ni(2)-S(3)	89.02(9)
Cu(2)-S(2)	2.253(2)	S(1)-Cu(1)-S(3)	117.83(9)
S(1)-C(8)	1.837(9)	S(1)-Cu(1)-Br(1)	121.97(7)
S(2)-C(12)	1.855(9)	S(3)-Cu(1)-Br(1)	118.56(7)
S(3)-C(26)	1.856(8)	S(4)-Cu(2)-S(2)	117.76(9)
S(4)-C(22)	1.853(8)	S(4)-Cu(2)-Br(2)	119.02(7)
N(1)-C(7)	1.506(10)	S(2)-Cu(2)-Br(2)	121.62(7)
N(1)-C(1)	1.509(9)	C(8)-S(1)-Ni(1)	97.5(3)
N(1)-C(6)	1.510(10)	C(8)-S(1)-Cu(1)	111.0(3)
N(2)-C(3)	1.488(10)	Ni(1)-S(1)-Cu(1)	99.35(9)
N(2)-C(11)	1.494(11)	C(12)-S(2)-Ni(1)	98.7(3)
N(2)-C(4)	1.520(10)	C(12)-S(2)-Cu(2)	106.3(3)
N(3)-C(17)	1.486(10)	Ni(1)-S(2)-Cu(2)	102.19(9)
N(3)-C(25)	1.502(10)	C(26)-S(3)-Ni(2)	97.9(3)
N(3)-C(18)	1.520(10)	C(26)-S(3)-Cu(1)	109.5(3)
N(4)-C(15)	1.485(10)	Ni(2)-S(3)-Cu(1)	112.12(10)
N(4)-C(21)	1.511(10)	C(22)-S(4)-Ni(2)	100.3(3)
N(4)-C(20)	1.512(10)	C(22)-S(4)-Cu(2)	109.0(3)
C(1)-C(2)	1.515(11)	Ni(2)-S(4)-Cu(2)	93.70(9)
C(2)-C(3)	1.521(12)	C(7)-N(1)-C(1)	104.3(6)
C(4)-C(5)	1.510(11)	C(7)-N(1)-C(6)	110.6(6)
C(5)-C(6)	1.520(11)	C(1)-N(1)-C(6)	110.0(6)
C(7)-C(8)	1.508(11)	C(7)-N(1)-Ni(1)	111.5(5)
C(8)-C(10)	1.524(11)	C(1)-N(1)-Ni(1)	108.7(5)
C(8)-C(9)	1.540(11)	C(6)-N(1)-Ni(1)	111.4(5)
C(11)-C(12)	1.506(12)	C(3)-N(2)-C(11)	106.7(6)
C(12)-C(13)	1.526(11)	C(3)-N(2)-C(4)	108.5(6)
C(12)-C(14)	1.534(12)	C(11)-N(2)-C(4)	111.8(6)
C(15)-C(16)	1.504(11)	C(3)-N(2)-Ni(1)	108.8(5)
C(16)-C(17)	1.522(11)	C(11)-N(2)-Ni(1)	111.2(5)
C(18)-C(19)	1.516(11)	C(4)-N(2)-Ni(1)	109.7(5)
C(19)-C(20)	1.521(11)	C(17)-N(3)-C(25)	105.4(6)
C(21)-C(22)	1.483(12)	C(17)-N(3)-C(18)	109.7(6)
C(22)-C(24)	1.514(11)	C(25)-N(3)-C(18)	110.1(6)
C(22)-C(23)	1.545(11)	C(17)-N(3)-Ni(2)	109.6(5)
C(25)-C(26)	1.503(11)	C(25)-N(3)-Ni(2)	112.9(5)
C(26)-C(27)	1.515(11)	C(18)-N(3)-Ni(2)	109.0(5)
C(26)-C(28)	1.525(11)	C(15)-N(4)-C(21)	105.5(6)
N(1S)-C(1S)	1.148(11)	C(15)-N(4)-C(20)	110.5(6)

Table A-15. Continued

C(21)-N(4)-C(20)	110.3(7)	N(4)-C(15)-C(16)	115.3(7)
C(15)-N(4)-Ni(2)	110.2(5)	C(15)-C(16)-C(17)	112.7(7)
C(21)-N(4)-Ni(2)	110.3(5)	N(3)-C(17)-C(16)	116.1(7)
C(20)-N(4)-Ni(2)	109.9(5)	C(19)-C(18)-N(3)	113.4(7)
N(1)-C(1)-C(2)	113.2(6)	C(18)-C(19)-C(20)	117.2(7)
C(1)-C(2)-C(3)	114.1(7)	N(4)-C(20)-C(19)	111.9(7)
N(2)-C(3)-C(2)	115.6(7)	C(22)-C(21)-N(4)	117.0(7)
C(5)-C(4)-N(2)	114.0(7)	C(21)-C(22)-C(24)	110.3(7)
C(4)-C(5)-C(6)	116.6(7)	C(21)-C(22)-C(23)	114.9(7)
N(1)-C(6)-C(5)	112.8(7)	C(24)-C(22)-C(23)	109.0(7)
N(1)-C(7)-C(8)	113.5(7)	C(21)-C(22)-S(4)	106.9(6)
C(7)-C(8)-C(10)	109.5(7)	C(24)-C(22)-S(4)	109.8(6)
C(7)-C(8)-C(9)	115.1(7)	C(23)-C(22)-S(4)	105.7(6)
C(10)-C(8)-C(9)	107.1(7)	N(3)-C(25)-C(26)	113.7(7)
C(7)-C(8)-S(1)	106.1(6)	C(25)-C(26)-C(27)	115.3(7)
C(10)-C(8)-S(1)	110.7(6)	C(25)-C(26)-C(28)	109.4(7)
C(9)-C(8)-S(1)	108.3(6)	C(27)-C(26)-C(28)	109.1(7)
N(2)-C(11)-C(12)	114.6(7)	C(25)-C(26)-S(3)	104.6(6)
C(11)-C(12)-C(13)	114.7(8)	C(27)-C(26)-S(3)	109.2(6)
C(11)-C(12)-C(14)	109.8(7)	C(28)-C(26)-S(3)	109.1(6)
C(13)-C(12)-C(14)	109.6(7)	N(1S)-C(1S)-C(2S)	178.0(10)
C(11)-C(12)-S(2)	106.2(6)		
C(13)-C(12)-S(2)	107.5(6)		
C(14)-C(12)-S(2)	108.9(6)		

Table A-16. Crystal data and structure refinement for **$[(Ni\text{-}1^*)_3Cu_2](Br)_2$**.

Identification code	mm36m	
Empirical formula	C45 H90 Br2 Cl6 Cu2 N6 Ni3 S6	
Formula weight	1601.34	
Temperature	110(2) K	
Wavelength	0.71073 Å	
Crystal system	Monoclinic	
Space group	C2/c	
Unit cell dimensions	a = 42.629(4) Å	α= 90°.
	b = 13.7696(13) Å	β= 109.534(2)°.
	c = 24.700(2) Å	γ = 90°.
Volume	13664(2) $Å^3$	
Z	8	
Density (calculated)	1.557 Mg/m^3	
Absorption coefficient	3.048 mm^{-1}	
F(000)	6576	
Crystal size	? x ? x ? mm^3	
Theta range for data collection	1.01 to 25.00°.	
Index ranges	-50<=h<=33, -16<=k<=16, -29<=l<=29	
Reflections collected	34956	
Independent reflections	11980 [R(int) = 0.0680]	
Completeness to theta = 25.00°	99.4 %	
Refinement method	Full-matrix least-squares on F^2	
Data / restraints / parameters	11980 / 463 / 688	
Goodness-of-fit on F^2	1.012	
Final R indices [I>2sigma(I)]	R1 = 0.0718, wR2 = 0.1796	
R indices (all data)	R1 = 0.1226, wR2 = 0.2233	
Largest diff. peak and hole	1.903 and -1.748 $e.Å^{-3}$	

Table A-17. Atomic coordinates (x 10^4) and equivalent isotropic displacement parameters ($Å^2$x 10^3) for **[(Ni-1*)$_3$Cu$_2$](Br)$_2$**. U(eq) is defined as one third of the trace of the orthogonalized U^{ij} tensor.

	x	y	z	U(eq)
C(1Q)	10000	9379(9)	2500	61(5)
Cl(1Q)	9643(1)	10123(3)	2365(2)	60(2)
C(1R)	10000	5691(8)	2500	59(5)
Cl(1R)	9756(1)	4992(4)	2794(2)	70(2)
C(1S)	7377(7)	8500(30)	1550(30)	62(2)
Cl(1S)	7627(4)	9526(12)	1740(6)	62(2)
Cl(2S)	6986(3)	8692(8)	1596(6)	62(2)
C(1S')	7416(10)	8590(30)	1630(30)	62(2)
Cl(1')	7679(4)	9567(14)	1872(7)	62(2)
Cl(2')	7092(3)	8569(9)	1895(6)	62(2)
C(1S^)	7501(9)	9170(40)	1504(16)	62(2)
Cl(1^)	7789(4)	9930(12)	1980(7)	62(2)
Cl(2^)	7189(4)	8806(12)	1760(7)	62(2)
C(1T)	9020(6)	4230(30)	3570(30)	171(3)
Cl(1T)	9374(5)	3611(16)	3981(10)	171(3)
Cl(2T)	8669(5)	3545(18)	3522(10)	171(3)
C(1T")	9031(12)	4130(20)	3609(12)	171(3)
Cl(1")	8880(4)	3015(11)	3760(6)	171(3)
Cl(2")	9060(3)	4144(10)	2928(6)	171(3)
C(1U)	8389(5)	8200(40)	7356(13)	106(3)
Cl(1U)	8601(3)	7869(11)	6894(6)	106(3)
Cl(2U)	7967(3)	8201(10)	6966(6)	106(3)
C(1U#)	8330(30)	8540(50)	7600(30)	106(3)
Cl(1#)	8239(10)	7570(30)	7130(15)	106(3)
Cl(2#)	8642(10)	8250(30)	8228(15)	106(3)
C(1U%)	8340(20)	7680(40)	6638(18)	106(3)
Cl(1%)	8616(7)	8543(19)	7132(12)	106(3)
Cl(2%)	8305(6)	6608(17)	6983(11)	106(3)
Br(1)	7927(1)	2976(1)	6058(1)	32(1)
Br(2)	9585(1)	2549(1)	6460(1)	26(1)
Br(2')	7352(2)	8651(6)	287(3)	31(2)
Cu(1)	9121(1)	8002(1)	4954(1)	33(1)
Cu(2)	8393(1)	7772(1)	4204(1)	27(1)
Ni(1)	8936(1)	7397(1)	3554(1)	22(1)
S(1)	9233(1)	6836(2)	4391(1)	30(1)
S(2)	8516(1)	6614(2)	3648(1)	24(1)
N(1)	9332(2)	8027(6)	3459(4)	31(1)
N(2)	8658(2)	7877(6)	2781(3)	29(1)
C(1)	9277(3)	9088(7)	3372(4)	33(2)
C(2)	9006(3)	9364(8)	2830(4)	35(2)
C(3)	8666(3)	8961(7)	2767(5)	33(2)
C(4)	8783(3)	7456(7)	2326(4)	30(2)
C(5)	9122(2)	6977(7)	2577(4)	29(2)
C(6)	9405(3)	7588(7)	2954(4)	29(2)
C(7)	9633(3)	7928(8)	3997(4)	34(2)

Table A-17. Continued

C(8)	9650(3)	6991(8)	4321(5)	39(2)
C(9)	9722(3)	6093(8)	4035(5)	43(3)
C(10)	9913(3)	7104(10)	4917(5)	52(3)
C(11)	8299(2)	7630(7)	2658(4)	30(2)
C(12)	8233(3)	6647(7)	2895(4)	32(2)
C(13)	8308(3)	5780(7)	2581(5)	35(2)
C(14)	7875(3)	6620(8)	2873(5)	38(2)
Ni(2)	8815(1)	6405(1)	5488(1)	27(1)
S(3)	9099(1)	7702(2)	5858(1)	40(1)
S(4)	8388(1)	7333(2)	5094(1)	39(1)
N(3)	9205(2)	5575(6)	5879(4)	40(2)
N(4)	8542(2)	5225(6)	5195(4)	44(2)
C(15)	9281(3)	4900(8)	5463(5)	40(2)
C(16)	9018(3)	4174(8)	5174(5)	44(2)
C(17)	8693(3)	4624(8)	4857(5)	44(2)
C(18)	8522(3)	4649(8)	5719(5)	46(2)
C(19)	8767(3)	4989(8)	6275(5)	43(2)
C(20)	9123(3)	4962(8)	6334(5)	43(2)
C(21)	9516(3)	6162(9)	6143(5)	46(2)
C(22)	9468(3)	7144(9)	6389(5)	51(2)
C(23)	9398(4)	7093(10)	6957(5)	64(3)
C(24)	9772(4)	7778(10)	6454(6)	67(3)
C(25)	8203(3)	5490(9)	4811(6)	53(2)
C(26)	8059(3)	6407(10)	4980(6)	58(2)
C(27)	7976(3)	6323(12)	5528(6)	74(4)
C(28)	7756(3)	6706(12)	4476(7)	73(4)
Ni(3)	8536(1)	9918(1)	4765(1)	24(1)
S(5)	9003(1)	9561(2)	4635(1)	36(1)
S(6)	8285(1)	9347(2)	3912(1)	30(1)
N(5)	8772(2)	10531(6)	5508(4)	32(2)
N(6)	8109(2)	10257(6)	4864(3)	28(1)
C(29)	8681(3)	10079(7)	5991(5)	34(2)
C(30)	8328(3)	10223(8)	5951(4)	33(2)
C(31)	8085(2)	9854(7)	5404(4)	30(2)
C(32)	8079(2)	11367(7)	4881(4)	29(2)
C(33)	8505(3)	11879(7)	4948(5)	34(2)
C(34)	8695(3)	11607(7)	5486(5)	35(2)
C(35)	9147(3)	10392(8)	5679(5)	40(2)
C(36)	9273(3)	10383(8)	5175(6)	44(2)
C(37)	9264(3)	11396(9)	4897(6)	55(3)
C(38)	9636(3)	10019(9)	5390(6)	54(3)
C(39)	7819(3)	9822(8)	4383(5)	35(2)
C(40)	7864(3)	9826(8)	3796(5)	39(2)
C(41)	7856(3)	10824(8)	3511(5)	48(3)
C(42)	7601(3)	9147(9)	341(5)	50(3)

Table A-18. Bond lengths [Å] and angles [°] for **$[(Ni\text{-}1^*)_3Cu_2](Br)_2$**.

C(1Q)-Cl(1Q)#1	1.772(8)	C(12)-C(14)	1.511(14)
C(1Q)-Cl(1Q)	1.772(8)	C(12)-C(13)	1.513(13)
C(1R)-Cl(1R)	1.744(9)	Ni(2)-N(3)	1.982(9)
C(1R)-Cl(1R)#1	1.744(9)	Ni(2)-N(4)	1.990(9)
C(1S)-Cl(2S)	1.730(17)	Ni(2)-S(4)	2.172(3)
C(1S)-Cl(1S)	1.733(17)	Ni(2)-S(3)	2.173(3)
C(1S')-Cl(2')	1.729(17)	S(3)-C(22)	1.856(14)
C(1S')-Cl(1')	1.733(16)	S(4)-C(26)	1.856(13)
C(1S^)-Cl(2^)	1.729(18)	N(3)-C(15)	1.497(13)
C(1S^)-Cl(1^)	1.733(18)	N(3)-C(21)	1.502(15)
C(1T)-Cl(1T)	1.731(18)	N(3)-C(20)	1.537(14)
C(1T)-Cl(2T)	1.734(18)	N(4)-C(25)	1.485(15)
C(1T")-Cl(2")	1.729(19)	N(4)-C(17)	1.485(15)
C(1T")-Cl(1")	1.746(17)	N(4)-C(18)	1.542(13)
C(1U)-Cl(2U)	1.732(18)	C(15)-C(16)	1.494(16)
C(1U)-Cl(1U)	1.740(18)	C(16)-C(17)	1.487(16)
C(1U#)-Cl(2#)	1.729(19)	C(18)-C(19)	1.496(16)
C(1U#)-Cl(1#)	1.736(19)	C(19)-C(20)	1.475(16)
C(1U%)-Cl(1%)	1.735(19)	C(21)-C(22)	1.524(16)
C(1U%)-Cl(2%)	1.738(18)	C(22)-C(24)	1.525(18)
Cu(1)-S(1)	2.275(3)	C(22)-C(23)	1.531(17)
Cu(1)-S(3)	2.281(3)	C(25)-C(26)	1.523(19)
Cu(1)-S(5)	2.285(3)	C(26)-C(27)	1.512(18)
Cu(1)-Cu(2)	3.0545(17)	C(26)-C(28)	1.520(18)
Cu(2)-S(2)	2.276(3)	Ni(3)-N(5)	1.966(9)
Cu(2)-S(6)	2.283(3)	Ni(3)-N(6)	1.973(8)
Cu(2)-S(4)	2.288(3)	Ni(3)-S(6)	2.168(3)
Ni(1)-N(1)	1.982(8)	Ni(3)-S(5)	2.177(3)
Ni(1)-N(2)	1.992(8)	S(5)-C(36)	1.832(12)
Ni(1)-S(2)	2.170(3)	S(6)-C(40)	1.836(11)
Ni(1)-S(1)	2.174(3)	N(5)-C(29)	1.507(13)
S(1)-C(8)	1.855(11)	N(5)-C(34)	1.515(12)
S(2)-C(12)	1.859(11)	N(5)-C(35)	1.522(13)
N(1)-C(1)	1.485(13)	N(6)-C(31)	1.487(12)
N(1)-C(6)	1.507(12)	N(6)-C(39)	1.522(13)
N(1)-C(7)	1.512(13)	N(6)-C(32)	1.535(12)
N(2)-C(3)	1.493(12)	C(29)-C(30)	1.488(14)
N(2)-C(11)	1.496(12)	C(30)-C(31)	1.495(14)
N(2)-C(4)	1.510(12)	C(32)-C(33)	1.516(14)
C(1)-C(2)	1.496(15)	C(33)-C(34)	1.529(15)
C(2)-C(3)	1.513(14)	C(35)-C(36)	1.512(16)
C(4)-C(5)	1.520(14)	C(36)-C(38)	1.545(16)
C(5)-C(6)	1.512(14)	C(36)-C(37)	1.550(16)
C(7)-C(8)	1.506(15)	C(39)-C(40)	1.527(15)
C(8)-C(9)	1.507(16)	C(40)-C(42)	1.526(15)
C(8)-C(10)	1.530(16)	C(40)-C(41)	1.533(16)
C(11)-C(12)	1.538(14)	Cl(1Q)#1-C(1Q)-Cl(1Q)	109.3(7)

Table A-18. Continued

		N(1)-C(6)-C(5)	113.0(8)
Cl(1R)-C(1R)-Cl(1R)#1	113.0(7)	C(8)-C(7)-N(1)	114.9(8)
Cl(2S)-C(1S)-Cl(1S)	112.2(16)	C(9)-C(8)-C(7)	115.8(9)
Cl(2')-C(1S')-Cl(1')	116.4(16)	C(9)-C(8)-C(10)	109.6(10)
Cl(2^)-C(1S^)-Cl(1^)	112.6(17)	C(7)-C(8)-C(10)	108.3(9)
Cl(1T)-C(1T)-Cl(2T)	109.8(19)	C(9)-C(8)-S(1)	107.5(7)
Cl(2")-C(1T")-Cl(1")	111.8(17)	C(7)-C(8)-S(1)	105.7(7)
Cl(2U)-C(1U)-Cl(1U)	107.8(16)	C(10)-C(8)-S(1)	109.8(8)
Cl(2#)-C(1U#)-Cl(1#)	110(2)	N(2)-C(11)-C(12)	115.4(8)
Cl(1%)-C(1U%)-Cl(2%)	109(2)	C(14)-C(12)-C(13)	110.2(9)
S(1)-Cu(1)-S(3)	123.27(11)	C(14)-C(12)-C(11)	108.6(8)
S(1)-Cu(1)-S(5)	121.29(11)	C(13)-C(12)-C(11)	113.7(8)
S(3)-Cu(1)-S(5)	115.40(11)	C(14)-C(12)-S(2)	110.3(7)
S(1)-Cu(1)-Cu(2)	86.23(8)	C(13)-C(12)-S(2)	108.6(7)
S(3)-Cu(1)-Cu(2)	101.85(9)	C(11)-C(12)-S(2)	105.3(7)
S(5)-Cu(1)-Cu(2)	79.99(8)	N(3)-Ni(2)-N(4)	90.0(4)
S(2)-Cu(2)-S(6)	122.62(10)	N(3)-Ni(2)-S(4)	177.7(3)
S(2)-Cu(2)-S(4)	118.16(10)	N(4)-Ni(2)-S(4)	90.9(3)
S(6)-Cu(2)-S(4)	119.21(10)	N(3)-Ni(2)-S(3)	90.8(3)
S(2)-Cu(2)-Cu(1)	92.63(7)	N(4)-Ni(2)-S(3)	176.5(3)
S(6)-Cu(2)-Cu(1)	98.73(8)	S(4)-Ni(2)-S(3)	88.23(13)
S(4)-Cu(2)-Cu(1)	77.23(9)	C(22)-S(3)-Ni(2)	100.2(4)
N(1)-Ni(1)-N(2)	89.9(3)	C(22)-S(3)-Cu(1)	118.2(4)
N(1)-Ni(1)-S(2)	176.1(3)	Ni(2)-S(3)-Cu(1)	87.17(11)
N(2)-Ni(1)-S(2)	91.2(2)	C(26)-S(4)-Ni(2)	98.2(4)
N(1)-Ni(1)-S(1)	91.1(3)	C(26)-S(4)-Cu(2)	106.7(5)
N(2)-Ni(1)-S(1)	178.5(3)	Ni(2)-S(4)-Cu(2)	108.09(11)
S(2)-Ni(1)-S(1)	87.70(10)	C(15)-N(3)-C(21)	105.7(9)
C(8)-S(1)-Ni(1)	98.1(4)	C(15)-N(3)-C(20)	108.3(8)
C(8)-S(1)-Cu(1)	112.2(4)	C(21)-N(3)-C(20)	111.3(9)
Ni(1)-S(1)-Cu(1)	98.99(11)	C(15)-N(3)-Ni(2)	111.2(7)
C(12)-S(2)-Ni(1)	99.4(3)	C(21)-N(3)-Ni(2)	112.0(7)
C(12)-S(2)-Cu(2)	112.7(3)	C(20)-N(3)-Ni(2)	108.3(7)
Ni(1)-S(2)-Cu(2)	94.65(10)	C(25)-N(4)-C(17)	106.5(9)
C(1)-N(1)-C(6)	109.9(7)	C(25)-N(4)-C(18)	110.4(9)
C(1)-N(1)-C(7)	105.2(8)	C(17)-N(4)-C(18)	110.7(9)
C(6)-N(1)-C(7)	110.1(8)	C(25)-N(4)-Ni(2)	111.0(7)
C(1)-N(1)-Ni(1)	110.4(6)	C(17)-N(4)-Ni(2)	110.6(7)
C(6)-N(1)-Ni(1)	110.0(6)	C(18)-N(4)-Ni(2)	107.7(7)
C(7)-N(1)-Ni(1)	111.1(6)	C(16)-C(15)-N(3)	116.5(10)
C(3)-N(2)-C(11)	104.6(7)	C(17)-C(16)-C(15)	113.2(9)
C(3)-N(2)-C(4)	110.5(7)	C(16)-C(17)-N(4)	115.1(10)
C(11)-N(2)-C(4)	110.5(8)	C(19)-C(18)-N(4)	113.2(9)
C(3)-N(2)-Ni(1)	110.1(6)	C(20)-C(19)-C(18)	117.4(10)
C(11)-N(2)-Ni(1)	111.1(6)	C(19)-C(20)-N(3)	113.2(9)
C(4)-N(2)-Ni(1)	110.0(6)	N(3)-C(21)-C(22)	115.8(10)
N(1)-C(1)-C(2)	114.7(8)	C(24)-C(22)-C(21)	109.1(11)
C(1)-C(2)-C(3)	115.2(8)	C(24)-C(22)-C(23)	110.4(11)
N(2)-C(3)-C(2)	113.1(8)	C(21)-C(22)-C(23)	114.7(11)
N(2)-C(4)-C(5)	112.7(8)	C(24)-C(22)-S(3)	109.0(9)
C(6)-C(5)-C(4)	117.7(8)	C(21)-C(22)-S(3)	105.9(8)

Table A-18. Continued

C(23)-C(22)-S(3)	107.5(10)	C(31)-N(6)-C(39)	105.5(7)
N(4)-C(25)-C(26)	115.1(11)	C(31)-N(6)-C(32)	108.9(7)
C(27)-C(26)-C(28)	111.5(11)	C(39)-N(6)-C(32)	111.1(8)
C(27)-C(26)-C(25)	114.7(11)	C(31)-N(6)-Ni(3)	111.4(6)
C(28)-C(26)-C(25)	108.1(13)	C(39)-N(6)-Ni(3)	110.7(6)
C(27)-C(26)-S(4)	108.0(11)	C(32)-N(6)-Ni(3)	109.2(6)
C(28)-C(26)-S(4)	109.3(9)	C(30)-C(29)-N(5)	114.5(9)
C(25)-C(26)-S(4)	105.0(8)	C(29)-C(30)-C(31)	113.2(8)
N(5)-Ni(3)-N(6)	89.3(3)	N(6)-C(31)-C(30)	116.3(8)
N(5)-Ni(3)-S(6)	175.4(3)	C(33)-C(32)-N(6)	112.6(8)
N(6)-Ni(3)-S(6)	91.6(3)	C(32)-C(33)-C(34)	115.2(8)
N(5)-Ni(3)-S(5)	91.5(3)	N(5)-C(34)-C(33)	112.0(8)
N(6)-Ni(3)-S(5)	178.6(3)	C(36)-C(35)-N(5)	113.6(10)
S(6)-Ni(3)-S(5)	87.48(11)	C(35)-C(36)-C(38)	108.1(11)
C(36)-S(5)-Ni(3)	97.7(4)	C(35)-C(36)-C(37)	113.3(9)
C(36)-S(5)-Cu(1)	108.5(4)	C(38)-C(36)-C(37)	108.5(9)
Ni(3)-S(5)-Cu(1)	105.57(12)	C(35)-C(36)-S(5)	107.3(7)
C(40)-S(6)-Ni(3)	99.3(4)	C(38)-C(36)-S(5)	111.3(8)
C(40)-S(6)-Cu(2)	118.4(4)	C(37)-C(36)-S(5)	108.5(9)
Ni(3)-S(6)-Cu(2)	93.18(10)	N(6)-C(39)-C(40)	114.3(8)
C(29)-N(5)-C(34)	108.8(8)	C(39)-C(40)-C(42)	106.9(10)
C(29)-N(5)-C(35)	104.6(8)	C(39)-C(40)-C(41)	115.7(9)
C(34)-N(5)-C(35)	109.2(8)	C(42)-C(40)-C(41)	110.4(10)
C(29)-N(5)-Ni(3)	112.1(6)	C(39)-C(40)-S(6)	106.1(7)
C(34)-N(5)-Ni(3)	110.4(7)	C(42)-C(40)-S(6)	110.7(8)
C(35)-N(5)-Ni(3)	111.6(6)	C(41)-C(40)-S(6)	107.0(8)

Symmetry transformations used to generate equivalent atoms: #1 -x+2,y,-z+1/2

Table A-19. Crystal data and structure refinement for **[(Ni-1*)$_2$(CuBr)$_4$]**.

Identification code	mm35cb	
Empirical formula	C72 H135 Br8 Cu8 N16 Ni4 S8	
Formula weight	2823.83	
Temperature	110(2) K	
Wavelength	0.71073 Å	
Crystal system	Monoclinic	
Space group	P2(1)/n	
Unit cell dimensions	a = 13.5542(12) Å	α = 90°.
	b = 32.169(3) Å	β = 100.459(2)°.
	c = 23.427(2) Å	γ = 90°.
Volume	10044.9(15) Å^3	
Z	4	
Density (calculated)	1.867 Mg/m^3	
Absorption coefficient	5.780 mm^{-1}	
F(000)	5640	
Crystal size	? x ? x ? mm^3	
Theta range for data collection	1.09 to 25.00°.	
Index ranges	-16<=h<=16, -38<=k<=27, -26<=l<=27	
Reflections collected	51956	
Independent reflections	17570 [R(int) = 0.2582]	
Completeness to theta = 25.00°	99.3 %	
Refinement method	Full-matrix least-squares on F^2	
Data / restraints / parameters	17570 / 549 / 942	
Goodness-of-fit on F^2	0.911	
Final R indices [I>2sigma(I)]	R1 = 0.0855, wR2 = 0.1911	
R indices (all data)	R1 = 0.2489, wR2 = 0.2593	
Largest diff. peak and hole	1.714 and -1.665 e.Å^{-3}	

Table A-20. Atomic coordinates (x 10^4) and equivalent isotropic displacement parameters (Å^{2}x 10^3) for **[(Ni-1*)$_2$(CuBr)$_4$]**. U(eq) is defined as one third of the trace of the orthogonalized U^{ij} tensor.

	x	y	z	U(eq)
Br(1A)	2189(2)	7780(1)	8564(1)	25(1)
Br(2A)	1281(2)	5640(1)	7373(1)	34(1)
Br(3A)	3656(2)	6837(1)	10899(1)	46(1)
Br(4A)	2443(2)	4973(1)	9672(1)	27(1)
Cu(1A)	2189(2)	7092(1)	8771(1)	21(1)
Cu(2A)	1648(2)	6079(1)	8187(1)	33(1)
Cu(3A)	2916(2)	6628(1)	9971(1)	24(1)
Cu(4A)	2282(2)	5676(1)	9376(1)	19(1)
Ni(1A)	3965(2)	6093(1)	8645(1)	17(1)
Ni(2A)	499(2)	6338(1)	9671(1)	16(1)
S(1A)	2850(4)	6563(1)	8341(2)	16(1)
S(2A)	3575(4)	6122(2)	9509(2)	20(1)
S(3A)	1441(4)	6858(2)	9488(2)	18(1)
S(4A)	858(4)	5978(2)	8936(2)	21(1)
N(1A)	4310(12)	6067(5)	7867(7)	26(2)
N(2A)	5004(12)	5669(5)	8938(7)	27(2)
N(3A)	190(11)	6643(5)	10343(7)	20(2)
N(4A)	-362(11)	5862(5)	9853(7)	21(2)
C(1A)	4151(15)	5628(6)	7580(9)	26(3)
C(2A)	4806(15)	5312(6)	7955(9)	26(3)
C(3A)	4750(15)	5274(6)	8587(9)	27(3)
C(4A)	6012(14)	5826(6)	8851(9)	27(3)
C(5A)	5982(15)	6207(6)	8575(9)	26(3)
C(6A)	5428(14)	6210(6)	7894(9)	26(3)
C(7A)	3638(15)	6329(6)	7425(9)	26(3)
C(8A)	3266(15)	6742(6)	7662(9)	25(3)
C(9A)	4114(13)	7077(6)	7839(9)	21(4)
C(10A)	2380(14)	6908(6)	7225(9)	30(4)
C(11A)	4989(15)	5544(6)	9564(8)	25(3)
C(12A)	4737(14)	5900(6)	9918(9)	25(3)
C(13A)	5563(15)	6252(6)	10038(9)	30(4)
C(14A)	4597(15)	5722(6)	10512(9)	33(4)
C(15A)	502(14)	6407(6)	10889(8)	22(3)
C(16A)	-44(14)	6001(6)	10928(9)	22(3)
C(17A)	37(14)	5721(6)	10441(8)	22(3)
C(18A)	-1449(13)	6011(6)	9797(9)	22(3)
C(19A)	-1531(14)	6479(6)	9772(9)	21(3)
C(20A)	-958(13)	6729(6)	10259(8)	19(3)
C(21A)	724(14)	7060(6)	10438(8)	20(3)
C(22A)	902(14)	7275(6)	9892(9)	20(3)
C(23A)	-16(14)	7454(6)	9486(9)	26(4)
C(24A)	1690(14)	7624(6)	10056(9)	22(4)
C(25A)	-332(14)	5514(6)	9454(8)	23(3)
C(26A)	-237(14)	5623(6)	8835(9)	22(3)
C(27A)	-1154(14)	5833(6)	8555(9)	27(4)
C(28A)	-9(14)	5227(6)	8595(9)	24(4)
Br(1B)	7482(2)	9960(1)	9877(1)	46(1)

Table A-20. Continued

Br(2B)	8827(2)	7897(1)	10977(1)	27(1)
Br(3B)	6012(2)	9181(1)	7478(1)	60(1)
Br(4B)	7306(2)	7197(1)	8588(1)	31(1)
Cu(1B)	7334(2)	9255(1)	9598(1)	24(1)
Cu(2B)	7983(2)	8217(1)	10129(1)	20(1)
Cu(3B)	6623(2)	8831(1)	8341(1)	27(1)
Cu(4B)	6839(2)	7885(1)	8715(1)	29(1)
Ni(1B)	9026(2)	8876(1)	8909(1)	14(1)
Ni(2B)	5518(2)	8562(1)	9794(1)	16(1)
S(1B)	8590(4)	8785(2)	9755(2)	18(1)
S(2B)	7959(4)	8510(2)	8512(2)	18(1)
S(3B)	5930(4)	8958(2)	9117(2)	20(1)
S(4B)	6485(4)	8063(1)	9598(2)	20(1)
N(1B)	10022(11)	9302(4)	9277(7)	18(2)
N(2B)	9410(11)	8970(5)	8164(7)	20(2)
N(3B)	4669(12)	9036(5)	9999(7)	26(2)
N(4B)	5162(12)	8229(5)	10420(7)	24(2)
C(1B)	9815(14)	9722(6)	8980(8)	18(2)
C(2B)	9941(14)	9731(6)	8356(8)	20(3)
C(3B)	9257(14)	9416(5)	7997(9)	21(3)
C(4B)	10510(13)	8859(6)	8180(8)	19(3)
C(5B)	11037(14)	8787(6)	8787(8)	21(3)
C(6B)	11064(14)	9170(6)	9188(8)	19(3)
C(7B)	10019(14)	9380(6)	9898(8)	18(3)
C(8B)	9738(14)	8974(6)	10223(9)	21(3)
C(9B)	10552(15)	8637(6)	10315(9)	29(4)
C(10B)	9503(14)	9105(6)	10812(8)	24(4)
C(11B)	8765(15)	8735(6)	7653(8)	22(3)
C(12B)	8533(16)	8302(6)	7851(9)	27(3)
C(13B)	9252(16)	7982(6)	7970(9)	30(4)
C(14B)	7590(16)	8138(7)	7375(9)	34(4)
C(15B)	5024(15)	9163(6)	10600(9)	30(3)
C(16B)	4977(15)	8839(6)	11043(9)	30(3)
C(17B)	5527(15)	8531(6)	10997(9)	28(3)
C(18B)	4035(14)	8152(6)	10342(9)	25(3)
C(19B)	3456(14)	8522(6)	9882(9)	24(3)
C(20B)	3560(14)	8873(6)	9938(9)	25(3)
C(21B)	4730(15)	9406(6)	9626(9)	27(3)
C(22B)	4830(15)	9301(6)	9020(9)	26(3)
C(23B)	3938(15)	9093(6)	8629(9)	32(4)
C(24B)	5072(15)	9714(6)	8720(9)	29(4)
C(25B)	5680(14)	7800(6)	10491(8)	22(3)
C(26B)	5871(14)	7626(6)	9917(9)	21(3)
C(27B)	4971(14)	7477(6)	9494(9)	24(4)
C(28B)	6624(13)	7248(5)	10041(9)	19(4)
N(1S)	5587(12)	7993(6)	8105(7)	44(2)
C(1S)	4908(14)	8079(7)	7756(9)	44(2)
C(2S)	4041(14)	8177(7)	7305(9)	44(2)
N(2S)	2450(14)	8576(7)	6225(8)	57(3)
C(3S)	1889(17)	8389(8)	6441(10)	57(3)
C(4S)	1276(16)	8155(8)	6767(10)	57(3)
N(3S)	7640(20)	6417(9)	6502(13)	115(4)

C(5S)	7310(30)	6725(10)	6640(16)	115(4)
C(6S)	6730(20)	7069(10)	6786(15)	115(4)
N(4S)	6671(17)	5502(7)	7152(12)	92(3)
C(7S)	7415(19)	5417(9)	7008(15)	92(3)
C(8S)	8304(19)	5369(9)	6773(14)	92(3)
N(5S)	3661(16)	4361(8)	7927(10)	33(5)
C(9S)	2856(18)	4454(10)	7956(13)	33(5)
C(10S)	1882(18)	4528(10)	8079(12)	33(5)
N(5A)	2620(40)	5064(15)	6420(19)	17(10)
C(9A)	2710(50)	4903(18)	6870(20)	26(9)
C(10A)	3080(50)	4620(19)	7340(20)	34(7)
N(6S)	9620(20)	7241(8)	6864(10)	99(4)
C(11S)	9620(30)	7056(9)	7283(12)	99(4)
C(12S)	9640(30)	6859(9)	7818(11)	99(4)
N(7S)	7480(20)	4943(10)	8918(14)	144(4)
C(13S)	7270(20)	4642(11)	8648(17)	144(4)
C(14S)	7300(20)	4233(10)	8516(16)	144(4)

Table A-21. Bond lengths [Å] and angles [°] for **[(Ni-1*)$_2$(CuBr)$_4$]**.

Br(1A)-Cu(1A)	2.327(3)	C(19A)-C(20A)	1.49(2)
Br(2A)-Cu(2A)	2.351(4)	C(21A)-C(22A)	1.51(3)
Br(3A)-Cu(3A)	2.323(3)	C(22A)-C(23A)	1.53(3)
Br(4A)-Cu(4A)	2.362(3)	C(22A)-C(24A)	1.55(2)
Cu(1A)-S(3A)	2.243(6)	C(25A)-C(26A)	1.52(3)
Cu(1A)-S(1A)	2.245(5)	C(26A)-C(27A)	1.55(2)
Cu(2A)-S(1A)	2.236(5)	C(26A)-C(28A)	1.56(2)
Cu(2A)-S(4A)	2.246(6)	Br(1B)-Cu(1B)	2.357(3)
Cu(2A)-Cu(4A)	3.052(4)	Br(2B)-Cu(2B)	2.343(3)
Cu(3A)-S(2A)	2.229(6)	Br(3B)-Cu(3B)	2.332(4)
Cu(3A)-S(3A)	2.237(6)	Br(4B)-Cu(4B)	2.385(3)
Cu(4A)-S(2A)	2.244(5)	Cu(1B)-S(3B)	2.242(5)
Cu(4A)-S(4A)	2.250(6)	Cu(1B)-S(1B)	2.257(5)
Ni(1A)-N(1A)	1.963(17)	Cu(2B)-S(4B)	2.238(6)
Ni(1A)-N(2A)	1.990(16)	Cu(2B)-S(1B)	2.247(5)
Ni(1A)-S(1A)	2.166(5)	Cu(3B)-S(3B)	2.231(6)
Ni(1A)-S(2A)	2.185(6)	Cu(3B)-S(2B)	2.237(6)
Ni(2A)-N(3A)	1.964(16)	Cu(4B)-N(1S)	2.040(14)
Ni(2A)-N(4A)	2.012(15)	Cu(4B)-S(4B)	2.281(6)
Ni(2A)-S(3A)	2.193(5)	Cu(4B)-S(2B)	2.378(5)
Ni(2A)-S(4A)	2.198(6)	Ni(1B)-N(2B)	1.933(15)
S(1A)-C(8A)	1.87(2)	Ni(1B)-N(1B)	2.005(15)
S(2A)-C(12A)	1.83(2)	Ni(1B)-S(2B)	2.171(5)
S(3A)-C(22A)	1.86(2)	Ni(1B)-S(1B)	2.188(6)
S(4A)-C(26A)	1.854(19)	Ni(2B)-N(4B)	1.947(17)
N(1A)-C(7A)	1.51(2)	Ni(2B)-N(3B)	2.019(16)
N(1A)-C(1A)	1.56(2)	Ni(2B)-S(4B)	2.173(5)
N(1A)-C(6A)	1.57(2)	Ni(2B)-S(3B)	2.185(6)
N(2A)-C(4A)	1.50(2)	S(1B)-C(8B)	1.85(2)
N(2A)-C(3A)	1.52(2)	S(2B)-C(12B)	1.85(2)
N(2A)-C(11A)	1.52(2)	S(3B)-C(22B)	1.83(2)
N(3A)-C(15A)	1.48(2)	S(4B)-C(26B)	1.858(19)
N(3A)-C(21A)	1.52(2)	N(1B)-C(7B)	1.48(2)
N(3A)-C(20A)	1.56(2)	N(1B)-C(1B)	1.52(2)
N(4A)-C(25A)	1.45(2)	N(1B)-C(6B)	1.53(2)
N(4A)-C(17A)	1.48(2)	N(2B)-C(3B)	1.49(2)
N(4A)-C(18A)	1.53(2)	N(2B)-C(4B)	1.54(2)
C(1A)-C(2A)	1.52(3)	N(2B)-C(11B)	1.55(2)
C(2A)-C(3A)	1.50(3)	N(3B)-C(15B)	1.46(2)
C(4A)-C(5A)	1.51(2)	N(3B)-C(21B)	1.49(2)
C(5A)-C(6A)	1.43(3)	N(3B)-C(20B)	1.57(2)
C(7A)-C(8A)	1.56(3)	N(4B)-C(17B)	1.50(2)
C(8A)-C(10A)	1.53(3)	N(4B)-C(18B)	1.52(2)
C(8A)-C(9A)	1.58(3)	N(4B)-C(25B)	1.54(2)
C(11A)-C(12A)	1.49(3)	C(1B)-C(2B)	1.50(2)
C(12A)-C(14A)	1.55(3)	C(2B)-C(3B)	1.52(2)
C(12A)-C(13A)	1.58(3)	C(4B)-C(5B)	1.48(2)
C(15A)-C(16A)	1.51(2)	C(5B)-C(6B)	1.55(2)
C(16A)-C(17A)	1.47(2)	C(7B)-C(8B)	1.59(2)
C(18A)-C(19A)	1.51(2)	C(8B)-C(10B)	1.53(3)

C(8B)-C(9B)	1.53(3)	C(11B)-C(12B)	1.55(3)

Table A-21. Continued

C(12B)-C(13B)	1.50(3)	N(2A)-Ni(1A)-S(2A)	89.1(5)
C(12B)-C(14B)	1.52(3)	S(1A)-Ni(1A)-S(2A)	90.2(2)
C(15B)-C(16B)	1.48(3)	N(3A)-Ni(2A)-N(4A)	90.2(6)
C(16B)-C(17B)	1.52(3)	N(3A)-Ni(2A)-S(3A)	89.6(5)
C(18B)-C(19B)	1.49(2)	N(4A)-Ni(2A)-S(3A)	179.7(5)
C(19B)-C(20B)	1.46(2)	N(3A)-Ni(2A)-S(4A)	178.2(5)
C(21B)-C(22B)	1.49(3)	N(4A)-Ni(2A)-S(4A)	88.3(5)
C(22B)-C(23B)	1.53(3)	S(3A)-Ni(2A)-S(4A)	91.9(2)
C(22B)-C(24B)	1.57(3)	C(8A)-S(1A)-Ni(1A)	101.2(6)
C(25B)-C(26B)	1.52(3)	C(8A)-S(1A)-Cu(2A)	113.6(7)
C(26B)-C(27B)	1.50(2)	Ni(1A)-S(1A)-Cu(2A)	90.6(2)
C(26B)-C(28B)	1.58(2)	C(8A)-S(1A)-Cu(1A)	110.8(6)
N(1S)-C(1S)	1.148(7)	Ni(1A)-S(1A)-Cu(1A)	133.9(3)
C(1S)-C(2S)	1.465(7)	Cu(2A)-S(1A)-Cu(1A)	105.2(2)
N(2S)-C(3S)	1.156(15)	C(12A)-S(2A)-Ni(1A)	97.9(7)
C(3S)-C(4S)	1.439(16)	C(12A)-S(2A)-Cu(3A)	114.4(7)
N(3S)-C(5S)	1.159(16)	Ni(1A)-S(2A)-Cu(3A)	131.8(3)
C(5S)-C(6S)	1.428(16)	C(12A)-S(2A)-Cu(4A)	113.5(6)
N(4S)-C(7S)	1.154(15)	Ni(1A)-S(2A)-Cu(4A)	99.1(2)
C(7S)-C(8S)	1.421(16)	Cu(3A)-S(2A)-Cu(4A)	99.4(2)
N(5S)-C(9S)	1.144(16)	C(22A)-S(3A)-Ni(2A)	98.8(6)
C(9S)-C(10S)	1.422(16)	C(22A)-S(3A)-Cu(3A)	112.2(7)
N(5A)-C(9A)	1.161(17)	Ni(2A)-S(3A)-Cu(3A)	98.4(2)
C(9A)-C(10A)	1.448(18)	C(22A)-S(3A)-Cu(1A)	114.3(6)
N(6S)-C(11S)	1.148(15)	Ni(2A)-S(3A)-Cu(1A)	139.5(3)
C(11S)-C(12S)	1.416(16)	Cu(3A)-S(3A)-Cu(1A)	90.3(2)
N(7S)-C(13S)	1.162(16)	C(26A)-S(4A)-Ni(2A)	98.5(7)
C(13S)-C(14S)	1.428(17)	C(26A)-S(4A)-Cu(2A)	118.4(7)
		Ni(2A)-S(4A)-Cu(2A)	137.7(3)
S(3A)-Cu(1A)-S(1A)	110.7(2)	C(26A)-S(4A)-Cu(4A)	113.1(6)
S(3A)-Cu(1A)-Br(1A)	125.15(17)	Ni(2A)-S(4A)-Cu(4A)	99.2(2)
S(1A)-Cu(1A)-Br(1A)	123.99(17)	Cu(2A)-S(4A)-Cu(4A)	85.5(2)
S(1A)-Cu(2A)-S(4A)	114.5(2)	C(7A)-N(1A)-C(1A)	101.0(14)
S(1A)-Cu(2A)-Br(2A)	126.15(18)	C(7A)-N(1A)-C(6A)	108.8(14)
S(4A)-Cu(2A)-Br(2A)	119.04(18)	C(1A)-N(1A)-C(6A)	109.7(14)
S(1A)-Cu(2A)-Cu(4A)	94.18(16)	C(7A)-N(1A)-Ni(1A)	113.5(12)
S(4A)-Cu(2A)-Cu(4A)	47.31(14)	C(1A)-N(1A)-Ni(1A)	113.6(12)
Br(2A)-Cu(2A)-Cu(4A)	117.90(13)	C(6A)-N(1A)-Ni(1A)	109.9(12)
S(2A)-Cu(3A)-S(3A)	113.4(2)	C(4A)-N(2A)-C(3A)	109.2(15)
S(2A)-Cu(3A)-Br(3A)	121.53(18)	C(4A)-N(2A)-C(11A)	113.0(15)
S(3A)-Cu(3A)-Br(3A)	124.86(18)	C(3A)-N(2A)-C(11A)	104.9(14)
S(2A)-Cu(4A)-S(4A)	112.0(2)	C(4A)-N(2A)-Ni(1A)	109.1(11)
S(2A)-Cu(4A)-Br(4A)	122.93(17)	C(3A)-N(2A)-Ni(1A)	108.0(12)
S(4A)-Cu(4A)-Br(4A)	125.09(17)	C(11A)-N(2A)-Ni(1A)	112.4(12)
S(2A)-Cu(4A)-Cu(2A)	86.45(16)	C(15A)-N(3A)-C(21A)	105.8(14)
S(4A)-Cu(4A)-Cu(2A)	47.20(15)	C(15A)-N(3A)-C(20A)	108.8(14)
Br(4A)-Cu(4A)-Cu(2A)	132.10(12)	C(21A)-N(3A)-C(20A)	107.5(14)
N(1A)-Ni(1A)-N(2A)	91.1(7)	C(15A)-N(3A)-Ni(2A)	111.4(12)
N(1A)-Ni(1A)-S(1A)	89.6(5)	C(21A)-N(3A)-Ni(2A)	113.1(11)
N(2A)-Ni(1A)-S(1A)	178.7(5)	C(20A)-N(3A)-Ni(2A)	109.9(11)
N(1A)-Ni(1A)-S(2A)	179.8(6)		

Table A-21. Continued

C(25A)-N(4A)-C(17A)	108.2(14)
C(25A)-N(4A)-C(18A)	109.6(14)
C(17A)-N(4A)-C(18A)	110.2(15)
C(25A)-N(4A)-Ni(2A)	112.2(12)
C(17A)-N(4A)-Ni(2A)	107.3(11)
C(18A)-N(4A)-Ni(2A)	109.4(11)
C(2A)-C(1A)-N(1A)	109.6(16)
C(3A)-C(2A)-C(1A)	119.7(17)
C(2A)-C(3A)-N(2A)	114.8(16)
N(2A)-C(4A)-C(5A)	115.0(16)
C(6A)-C(5A)-C(4A)	120.9(17)
C(5A)-C(6A)-N(1A)	111.8(17)
N(1A)-C(7A)-C(8A)	115.2(16)
C(10A)-C(8A)-C(7A)	109.0(17)
C(10A)-C(8A)-C(9A)	112.7(16)
C(7A)-C(8A)-C(9A)	114.1(16)
C(10A)-C(8A)-S(1A)	110.9(14)
C(7A)-C(8A)-S(1A)	102.0(13)
C(9A)-C(8A)-S(1A)	107.7(14)
C(12A)-C(11A)-N(2A)	112.1(16)
C(11A)-C(12A)-C(14A)	107.1(16)
C(11A)-C(12A)-C(13A)	115.1(17)
C(14A)-C(12A)-C(13A)	107.7(17)
C(11A)-C(12A)-S(2A)	105.7(14)
C(14A)-C(12A)-S(2A)	112.3(14)
C(13A)-C(12A)-S(2A)	109.1(13)
N(3A)-C(15A)-C(16A)	115.4(16)
C(17A)-C(16A)-C(15A)	112.0(17)
C(16A)-C(17A)-N(4A)	118.7(16)
C(19A)-C(18A)-N(4A)	112.2(15)
C(20A)-C(19A)-C(18A)	118.9(17)
C(19A)-C(20A)-N(3A)	111.8(15)
C(22A)-C(21A)-N(3A)	115.1(16)
C(21A)-C(22A)-C(23A)	117.4(16)
C(21A)-C(22A)-C(24A)	109.2(16)
C(23A)-C(22A)-C(24A)	109.0(16)
C(21A)-C(22A)-S(3A)	103.8(13)
C(23A)-C(22A)-S(3A)	107.8(13)
C(24A)-C(22A)-S(3A)	109.3(13)
N(4A)-C(25A)-C(26A)	116.1(16)
C(25A)-C(26A)-C(27A)	116.8(17)
C(25A)-C(26A)-C(28A)	111.0(16)
C(27A)-C(26A)-C(28A)	106.0(15)
C(25A)-C(26A)-S(4A)	103.0(13)
C(27A)-C(26A)-S(4A)	110.0(13)
C(28A)-C(26A)-S(4A)	110.1(13)
S(3B)-Cu(1B)-S(1B)	110.0(2)
S(3B)-Cu(1B)-Br(1B)	124.80(17)
S(1B)-Cu(1B)-Br(1B)	125.15(17)
S(4B)-Cu(2B)-S(1B)	108.9(2)
S(4B)-Cu(2B)-Br(2B)	128.98(18)
S(1B)-Cu(2B)-Br(2B)	122.05(17)
S(3B)-Cu(3B)-S(2B)	114.3(2)
S(3B)-Cu(3B)-Br(3B)	118.79(18)
S(2B)-Cu(3B)-Br(3B)	126.63(18)
N(1S)-Cu(4B)-S(4B)	107.8(6)
N(1S)-Cu(4B)-S(2B)	102.6(6)
S(4B)-Cu(4B)-S(2B)	104.4(2)
N(1S)-Cu(4B)-Br(4B)	103.0(5)
S(4B)-Cu(4B)-Br(4B)	122.93(17)
S(2B)-Cu(4B)-Br(4B)	114.25(17)
N(2B)-Ni(1B)-N(1B)	90.7(6)
N(2B)-Ni(1B)-S(2B)	89.4(5)
N(1B)-Ni(1B)-S(2B)	179.4(5)
N(2B)-Ni(1B)-S(1B)	178.8(5)
N(1B)-Ni(1B)-S(1B)	88.4(5)
S(2B)-Ni(1B)-S(1B)	91.5(2)
N(4B)-Ni(2B)-N(3B)	90.4(7)
N(4B)-Ni(2B)-S(4B)	89.6(5)
N(3B)-Ni(2B)-S(4B)	177.6(5)
N(4B)-Ni(2B)-S(3B)	177.5(5)
N(3B)-Ni(2B)-S(3B)	87.9(5)
S(4B)-Ni(2B)-S(3B)	92.0(2)
C(8B)-S(1B)-Ni(1B)	99.1(7)
C(8B)-S(1B)-Cu(2B)	111.5(6)
Ni(1B)-S(1B)-Cu(2B)	129.9(2)
C(8B)-S(1B)-Cu(1B)	114.0(6)
Ni(1B)-S(1B)-Cu(1B)	94.7(2)
Cu(2B)-S(1B)-Cu(1B)	106.8(2)
C(12B)-S(2B)-Ni(1B)	100.8(7)
C(12B)-S(2B)-Cu(3B)	111.1(7)
Ni(1B)-S(2B)-Cu(3B)	96.5(2)
C(12B)-S(2B)-Cu(4B)	111.7(7)
Ni(1B)-S(2B)-Cu(4B)	143.7(3)
Cu(3B)-S(2B)-Cu(4B)	86.63(19)
C(22B)-S(3B)-Ni(2B)	97.6(7)
C(22B)-S(3B)-Cu(3B)	117.5(7)
Ni(2B)-S(3B)-Cu(3B)	133.2(2)
C(22B)-S(3B)-Cu(1B)	113.8(7)
Ni(2B)-S(3B)-Cu(1B)	100.9(2)
Cu(3B)-S(3B)-Cu(1B)	92.5(2)
C(26B)-S(4B)-Ni(2B)	98.2(7)
C(26B)-S(4B)-Cu(2B)	111.8(6)
Ni(2B)-S(4B)-Cu(2B)	103.9(2)
C(26B)-S(4B)-Cu(4B)	111.0(7)
Ni(2B)-S(4B)-Cu(4B)	127.8(3)
Cu(2B)-S(4B)-Cu(4B)	103.9(2)
C(7B)-N(1B)-C(1B)	105.4(14)
C(7B)-N(1B)-C(6B)	110.5(14)
C(1B)-N(1B)-C(6B)	106.4(14)
C(7B)-N(1B)-Ni(1B)	114.8(11)

Table A-21. Continued

C(1B)-N(1B)-Ni(1B)	110.8(11)
C(6B)-N(1B)-Ni(1B)	108.6(11)
C(3B)-N(2B)-C(4B)	109.8(14)
C(3B)-N(2B)-C(11B)	103.6(14)
C(4B)-N(2B)-C(11B)	107.7(14)
C(3B)-N(2B)-Ni(1B)	109.8(12)
C(4B)-N(2B)-Ni(1B)	111.0(11)
C(11B)-N(2B)-Ni(1B)	114.6(11)
C(15B)-N(3B)-C(21B)	107.2(15)
C(15B)-N(3B)-C(20B)	108.8(15)
C(21B)-N(3B)-C(20B)	111.6(15)
C(15B)-N(3B)-Ni(2B)	109.8(12)
C(21B)-N(3B)-Ni(2B)	111.7(12)
C(20B)-N(3B)-Ni(2B)	107.6(11)
C(17B)-N(4B)-C(18B)	109.6(15)
C(17B)-N(4B)-C(25B)	102.7(14)
C(18B)-N(4B)-C(25B)	107.2(15)
C(17B)-N(4B)-Ni(2B)	110.7(12)
C(18B)-N(4B)-Ni(2B)	112.2(12)
C(25B)-N(4B)-Ni(2B)	113.8(12)
C(2B)-C(1B)-N(1B)	114.8(15)
C(1B)-C(2B)-C(3B)	111.0(16)
N(2B)-C(3B)-C(2B)	117.1(16)
C(5B)-C(4B)-N(2B)	110.7(15)
C(4B)-C(5B)-C(6B)	115.4(16)
N(1B)-C(6B)-C(5B)	112.7(15)
N(1B)-C(7B)-C(8B)	112.0(15)
C(10B)-C(8B)-C(9B)	109.3(16)
C(10B)-C(8B)-C(7B)	108.2(15)
C(9B)-C(8B)-C(7B)	114.7(16)
C(10B)-C(8B)-S(1B)	109.7(13)
C(9B)-C(8B)-S(1B)	111.0(13)
C(7B)-C(8B)-S(1B)	103.7(13)
N(2B)-C(11B)-C(12B)	111.8(16)
C(13B)-C(12B)-C(14B)	109.8(17)
C(13B)-C(12B)-C(11B)	115.4(17)
C(14B)-C(12B)-C(11B)	108.9(17)
C(13B)-C(12B)-S(2B)	108.6(15)
C(14B)-C(12B)-S(2B)	110.2(15)
C(11B)-C(12B)-S(2B)	103.7(13)
N(3B)-C(15B)-C(16B)	115.4(17)
C(15B)-C(16B)-C(17B)	118.2(18)
N(4B)-C(17B)-C(16B)	110.6(16)
C(19B)-C(18B)-N(4B)	112.2(16)
C(20B)-C(19B)-C(18B)	118.9(17)
C(19B)-C(20B)-N(3B)	114.5(16)
C(22B)-C(21B)-N(3B)	113.6(16)
C(21B)-C(22B)-C(23B)	118.1(18)
C(21B)-C(22B)-C(24B)	107.3(17)
C(23B)-C(22B)-C(24B)	108.0(17)
C(21B)-C(22B)-S(3B)	103.4(14)
C(23B)-C(22B)-S(3B)	110.3(14)
C(24B)-C(22B)-S(3B)	109.5(13)
C(26B)-C(25B)-N(4B)	112.4(15)
C(27B)-C(26B)-C(25B)	116.8(17)
C(27B)-C(26B)-C(28B)	107.2(15)
C(25B)-C(26B)-C(28B)	109.3(16)
C(27B)-C(26B)-S(4B)	110.1(13)
C(25B)-C(26B)-S(4B)	103.7(13)
C(28B)-C(26B)-S(4B)	109.5(13)
C(1S)-N(1S)-Cu(4B)	176(2)
N(1S)-C(1S)-C(2S)	178(3)
N(2S)-C(3S)-C(4S)	174(3)
N(3S)-C(5S)-C(6S)	170(4)
N(4S)-C(7S)-C(8S)	171(4)
N(5S)-C(9S)-C(10S)	170(3)
N(5A)-C(9A)-C(10A)	159(6)
N(6S)-C(11S)-C(12S)	177(4)
N(7S)-C(13S)-C(14S)	162(4)

Table A-22. Crystal data and structure refinement for [(**Ni-1**)Rh(CO)(PPh_3)][Cl].

Identification code	mdm	
Empirical formula	C29 H37 Cl N2 Ni O2 P Rh S2	
Formula weight	737.77	
Temperature	110(2) K	
Wavelength	0.71073 Å	
Crystal system	Triclinic	
Space group	P-1	
Unit cell dimensions	a = 9.119(5) Å	α= 82.768(5)°.
	b = 11.111(5) Å	β= 79.333(5)°.
	c = 14.916(5) Å	γ = 83.661(5)°.
Volume	1467.5(12) $Å^3$	
Z	2	
Density (calculated)	1.670 Mg/m^3	
Absorption coefficient	1.523 mm^{-1}	
F(000)	756	
Crystal size	0.30 x 0.20 x 0.20 mm^3	
Theta range for data collection	1.85 to 27.52°.	
Index ranges	-11<=h<=11, -7<=k<=14, -19<=l<=19	
Reflections collected	9086	
Independent reflections	6294 [R(int) = 0.0211]	
Completeness to theta = 27.52°	92.9 %	
Absorption correction	Semi-empirical from equivalents	
Max. and min. transmission	0.7505 and 0.6580	
Refinement method	Full-matrix least-squares on F^2	
Data / restraints / parameters	6294 / 0 / 352	
Goodness-of-fit on F^2	1.078	
Final R indices [I>2sigma(I)]	R1 = 0.0562, wR2 = 0.1327	
R indices (all data)	R1 = 0.0715, wR2 = 0.1429	
Largest diff. peak and hole	3.439 and -0.494 e.$Å^{-3}$	

Table A-22. Atomic coordinates (x 10^4) and equivalent isotropic displacement parameters ($Å^2$x 10^3) for [(**Ni-1**)Rh(CO)(PPh_3)][Cl]. U(eq) is defined as one third of the trace of the orthogonalized U^{ij} tensor.

	x	y	z	U(eq)
Rh(1)	8998(1)	956(1)	3402(1)	20(1)
Ni(1)	8786(1)	922(1)	1425(1)	20(1)
O(2)	3417(4)	4865(4)	1147(3)	41(1)
S(1)	10673(1)	1355(1)	1977(1)	23(1)
S(2)	8625(1)	-573(1)	2512(1)	22(1)
P(1)	9439(1)	2495(1)	4156(1)	18(1)
O(1)	6579(4)	138(3)	4909(2)	35(1)
Cl(2)	6017(1)	6674(1)	607(1)	29(1)
N(1)	8933(4)	2371(4)	530(2)	24(1)
N(2)	6923(4)	564(4)	1064(2)	23(1)
C(1)	10659(6)	2957(4)	1466(3)	27(1)
C(2)	10351(5)	2955(4)	506(3)	26(1)
C(3)	8986(5)	2058(5)	-428(3)	26(1)
C(4)	7596(5)	1523(5)	-571(3)	29(1)
C(5)	7196(5)	394(5)	58(3)	27(1)
C(6)	7591(5)	3276(4)	777(3)	28(1)
C(7)	6364(5)	2720(5)	1504(3)	29(1)
C(8)	5743(5)	1620(5)	1271(3)	27(1)
C(9)	6391(5)	-611(4)	1577(3)	26(1)
C(10)	6628(5)	-722(5)	2567(3)	26(1)
C(11)	7535(5)	445(4)	4359(3)	26(1)
C(12)	8290(4)	2639(4)	5286(3)	20(1)
C(13)	7441(5)	3717(4)	5514(3)	23(1)
C(14)	6579(5)	3779(5)	6380(3)	26(1)
C(15)	6547(5)	2776(5)	7027(3)	28(1)
C(16)	7413(5)	1696(5)	6816(3)	27(1)
C(17)	8275(5)	1631(4)	5952(3)	26(1)
C(18)	11334(5)	2527(4)	4374(3)	19(1)
C(19)	11587(5)	2890(4)	5198(3)	23(1)

Table A-22. Continued

C(20)	13037(5)	2985(4)	5327(3)	24(1)
C(21)	14248(5)	2699(4)	4653(3)	26(1)
C(22)	14008(5)	2334(5)	3853(3)	29(1)
C(23)	12564(5)	2232(5)	3705(3)	27(1)
C(24)	9071(5)	3972(4)	3509(3)	21(1)
C(25)	7716(5)	4195(4)	3182(3)	23(1)
C(26)	7446(5)	5241(4)	2597(3)	26(1)
C(27)	8528(5)	6070(4)	2330(3)	27(1)
C(28)	9858(6)	5863(4)	2666(3)	26(1)
C(29)	10140(5)	4814(4)	3251(3)	24(1)

Table A-22. Bond lengths [Å] and angles [°] for [(**Ni-1**)Rh(CO)(PPh_3)][Cl]

Rh(1)-C(11)	1.853(5)	C(16)-C(17)	1.386(6)
Rh(1)-P(1)	2.2710(13)	C(18)-C(23)	1.395(6)
Rh(1)-S(2)	2.3719(13)	C(18)-C(19)	1.407(6)
Rh(1)-S(1)	2.3994(13)	C(19)-C(20)	1.388(6)
Rh(1)-Ni(1)	2.9955(12)	C(20)-C(21)	1.386(6)
Ni(1)-N(1)	1.958(4)	C(21)-C(22)	1.385(7)
Ni(1)-N(2)	1.968(4)	C(22)-C(23)	1.388(6)
Ni(1)-S(1)	2.1628(15)	C(24)-C(29)	1.395(6)
Ni(1)-S(2)	2.1665(14)	C(24)-C(25)	1.398(6)
S(1)-C(1)	1.856(5)	C(25)-C(26)	1.390(6)
S(2)-C(10)	1.832(5)	C(26)-C(27)	1.394(7)
P(1)-C(18)	1.821(4)	C(27)-C(28)	1.373(7)
P(1)-C(24)	1.826(5)	C(28)-C(29)	1.397(7)
P(1)-C(12)	1.828(4)		
O(1)-C(11)	1.132(6)	C(11)-Rh(1)-P(1)	91.70(15)
N(1)-C(2)	1.503(6)	C(11)-Rh(1)-S(2)	92.33(15)
N(1)-C(3)	1.503(6)	P(1)-Rh(1)-S(2)	175.72(4)
N(1)-C(6)	1.516(6)	C(11)-Rh(1)-S(1)	167.87(15)
N(2)-C(5)	1.508(6)	P(1)-Rh(1)-S(1)	99.97(5)
N(2)-C(9)	1.509(6)	S(2)-Rh(1)-S(1)	75.92(5)
N(2)-C(8)	1.524(6)	C(11)-Rh(1)-Ni(1)	123.27(14)
C(1)-C(2)	1.509(6)	P(1)-Rh(1)-Ni(1)	130.26(3)
C(3)-C(4)	1.518(7)	S(2)-Rh(1)-Ni(1)	45.81(3)
C(4)-C(5)	1.505(7)	S(1)-Rh(1)-Ni(1)	45.63(4)
C(6)-C(7)	1.531(7)	N(1)-Ni(1)-N(2)	91.37(16)
C(7)-C(8)	1.505(7)	N(1)-Ni(1)-S(1)	91.35(12)
C(9)-C(10)	1.520(6)	N(2)-Ni(1)-S(1)	173.24(11)
C(12)-C(13)	1.397(6)	N(1)-Ni(1)-S(2)	174.76(12)
C(12)-C(17)	1.399(6)	N(2)-Ni(1)-S(2)	91.46(12)
C(13)-C(14)	1.387(6)	S(1)-Ni(1)-S(2)	85.37(5)
C(14)-C(15)	1.378(7)	N(1)-Ni(1)-Rh(1)	123.07(12)
C(15)-C(16)	1.399(7)	N(2)-Ni(1)-Rh(1)	121.09(11)

Table A-22. Continued

S(1)-Ni(1)-Rh(1)	52.47(3)	N(1)-C(6)-C(7)	112.6(4)
S(2)-Ni(1)-Rh(1)	51.72(4)	C(8)-C(7)-C(6)	116.3(4)
C(1)-S(1)-Ni(1)	96.30(16)	C(7)-C(8)-N(2)	113.7(4)
C(1)-S(1)-Rh(1)	116.32(16)	N(2)-C(9)-C(10)	110.5(4)
Ni(1)-S(1)-Rh(1)	81.90(5)	C(9)-C(10)-S(2)	105.8(3)
C(10)-S(2)-Ni(1)	95.99(16)	O(1)-C(11)-Rh(1)	175.8(4)
C(10)-S(2)-Rh(1)	111.50(16)	C(13)-C(12)-C(17)	118.8(4)
Ni(1)-S(2)-Rh(1)	82.47(5)	C(13)-C(12)-P(1)	122.6(3)
C(18)-P(1)-C(24)	103.7(2)	C(17)-C(12)-P(1)	118.6(3)
C(18)-P(1)-C(12)	102.89(19)	C(14)-C(13)-C(12)	120.5(4)
C(24)-P(1)-C(12)	103.8(2)	C(15)-C(14)-C(13)	120.5(4)
C(18)-P(1)-Rh(1)	117.44(15)	C(14)-C(15)-C(16)	119.8(4)
C(24)-P(1)-Rh(1)	110.89(15)	C(17)-C(16)-C(15)	119.9(4)
C(12)-P(1)-Rh(1)	116.45(15)	C(16)-C(17)-C(12)	120.6(4)
C(2)-N(1)-C(3)	105.8(3)	C(23)-C(18)-C(19)	118.8(4)
C(2)-N(1)-C(6)	109.7(4)	C(23)-C(18)-P(1)	120.2(3)
C(3)-N(1)-C(6)	109.3(3)	C(19)-C(18)-P(1)	121.0(3)
C(2)-N(1)-Ni(1)	111.3(3)	C(20)-C(19)-C(18)	120.1(4)
C(3)-N(1)-Ni(1)	111.5(3)	C(21)-C(20)-C(19)	120.4(4)
C(6)-N(1)-Ni(1)	109.2(3)	C(22)-C(21)-C(20)	119.8(4)
C(5)-N(2)-C(9)	106.6(4)	C(21)-C(22)-C(23)	120.5(4)
C(5)-N(2)-C(8)	110.8(3)	C(22)-C(23)-C(18)	120.4(4)
C(9)-N(2)-C(8)	110.3(3)	C(29)-C(24)-C(25)	119.3(4)
C(5)-N(2)-Ni(1)	110.1(3)	C(29)-C(24)-P(1)	122.8(3)
C(9)-N(2)-Ni(1)	110.8(3)	C(25)-C(24)-P(1)	117.5(3)
C(8)-N(2)-Ni(1)	108.2(3)	C(26)-C(25)-C(24)	120.2(4)
C(2)-C(1)-S(1)	105.8(3)	C(25)-C(26)-C(27)	120.2(4)
N(1)-C(2)-C(1)	110.5(4)	C(28)-C(27)-C(26)	119.6(4)
N(1)-C(3)-C(4)	114.4(4)	C(27)-C(28)-C(29)	120.9(4)
C(5)-C(4)-C(3)	115.0(4)	C(24)-C(29)-C(28)	119.8(4)
C(4)-C(5)-N(2)	114.2(4)		

Symmetry transformations used to generate equivalent atoms:

VITA

Marilyn Vena Rampersad was born in Trinidad and Tobago. At 16 years of age she immigrated to the United States where she resided in New York City for 10 years. She completed her Bachelor of Arts Degree in psychology and chemistry at Hunter College of the City University of New York in May of 2001. In the summer of 2001 she moved to College Station, Texas where she studied at Texas A&M University under the tutelage of Dr. Marcetta Y. Darensbourg. She graduated with a Ph.D. in December, 2005 and can be contacted through her advisor, Dr. Marcetta Darensbourg in the Chemistry Department at Texas A&M University, mailstop 3255 , College Station, TX, 77843.